

BIOLOGICAL ACTIVITY AND CALCIUM CARBONATE DYNAMICS IN GREENLAND SEA ICE

– IMPLICATION FOR THE INORGANIC CARBON CYCLE

Dorte H. Søgaard
PhD thesis 2014

BIOLOGICAL ACTIVITY AND CALCIUM CARBONATE DYNAMICS IN GREENLAND SEA ICE – IMPLICATION FOR THE INORGANIC CARBON CYCLE

PhD thesis 2014
Dorte H. Søgaard



Data sheet

Title: Biological activity and calcium carbonate dynamics in Greenland sea ice
– Implication for the inorganic carbon cycle

Subtitle: PhD thesis

Author: Dorte H. Søgaard

Affiliations: Greenland Climate Research Centre (c/o Greenland Institute of Natural Resources),
Kivioq 2, Box 570, 3900 Nuuk, Greenland
University of Southern Denmark, Campusvej 55, 5230 Odense M, Denmark

Publisher: Greenland Institute of Natural Resources, Nuuk Greenland

Year of publication: 2014

PhD supervisors

Internal: Professor Ronnie N Glud
University of Southern Denmark
Campusvej 55
5230 Odense M, Denmark

External: Professor Søren Rysgaard
Arctic Research Centre, Department of Bioscience
Ny Munkegade 116, building 1540
8000 Aarhus C, Denmark

Please cite as: Søgaard D.H. (2014) Biological activity and calcium carbonate dynamics in Greenland sea ice – Implication for the inorganic carbon cycle. PhD thesis. Greenland Climate Research Centre and Department of Biology, University of Southern Denmark. Greenland Institute of Natural Resources, 148 pp.

Keywords: Subarctic sea ice • High Arctic sea ice • Air-sea CO₂ exchange • Greenland • Spatial variability • Calcium carbonate • Net autotrophic activity • Net heterotrophic activity

Reproduction permitted provided the source is explicitly acknowledged

Layout: Tinna Christensen

Cover photo: Jakob Sievers

Number of pages: 148

Printed by: Rosendahls – Schultz Grafisk a/s

ISBN: 87-91214-68-8
EAN: 9788791214684

Circulation: 160

Electronic version: www.natur.gl

Contents

List of publications	5
Preface	6
Acknowledgements	7
Abstract	8
Dansk abstrakt (abstract in Danish)	9
Eqikkaaneq (abstract in Greenlandic)	10
CHAPTER 1 – INTRODUCTION	11
1.1 Setting the scene	12
1.1.1 General oceanography of the study areas	13
1.2 Phase I: Transition from open water to ice-covered oceans	14
1.2.1 Sea ice formation – abiotic processes	15
1.2.2 Microorganisms in newly formed sea ice	18
1.2.3 Frost flowers and brine skim formation – abiotic processes	19
1.3 Phase II: Growing winter sea ice	20
1.3.1 Abiotic processes in growing winter ice	21
1.3.2 Growth limitation of microorganisms in winter sea ice	22
1.4 Phase III: Transition from ice-covered ocean to open waters	23
1.4.1 Abiotic processes in melting sea ice	23
1.4.2 Biotic processes in spring/summer sea ice	24
1.4.3 The open water period	28
1.5 Ocean and sea ice in the context of global change	29
1.6 Conclusions and perspectives	30
1.7 Glossary	31
1.8 Literature cited	34



CHAPTER 2 – PUBLICATIONS

41

Paper I	The relative contributions of biological and abiotic processes to carbon dynamics in subarctic sea ice	43
Paper II	Ikaite crystal distribution in winter sea ice and implications for CO ₂ system dynamics	61
Paper III	Frost flowers on young Arctic sea ice: The climatic, chemical and microbial significance of an emerging ice type	75
Paper IV	Autotrophic and heterotrophic activity in Arctic first-year sea ice: seasonal study from Malene Bight, SW Greenland	95
Paper V	Growth limitation of three Arctic sea ice algal species: effects of salinity, pH, and inorganic carbon availability	111
Paper VI	Short-term variability in bacterial abundance, cell properties, and incorporation of leucine and thymidine in subarctic sea ice	121
Paper VII	High air-sea CO ₂ uptake rates in nearshore and shelf areas of Southern Greenland: Temporal and spatial variability	139

List of publications

Part of the dissertation

Paper I: Sogaard DH, Thomas DN, Rysgaard S, Glud RN, Norman L, Kaartokallio H, Juul-Pedersen T, Geilfus N-X (2013) The relative contributions of biological and abiotic processes to carbon dynamics in subarctic sea ice. *Polar Biol* 36:1761 – 1777, doi:10.1007/s003-013-1396-6

Paper II: Rysgaard S, Sogaard DH, Cooper M, Pucko M, Lennert K, Papakyriakou TN, Wang F, Geilfus NX, Glud RN, Ehn J, McGinnis DF, Attard K, Sievers J, Deming JW, Barber D (2013) Ikaite crystal distribution in winter sea ice and implications for CO₂ system dynamics. *TC* 7:707 – 718, doi:10.5194/tc7-707-2013

Paper III: Barber DG, Ehn JK, Pucko M, Rysgaard S, Papakyriakou T, Deming J, Galley R, Sogaard DH (2014) Frost flowers on young Arctic sea ice: The climatic, chemical and microbial significance of an emerging ice type. *J Geophys Res-Atmos*, doi:10.1002/2014JD021736

Paper IV: Sogaard DH, Kristensen M, Rysgaard S, Glud RN, Hansen PJ, Hilligsøe KM (2010) Autotrophic and heterotrophic activity in Arctic first-year sea ice: seasonal study from Malene Bight, SW Greenland. *Mar Ecol Prog Ser* 419:31 – 45, doi:10.3354/meps08845*

Paper V: Sogaard DH, Hansen PJ, Rysgaard S, Glud RN (2011) Growth limitation of three Arctic sea ice algal species: effects of salinity, pH, and inorganic carbon availability. *Polar Biol* 34:1157 – 1165, doi:10.1007/s00300-011-0976-3**

Paper VI: Kaartokallio H, Sogaard DH, Norman L, Rysgaard S, Tison JL, Delille B, Thomas DN (2013) Short-term variability in bacterial abundance, cell properties, and incorporation of leucine and thymidine in subarctic sea ice. *Aquat Microb Ecol* 71:57 – 73, doi:10.3354/ame01667

Paper VII: Rysgaard S, Mortensen J, Juul-Pedersen T, Sørensen LL, Lennert K, Sogaard DH, Arendt KE, Blicher ME, Sejr MK, Bendtsen J (2012) High air-sea CO₂ uptake rates in nearshore and shelf areas of Southern Greenland: Temporal and spatial variability. *Mar Chem* 128-129:26 – 33, doi:10.1016/j.marchem.2011.11.002

Related work not included in the dissertation

Long MH, Koopmans D, Berg P, Rysgaard S, Glud RN, Sogaard DH (2012) Oxygen exchange and ice melt measured at the ice-water interface by eddy correlation. *BG* 9:1957 – 1967, doi:10.5194/bg-9-1-2012

Geilfus N-X, Galley RJ, Cooper M, Halden N, Hare A, Wang F, Sogaard DH, Rysgaard S (2013b) Gypsum crystals observed in experimental and natural sea ice. *Geophys Res Lett* 40: 1 – 6, doi:10.1002/2013GL058479

Sørensen LL, Jensen B, Glud RN, McGinnis DF, Sejr MK, Sievers J, Sogaard DH, Tison JL, Rysgaard S (2014) Parameterization of atmospheric-surface exchange of CO₂ over sea ice. *TC* 8:853 – 866, doi:10.5194/tc-8-853-2014

Juul-Pedersen, Arendt KE, Mortensen J, Blicher M, Sogaard DH, Rysgaard S (submitted) Seasonal and interannual phytoplankton production in a sub-arctic fjord (Godthåbsfjord) connected to the Greenland Ice Sheet. *Mar Ecol Prog Ser*

Sogaard DH, Glud RN, Rysgaard S, Jody Deming (in prep) A comparative study of biotic- and abiotic-induced oxygen and inorganic carbon dynamics in meter thick winter and young thin polynya ice. Prepared for *Mar Ecol Prog Ser*

Meire L, Sogaard DH, Juul-Pedersen T, Blicher M, Rysgaard S, Glud RN, Sejr M, Arendt K, Lennert K, Mortensen J (in prep) Influence of glacier runoff and biology on the CO₂ uptake in a Subarctic Greenlandic fjord (Godthåbsfjord, SW Greenland). Prepared for *Mar Chem*

*) The data material was a part of my master's thesis, but the data processing, writing the paper and the review process was done during my Ph.D. study.

**) A small part of the data material was a part of a model project, but the rest of the data, the data processing, writing the paper and the review process was done during my Ph.D. study.

Photo: Jakob Sievers..



Preface

This dissertation is the result of a 3-year Ph.D. project conducted at the Greenland Climate Research Center (GCRC) and the Greenland Institute of Natural Resources (GINR). The project was funded by the Commission for Scientific Research in Greenland (KVUG). Much of the work has been conducted with logistical support by GCRC, GINR, the Department for Education, Church, Culture and Equality (IIKNN), the Marine Basis Monitoring Programmes of Greenland Ecosystem Monitoring (GEM; www.g-e-m.dk), the Canada Excellence Research Chair (CERC) program and the Danish Agency for Science, Technology and Innovation.

One of the first descriptions of the transport of CO₂ across the sea ice-ocean interface (i.e., the sea ice CO₂ pump) was made by E.P. Jones and A.R. Coote (1981) in the year I was born. Now 33 years later the understanding of the seasonal events controlling the inorganic carbon dynamics in ice-covered seas is still a challenging subject. A very important factor in climate change is the global carbon budget; and, in order to refine it, we need detailed measurements of the seasonal inorganic carbon dynamics in ice-covered seas.

My dissertation consists of two chapters: Chapter 1 is structured as a review with a detailed discussion of the processes driving the inorganic carbon cycle in high latitude waters during all phases of the sea ice growth and decay cycle (sections 1.2 – 1.4). In addition, there is a discussion of the Arctic Ocean and sea ice coverage in the context of global change (section 1.5) and, finally an outline and discussion of future studies needed to improve our understanding of the seasonal events controlling the dynamics of inorganic carbon in high latitude oceans (section 1.6); Chapter 2 consists of seven published peer-reviewed papers. The findings in this thesis provide strong evidence for the idea of a sea-ice-driven carbon pump in Subarctic and High Arctic sea ice, improve the state of knowledge on the relative contribution of biotic and abiotic processes to carbon dynamics within sea ice, and present a compilation of the current knowledge of the seasonal inorganic carbon dynamics in ice-covered seas during sea ice growth and decay. Furthermore, it provides new knowledge of the influence of biological processes and glacier runoff on the pCO₂ flux in Arctic coastal waters.

Photo: Jakob Sievers.



Acknowledgements

I owe tremendous thanks to my supervisors Søren Rysgaard (Aarhus University) and Ronnie N. Glud (University of Southern Denmark) for excellent supervision and support, for making this project possible in the first place as well as introducing me to the field work in Malene Bight, SW Greenland and Young Sound, NE Greenland and for many quality hours spend in the Arctic winter.

Thanks to John Mortensen and Lorenz Meire for a fruitful co-operation on the subject of the influence of glacier runoff and biology on the CO₂ uptake in a Subarctic Greenlandic fjord. Nicolas-Xavier Geilfus (ARC) is thanked for constructive ideas and discussions during our study of ikaite in sea ice.

Thanks to the warm welcome from GINR when I arrived in Greenland in 2007. Special thanks to director Klaus Nygaard (GINR) for supporting me financially and logistically. Thanks to my colleagues at GINR for an inspiring and pleasant working environment – especially Martin E. Blicher, Kristine E. Arendt, Thomas Juul Pedersen, John Mortensen, Katrine Raundrup and Rasmus Hedeholm for scientific advice and for correction of my manuscripts.



This project could not have been completed without help in the field: Thomas Krogh, Michael S. Schrøder, Thomas Juul-Pedersen, Paul Batty, Kristine E. Arendt, Martin E. Blicher, Morten Kristensen, Lorentz Meire, Kunuk Lennert, Ivali Lennert and Egon Frandsen.

Thanks to all my co-authors for comments on manuscripts but especially for broadening my scientific horizon by challenging my work.

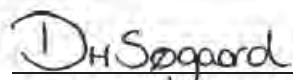
A special thanks to my best friend Charlotte F. Michelsen for helping me whenever needed and for proof reading my thesis.

I am grateful for the support of my family: my parents Bent and Hanne Søgaaard, my sister Susanne Søgaaard, my grandparents Margit and Børge Sørensen and my in-laws Ulla and Peter Schrøder for always encouraging me to explore new horizons and for providing unwavering support.

Deep felt thanks to Michael S. Schrøder, my wonderful husband, who has participated right from the beginning – in the field with statistical support, for having patience with me at busy times, for engaging in interesting discussions, for providing a profound sense of stability and for giving me my two daughters Sif and Naja. You followed me to Greenland and made this project possible. I will forever be grateful for this.

Ilaquttakka asasakka uannut pingaarnerpaavusi!

Nuuk, August 2014


Dorte H. Søgaaard



Abstract

The contribution of sea-ice-covered regions to the global air-sea CO₂ exchange was, until recently, assumed to be insignificant primarily because sea ice was considered impermeable. The discovery of a sea ice CO₂ pump and the recognition that extensive and productive microbial communities exist within sea ice, however, has changed this general perception. Therefore, an improved understanding of the current role of sea ice in the overall carbon budget is needed. The main focus of this PhD study was: 1) to investigate the factors that control the spatial and temporal distribution of calcium carbonate and other important biogeochemical parameters in Greenland sea ice, 2) to discuss the potential interactions between these parameters, and 3) to assess how these parameters affect the sea ice CO₂ system.

Here, I report measurements of calcium carbonate dynamics, biological activity, total alkalinity (TA), total inorganic carbon (TCO₂) and other biogeochemical parameters from sea ice in Greenland. First, I look at the dynamics of these parameters at temporal and spatial scales in Subarctic sea ice and, secondly look at the dynamics of these parameters in High Arctic winter sea ice on a more patchy level. Altogether, my results indicate that the TCO₂ depletion of the Subarctic and High Arctic sea ice is mainly controlled by physical export through brine drainage and CaCO₃ precipitation/dissolution – a conclusion that, therefore, strengthens the concept of the sea-ice-driven carbon pump in high latitude waters. Furthermore, the different studies combined revealed that the relative contribution of primary production to TCO₂ depletion is minor compared to the contribution of calcium carbonate precipitation. However, the biological contribution to the TCO₂ depletion might be much higher in areas with high primary production. Consequently, the evaluation of the sea ice sink described in this thesis may not be representative of the Arctic as a whole since the uptake of CO₂ by biological activity seems to be much lower in Greenland sea ice compared to other regions. Extensive investigations are, however, still needed to elucidate local and regional variation in biological activity in sea ice in Greenland and in other Arctic regions.

The highest concentrations of calcium carbonate ever reported in natural sea ice was measured in approximately 5-month-old High Arctic land-fast sea ice, followed by high concentrations in newly formed High Arctic polynya sea ice; whereas the lowest concentrations observed during our studies were in Subarctic land-fast sea ice. Variations in sea ice properties such as temperature, salinity, pH, ice texture and freshwater input are likely responsible for some of the differences found in calcium carbonate concentrations between sites.

Consequently, the different studies revealed large variations in calcium carbonate concentration and other biogeochemical parameters at different temporal and spatial scales, emphasising the importance of full-season studies covering the meter-hundred meter spatial scale in order to make reliable carbon budgets.

This PhD thesis also presents a survey of the influence of biological processes and glacier runoff on the pCO₂ dynamics in Subarctic coastal waters. The study revealed that the Subarctic Godthåbsfjord system in SW Greenland can be considered as a strong sink of CO₂ and that the CO₂ uptake is highly regulated by biological processes and by mixing glacial meltwater and coastal waters. Moreover, the CO₂ uptake is strongest nearest to the outlet from the Greenland Ice Sheet. If our estimates are representative of similar Subarctic fjord system in Greenland, then the coastal areas of Greenland constitutes a larger sink than anticipated and this knowledge should be included in future global carbon budgets.

Dansk abstrakt (abstract in Danish)

Indtil for nylig har man anset betydningen af isdækkede havområder for den globale udveksling af CO₂ mellem hav og luft for at være ubetydelig, især fordi havis er blevet anset for at være uigennemtrængelig. Opdagelsen af en CO₂-pumpe drevet af havis, samt anerkendelsen af, at der eksisterer omfattende og produktive mikrobielle samfund i havis, har dog ændret denne generelle opfattelse. En bedre forståelse af havisens aktuelle rolle i det samlede CO₂-budget er derfor nødvendig. Fokus for dette ph.d.-studium blev derfor: 1) at undersøge de faktorer, der styrer den rumlige og tidsmæssige fordeling af kalciumkarbonat og andre vigtige biogeokemiske parametre i grønlandsk havis 2) at diskutere de potentielle interaktioner mellem disse parametre og 3) at vurdere, hvordan disse parametre påvirker havisens CO₂-system.

Denne ph.d.-afhandling viser målinger af kalciumkarbonatdynamik, biologisk aktivitet, total alkalinitet (TA), totalt uorganisk kulstof (TCO₂) og andre biogeokemiske parametre fra havis i Grønland. Først undersøges disse parametres dynamik i tidsmæssige og rumlige skalaer i subarktisk havis, og desuden undersøges parametrene dynamik i højarktisk nydannet polynya- og vinter-havis.

Alt i alt viser mine resultater, at TCO₂-tabet i den subarktiske og højarktiske havis hovedsageligt styres af fysisk eksport af salt og TCO₂ ud af havisen til det underliggende havvand og kalciumkarbonat-udfældning/opløsning. Dette styrker beviset om en CO₂-pumpe drevet af havis i det grønlandske farvande. Desuden afslørede de forskellige undersøgelser tilsammen, at det relative bidrag af primærproduktion til TCO₂-tabet er mindre sammenlignet med bidrag fra udfældningen af kalciumkarbonat. Men det biologiske bidrag til det samlede TCO₂-tab er muligvis meget højere i områder med høj primærproduktion. Derfor er den evaluering af det biologiske bidrag til havis pumpen, som er beskrevet i denne afhandling, muligvis ikke repræsentativ for Arktis som helhed, siden optagelsen af CO₂ af biologisk aktivitet synes at være meget lavere i grønlandsk havis end i havis i andre regioner. Der er dog stadig behov for omfattende undersøgelser til yderligere at belyse lokale og regionale forskelle i biologisk aktivitet i havisen i Grønland og i andre arktiske regioner.

De undersøgelser, der præsenteres her, viste, at de højeste koncentrationer af kalciumkarbonat, der nogensinde er målt i naturlig havis, blev målt i cirka fem måneder gammel højarktisk, landfast havis, efterfulgt af høje koncentrationer i nydannet højarktisk polynya-havis, mens de laveste koncentrationer, vi observerede under vores undersøgelser, var i subarktisk, landfast havis. Variationer i havisens egenskaber, såsom temperatur, saltindhold, pH-niveau, isens tekstur, og ferskvandspåvirkning, kan sandsynligvis forklare nogle af de forskelle, der er fundet i kalciumkarbonatkoncentrationer forskellige steder.

Sammenfattende kan det siges, at de resultater, der præsenteres her, viste store variationer i kalciumkarbonatkoncentration og andre biogeokemiske parametre på forskellige tidsmæssige og rumlige skalaer, og det understreger betydningen af at lave undersøgelser gennem alle årstider, der dækker den meter-hundrede meter rumlige skala, hvis man skal kunne lave pålidelige CO₂-budgetter.

Denne ph.d.-afhandling viser også resultaterne fra en undersøgelse af påvirkningen af biologiske processer og gletsjerafsmeltningen på pCO₂-dynamikken i et subarktisk fjordsystem. Undersøgelsen viste, at det subarktiske Godthåbsfjord-system i Sydvestgrønland optager store mængder af CO₂, og at CO₂-optaget er stærkt reguleret af de biologiske processer og af opblanding af gletsjersmeltevand og kystnært vand. Derudover er CO₂-optaget stærkest tættest på afsmeltningen fra den grønlandske indlandsis. Hvis vores estimat er repræsentativt for lignende subarktiske fjordsystemer i Grønland, så spiller Grønlands kystnære områder en større rolle end forventet, og der bør tages højde for denne viden i fremtidige globale CO₂-budgetter.

Eqikkaaneq (abstract in Greenlandic)

Imartat sikusimasut nunarsuarmi silaannaap immallu CO₂-mik paarlaasseqatigiittarnerannut peqataanerat, ungasinngitsoq tikillugu, soqutaanngitsutut isigineqarsimagaluarpoq immap sikuata sumilluunniit kaanngaasarani ussissutut isigineqarsimanera pissutaanerulluni. Immalli siukuani CO₂-p ingerlatitsisuanik (pumpianik) taaneqartartup paasineqarneratigut immallu sikuani pinngorartitsilluartaartunik uumassusilinnik tappiorannartoqarfissuunerata ilisimalerneratigut, taamatut isiginninneq allanngorsimavoq. Taamaammat immap sikuata umassuseqarfiani carbon-ip nikerarnerata (naatsorsuutaalusoq) inissisimanera itinerusumik paasiniarneqartariaqarpoq. Taamaammat ilisimatusaatigalugu misissuinermit matumani pingaarnertut sammineqartoq tassaavoq: 1) Kalaallit Nunaata imaata sikuani kalkip (calcium carbonatip) aamma pinngoqqaatinik uumassusilinnillu peqassutsimut sunniutaasut pingaarutillit piffissami sumiiffimmilu nikerarnerat misissussallugit, 2) pissutsit tamakku akunnerminni imminnut sunneqatigiitarsinnaanerisa nalilersornissaat, aamma 3) pissutsit tamakku immap sikuani CO₂-p ingerlaartarneranut sunniutaasa misissornissaat.

Matumani calcium carbonatip allanngorarnerisa uuttortarneqartarnissaat eqqarsaatigaara, uumassuseqassutsip nikerarnera, seernartup akerliata basiskip annertussusia (TA), carbon uumassuseqanngitsumeersup annertussusia (TCO₂) Kalaallillu Nunaanni immap sikuani pinngoqqaatit uumassusillillu sunniisartut allat. Siullertut, Issittup issaasannerusortaata (subarktis-ip) imaata sikuani sunniisartut tamakku piffissap sumiiffillu nikerarnerini allanngorarneri tulliatullu Issittumi issinnerusup (højarktis-ip) ukiuunerani immap sikuani sunniisartut taakkua allanngorarnerisa nalaatornerusumik pissuseqarluni misissuiffigineqartarnissaat eqqarsaatigaara. Ataatsimut isigalugu, inernerit pissarsiaa takutippaat Issittup issittortaani issaasannerusortaani immap sikuani TCO₂-p (CO₂-p tamakkiisup) nungukkiartortarnera annermik immap tarajuusup seerinerasigut kalkillu (CaCO₃-llu) nakkaanerata/arrornerata aquunnerugaat taamaammallu avannarpasissup imartaani immap sikuata ingerlataanik carbon pumpeqarnera qularnaallilluni. Aammattaaq, misissuinerit assigiinngitsut ataatsimut takutippaat naasut (tappiorannartut) pinngorartitsinerisa (primærproduktionip) TCO₂-p nungukkiartorneranut sunneqataanerat calcium carbonatip nakkaaneranut sanilliullugu annikinnerusup. Taamaakkaluartoq, sumiiffinni tappiorannartunik quajaateqqanik uumasuaqqanillu pilersitsiortorfiulluartauni uumassusillit tamarmiullutik TCO₂-p nungukkiartorneranut sunniutigisartagaat annerungaatsiarsinnaasoq ilimanarpoq. Tamaattorli, suliami matumani

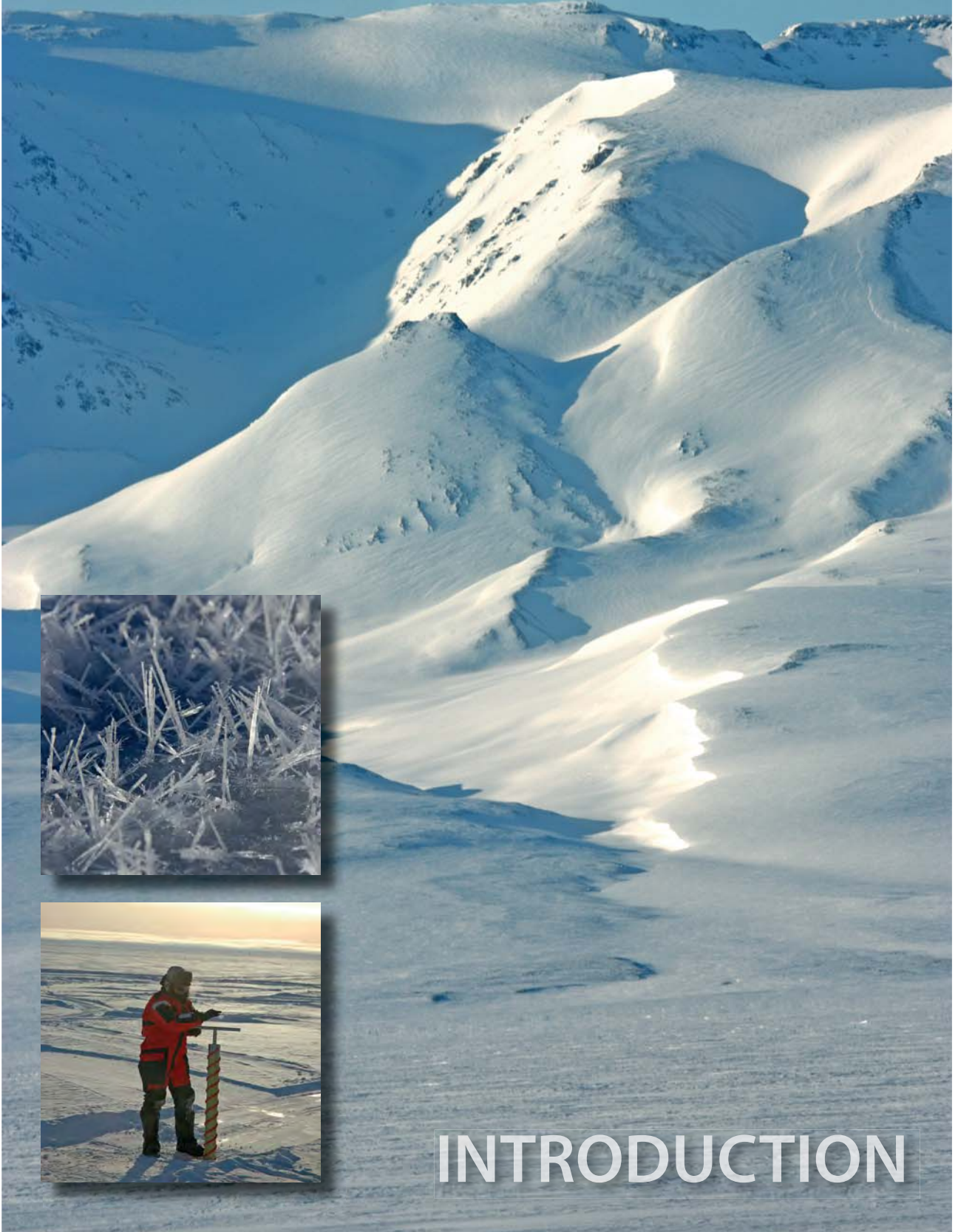
sammineqartup immap sikuata tigooraasuunerata nalilersorneqarnera Issittumut tamanut atuuttuunngeratarsinnaavoq, sumiiffinnut allanut naleqqiullugu Kalaallit Nunaata imaata sikuani CO₂-mik tigooraaneq sumiiffinnut allanut naleqqiullugu annikinneralaarsuusutut isikkoqarmat. Kalaallit Nunaata Issittumilu allani imaani pissutsit assigiinngisitaarnerannik paasinninneruniarluni misissuinerit amerlasuut sulii pisariaqartinneqarput.

Misissuinerit matumani takutinneqartut Issittumi issinnerpaap immap sikuani qaammatini tallimani aalaakkaasimasumi sikuup calcium carbonatinik akoqarnera uuttortarneqarsimasuni qullasinnerpaajusartoq, tulleralugit (højarktis) aakkarnersuit sikoqqammersimasuni uuttortakat annertuut, uuttortakkallu appasinnerpaatut inissisimasut Issittut issaasannersaani (subarktis) sikumi aalaakkaasumi uuttortarneqarsimallutik. Immap sikuani assigiinngitsut uuttortarneqartut nalingisa allanngorarneri soorlu, kissasusiata, tarajoqassusiata, pH-ata, sikuup qaavata ilusiata, imermik kuuffigineqarnera uumassuseqarneratalu sumiiffinni calcium carbonateqassusianut assigiinngisitsisarneranut pissutaasimasinnaalluarpur.

Tamatuma malitsigisaanik, misissuinerit assigiinngitsut calcium carbonateqassutsimik uumassusilinnillu pinngoqqaateqassutsimik takussutissiisinnasut allat piffissap sumiiffillu ingerlaviginerini assigiinngisitaangaatsiarnerat takutippaat, carbonimik naatsorsuutit tatiginassusillit suliarinaraanni ukioq kaajallallugu meterikkaani-hunnoruju meterikkaanik misissuinnissat pisariaqartussaassappur.

PhD-nngorniutigalugu allaaserisap matumap aamma takutippaat ukiuni arfinilinni Issittumi issaasannerusumi sinerissap qanittuani pCO₂-p allanngorarnerata immani uumassusillit pisoqartitsinerinit sermillu kuutsitsinerinit sunnerneqartarnerisa misissuiffigineqarnerat. Misissuinerup takutippaat Kalaallit Nunaata kujataata kitaaniittoq Nuup Kangerlua Issittumi issaasattumiittumi CO₂-mik tigooraangaatsiartuusutut naatsorsuunneqarsinnaasoq, CO₂-millu tigooqqaanerup uumassusillit pisoqartitsinerisa aammalu sermip erngata sinerissallu imaata akuleruttarnerisa aqutaringaatsiaraat. Aammattaaq, CO₂-mik tigooqqaaneq Sermersuup kuuffiata qaninnerpaasaani annerpaajusoq. Peqatigitillugulu Kalaallit Nunaanni Issittumi issaasattumi kangerlunnut assingusunut uuttuutaasinnaappat, taava Kalaallit Nunaata sineriaata qanittui ilimagisamiit CO₂-mik tigooraasuunerupput paasisarlu tamanna siunissami nunarsuarmut tamarmut carbonimut naatsorsuusiordermi ilaattinneqartariaqarluni.

CHAPTER 1



INTRODUCTION

1.1 Setting the scene

The main driver of climate warming is the accumulation of greenhouse gases such as CO₂ and CH₄, where CO₂ is the most important in terms of radiative forcing (Ramaswamy et al. 2001). Over the last 150 years, the atmospheric concentration of CO₂ has increased by 43 % from a preindustrial value of about 280 ppm to 399 ppm in July 2014 primarily due to anthropogenic activities. Approximately 30 % of anthropogenic CO₂ emissions have been absorbed by the oceans (Sabine et al. 2004). Thus, the global oceans play a crucial role in buffering the effects of anthropogenic CO₂ emissions through physical, chemical and biological processes (Takahashi et al. 2009 and references therein). Consequently, to understand the global carbon cycle, it is very important to understand the CO₂ sinks and sources in all areas of the world's oceans. The precipitation of calcium carbonate in natural sea ice has been predicted for more than 50 years (Assur 1958), but it was not until 1981 that the connection between precipitation of calcium carbonate and the "sea ice CO₂ pump" was suggested by Jones and Coote (1981). They wrote:

"In the winter season as sea ice forms and calcium carbonate precipitates from the brine in the sea ice, carbonate ions are removed causing the following reaction to occur within the brine. $\text{Ca}^{2+} + 2\text{HCO}_3^- + 6\text{H}_2\text{O} = \text{H}_2\text{O} + (\text{CO}_2)_{\text{aq}} + \text{CaCO}_3 \cdot 6\text{H}_2\text{O}$ (1). [...] The processes involving sea ice formation and subsequent melting represent a CO₂ pump: in summer, CO₂ is transferred from the atmosphere into the ocean, and in winter it is transferred from the surface of the ocean to deeper regions. The key to the operation of this CO₂ pump is the separation of the products of (1) that occurs during the formation of sea ice. [...] It is difficult to be precise regarding how much calcium carbonate would be present in naturally formed sea ice because of the complicated and varied processes that occur during ice formation and aging [...] about 1 % of the total carbon dioxide entering the ocean enters through the formation of sea ice."

What have we learned since then?

Until recently, the contribution of sea-ice-covered regions to the overall oceanic-atmospheric CO₂ exchange was assumed to be insignificant mainly because sea ice was considered impermeable (e.g., Gibson and Trull 1999, Tison et al. 2002). Recent studies, however, demonstrate that the sea ice-driven CO₂ pump does exist in natural sea ice (e.g., Rysgaard et al. 2007; 2009; 2012, Dieckmann et al. 2008) and that this pump is very effective and may be equivalent to 17 – 42 % of the annual air-sea CO₂ flux in open ocean waters

at high latitudes (> 62° N and > 50° S; Rysgaard et al. 2011, Loose et al. 2011a). In addition, high latitude shelf areas and fjord systems are also suggested to be strong sinks of CO₂, responsible for a high uptake of the total ocean uptake (Bates and Mathis 2009). Therefore, sea ice and high latitude shelf areas and fjord systems should be considered an essential part of the global carbon cycle.

However, little is known about the seasonal dynamics of inorganic carbon in these high latitude waters and important questions remain unanswered about the significance of biotic and abiotic processes in these waters. Furthermore, knowledge of the spatial and temporal occurrence of calcium carbonate and other biogeochemical parameters in sea ice are still not well described.

Based on this lack of knowledge I formulated the following objectives for my PhD study:

- Expand the knowledge of the spatial and temporal events controlling the inorganic carbon dynamics in sea ice by measuring the vertical distribution of calcium carbonate as well as total inorganic carbon (TCO₂), total alkalinity (TA), inorganic nutrients, dissolved organic carbon (DOC), dissolved organic nitrogen (DON), bulk salinity, temperature and primary and bacterial productivity (**Papers I – IV**).
- Assess the significance of calcium carbonate precipitation in different types of sea ice, i.e., warm Subarctic sea ice, cold High Arctic sea ice, sea ice near the Greenland Ice Sheet, frost flowers and brine skim and its possible role as sink or source for atmospheric CO₂ (**Papers I – III**).
- Examine the factors controlling the sea ice algal and bacterial growth by measuring: the effects of salinity, pH and inorganic carbon availability on three sea ice algal species (Paper V) and the simultaneous incorporation of thymidine (tdR) and leucine (leu), bacterial abundance, cell properties and activity for sea ice bacterial communities in Subarctic sea ice in SW Greenland (**Paper VI**).
- Investigate the influence of biotic and abiotic parameters for the air-sea CO₂ flux by measuring pelagic primary productivity, salinity, nutrients, vertical export, TCO₂ and TA in a Subarctic fjord in SW Greenland (**Paper VII**).

In order to provide an overview of the seasonal inorganic carbon dynamics in high latitude oceans and to put the main findings of my PhD work as presented in Papers I – VII into a broader context, I derived figure 1. This figure enlarges the perspective of the work done by me and other scientists and presents a compilation of the current knowledge of the seasonal events controlling the dynamics of inorganic carbon in high latitude oceans with a special emphasis on Greenland coastal systems.

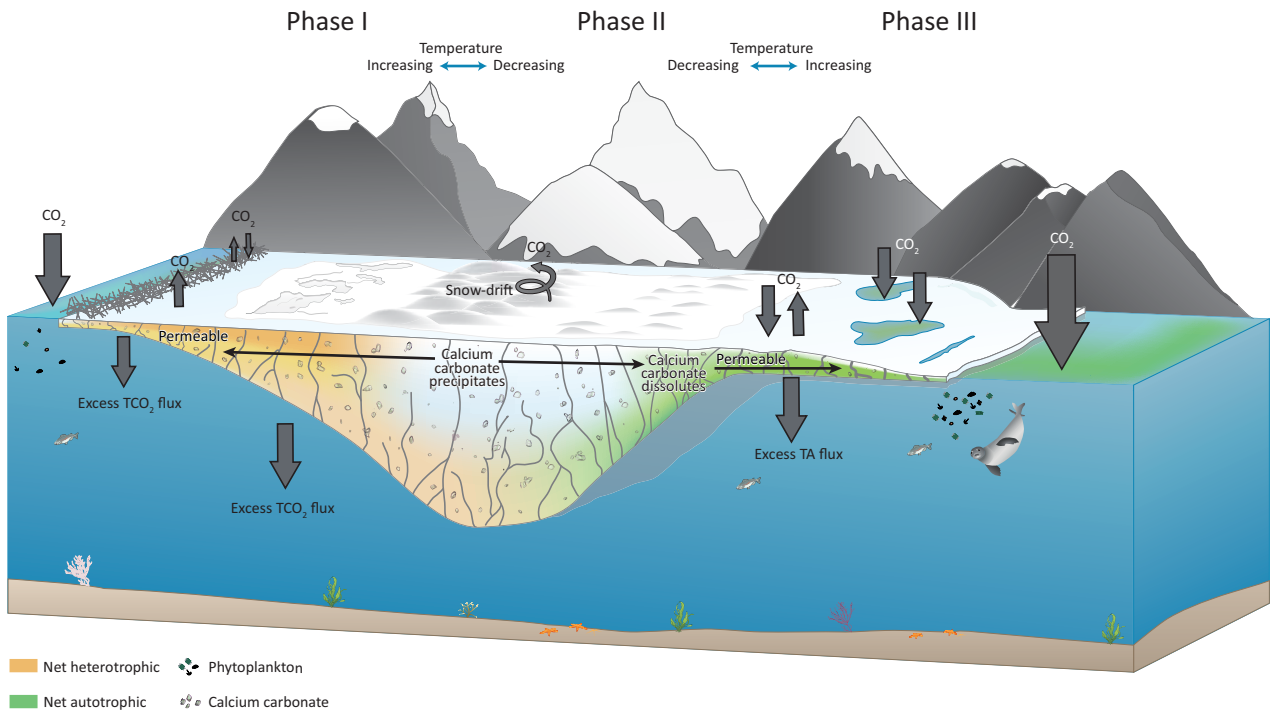
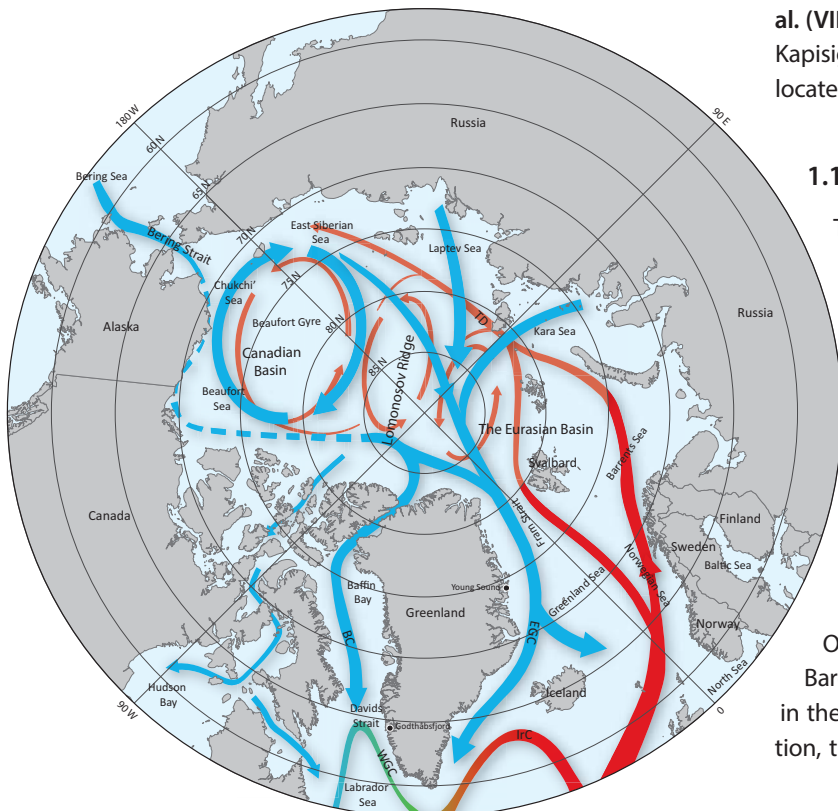


Figure 1. Conceptual model of the seasonal events controlling the dynamics of inorganic carbon (grey arrows) in ice-covered seas during all phases (I, II and III) of the sea ice formation and decay cycle. Modified after Miller et al. (2011) and Rysgaard et al. (2011).

Figure 2. A schematic diagram showing the Arctic Ocean circulation as well as the different locations in or near the Arctic Ocean. The more salty surface waters from the Atlantic penetrate the Arctic Ocean (red arrows). As it get colder it sink beneath (now pink) the cold, less salty waters in the Arctic Ocean (blue arrows). The Transpolar drift (TD), the East Greenland Current (EGC), the West Greenland Current (WGC), the Irminger Current (IRC) and the Baffin Current (BC). Modified from <http://www.divediscover.whoi.edu>.

Prior to discussing the interaction between the newly formed sea ice, frost flowers, and brine skim and the atmosphere and the underlying sea water (Fig. 1; phase I), a general description is provided of the ocean settings in the areas on which the studies in this thesis were conducted, i.e., the High Arctic Tyroler fjord – Young Sound area in NE Greenland (Fig. 2; Rysgaard et al. (II), Barber et al. (III)) and the Subarctic Godthåbsfjord system in SW Greenland (Fig. 2; Rysgaard et al. (VII)) – where also Malene Bight (Søgaard et al. (IV)) and Kapisigdlit Bight (Søgaard et al. (I), Kaartokallio et al. (VI)) is located (Fig. 2).



1.1.1 General oceanography of the study areas

The general circulation of the Arctic Ocean consists of a circular wind-driven current over the Canada Basin, referred to as the Beaufort Gyre, a flow of cold and less saline polar surface waters that leak out from the Arctic Ocean through several gateways, i.e., the Fram Strait and the Canadian Arctic Archipelago, and a flow of warm saline Atlantic surface waters from the south that penetrates the Arctic Basin and sinks beneath the polar waters (Fig. 2; Jakobsson et al. 2004). The distribution of cold and warm water masses in the Arctic Ocean has a great influence of the sea ice production and distribution in the Arctic Ocean as the heat supply from the Atlantic waters in the Barents Sea results in an ice edge much further north than in the waters adjacent to Greenland (Weeks 2010). In addition, the oceanographic characteristics described above af-

fects the water mass properties and contribute to differences in the marine systems as well as in sea ice production and distribution in Greenland coastal areas and fjords.

With respect to the Young Sound Area in NE Greenland (Fig. 2; **Rysgaard et al. (II)**, **Barber et al. (III)**), the East Greenland Current (i.e., a continuation of the Transpolar Current) has an important influence on the water mass properties in this area – especially due to the large amounts of sea ice it carries along with it. Another oceanographic feature in this area is the large seasonal input of freshwater from the Greenland Ice Sheet, terrestrial runoff and melt water from both sea ice and calved glacial ice (Rysgaard and Glud 2007). Furthermore, the area outside Young Sound is a polynya site, where new sea ice is produced and frequently blown away, thereby allowing new ice to form again and again (Pedersen et al. 2010). The marine system in the Godthåbsfjord area in SW Greenland (Fig. 2; **Søgaard et al. (I)**, **Søgaard et al. (IV)**, **Kaartokallio et al. (VI)**, **Rysgaard et al. (VII)**) is affected by three principal water masses, atmospheric heat exchange and melt/freeze processes (Mortensen et al. 2011, 2013). Two of the three principal water masses are found outside the fjord – sub-polar

mode water and coastal water; whereas the third, freshwater, comes from meltwater runoff from the Greenland Ice Sheet, terrestrial runoff, meltwater from sea ice and calved glacial ice (Mortensen et al. 2011, 2013). The freshwater input in this area from the Greenland Ice Sheet induces a seasonal stratification of the upper part of the water column and is a source of large amounts of bioavailable nutrient (Arendt 2011, Calbet 2011, Lydersen et al. 2014).

1.2 Phase I: Transition from open water to ice-covered oceans

In this section, the mechanisms behind sea ice formation, phase I, are described as well as the microorganisms in newly formed sea ice and their contribution to the CO₂ dynamics in this phase (sections 1.2.1 and 1.2.2). In addition, the mechanisms behind brine skim and frost flower formation are briefly described (1.2.3). The processes driving CO₂ exchange in the transition period from open water to ice-covered seas are discussed and whether phase I acts as net sink or source of CO₂ to the atmosphere.

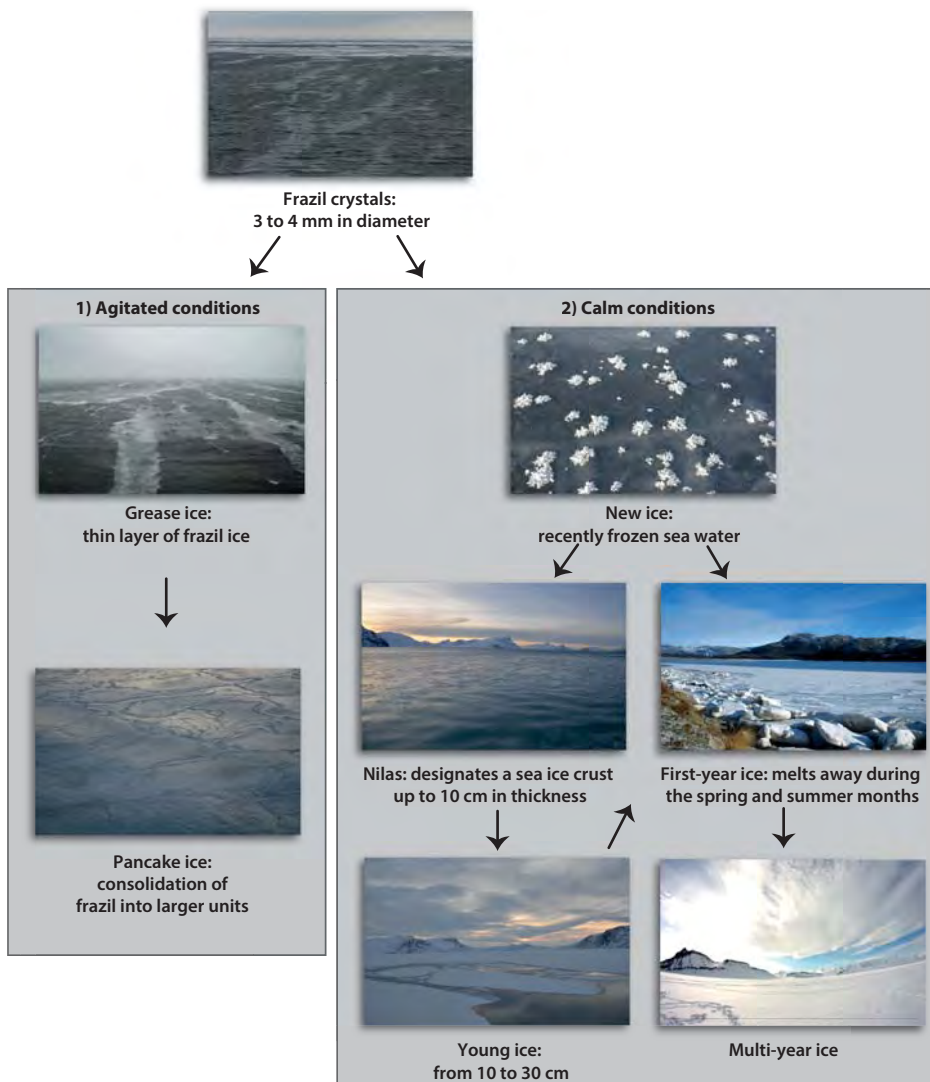


Figure 3. Sea ice development stages 1) agitated conditions with ice growth in wave-field and 2) calm conditions with ice growth through quiescent bottom freezing.

1.2.1 Sea ice formation – abiotic processes

In autumn and winter, when the ocean surface layer is cooled down to temperatures close to -1.86°C (freezing point of seawater with a salinity of 34), ice crystals start to grow on the surface (Weeks 2010) and form a soupy suspension known as frazil ice crystals (i.e., 3 to 4 mm in diameter; Fig. 3).

Under calm conditions, the ice crystals freeze together to form a sheet of new ice called Nilas, which designates a sea ice crust up to 10 cm in thickness with randomly-oriented ice crystals (i.e., granular ice texture; Timco and Weeks 2010; Fig. 3 and Fig. 4). It is at this point that frost flowers are sometimes formed from the brine skim on the ice surface (described in more detail in section 1.2.4). As the sheet ice thickens through congelation at the ice-water interface, the transitional granular/columnar ice layer forms (Eicken and Lange 1989). This layer is a few centimetres thick transition zone that is mainly characterised by elongated grains (Fig. 4).

Below the transitional granular/columnar layer, the sea ice consists of columnar ice, characterised by vertically-elongated ice crystals (Fig. 4 and Fig. 5). The sea ice is classified as young ice when the ice sheet becomes thicker than 10 cm and first-year sea ice when the ice sheet becomes thicker than 30 cm (Fig. 3; Weeks 2010). If the first-year ice survives at least one melting season (i.e., one summer), it is called multi-year ice (Fig. 3).

Under more agitated conditions with ice growth in wave-fields, frazil crystals consolidate into grease. The grease ice layer consolidates into ice discs known as pancakes (Fig. 3). As they grow from a few centimetres to a few meters across, they solidify and thicken mechanically by rafting on top of each other. Pancakes freeze together to form cakes and floes, which contain a large amount of ice with a granular texture (Fig. 4). With ongoing freezing, the pancakes adhere into a continuous ice sheet by bottom freezing at the ice-water interface.

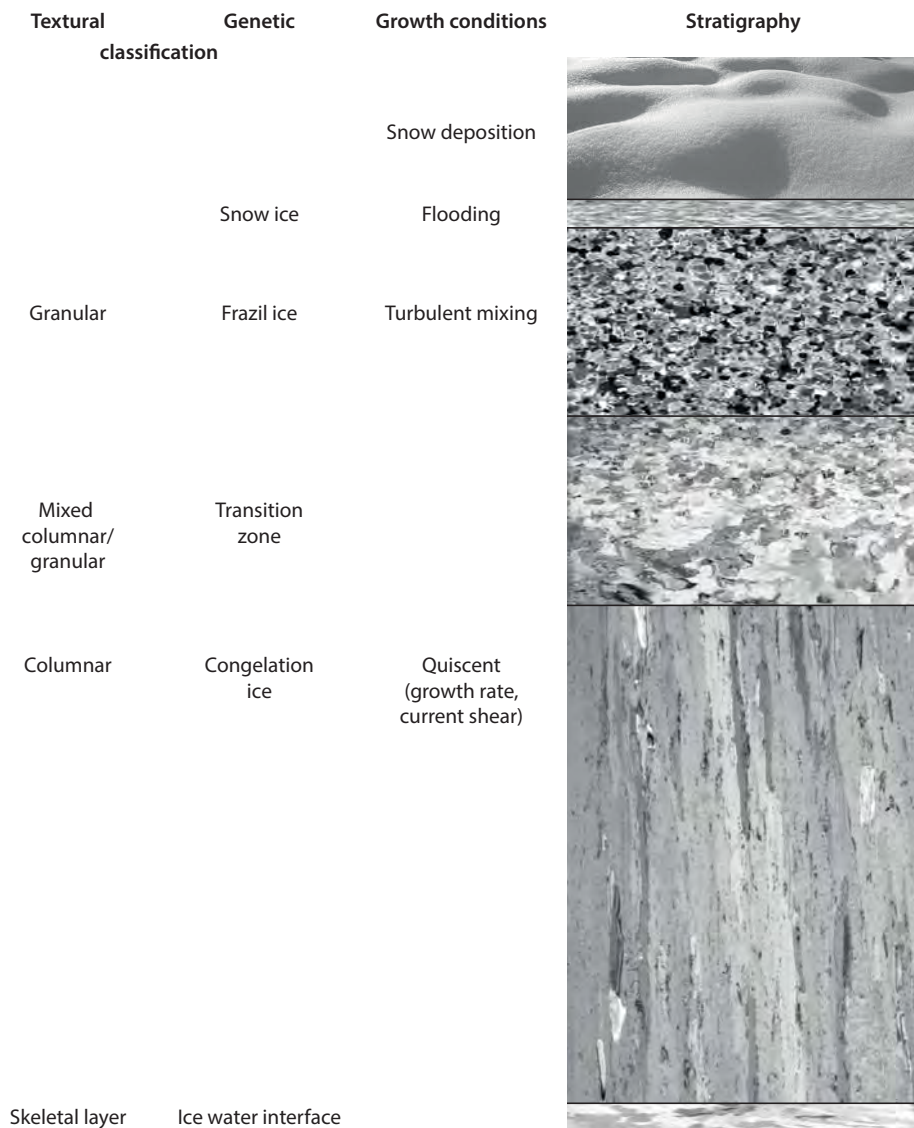


Figure 4. Schematic summarizing the main ice texture and growth conditions for first-year sea ice. The figure is adapted from Eicken (2003). The horizontal thin-section photographs is of first-year sea ice from Young Sound in NE Greenland for detailed description see Rysgaard et al. (II) (photo courtesy of M. Pucko).

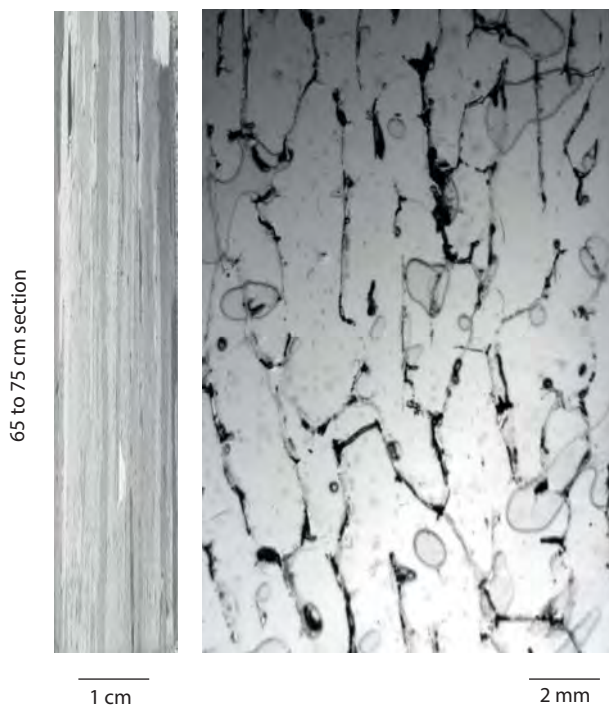


Figure 5. Thin section of first year sea ice showing ice platelets and the brine pockets along the grain boundaries. For detailed description see **Rysgaard et al. (II)** (Photo courtesy of M. Pucko).

The frazil – congelation sea ice growth process described above is the process that occurs most frequently, but other sea ice types exists, e.g., snow ice and superimposed ice. Snow ice is formed through sea water flooding due to negative freeboard and thick snow cover (Fristsen et al. 1998), and it is quite porous (Eicken 2003, **Rysgaard et al. (II)**, **Søgaard et al. (IV)**). Superimposed ice occurs during spring and summer when the snow melts internally and melt water refreezes either in the snow or at the snow-ice interface, when the temperature gradients within snow and ice are negative (Hass et al. 2001, Nicolaus et al. 2009).

As soon as sea water solidifies, some of the salts and gases present in the seawater are rejected, whereas the rest are trapped within the brine pockets, channels and tubes (Fig. 5; Weeks and Ackley 1982, Petrich and Eicken 2010). A reduction in sea ice temperature decreases the brine volume and, concurrently, increases the brine salinity and brine $p\text{CO}_2$ through a decrease in brine CO_2 solubility (Cox and Weeks 1983, Papadimitriou et al. 2004). Thus, at this point, the $p\text{CO}_2$ in the sea ice brine is higher than that in the air above the sea ice; and, therefore, the sea ice brine has the potential to release CO_2 to the atmosphere. However, when the sea ice temperature reaches -5°C , the brine volume decreases; a brine volume of 5% is generally considered the threshold at which the sea ice matrix becomes impermeable, thus preventing air-sea ice gas exchange (Golden et al. 1998, Zhou et al. 2013). This percolation threshold varies with changes in the ice crystal structures – e.g., granular ice shows a higher percolation threshold than columnar ice

(Fig. 4; Weeks 2010). In addition, as temperature decreases and solute concentration increases, calcium carbonate precipitates (Marion et al. 2001). On the basis of thermodynamic equilibrium calculation, calcium carbonate precipitation was predicted to occur during natural sea ice formation (Assur 1958), which was later confirmed first in freezing sea water by Richardson (1976), then in artificial sea ice (Tison et al. 2002) and, finally, in Antarctic and Arctic sea ice as ikaite (Dieckmann et al. 2008; 2010, Rysgaard et al. 2011; 2012, Fischer et al. 2013, Geilfus et al. 2013a, Nomura et al. 2013b, **Rysgaard (II)**). At present, it is still not clear whether ikaite is the only calcium carbonate phase formed in sea ice (Dieckmann et al. 2010).

The calcium carbonate formation increases the amount of CO_2 in the brine beyond that attributed solely to the solubility effect. The calcium carbonate crystals are trapped within the interstices between the ice crystals (**Rysgaard (II)**), whereas the CO_2 released through calcium carbonate production within the brine can be lost from the sea ice. Therefore, as sea ice grows, brine drainage leads to an export of gases from the sea ice, leaving sea ice depleted in CO_2 compared to ambient seawater (Rysgaard et al. 2007, Crabeck et al. 2014, **Søgaard et al. (I)**). Brine drainage from sea ice causes the formation of highly saline dense cold

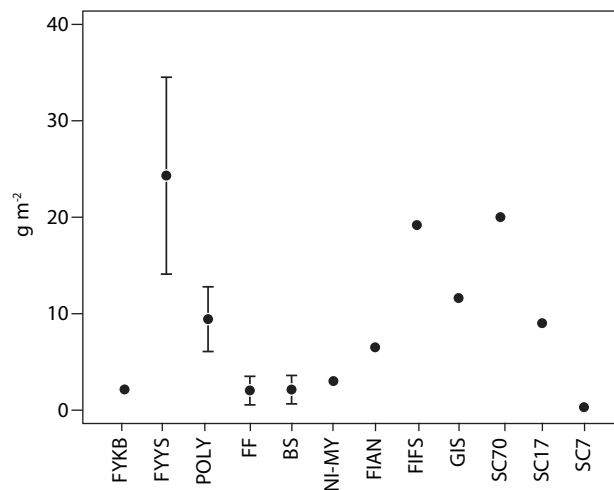


Figure 6. Calcium carbonate concentration in different ice types in the Arctic and Antarctic: FYKB= First-year sea ice in Kapisigdlit Bight, SW Greenland (**Søgaard et al. (I)**), FYYS=First-year sea ice in Young Sound, NE Greenland and POLY=newly formed polynya ice in Young Sound, NE Greenland (**Rysgaard et al. (II)**), FF= frost flowers and BS=brine skim in Young Sound, NE Greenland (**Barber et al. (III)**), NI-MY=Nilas to multi-year ice in the Antarctic from Dieckmann et al. (2008), FIAN=Fast ice in Antarctic from Fischer et al. (2013), FIFS=Fast ice in Fram Strait from Rysgaard et al. (2012), GIS=Sea ice near the Greenland Ice Sheet (**unpublished data D.H. Søgaard**), SC70=70 cm thick snow cover and SC17=17 cm thick snow cover in Young Sound, NE Greenland (**unpublished data D.H. Søgaard**) and SC7=7 cm thick snow cover in Kapisigdlit Bight, SW Greenland (**Søgaard et al. (I)**).

Table 1. Sea ice bulk conditions of TCO₂, TA and salinity during different field campaigns.

Area and Site	Date	Type	TCO ₂ (μmol kg ⁻¹)	TA (μmol kg ⁻¹)	TA:TCO ₂	Bulk salinity	Reference
Greenland							
Kapisigdlit Bight	17 February 2010	Newly formed sea ice	281	359	1.28	4.6	Søgaard et al. (I)
Kapisigdlit Bight	11 to 15 March 2010	Winter sea ice	233	280	1.20	5.6	Søgaard et al. (I)
Kapisigdlit Bight	8 April to 1 May 2010	Spring/summer sea ice	282	356	1.26	2.8	Søgaard et al. (I)
Young Sound	17 March 2012	Winter sea ice	406	516	1.27	6.5	Rysgaard et al. (II)
Young Sound	20 March 2012	Newly formed polynya sea ice	502	605	1.21	7.8	Rysgaard et al. (II)
Greenland/Svalbard							
Fram Strait	25 to 29 June 2010	Spring/summer sea ice	221	420	1.90	3.9	Rysgaard et al. (2012)

water that sinks to deeper layers and contributes to the global ocean circulation. Furthermore, observations in the Arctic suggest that TCO₂ can be transported below the pycnocline and, subsequently, be incorporated into intermediate and deep-water masses (Rysgaard et al. 2007; Rysgaard et al. 2011).

Knowledge on precipitation of calcium carbonate in newly formed sea ice and its effect on inorganic carbon dynamics are still not well described. This issue is addressed in two of our papers (Søgaard et al. (I), Rysgaard et al. (II)), where we report measurements of calcium carbonate concentration of 1 g m⁻² in a 2 weeks old Subarctic sea ice in Kapisigdlit Bight in SW Greenland (Fig. 2 and Fig. 6) and 10 g m⁻² in a less than one-week-old High Arctic sea ice in Young Sound, NE Greenland (Fig. 2 and Fig. 6). The amount of calcium carbonate in the newly formed High Arctic sea ice (Rysgaard et al. (II)) was 2 to 5 times higher than those measured in other sea ice types in both Arctic and Antarctic waters and also 10 times higher than concentrations measured in newly formed Subarctic sea ice in Kapisigdlit Bight in SW Greenland (Fig. 2 and Fig. 6; Søgaard et al. (I)). However, the calcium carbonate concentration in the newly formed High Arctic sea ice was lower than concentrations observed in first-year sea ice and in 70 cm-thick snow cover at the same sampling location in NE Greenland (Fig. 2 and Fig. 6; Rysgaard et al. (II)) as well as in land-fast ice in Fram Strait (Fig. 6.; Rysgaard et al. 2012). These results indicate very dynamic conditions of calcium carbonate formation even on short timescales but also indicate considerable spatial distribution of calcium carbonate (Søgaard et al. (I)).

The potential influence of melting the entire newly formed ice cover in Kapisigdlit Bight in SW Greenland (Fig. 2; Søgaard et al. (I)) and Young Sound in NE Greenland (Fig. 2; Rysgaard et al. (II)) into a 20 m thick mixed layer (typical for summer conditions in these location) on the CO₂ flux can be determined using the measured ice carbon chemistry (Table 1) and the initial mixed layer characteristics (Table 2) from the two different regions. Assuming that melt occurs over one month, the resultant air-sea CO₂ flux to return to pre-melt conditions would be - 3.4 mmol C m⁻² d⁻¹ in Kapisigdlit Bight in SW Greenland (Fig. 2) and - 2.3 mmol C m⁻² d⁻¹ in Young Sound in NE Greenland (Fig. 2). The potential air-sea CO₂ flux vary by a factor of 0.7 with the highest potential air-sea CO₂ flux estimated in Subarctic sea ice (Søgaard et al. (I), Rysgaard et al. (II)). The reason for this difference is unclear but indicates that the age of the sea ice plays an important role for this potential flux. In addition, this finding suggests that TA and TCO₂ feature high variability between ice locations and clearly emphasizes the importance of studies covering the spatial variability in these parameters in order to make reliable carbon budgets.

In these calculations, we assume that sea ice formation occurs only once. However, in polynya areas, sea ice with low bulk concentrations of CO₂ and high alkalinities is produced (Rysgaard et al. (II)) and frequently blown away from the area, which thereby allows new ice to form again and again. The function of a polynya and the influence on CO₂ exchange are not well understood, but the production of new sea ice in these areas may contribute to a significant CO₂ release to the atmosphere, which is balanced by the dissolution of calcium

Table 2. Surface water conditions below sea ice of TCO₂, TA and salinity during different field campaigns.

Area and Site	Date	TCO ₂ (μmol kg ⁻¹)	TA (μmol kg ⁻¹)	TA:TCO ₂	Bulk salinity	Reference
Greenland						
Kapisigdlit Bight	17 February 2010	2110	2180	1.03	33	Søgaard et al. (I)
Kapisigdlit Bight	11 to 15 March 2010	2095	2230	1.06	32.7	Søgaard et al. (I)
Kapisigdlit Bight	8 April to 1 May 2010	2015	2138	1.06	32.7	Søgaard et al. (I)
Young Sound	17 March 2012	2101	2276	1.08	31.7	Rysgaard et al. (II)
Young Sound	20 March 2012	2070	2205	1.07	31.7	Rysgaard et al. (II)
Greenland/Svalbard						
Fram Strait	25 to 29 June 2010	1987	2203	1.11	32.6	Rysgaard et al. (2012)

carbonate when the sea ice melts. On the other hand, it is possible that polynya areas act as a downward vertical transport mechanism to remove CO₂ rejected from sea ice away from the surface layer and, therefore, ensure a net CO₂ flux into the ocean over the entire year (Rysgaard et al. 2011). Our findings of high calcium carbonate concentrations in newly formed polynya ice suggest that polynya formation increases the potential for seawater uptake of CO₂ (Rysgaard et al. (II)).

Another scenario is that the formation of calcium carbonate and the concentration of solutes in newly formed polynya sea ice lead to CO₂ de-gassing. If all CO₂ produced during the precipitation of calcium carbonate (1) were released to the atmosphere, then the consumption of CO₂ during dissolution of the calcium carbonate mineral in the melting phase would balance the efflux during precipitation (Rysgaard et al. 2011; 2012). Thus, calcium carbonate would not contribute to the polar carbon cycle. However, as soon as an excess of CO₂ is rejected together with brine to the underlying water column and transported away from the sea ice formation region, then the mineral may potentially have an important role in the polar carbon cycle as proposed by Rysgaard et al. (2007; 2011 and 2012). However, it is still critical that the surface sea water layer is exposed for a sufficient time so that the mixed layer has time to equilibrate with the atmosphere, which may not be the case in High Arctic areas with short open water periods (Fransson et al. 2009).

In the newly formed sea ice in Young Sound in NE Greenland, we observed high concentrations of calcium carbonate, and at this early stage, the sea ice was still permeable with a brine volume over 5% (Søgaard et al. (I), Rysgaard et al. (II)). As mentioned earlier, precipitation of calcium carbonate increases the amount of CO₂ in the brine beyond that attributed solely to the solubility (1). As a consequence, CO₂ may diffuse to the atmosphere (Fig. 1; Papadimitriou et al 2004, Nomura et al. 2006; 2010a; 2010b, Loose et al. 2011a, Rysgaard et al. 2011). Since high ice permeability is usually encountered in newly formed sea ice, we would expect some ice-atmosphere fluxes during sea ice formation. Indeed, we measured a CO₂ efflux of $3.67 \pm 1.99 \text{ mmol m}^{-2} \text{ d}^{-1}$ above newly formed sea ice in Young Sound in NE Greenland (Fig. 2), using chamber flux measurements (Barber et al. (III)), which is consistent with laboratory experiments by Nomura et al. (2006; 2010) and to findings by Geilfus et al. (2013), who estimated a CO₂ release from young growing sea ice of 4.2 – 9.9 mmol m⁻² d⁻¹. This suggested a release of CO₂ from newly formed sea ice. However, recent studies have shown that the largest flux of TCO₂ and CO₂ is driven by brine drainage to the underlying water column and subsequently incorporation into deep-water masses (Rysgaard et al. 2007, Sejr et al. 2011).

1.2.2 Microorganisms in newly formed sea ice

Microorganisms in sea ice have been reported for more than 160 years (Horner 1985 and references herein); but, to our best knowledge, the biological processes during the initial stages of sea ice formation have not been well described. The initial stages of sea ice formation generally begin when there are still substantial microbial populations left in the water column (described in section 1.4.3). As a result, particles such as viruses, bacteria and heterotrophic (e.g., flagellates and ciliates) and autotrophic (e.g., diatoms) protists are often scavenged from the water column as the newly formed frazil ice rise to the surface (Fig. 3; Garrison et al. 1990, Reimnitz et al. 1992, Grossmann and Gleitz 1993, Gradinger and Ikävalko 1998, Kaartokallio et al. 2006). It is also possible that floating ice algal aggregates can be refrozen into the sea ice during autumn and, therefore, act as a seeding stock (Assmy et al. 2013 and reference herein).

Organisms larger than 10 µm are selectively scavenged from the water column into the sea ice and can accumulate at concentrations higher than that in the underlying sea water (Gradinger and Ikävalko 1998, Riedel et al. 2007, Mikkelsen et al. 2008, Rózanska et al. 2008). Bacteria seem to become entrained in the sea ice along with micro-algae (e.g., Riedel et al. 2007). The bacterial cells may attach to the outer surface of the algae (e.g., epiphytic attachment), or to particles in the water column, which can subsequently transport them into the sea ice. The sea ice bacterial community closely resembles the sea water bacterial community in oligotrophic systems; thus, selection processes during sea ice formation seem to play a minor role (Collins et al. 2010). By contrast, in more productive regions, selection processes due to viral lysis of the heterotrophic bacterial community is possible (Collins et al. 2011).

Once incorporated into the sea ice, the microorganisms are challenged with changes in space, light availability, salinity, nutrients, TCO₂ and O₂ concentrations, temperature and pH (Gradinger and Ikävalko 1998, Søgaard et al. (I), Søgaard et al. (IV – V), Kaartokallio et al. (VI)). These micro-environmental differences can lead to dramatic differences in the composition and magnitude of the microbial community living there. Sea ice environments are dominated by psychrotolerant and/or psychrophilic organisms (Cameotra and Makkar 1998), and adaptation to low temperatures in all cellular components is of great importance for algae and bacteria living in cold environments.

For some sea ice algae and protozoans, one reproductive strategy is the formation of robust stress resistant cysts, which can lie dormant until suitable conditions for growth are present. Sea ice algae that are stressed by extreme ice salinities are likely to exhibit increased halo tolerance and some studies show that sea ice diatoms remain physiologically active at salinities above 100 (Stoecker et al. 1997). A recent study

showed that diatoms are the most successful colonisers of newly formed sea ice (Gradinger and Ikävalko 1998). In addition, we have shown that diatoms are less affected by increasing salinities, which might explain the high abundance of diatoms in sea ice (Søgaard et al. (V)). The differences in tolerance between sea ice algal species have been ascribed to various abilities for osmotic acclimations, e.g., production of osmolytes (such as dimethylsulphoniopropionate; DMSP), which balances the ionic pressure during changes in salinity (Gleitz and Thomas 1992, Arrigo et al. 2010). In addition to high salinities, sea ice algae must also adapt to the low light conditions in the sea ice, where facultative heterotrophy is an important survival strategy (Horner and Alexander 1972). Sea ice algae are known to be adapted to low ambient light levels and are able to grow beneath several meters of ice and snow only receiving < 1 % of the solar irradiance (Horner & Schrader 1982, Gosselin et al. 1990, Gradinger and Ikävalko 1998, Mock and Gradinger 1999, Lazzara et al. 2007).

Cold adaptation by sea ice bacteria include maintaining membrane fluidity (Gounot & Russell 1999), modification of amino acid composition of the proteome (Deming 2010), i.e., conferring flexibility to proteins for their enzymatic functions, and storage of intercellular reserves in the form of large polymers or polyhydroxyalkanoates (PHA; Deming 2010, Kaartokallio et al. (VI)). Sea ice bacteria also release antifreeze proteins, cold-active enzymes and exopolymeric substances (EPS; Feller and Gerday 2003, Marx et al. 2009, Deming 2010). In addition to low temperatures, the sea ice bacteria also need to adapt to extremely high salinities and to protect themselves against osmotic shock. These adaptation processes include the production or accumulation of intracellular, compatible solutes (typically sugars and amino acids), changes in membrane fatty acid composition and by the production of salt-tolerant enzymes (Thomas and Dieckmann 2002, Bowman 2008).

High concentrations of EPS have been measured in Arctic sea ice throughout the sea ice season, and EPS is released both by bacteria and algae in sea ice. The role of EPS in sea ice is to protect the algal and bacterial cells against the harsh environmental conditions, assist in cell locomotion, serve as a carbon-rich substrate, provide a defence against grazing and create a microhabitat in which bacterial attachment is favoured thereby increasing bacteria-mediated processes (Deming 2010).

The productivity of the microorganisms inhabiting sea ice during the first stages of ice formation and development is not well described. However, in Søgaard et al. (I) and Søgaard et al. (IV), we showed that the ice-associated biological community in newly formed sea ice was net heterotrophic with a bacterial carbon demand of 0.50 mg C m⁻² d⁻¹ in Kapisigdlit Bight in SW Greenland (Fig. 2) and 0.20 mg C m⁻² d⁻¹ in Malene Bight in SW Greenland (Fig. 2). An obvious

question is whether the biological processes affect the TCO₂ concentration within the sea ice in this phase. The relative effects of the biological activity and precipitation of calcium carbonate on the air-sea exchange of CO₂ can be estimated. At both locations in the newly formed ice (i.e., Kapisigdlit Bight and Malene Bight; Fig. 2) the ice-associated biological communities were net heterotrophic with a CO₂ production rate of 4.10 to 2.10 mg m⁻² which were very low compared to the integrated calcium carbonate concentration of 1,000 mg m⁻² (Søgaard et al. (I)). In our studies the highest bacterial production was observed at the base of the newly formed sea ice (Søgaard et al. (I), Søgaard et al. (IV)). Consequently, this indicates that although the relative contribution of the biological processes to the carbon dynamics is low, it is still possible that the observed CO₂ efflux above newly formed sea ice in some areas (see description in section 1.2.1) is driven, in part, by the respiration of the heterotrophic community at the base of the sea ice.

1.2.3 Frost flowers and brine skim formation – abiotic processes

During the initial hours of sea ice formation, a highly saline layer of brine skim is often observed on the surface of the new and young ice (Drinkwater and Crocker 1988, Perovich and Richter-Menge 1994, Isleifson et al. 2014). The skim layer is typically 1 – 2 mm thick and is highly saline, yielding salinities in the order of 30 to 120 (Douglas et al. 2012, Geilfus et al. 2013a, Barber et al. (III)). It is suggested that this skim layer is formed by brine transport as the brine channels constrict during sea ice growth (Martin et al. 1995).

In calm wind conditions (< 5 m s⁻¹), frost flowers may form on top of the newly formed ice and brine skim as distinct nodules and, then, expand from their nucleation sites radially outwards in all directions (Style and Worster 2009, Barber et al. (III)). In the literature, there is still an ongoing debate whether frost flowers form due to sublimation or evaporation from the sea ice surface rather than from deposition from the atmosphere (Domine et al. 2005). In the meantime, our measurements show that the initial δ¹⁸O values in the frost flowers are close to 0 ‰, which is similar to the signature of the surface slush layer (Barber et al. (III)), suggesting that newly formed frost flowers are composed primarily of brine. This is also supported by previous work showing that brine can be wicked into frost flowers from brine skim (Perovich and Richter-Menge 1994, Martin et al. 1995, Roscoe et al. 2011, Isleifson et al. 2012).

Frost flowers are modified significantly within a few days, since they are extremely effective collectors of blowing snow, which suggests a temporal increase in the atmospheric fraction in the frost flowers (Barber et al. (III)). As a consequence, they are integrated into the snow layer on top of the sea ice (Perovich and Richter-Menge 1994).

Although the mechanisms behind frost flower formation are relatively well described, the biological components in frost flowers are not well-known (Bowman and Deming 2010, Bowman et al. 2013, Eronen-Rasimus et al. 2014). In **Barber et al. (III)**, we showed that the bacterial concentrations generally increase with salinity in frost flowers. It also confirms that the bacterial community in frost flowers is significantly different from that in the underlying sea water.

In our study, we found high calcium carbonate concentrations of 2.00 – 2.12 g m⁻² (Fig. 6; **Barber et al. (III)**) in these newly formed saline layers (<1 h old), which is similar to calcium carbonate concentrations found in frost flowers and brine skim in an outdoor pool of the Sea-Ice Environmental Research Facility (SERF; Rysgaard et al. 2014), but they are several times higher than concentrations reported from Barrow, Alaska (Geilfus et al. 2013a). If we compare the amount of calcium carbonate in the frost flowers and brine skim (Fig. 6; **Barber et al. (III)**) with the total amount of calcium carbonate in the entire sea ice column in Young Sound in NE Greenland (Fig. 2 and Fig. 6; **Rysgaard et al. (II)**), it accounted for approximately 8 %. This is in general agreement with other studies in which frost flowers and brine skim in newly formed sea ice fully covered by frost flowers accounted for 1-5 % of the total calcium carbonate (Domine 2005, Rysgaard et al. 2014).

An explanation for the occurrence of calcium carbonate in the frost flowers and brine skim could be the upward migration of brine with calcium carbonate from the underlying sea ice (Geilfus et al. 2013a) and, subsequently, the incorporation of this brine into frost flowers and brine skim on the ice surface. The observation of high calcium carbonate concentrations in the newly formed sea ice within the same season and at the same sampling station supports this idea (Fig. 6; **Rysgaard et al. (II)**). Furthermore, we observed that the newly formed frost flowers were composed primarily of brine from the underlying sea ice (**Barber et al. (III)**). However, it is possible that precipitation of calcium carbonate continued after the brine skim and frost flowers were formed due to low air temperature at the sampling station, allowing the precipitation of salts to occur within these structures (**Barber et al. (III)**).

The upward migration of brine from the ice column to the frost flowers and brine skim (**Barber et al. (III)**) facilitates salt transport to the atmosphere and increases the specific surface area of the ice, which may potentially promote CO₂ exchange between the ice and the atmosphere (Rankin et al. 2000; 2002, Alvarez-Aviles et al. 2008, Bowman and Deming 2010, Geilfus et al. 2013a, **Barber et al. (III)**). Our results indicate an efflux of CO₂ at the brine wetted newly formed sea ice surface (3.35 ± 0.86 mmol m⁻² d⁻¹, n=8), but there were no striking differences in the CO₂ flux if frost flowers were inside the chamber footprint (3.02 ± 0.76 mmol m⁻² d⁻¹, n=4) or out-

side the footprint (3.67 ± 1.99 mmol m⁻² d⁻¹, n=4), suggesting that the formation of frost flowers only promotes minor CO₂ de-gassing (**Barber et al. (III)**). However, another study showed that frost flower formation releases high amounts of CO₂, produced during the precipitation of calcium carbonate (Geilfus et al. 2013a). Nevertheless, when the precipitated calcium carbonate from frost flower formation is dissolved later during summer thaw, this leads to a similar CO₂ uptake from the atmosphere; and, therefore, this will, most likely, not have a net effect on the CO₂ exchange between the atmosphere and ocean (Fig. 1; phase II). We found high amounts of calcium carbonate (9 – 20 g m⁻²; Fig. 6) in the snow cover above the sea ice in Young Sound, NE Greenland (Fig. 2), which has also been shown for snow on top of sea ice in other Arctic locations (**Søgaard et al. (IV)**). If the precipitated calcium carbonate is incorporated into the snow cover together with the CO₂ released through calcium carbonate production (1), then it is possible that the CO₂ is lost from the snow cover to the atmosphere under conditions with high wind speed (Fig. 1; wind-drift). The overall outcome is that the dissolution of calcium carbonate during the summer thaw, most likely, will have no net effect on the CO₂ exchange between the atmosphere and ocean. As a result of the way frost flowers are formed and their later integration into the snow cover, frost flowers present a unique way for the ocean and sea ice to interact with the atmosphere.

The events controlling the dynamics of inorganic carbon in the transition from open water to an ice-covered ocean in autumn and winter have been outlined in the sections above (Fig. 1; phase I). Altogether, my results from this phase I indicate that CO₂ is released to the atmosphere while, at the same time, TCO₂ is rejected together with brine to the underlying sea water (Fig. 1). Formation of new ice may lead to a de-gassing of CO₂ in part, because of the increase in concentration of solutes but also because of the formation of calcium carbonate. However, it may also be a result of respiration by the net heterotrophic community at the ice base in newly formed sea ice. High concentrations of calcium carbonate occur both in frost flowers and brine skim, accounting for approximately 5% of the total calcium carbonate in the entire sea ice column. However, the fate of the precipitated calcium carbonate still remains unclear.

1.3 Phase II: Growing winter sea ice

In this section, the processes driving CO₂ exchange in the growing winter sea ice are discussed (1.3.1) and whether this phase acts as a net sink or source of CO₂ to the atmosphere. A short description of the microorganisms in winter sea ice and their contribution to the CO₂ dynamics during phase II is also provided (1.3.2).

1.3.1 Abiotic processes in growing winter ice

During winter (Fig. 1; phase II), the largest flux of TCO_2 and CO_2 is driven by brine drainage to the underlying water column, leaving sea ice depleted in CO_2 compared to ambient seawater (Fig. 1). This is supported by results in **Søgaard et al. (I)** indicating that the TCO_2 depletion in sea ice in Kapisigdlit Bight in SW Greenland (Fig. 2) was mainly controlled by brine drainage to the underlying water. There are three types of desalination mechanisms: 1) brine expulsion, 2) gravity drainage and 3) brine pocket migration. The first two desalination mechanisms are the only ones of quantitative importance (Eicken 2003). Brine expulsion is the migration of brine driven by the cooling of the sea ice, which results in pressure buildup in the brine pocket. This allows the brine to escape from the brine pocket and migrate toward the warmer end of the ice sheet (Weeks 2010). Gravity drainage includes all processes in which the brine, under the influence of gravity, drains out of the sea ice into the underlying water column (Cox and Weeks 1974). These two desalination mechanisms result in the rejection of large amounts of TCO_2 and CO_2 to the underlying water column along with the expelled brine during sea ice growth (Killawee et al. 1998, Anderson et al. 2004, Rysgaard et al. 2007), which subsequently increases the $p\text{CO}_2$ concentration below the sea ice (Fig. 1; Gibson and Trull 1999, Semiletov et al. 2004; 2007, Delille 2006; 2010). TCO_2 is assumed to be removed from the surface oceanic mixed layer to deeper water masses via the sinking of the expelled dense brine (Nansen 1906, Rysgaard et al. 2011). However, the fate of the rejected TCO_2 in the water column is still poorly understood.

During winter calcium carbonate precipitation continues in sea ice (**Søgaard et al. (I)**, **Rysgaard et al. (II)**). Our measurement from growing Subarctic winter sea ice in Kapisigdlit Bight (Fig. 2) showed high calcium carbonate concentrations (i.e., 9 g m^{-2} ; **Søgaard et al. (I)**), which was 4 times higher than the average seasonal calcium carbonate concentration in sea ice measured in this area (i.e., 2.13 g m^{-2} ; **Søgaard et al. (I)**). In addition, in winter ice in the High Arctic in Young Sound, NE Greenland (Fig. 2), we observed the highest calcium carbonate concentrations ever measured to our knowledge in natural sea ice (i.e., 25 g m^{-2} ; **Rysgaard et al. (II)**), suggesting that winter (Fig. 1; phase II) is extremely important for the annual calcium carbonate precipitation (Fig. 6). Furthermore, it indicates that the calcium carbonate concentration in the brine increases with decreasing temperatures as the highest calcium carbonate concentrations are observed in cold winter High Arctic sea ice (**Rysgaard et al. (II)**).

Calcium carbonate is mainly found as ikaite in the natural sea ice environment, and we confirmed that the calcium carbonate found in the winter sea ice in the Young Sound area in NE Greenland (Fig. 2) was, indeed, ikaite (**Rysgaard et al. (II)**). Precipitation of ikaite requires near-freezing temperatures and

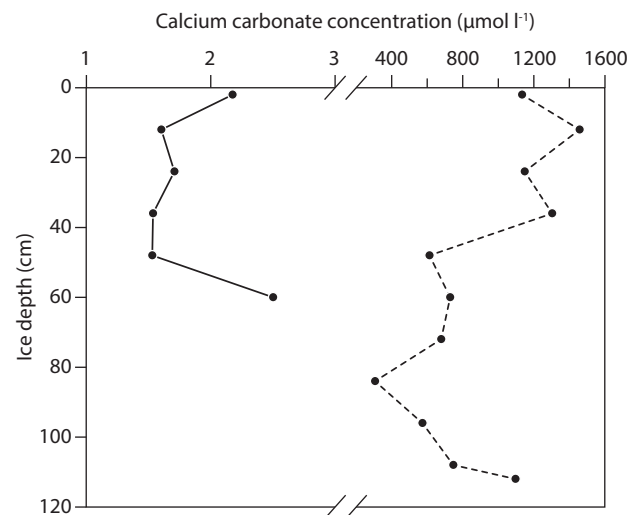


Figure 7. Vertical distribution of the calcium carbonate concentration in first-year winter sea ice in Kapisigdlit, SW Greenland (black line; **Søgaard et al. (I)**) and in first-year winter sea ice in Young Sound, NE Greenland (dashed black line; **unpublished data D. H. Søgaard**).

conditions of high alkalinity (Bischoff et al. 1993, Buchardt et al. 2001, Selleck et al. 2007, Hu et al. 2014). Previously, it was also postulated that elevated phosphate concentrations were critical for ikaite precipitation (Bischoff et al. 1993); however, this has been shown not to be the case (Hu et al. 2014). In the winter sea ice in Young Sound, NE Greenland and in Kapisigdlit Bight, SW Greenland (Fig. 2), we did observe low sea ice temperatures and conditions of high alkalinity with the pH following a C-shaped pH profile, i.e., high pH (> 9) in the surface and bottom sea ice layers and slightly lower pH conditions (8.5) in the internal sea ice layers (**Søgaard et al. (I)**, **Rysgaard et al. (II)**). The C-shaped pH profile in the sea ice is created when the brine inclusions in the upper ice layers are closed due to low ice permeability. This will restrict further CO_2 expulsion from the interior ice, which then results in CO_2 depletion relative to sea water and, thus, higher pH levels in the upper ice layers (Hare et al. 2013). The interior ice layer continues to receive CO_2 from calcium carbonate precipitation and CO_2 transport due to brine movement, which explains the low pH values encountered here. The bottom ice layer has open brine channels that continuously export brine to the underlying water resulting in CO_2 -depletion and high pH in this layer (Hare et al. 2013).

The calcium carbonate concentrations measured at two different locations followed the C-shaped pH profile with high calcium carbonate concentrations in the surface and bottom sea ice layers (Fig. 7; **Søgaard et al. (I)**). This suggests that the calcium carbonate precipitation in natural sea ice is also controlled by pH, as suggested in a laboratory study by Hu et al. (2014). This contradicts previous studies in which calcium carbonate is primarily found in the uppermost layers of sea ice (e.g., Fischer et al. 2013, Nomura et al. 2013b, Rysgaard et al. 2014).

The potential influence of melting the entire winter ice cover in Kapisigdlit Bight in SW Greenland (Fig. 2; **Søgaard et al. (I)**) and Young Sound in NE Greenland (Fig. 2; **Rysgaard et al. (II)**) into a 20 m thick mixed layer (typical for summer conditions in these location) on the CO₂ flux can be determined using the measured ice carbon chemistry (Table 1) and the initial mixed layer characteristics (Table 2) from the two different regions. Assuming that melt occurs over one month, the resultant air-sea CO₂ flux to return to pre-melt conditions would be – 4.8 mmol C m⁻² d⁻¹ in Kapisigdlit Bight in SW Greenland and – 5.9 mmol C m⁻² d⁻¹ in Young Sound in NE Greenland (Fig. 2). The potential air-sea CO₂ flux vary by a factor of 0.8 with the highest potential air-sea CO₂ flux estimated in High Arctic sea ice (**Søgaard et al. (II)**, **Søgaard et al. (IV)**). Our observations of calcium carbonate concentrations in sea ice vary by several orders of magnitude depending on the sea ice type and the locality (Fig. 6; **Søgaard et al. (I)**, **Rysgaard et al. (II)**), suggesting that TA, TCO₂ and calcium carbonate concentrations feature high horizontal variability. This issue is addressed in one of my papers (**Søgaard et al. (I)**) in which we found high spatial variability on the scale of metres to hundreds of metres for calcium carbonate concentration and other sea ice biogeochemical properties. Another important finding in these studies is that the presence of calcium carbonate in sea ice almost doubles the air-sea CO₂ flux as compared to melting of calcium carbonate-free sea ice, which emphasizes that the precipitation and dissolution of calcium carbonate is critical to the efficiency of the sea ice-driven carbon pump in these areas (**Søgaard et al. (I)**, **Rysgaard et al. (II)**).

Although the rejection of TCO₂ from growing sea ice to the underlying water column during winter is the dominant process in this phase, the sea ice-atmosphere fluxes should also be taken into account when describing the sea ice carbon budget. As mentioned above, our data showed that calcium carbonate concentration follows a C-shaped profile (Fig. 6; **Søgaard et al. (I)**). Since most of the calcium carbonate is found in the upper and lower sea ice layers, it suggests that the CO₂ produced during precipitation of calcium carbonate is both in close contact with the atmosphere and the underlying water column. The amount of CO₂ released to the atmosphere depends on the ice permeability, while CO₂ in the lower ice layers is rejected together with the brine to the underlying water column when there is an excess of CO₂ due to high permeability in this ice layer. The low temperatures during winter result in lower brine volumes and, subsequently, a decrease in permeability, which impedes the ice-atmosphere gas exchange (Loose et al. 2011a, Rysgaard et al. 2011) and results in insignificant fluxes above cold sea ice (Heinesch et al. 2010, Miller et al. 2011b, Geilfus et al. 2012b, Sørensen et al. 2014). However, small fluxes of CO₂ have been observed above cold winter sea ice under conditions with high wind speed (Heinesch et al. 2010, Miller et al. 2011a, Papakyriakou and Miller 2011, Else et al. 2011), indicating that CO₂ de-gassing might oc-

cur occasionally above winter sea ice (Fig. 1; snow-drift). The CO₂ de-gassing above winter sea ice is mainly due to the loss of stored CO₂ from the snow pack (Rysgaard et al. 2014). This is supported by a recent study showing low pH values in the snow cover above winter sea ice, indicating high CO₂ concentrations (Hare et al. 2013). In addition, we also found high amounts of calcium carbonate (0.12 – 20 g m⁻²; Fig. 6) in the snow cover above the sea ice in Young Sound, NE Greenland and in Kapisigdlit Bight in SW Greenland (Fig. 6; **Søgaard et al. (IV)**). If the precipitated calcium carbonate is incorporated into the snow cover together with the CO₂ released through calcium carbonate production (1), this process may be responsible for the observed snow-driven CO₂ degassing under conditions with high wind speeds above winter sea ice (Fig. 1; phase II). The snow cover also has an insulating effect (Sturm and Massom 2010, Fischer et al. 2013), maintaining sea ice temperatures high enough to allow a small CO₂ efflux from the ice column into the snow cover (Golden et al. 2007; Nomura et al. 2010a; 2010b, Hare et al. 2013). In addition, new snowfall or a redistribution of snow due to high winds to the same site may warm sea ice cover locally during winter, which may dissolve calcium carbonate (Rysgaard et al. 2014). This indicates dynamic conditions of calcium carbonate precipitation/dissolution, CO₂ and pH during winter.

1.3.2 Growth limitation of microorganisms in winter sea ice

In winter (Fig. 1; phase II), light availability in the sea ice is very low and the sympagic community remains net heterotrophic, counteracting the atmospheric CO₂ drawdown as respiration releases CO₂ (**Søgaard et al. (I)**, **Søgaard et al. (IV)**).

Our studies show that, although both biotic and abiotic processes can influence air-sea CO₂ exchange, the relative effects of biotic processes throughout the examined winter sea ice are very low (**Søgaard et al. (I)**). In addition, our studies revealed that the ice-associated biological community was net heterotrophic in this winter phase with high bacterial carbon demands (i.e., varies between 19.40 mg C m⁻² – 40.50 mg C m⁻²) compared to estimated primary production values (i.e., varies between 12.20 – 20.70 mg C m⁻²; **Søgaard et al. (I)**, **Søgaard et al. (IV)**). The bacterial carbon demand in winter sea ice varies between locations with recorded values of 0.80 – 26 mg C m⁻² d⁻¹ in Greenland sea ice (Long et al. 2012, **Søgaard et al. (I)**, **Søgaard et al. (IV)**), 0.02 – 1.5 mg C m⁻² d⁻¹ in the Baltic Sea (Kaartokallio 2004) and 5.96 mg C m⁻² d⁻¹ in sea ice in Resolute (Smith and Clement 1990). Regardless of location and bacterial carbon demand, minima in bacterial abundance have been observed during winter (Collins et al. 2008, Deming 2010 and references herein). The low bacterial abundance in sea ice during winter might be due to virally-mediated cell death (Collins et al. 2008),

grazing by bacterivorous protists (Rózanska et al. 2008), a reduction in habitable space or the formation of intracellular ice crystals and cell-puncturing by ice crystals (Collins and Deming 2011). Our studies indicate that high ice salinity is a key parameter influencing the constitution and activity of the bacterial community in winter sea ice (Kaartokallio et al. (VI)). Our findings also suggest that the sea ice is acting as a biofilm-like system rather than being analogous to open-water systems, which may be a survival strategy for the heterotrophic community in this hostile environment (Kaartokallio et al. (VI)).

As mentioned in section 1.3.1, the pH in winter sea ice follows a C-shape profile i.e., high pH (> 9) in the surface and bottom sea ice layers and slightly lower pH conditions (8.5) in the internal sea ice layers. This may have an effect on the growth of the microorganisms within the sea ice. Limited knowledge exists on how high pH affects growth rates of sea ice algae and bacteria. However, previous studies indicate that high extracellular pH may cause gross alterations in membrane transport processes and metabolic functions involved in internal pH regulation (Raven 1980) or cause alterations of cellular content of amino acids and their composition, which might affect cellular growth (e.g., Taraldsvik & Mykkestad 2000). Changes of pH influence the inter-speciation of inorganic carbon (CO_2 (aq), HCO_3^- , CO_3^{2-}). At pH 8 in sea water (TCO_2 approximately 2mM in marine waters), approximately 1 % of TCO_2 is present as CO_2 while, at pH 9, only 0.1 % of TCO_2 is present in this form (Hinga 2002). Potentially, the limitation of the CO_2 supply due to elevated pH may restrict photosynthesis and growth of phytoplankton (Hansen 2002). However, some phytoplankton species have active transport systems by which they utilize HCO_3^- in order to avoid TCO_2 limitation at elevated pH (Korb et al. 1997, Huertas et al. 2000, Hansen 2002).

We have shown that the growth rates of the sea ice diatom species (i.e., *Fragilariopsis nana* and *Fragilariopsis* sp.) were significantly reduced at pH > 9.0; and, at pH=9.5, they stopped growing irrespective of TCO_2 , indicating that pH had a direct effect on algal growth (Søgaard et al. (V)). In addition, our experiments revealed that a chlorophyte species commonly encountered in sea ice (i.e., *Chlamydomonas* sp.) had an extreme pH-tolerance since only a small reduction in its growth rate was observed above pH=9.5, but it was sensitive to low TCO_2 concentrations (Søgaard et al. (V)). Furthermore, the chlorophytes species out-grew two species of sea ice diatoms in a succession experiment, suggesting that an elevated pH played a potential role in the succession of Arctic sea ice algae in winter sea ice (Søgaard et al. (V)).

Sea ice algae are known to be adapted to low light levels and are able to grow at light intensities down to $0.36 - 20 \mu\text{mol photon m}^{-2} \text{s}^{-1}$ (Horner and Schrader 1982, Gosselin et al. 1990, Gradinger and Ikävalko 1998, Mock and Gradinger

1999). However, much lower light intensities are observed in the winter sea ice covered with heavy snow (Søgaard et al. (IV)). In our study, light was identified as the major limiting factor for algal productivity – with snow cover depth largely controlling light transmission in Subarctic sea ice in Malene Bight in SW Greenland during winter (Fig. 2; Søgaard et al. (IV)). This suggests that the low algal biomass and productivity in the winter sea ice in Malene Bight in SW Greenland is caused by poor light conditions (Søgaard et al. (IV)).

In the sections above, the sequence of events controlling the dynamics of inorganic carbon in growing winter sea ice (Fig. 1; phase II) is outlined. Very high amounts of calcium carbonate were observed in winter the High Arctic sea ice in Young Sound in NE Greenland (Fig. 2), and the concentration followed a C-shaped profile, suggesting that the CO_2 produced in this phase is both in close contact with the atmosphere and the underlying water column. In addition, the sea ice permeability was very low, suggesting that brine drainage were the dominant processes leading to TCO_2 depletion in the ice column during the winter months. Therefore, CO_2 de-gassing plays only a role in areas with high ice permeability, high wind speeds and/or heavy snow cover where ice temperatures are maintained high enough to allow for CO_2 efflux. Altogether, my results indicate that the role of biology in modulating inorganic carbon dynamics in this phase is minor, and is apparently delayed until spring and summer.

1.4 Phase III: Transition from ice-covered ocean to open waters

In this section, the abiotic processes driving CO_2 exchange in melting sea ice are discussed (1.4.1) and whether this phase acts as a net sink or source of CO_2 to the atmosphere. In addition, the microorganisms in melting sea ice and their contribution to the CO_2 dynamics in this phase are described (1.4.2) with a focus on the processes determining the magnitude of the primary production in Greenland sea ice and the considerable geographic differences in primary production. Finally, a short discussion of the balance of CO_2 sinks and sources in the open water period in section 1.4.3 is provided.

1.4.1 Abiotic processes in melting sea ice

The warming of sea ice is accompanied by a reduction in ice salinity, approaching zero salinity, because of internal ice melt and brine flushing due to the draining of meltwater from surface melt ponds (Untersteiner 1968, Cox and Weeks 1974, Fetterer and Untersteiner 1998). Brine inclusions and channels enlarge upon warming and form new pathways for brine and melt water. These new pathways form longer and bigger channels than the primary pathways in

growing ice. The melt water percolates downwards into the ice, flushing out salts into the upper ocean in this process (Petrich and Eicken 2010). As the sea ice warms, the ice porosity increases; and, therefore gas exchange between the sea ice and atmosphere is also expected to increase. This is supported by field measurements of a high CO₂ influx (i.e., – 259.2 mmol C m⁻² d⁻¹) in some areas and, in other areas, high de-gassing of CO₂ (i.e., up to 74.3 mmol C m⁻² d⁻¹) over the surface of sea ice (Zemmerlink et al. 2006, Delille 2006, Nomura et al. 2010a, Miller et al. 2011a, Papkyriakou and Miller 2011, Geilfus et al. 2012b). However, recent studies have observed the formation of superimposed ice during spring and summer (Hass et al. 2001, Nicolaus et al. 2009), and it has been suggested that the formation of this ice type may reduce or even stop the gas exchange between the sea ice and atmosphere (Delille et al. 2006, Geilfus et al. 2012b, Nomura et al. 2010a; 2010b; 2013).

As the ice temperatures continue to rise, it leads to a widening of brine channels and a subsequent mass drainage of brine (Fig. 1; phase III). The sea ice melt water is depleted in TCO₂ and potentially enriched in TA due to dissolution of ikaite (e.g., Nedashkovsky et al. 2009), which will result in a decrease in *p*CO₂ of the top water column (Rysgaard et al. 2012, Else et al. 2013a; Else et al. 2013b). This CO₂ depletion of the surface seawater leads to an increase in the air-sea flux of CO₂ (e.g., Rysgaard et al. 2007; 2009; 2011).

An important question is whether the sea ice acts as a sink or source of CO₂ to the atmosphere during the spring/summer period. An important feature during sea ice melt (Fig. 1; phase III) are the formation of flooded slush surface and melt ponds, which both constitute a net CO₂ sink during the ice melting season (Semiletov et al. 2004, Geilfus et al. 2012b; 2014, Nomura et al. 2013a). Melt ponds is common on Arctic sea ice and can, at times, cover up to 50 – 80 % of the sea ice area (Eicken et al. 2004, Lüthje et al. 2006). Recent estimates of the CO₂ influx over melt ponds suggest that melt ponds represent a sink for atmospheric CO₂ by – 0.04 to – 5.4 mmol m⁻² d⁻¹ during Arctic sea ice melt and that this CO₂ flux accounts for 5 – 15 % (Geilfus et al. 2012b; 2014) of the total uptake for the Arctic Ocean (Bates and Mathis 2009, Takahashi et al. 2009).

This estimated influx over melt ponds is higher than the potential air-sea CO₂ flux of – 3.7 mmol C m⁻² d⁻¹ calculated using the measured ice carbon chemistry (Table 1) and the initial mixed layer characteristics (Table 2) from the spring/summer sea ice in Kapisigdlit Bight in SW Greenland (Fig. 1; phase III and Fig. 2) – assuming that the melt occurs over one month.

In addition, our estimate is low compared to the potential air-sea CO₂ flux in Fram Strait (i.e., –10.6 mmol C m⁻² d⁻¹, Rysgaard et al. 2012). This difference might be because our

study was performed in Subarctic sea ice exposed to higher seasonal air temperatures than the aforementioned studies. A comparison of the calcium carbonate concentration in the sea ice between these two sites (i.e., High Arctic sea ice in the Fram Strait and Subarctic in Kapisigdlit Bight; Fig. 6), revealed a ten times lower calcium carbonate concentration in the Subarctic sea ice (Rysgaard et al. 2012, **Søgaard et al. (I)**). This difference in calcium carbonate concentration between the two sites might also explain, in part, the lower sea-ice-driven CO₂ uptake found at this Subarctic sea ice site. Another explanation for the lower potential air-sea CO₂ flux in Kapisigdlit Bight in SW Greenland (Fig. 2) might be that the sea ice is formed by sea water that is influenced by a freshwater input, which might have increased the total gas content of the sea ice in this area (Crabeck et al. 2014). Therefore, variations in sea ice properties such as temperature, salinity, ice texture, pH and freshwater input are likely responsible for some of the differences found in the calcium carbonate concentrations and the estimated potential air-sea CO₂ flux between these two sites.

As mentioned in section 1.3.1, our data show that the precipitation of calcium carbonate follow a C-shaped profile during winter (Fig. 7; **Søgaard et al. (I)**). However, just before the ice break-up, we observed that the calcium carbonate concentration followed an L-shaped profile with the highest concentration of calcium carbonate in the bottom layer of the Subarctic sea ice in Kapisigdlit Bight in SW Greenland (Fig. 2; **Søgaard et al. (I)**). This high concentration in the bottom ice layers might be due to a migration of the calcium carbonate crystals through the brine channels or could result from the effects of surface flooding and/or gravity drainage. Therefore, it is possible that both the precipitated calcium carbonate and the CO₂ produced are released to the underlying water column, and the two processes may balance out in terms of air-ice CO₂ fluxes. However, in our study, we did not observe calcium carbonate crystals in the sediment traps deployed under the Subarctic sea ice in Kapisigdlit Bight in SW Greenland (Fig. 2; **Søgaard et al. (I)**). This suggests that the precipitated calcium carbonate is not released to the underlying water column and again strengthens the idea of an effective sea-ice-driven carbon pump in this Subarctic sea ice (**Søgaard et al. (I)**).

1.4.2 Biotic processes in spring/summer sea ice

It is the sea ice algae bloom that marks the transition from winter to spring/summer in ice-covered waters, where phytoplankton typically starts blooming after light levels in the sea ice have passed a critical level (i.e., ranging from 0.36 to 20 μmol photons m⁻² s⁻¹) and sea ice algae will start to grow exponentially (Mock and Gradinger 1999, Horner and Schrader 1982, Gosselin et al. 1990, Gradinger and Ikävalko 1998, **Søgaard et al. (IV)**). Light has previously been identified as the major limiting factor for algal productivity, with

snow cover depth largely controlling light transmission in sea ice during winter and early spring (e.g. Rysgaard et al. 2001, Mikkelsen et al. 2008, SØgaard et al. (IV)). Hence, the snow depth influences the transition from phase II to phase III; the thicker the snow cover, the more the transition is delayed.

The sea ice algae community sustains itself as long as sufficient amounts of nutrients remain – either incorporated from the underlying water column during the initial ice formation or through an increased exchange by tidal current, gravity drainage and brine movement when the permeability in the sea ice is high (Arrigo et al. 2010). The algal bloom in the Arctic usually begins at the ice-water interface, in a lamellar bottom ice layer called the skeletal layer (Fig. 4; SØgaard et al. (IV)). Even though this layer only contributes marginally to the total mass of sea ice, it harbours one of the highest phytoplankton concentrations in the world's oceans (Arrigo et al. 2010), which is dominated by pennate diatoms often accounting for > 90 % of the total biomass (Rózanska et al. 2009). An explanation for the dominance of diatoms in spring and summer ice is that diatom species are only slightly affected by decreasing salinities, whereas the decreasing salinity may result in substantial losses of species such as ciliates and flagellate (Garrison and Buck 1986, Ryan et al. 2004, Ralph et al. 2007, Mikkelsen and Witkowski 2010, SØgaard et al. (V)). However, other studies have shown that, when the sea ice has reached an advanced stage of ice melt and the brine salinity decreases, the dominance of diatoms gradually decreases, and flagellates become more abundant (Mikkelsen et al. 2008, Leu et al. submitted). We found that the flagellate species studied (i.e., *Chlamydomonas* sp.) outgrew the sea ice diatoms (i.e., *Fragilariopsis nana* and *Fragilariopsis* sp.) in a succession experiment in which pH levels were elevated, suggesting that elevated pH levels play a possible role in the succession of Arctic sea ice algae (SØgaard et al. (V)). Extremely high pH (i.e. pH levels as high as 10.0) is observed in sea ice with high primary production (Gleitz et al. 1995, Thomas et al. 2001b) and, thus, prevails during spring when the irradiance increases (Cota and Horne 1989, Kühl et al. 2001). On the other hand our results suggest that sea ice diatoms (i.e., *Fragilariopsis nana* and *Fragilariopsis* sp.) are less affected by decreasing salinities compared to the flagellate species studied (i.e., *Chlamydomonas* sp) and thus may have a competitive advantage during spring and summer thaw when sea ice salinity become low (SØgaard et al. (V)).

The algal bloom period ends when the sea ice temperature rises above a critical limit (i.e., depends on bulk salinity) that leads to a high sea ice permeability and, subsequently a major brine drainage and loss of the sea ice community (Lavoie et al. 2005, Gradinger et al. 2009, Boetius et al. 2013). Thus, the seeding of algae by melting sea ice is

thought to provide a starter community for phytoplankton growth in the water column under some conditions (Kuosa et al. 1992). Furthermore, melting sea ice may serve as a source of organic matter (Lannuzel et al. 2007, Thomas et al. 2010). Previous studies show that significant primary production takes place under the sea ice during the spring thaw as the sea ice melt will rapidly increase light transmission and enhance surface stratification of the underlying water column (Arrigo et al. 2012, Nicolaus et al. 2012, Mundy et al. 2009; 2013). Furthermore, Glud et al. (2014) measured high primary production rates by buoyant algal aggregates under melting sea ice in the Fram Strait, and a recent study by Boetius et al. (2013) showed that these aggregates contributed to, at least, 45 % of total primary production (i.e., both ice-algal and pelagic production) and > 85 % of carbon export in 2012 in the Central Arctic. We measured high light levels, reaching values of > 500 $\mu\text{mol photons s}^{-1} \text{ m}^{-2}$ below thin winter sea ice, which is more than sufficient to promote an under-ice phytoplankton bloom (Barber et al. (III)). Therefore, this under-ice primary production could be important in the carbon budget of the Arctic Ocean – a process, that has not previously been considered.

The significance of heterotrophic processes typically increases during late-bloom and post-bloom conditions close to spring thaw (Vezina et al. 1997, Kaartokallio 2004). Our studies show that the sea ice habitat is acting as a biofilm-like system and that this system is dominated by PHA-producing bacteria (Kaartokallio et al. (VI)). The production of PHA is a possible way for the bacterial community to store excess carbon, which thereby enhances their survival in the planktonic environment following ice melt (Kaartokallio et al. (VI)). Even though relatively high heterotrophic activities are measured during ice melt in phase III, our studies suggest that the autotrophic activity exceeds the heterotrophic activity in this period, resulting in a net autotrophic community (SØgaard et al. (I), SØgaard et al. (IV)). Bacteria follow the progress of the ice algal bloom, increasing their abundance as the Chl a concentration increases (Deming 2010). Extremely high bacterial production rates on the order of 3.80 – 290 $\text{mg C m}^{-2} \text{ d}^{-1}$ were measured in spring sea ice in Young Sound, NE Greenland (Fig. 2; Glud et al. 2007) and in the melting sea ice in the Fram Strait (Glud et al. 2014), which were considerably higher than the primary production rates, indicating that the sea ice was net heterotrophic during summer in these areas. However, the bacterial production rates typically represent less than 60 % of primary production rates during spring and summer and often peak during post-bloom condition in spring/summer ice (Smith and Clement 1990, Gowing et al. 2004, Deming 2010, SØgaard et al. (I), SØgaard et al. (IV)).

The autotrophic assimilation of CO_2 is an important process that depletes the $p\text{CO}_2$ of sea ice brine and, ultimately, of

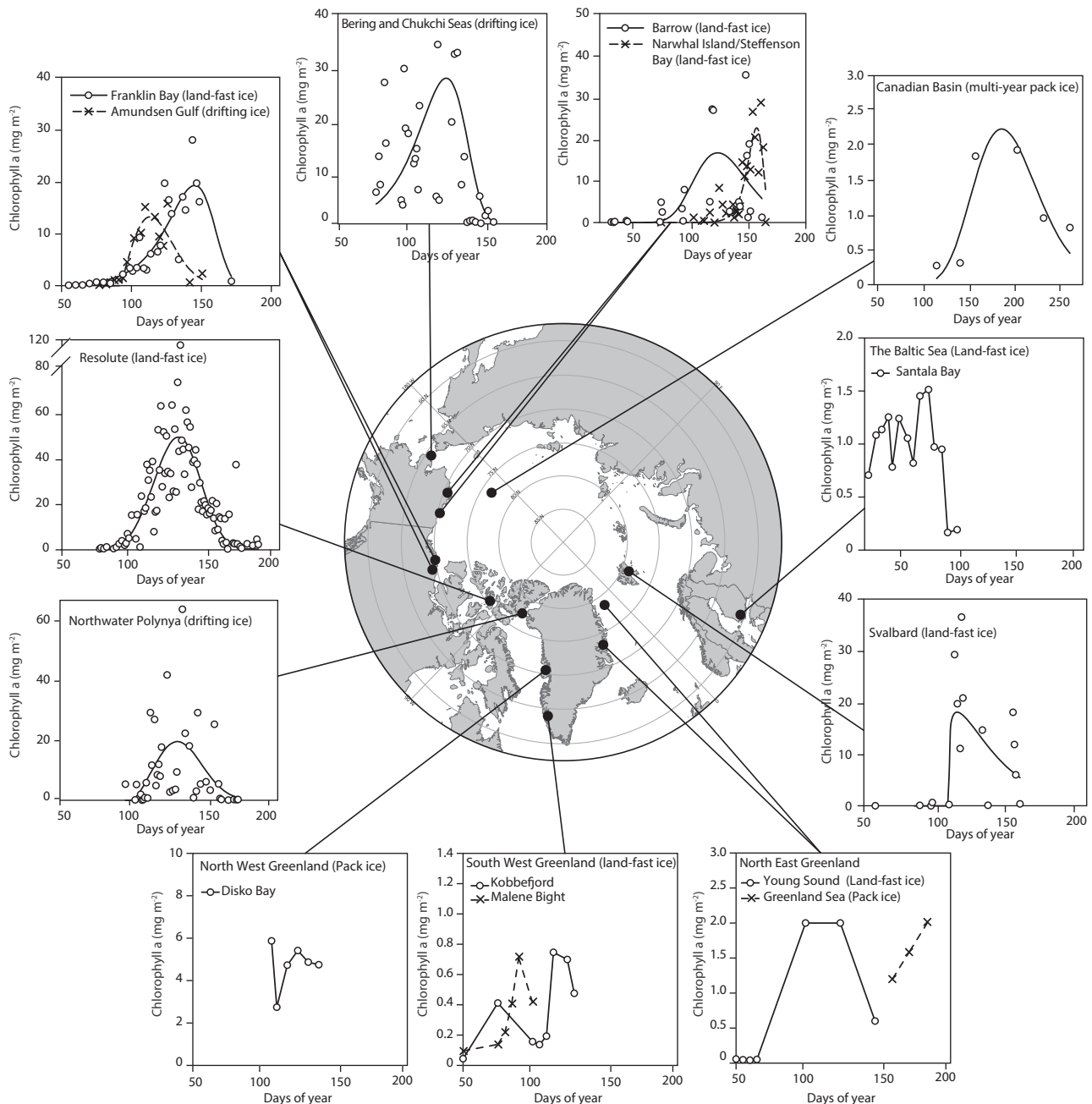


Figure 8. Seasonal development of sympagic Chl *a* values in different regions of the Arctic modified from Leu et al. submitted. Additional plots: the Baltic Sea data from Kaartokallio (2004), Young Sound, NE Greenland (**unpublished data D. H. Søgaard**, Rysgaard and Glud (Eds.) 2007), the Greenland Sea from Gradinger (1999), Disko Bay from Buck et al. 1998 and Malene Bight, SW Greenland (**Søgaard et al. (IV)**). Note the different scales for Chl *a*.

surface water when the sea ice melts (Arrigo et al. 2010). The relative effects of biological activity and calcium carbonate precipitation/dissolution on the air-sea CO₂ exchange can be estimated from measurements of primary production (**Søgaard et al. (I)**, **Søgaard et al. (IV)**). The measured primary production was 54 – 240 mg C m⁻² in Subarctic sea ice in Malene Bight and Kapisigdlit Bight in SW Greenland during spring and summer (Fig. 2; **Søgaard et al. (I)**, **Søgaard et al. (IV)**), which is low compared to the integrated calcium carbonate concentration of 2,440 mg m⁻² during this spring and summer phase (Fig. 6; **Søgaard et al. (I)**). This and other studies indicate that the contribution of primary production

to TCO₂ depletion in phase III is minor (<25%) compared to the contribution of calcium carbonate precipitation (**Søgaard et al. (I)**, Munro et al. 2010, Fransson et al. 2011, Geilfus et al. 2012b, Papadimitriou et al 2012, Rysgaard et al. 2012).

Algal biomass from sea ice in Greenland coastal areas range from 0.04 to 8.0 mg Chl *a* m⁻², which are similar to values recorded for sea ice in the central Arctic and the Baltic Sea (Fig. 8). However, these values are extremely low compared to values recorded for Arctic sea ice in general, which range from 53.8 mg Chl *a* m⁻² in the European Arctic to 340 mg Chl

a m⁻² near Resolute in the centre of the Canadian Archipelago (Fig. 8; Arrigo et al. 2010). Using a carbon-to-Chl a ratio of 20 to 40 for Arctic sea ice algae in general (Arrigo et al. 2010), the primary production was estimated to be around 1,076 to 13,600 mg C m⁻², which is within the range of or higher than the calcium carbonate concentrations of 2,130 to 25,000 mg m⁻² measured within Arctic sea ice from different locations and different ice development stages (Fig. 6; Søgaard et al. (I), Rysgaard et al. (II), Barber et al. (III), Søgaard et al. (IV)). This emphasizes that, in areas with high biological activity in the sea ice, the contribution of biotic processes to the CO₂ depletion can be substantially higher. Therefore, the evaluation of the sea ice sink described in this phase III may not be representative of the Arctic as a whole, since the uptake of CO₂ by biological activity seems to be much lower in Greenland sea ice compared to other regions.

The results above generate a very important question. Why is the primary production so low in Greenland sea ice? Sea ice associated microbial communities can contribute up to approximately 70 % of the integrated primary production in Arctic ecosystems (Horner & Schrader 1982, Legendre et al. 1992); but, generally and especially in coastal Greenland coastal waters, the contribution appears to be much less, amounting to approximately 1 % of the total production (Rysgaard et al. 2001, Mikkelsen et al. 2008, Søgaard et al. (IV)). Most fjords in Greenland receive large amounts of melt water with high concentrations of suspended sediments from the Greenland Ice Sheet, which in turn will influence the timing and duration of the pelagic primary production and also the composition of the pelagic species (Arendt et al. 2010; 2011, Juul-Pedersen et al. submitted). Such sediment-rich plumes can be observed even in winter, when they are identified by tidal re-suspension (Rysgaard et al. 2008, Mortensen et al. 2011). The low biomass and productivity in Greenland sea ice may be attributed to high fresh-

water run-off from the glaciers, which will influence light availability in the sea ice if suspended sediments are incorporated into the ice column. In the sea ice in Young Sound, NE Greenland (Fig. 2), however, neither the ice texture nor microscopic examination of both vertical and horizontal ice sections showed any suspended sediments (Rysgaard et al. (II)). It is still possible that the freshwater from melting glaciers locally affects the sea ice dynamics, due to surface flooding by less saline sea water and discharge below the sea ice. The accumulation of less saline sea water on top of and below the sea ice may change the sea ice microstructure (Crabeck et al. 2014), which may inhibit algal growth. The measured sea ice salinities (i.e., average less than 6.5; Table 3) in Greenland fjords reflect the low surface water salinities (Mortensen et al. 2011; 2013, Crabeck et al. 2014, Søgaard et al. (I)). The salinity in Greenland sea ice is, therefore, lower than in other sea ice regions in which high algal standing stocks were encountered (Fig. 8 and Table 3) and close to the bulk ice salinity ($2 < S < 4.7$) of sea ice grown under influence of brackish water in the Laptev Region of the Arctic Ocean (Eicken et al. 2005). A decrease in salinities within the sea ice play a potential role in the succession of Arctic sea ice algae (Søgaard et al. (V)), and this may, therefore, explain the lower algal biomass and productivity in Greenland sea ice. This is supported by the fact that our values of depth integrated algal biomass measured from sea ice in Greenland coastal areas are similar to values recorded for sea ice in the Baltic Sea (Fig. 8), which is also an area in which low sea ice bulk salinities are encountered (i.e., below 2). In addition, we observed periodic melting of the sea ice from below and subsequent re-growth, which could result in a lower bottom algal biomass, and therefore, lower algal productivities in the Greenland sea ice (Søgaard et al. (I), Søgaard et al. (IV)). This is supported by observations in Resolute, Canada, where melt rates of the bottom ice regulated the maximum biomass attained in this region (Lavoie et al. 2005).

Table 3. Bulk salinity, inorganic nutrient concentrations, snow depth and ice thickness of different Arctic regions. Modified from Leu et al. submitted.

Area and site	Bulk salinity	Silicate (μM)	Phosphate (μM)	Nitrate (μM)	Snow depth (cm)	Ice thickness (cm)	Reference
Greenland							
Young Sound	6.50	0.80	0.40	0.50	30 – 70	30 -110	Unpublished data D. H. Søgaard Søgaard et al. (IV) Søgaard et al. (V)
Kapisigdlit	4.40	4.70	0.50	1.70	0 – 7	0 – 81	
Malene Bight	5.20	1.10	0.20	1.90	0 -28	0 – 62	
The Baltic Sea							
Santala Bay	0.60	1.00	0.10	3.60	0	13 – 27	Kaartokallio (2004)
Svalbard							
Rijpfjorden	-	5	0.70	9	3 – 27	100	Leu et al. (2010)
Canada							
Amundsen Gulf	7.40	7.8 – 23.2	0.5 – 1.6	2.9 – 10.0	<5 - >15	120 – 180	Alou-Font et al. (2013) Cota et al. (1990), Mundy et al. (2013)
Resolute	8.00	11.8 – 28.6	1.1 – 1.7	4.3 – 8.9	5 - >30	136 - 176	

The low algal biomass and productivity recorded in Greenland may also be attributed to light limitation (Søgaard et al. (I), Søgaard et al. (IV)). In our study, we revealed that the snow and sea ice attenuations are generally higher than values reported elsewhere (Søgaard et al. (IV)), which might explain the low algal biomass and productivity in Greenland sea ice. Furthermore, we showed that the patch size of ice algal biomass followed the snow cover and sea ice temperature, suggesting that the light availability in sea ice is the main factor controlling sea ice algal patchiness in this area (Søgaard et al. (IV)). Considerable amounts of snowfall are usually observed in Greenland fjords (Søgaard et al. (I), Rysgaard et al. (II), Søgaard et al. (IV)), and we frequently observe that the upper sea ice column at different locations in Greenland are composed of snow-ice that is formed through flooding due to negative freeboard and thick snow cover (Søgaard et al. (I), Rysgaard et al. (II), Søgaard et al. (IV)). This may result in altered biochemical properties and light availabilities, which may inhibit algal growth and, thus, may substantially control the development of algal blooms (Perovich 1996). Therefore, a combination of heavy snowfall and the production of snow-ice/surface slush layers may cause the limitation of ice algae growth in Greenland sea ice. This is supported by the fact that the formation of a flooded slush surface layer has been widely observed in heavily-snow-covered sea ice during the ice melting season (e.g., Papadimitriou et al. 2009, Nomura et al. 2013a) and that low Chl *a* concentrations have been observed in surface flooded sea ice (Nomura et al. 2013a). Another explanation for the low algal productivity in Greenland sea ice could be the spectral composition of light penetrating the ice cover in Greenland, which is hampered by changes in the solar angle from the high mountains surrounding the fjords. This could potentially limit algal productivity through light limitation.

An additional potential factor that could limit sea ice algal growth and productivity is nutrient limitation. However, the levels of inorganic nutrients were similar to values reported for sea ice in other Arctic locations (Table 3; Thomas et al. 2010), which rules out low nutrient levels as a likely explanation for the low algal biomass and productivity in Greenland sea ice.

Unfortunately, the available data series on seasonal and spatial-bloom developments for many regions in Greenland are incomplete, which makes it impossible to deduce the most important factors limiting the algal biomass and productivity in Greenland sea ice. However, low light availability, lower sea ice bulk salinities and periodic melting of bottom ice seem to play an important role for the magnitude of the productivity.

In phase III, rapid brine dilution through internal sea ice melt will lead to a reduction in the sea ice CO₂ concen-

tration, which is further enhanced by the dissolution of calcium carbonate (Fig. 1; Rysgaard et al. 2011). In addition, sea ice melt enhances surface stratification of the underlying water column. The net result is an increase in TA and a lowering of CO₂ in the surface waters, enhancing the air-sea CO₂ flux. Our estimated air-sea CO₂ flux in this phase is only 35 % of the estimated flux from High Arctic sea ice in the Fram Strait. An explanation for this difference might be that our estimates were for Subarctic sea ice, suggesting that the magnitude of the air-sea CO₂ flux is determined by the geophysical (i.e., salinity and permeability) and thermodynamic (i.e., temperature) properties of the sea ice. Furthermore, the calcium carbonate concentration in the Subarctic sea ice in Kapisigdlit Bight (Fig. 2) were ten times lower than calcium carbonate concentration in the High Arctic sea ice in the Fram Strait. This difference in calcium carbonate concentration between the two sites might also explain, in part, the lower sea-ice-driven CO₂ uptake found at this Subarctic sea ice site. Our result also revealed that the autotrophic activity exceeded the heterotrophic activity, but the relative contribution of primary production to TCO₂ depletion was minor compared to the contribution of calcium carbonate precipitation/dissolution. However, the contribution of primary production to the TCO₂ depletion might be much higher in areas with higher primary production. In addition, our results suggest that the low light availability, lower sea ice bulk salinities and periodic melting of bottom ice seem to play an important role for the magnitude of the sea ice productivity in Greenland.

Once the sea ice cover has disappeared, conditions revert to those typical of open Arctic waters with CO₂ drawn down into biologically productive waters as outlined in the following.

1.4.3 The open water period

Once the sea ice has disappeared, increased TA and low CO₂ concentrations are observed in the stratified surface water, which will enhance the air-sea CO₂ flux (Rysgaard et al. 2011, Miller et al. 2011; Fig. 1, phase III). Furthermore, sea ice break-up triggers a pelagic spring bloom when nutrient-rich water is exposed to light. The melting sea ice creates an upper mixed layer separated from the underlying waters by a strong pycnocline (Mikkelsen et al. 2008, Leu et al. 2011), further reducing thereby the concentration of surface water CO₂ (Fig. 1; phase III). The pelagic bloom in areas with seasonal sea ice can be much higher than sea ice production with an annual production of 12 – 150 g C m⁻² (Sakshaug 2004 and references herein). There is a strong geographical variation in this pelagic primary production, depending on the timing of sea ice melt and, consequently, the light availability and nutrient levels. The pelagic phytoplankton bloom creates a strong biological pump that mainly controls the variability of sea-air CO₂ gas exchange in Arctic surface waters (e.g., Bates et al. 2006, Fransson et al. 2006). However,

at present, it is still difficult to quantify the respective roles of the pelagic biological pump during the ice-free period and the sea ice CO₂ pump on the air-sea CO₂ exchange on a large scale (Rysgaard et al. 2011). Recent estimates, however, predict them to be of equal size (Rysgaard et al. 2009). Furthermore, it is critical for the effectiveness of these high latitude areas acting as a potential sink for CO₂ that the surface sea water layer is exposed for a sufficient amount of time for the mixed layer to equilibrate with the atmosphere (Fransson et al. 2009, Rysgaard et al. 2011).

When considering the recent and ongoing changes in sea ice extent, thickness and transparency, a question arises: what impact may these changes have on the Arctic carbon pump? In the following section 1.5, I will describe the different changes in the Arctic caused by the climate change.

1.5 Ocean and sea ice in the context of global change

In the Arctic region (Fig. 2), the ice cover doubles its size from summer to winter with a total sea ice area ranging from 7.5 x 10⁶ km² to 15.5 x 10⁶ km², respectively (Table 4). Combining the total sea ice extent at the Arctic region (Fig. 2) and the Southern Ocean, the maximum extent covers about 7 % of the earth's surface, representing one of the largest biomes on earth (Table 4). Less than half of Arctic sea ice is multi-year sea ice (30 – 45 %), and this ice type has been reported as being in a rapid decline (Comiso et al. 2008; 2012, Haas et al. 2010, Stroeve et al. 2007; 2012), replaced instead by first-year sea ice in most areas (Comiso 2012). An increasing area of first-year sea ice may offer better growth conditions for sea ice algae because first-year sea ice is less thick, has a thinner snow cover (because there is less time to accumulate snow), a higher nutrient load, larger brine volumes and a higher melt pond coverage (i.e., increased transparency) than multi-year sea ice (Perovich et al. 2011, Lee et al. 2012, Nicolaus et al. 2012, Polashenski et al. 2012). These condi-

Table 4. Minimum and maximum ice area (× 10⁶ km²) in the Arctic region and ice extent in both emispheres averaged over the 1978-2010 period. Compiled after Comiso (2003 and 2008) and Cavalieri and Parkinson (2012).

	Arctic region	Both hemispheres
Min	7.5 (September)	19
Max	15.5 (March)	27.5

tions will most likely promote increasing algal blooms during the shorter ice-covered period.

In addition, the seasonal length of the ice-free period has increased, and a sea ice decline of about 3 % per decade has been observed (Fig. 9; Arrigo et al. 2008, Comiso et al. 2003; 2008, Cavalieri and Parkinson 2012) due to increased advection of warm water into the Arctic Ocean, atmospheric circulation patterns that favour advection of sea ice out of the Arctic Ocean through the Fram Strait (Fig. 2) and increased Arctic temperatures (e.g., Arrigo et al. 2008; Fig. 9). The observed changes in Arctic sea ice cover during the last decade and, in particular, the shift from multi-year sea ice to first-year sea ice cover could increase the importance of the sea-ice-driven carbon pump (Rysgaard et al. 2007; 2011), as this shift will increase the area that undergoes the cycle of sea ice formation and decay (sections 1.2 to 1.4). Contradicting this scenario, however, is the fact that the length of the average seasonal sea-ice-free period has increased in the same period (Comiso et al. 2008, Parkinson 2000), which potentially weakens the sea-ice-driven carbon pump. Furthermore, the area extent and periodicity of frost flowers and brine skim are expected to increase due to later freeze-up, thereby increasing the dynamic opening of mobile pack ice in autumn and winter (Isleifson et al. 2014). This will have significant implications for the CO₂ exchange and biogeochemical processes operating between the sea water-ice-atmosphere interfaces in these areas (Fig. 1; section 1.2.3; Barber et al. (III)).

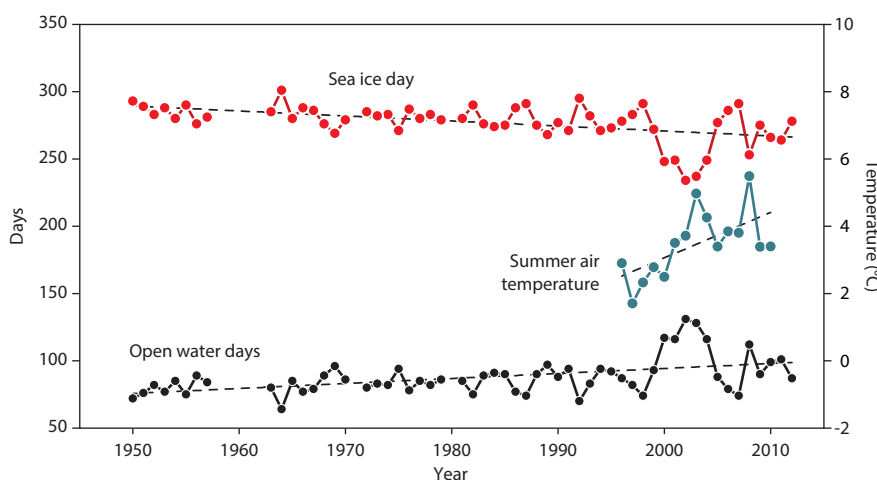


Figure 9. The average sea ice (red dots) and open water days (black dots) from 1949 to 2012 and the average summer air temperature (blue dots) from 1997 to 2010 in Young Sound, NE Greenland. The figure is updated from Rysgaard and Glud (2007) and is based on data from the Greenland Ecosystem Monitoring program. The slopes remains significantly ($p < 0.05$). However, the numerical slope is influenced by the extreme observations from 2000-2005.

In addition, melt ponds are a widespread and increasing surface feature of Arctic sea ice during spring and summer (Rösel and Kaleschke 2012), and their impact on inorganic carbon transport through sea ice might, therefore, increase in the future (see description in section 1.4.1).

The more transparent sea ice cover and earlier ice melt will also result in an increasing potential for pelagic primary production both below the thinner sea ice cover and in the open waters (Arrigo et al. 2012, Nicolaus et al. 2012, Mundy et al. 2013, Barber et al. (III)). Recent studies also indicate that the current sea ice thinning may enhance ice-algal export due to algal aggregation (Boetius et al. 2013). As a consequence, the biological drawdown of CO₂ is expected to increase as sea ice cover is reduced, which will lead to increased net oceanic uptake of CO₂ (Bates et al. 2006, Arrigo et al. 2008, Bates and Mathis 2009, MacGilchrist et al. 2014). However, recent studies show that the uptake capacity of the Arctic Ocean for atmospheric CO₂ is limited as a result of surface warming and increased stratification (Fransson et al. 2009, Cai et al. 2010, Brent et al. 2013, Else et al. 2013) and that these changes will also stimulate bacterial production and, consequently, limit the sink function of the Arctic Ocean when the sea ice cover is reduced (Xie et al. 2009). Furthermore, observation has shown that the Arctic river runoff has increased, which would lead to an even stronger stratification in the Arctic Ocean (Fransson et al. 2009). This will most likely result in a decrease in the annual biological production in these areas and, consequently, also limit the sink function of the Arctic Ocean in summer (Fransson et al. 2009).

The melt from the Greenland Ice Sheet has also increased as a response to global warming, adding more freshwater to the surface water in the coastal areas and fjords in Greenland (Inall et al. 2014 and references herein, Khan et al. 2014). What is the effect of glacial runoff on the air-sea CO₂ exchange in coastal areas and fjords in Greenland? Our studies revealed that the Godthåbsfjord system in SW Greenland was, indeed, a sink of CO₂ (Rysgaard et al. (VII)) and that the CO₂ dynamics were controlled by both the biological processes and mixing between glacial meltwater and coastal waters (Rysgaard et al. (VII)). The strength of the sink was particularly strong near the Greenland Ice Sheet, indicating spatial variations in air-sea CO₂ uptake. High amounts of CO₂ are taken up in the Godthåbsfjord (annual flux of – 83 to – 108 g C m⁻² yr⁻¹; Rysgaard et al. (VII)). This estimate is higher than flux estimates from other sites in the Greenland Sea (i.e., – 52 g C m⁻² yr⁻¹; Nakaoka et al. 2006), in Young Sound in NE Greenland (– 32 g C m⁻² yr⁻¹; Sejr et al. 2011; Fig. 2) and data from other Arctic shelf systems (Bates and Mathis 2009), underlining the importance of this Subarctic fjord system acting as a strong sink for CO₂ (Rysgaard et al. (VII)). If this uptake is typical for similar Subarctic fjord systems in Greenland, then the coastal areas of Greenland constitute a larger sink than anticipated. Furthermore, a re-

cent study from the Godthåbsfjord indicates that the glacial freshwater runoff is likely to be important for the stimulation effect on primary production (total annual production of 84.6 – 139.1 g C m⁻² yr⁻¹). This suggests that the timing, duration and magnitude of the glacial freshwater runoff are likely to be important for the CO₂ uptake in this Subarctic fjord system (Rysgaard et al. (VII), Juul-Pedersen et al. submitted). Therefore, an increased ablation of the Greenland Ice Sheet due to future warming could result in an increase in the annual biological production, which could potentially increase the air-sea CO₂ flux in these areas.

1.6 Conclusions and perspectives

So, what have we learned since the sea ice CO₂ pump was first suggested by Jones and Coote (1981) 33 years ago and later confirmed in natural sea ice by, e.g., Rysgaard et al. 2007? The studies of sea ice carbon dynamics over a complete seasonal cycle of sea ice formation and decay as presented in this thesis have, indeed, improved our understanding of the drivers of the sea ice CO₂ pump.

Collectively, the results in this thesis showed that the formation of sea ice results in transport of TCO₂ out of the ice column and, therefore, strengthens the idea of an effective sea-ice-driven carbon pump in both Subarctic and High Arctic sea ice in Greenland (Fig. 1). However, the extent to which TCO₂ is transported to the underlying water column and, subsequently, enters the intermediate and deep water masses has yet to be determined. The highest concentrations of calcium carbonate ever reported in natural sea ice was measured in approximately 5-month-old High Arctic land-fast sea ice, followed by high concentrations in newly formed High Arctic polynya sea ice; whereas the lowest concentrations observed during our studies were in Subarctic land-fast sea ice. Variations in sea ice properties such as temperature, salinity, pH, ice texture and freshwater input are likely responsible for some of the differences found in calcium carbonate concentrations between sites. It seems that the direction and magnitude of the air-ice flux appear to be determined by the stage of ice development, the properties of the sea ice carbonate system (i.e., TA, TCO₂, pCO₂) as well as sea ice geophysical (i.e., salinity and permeability) and thermodynamic (i.e., temperature) properties.

The contribution of primary production to the TCO₂ depletion was minor compared to the contribution of calcium carbonate precipitation/dissolution in my study areas; however, in areas of high primary production the contribution to the TCO₂ depletion might be significantly higher. As a result, the evaluation of the sea ice sink described in this thesis is not representative of the Arctic as a whole since the uptake of CO₂ by biological activity seems to be much lower in Greenland sea ice compared to other regions.

These results revealed large variation in calcium carbonate concentration and other biogeochemical properties at different temporal and spatial scales in sea ice, emphasising the importance of full-season studies covering the hundred-meter spatial scale in order to make reliable regional and eventually global carbon budgets.

Many questions still remain unanswered within this field of research, some of which I would like to address in the future. The first step would be to perform full-season studies of the inorganic carbon dynamics in different sea ice types and in different ice locations. It is important to perform continuous measurements of all components involved in the sea-ice-driven carbon cycle during a complete seasonal cycle, in different sea ice types and from different geographic areas. Furthermore, seasonal measurements of the resulting CO₂ fluxes across the atmosphere-ice-ocean boundary layer are needed. In addition to measuring these parameters with already established techniques, it is also important to develop new methods for measurements including *in situ* measurements in the microenvironment of brine channels and pockets.

This first step require in itself a focused effort and still other basic questions will undoubtedly present themselves: 1) Will the future changes in sea ice cover affect the capacity of the Arctic Ocean to take up atmospheric CO₂? 2) What is the fate of the rejected TCO₂ in the water column at different Arctic areas, and is it transported below the pycnocline? 3) What is the fate of the calcium carbonate and CO₂ in frost flowers and brine skim? 4) What is the importance of polynya areas to the air-sea CO₂ flux? 5) How important is the sea ice carbon pump compared to the solubility pump and biological pump? Here, I outline what are to me the most interesting unanswered questions to advance our knowledge of the events controlling the inorganic carbon dynamics in high latitude oceans.

The temporal and spatial variations in the air-sea CO₂ flux were discussed for the coastal seawater in Godthåbsfjord, SW Greenland (Fig. 2). This area is determined to be a strong sink of CO₂, which was highly regulated both by the biological processes and by mixing between glacial meltwater and coastal waters. The strength of this sink is particularly strong near the Greenland Ice sheet.

The next step will be to put these results into a global context to understand how important the role of Greenland coastal waters is in relation to the global carbon budget. Three basic questions present themselves: 1) What is the inter-annual pattern of the CO₂ sink and biological processes in Greenland in the Subarctic and High Arctic fjords? 2) What is the spatial pattern of the CO₂ sink and biological processes in Greenland? 3) Will these patterns change as

a consequence of ongoing global warming, which is more pronounced at these high latitudes? It is a nontrivial task to answer these questions as the coastal CO₂ flux and biological processes show high spatial and temporal heterogeneity. However, Greenland presents a unique opportunity to study changes in coastal biological and physical characteristics along a climate gradient from the Subarctic to the High Arctic.

Therefore, there are still a lot of important future research questions in terms of understanding the influence of the sea-ice-driven CO₂ pump and the role of Greenland coastal waters in relation to the global carbon cycle, and it is needed urgently since climate change threatens to take these frozen high latitude environments from us.

1.7 Glossary

Aggregates: are attached or free-floating mats or aggregates of, e.g., the centric diatom *Melosira arctica* beneath the sea ice, in melt ponds, frozen into the sea ice or sunk to the bottom of the deep-sea floor.

Air-sea CO₂ exchange: is primarily controlled by the air-sea difference in gas concentrations and the exchange coefficient. It takes about one year to equilibrate CO₂ in the surface ocean with atmospheric CO₂. Therefore, in some areas large air-sea differences in CO₂ concentrations can be observed. In my PhD thesis negative flux indicates sea ice or sea water uptake of CO₂.

Algae: general term for eukaryotic organisms ranging from unicellular genera, e.g., diatoms to multicellular forms, such as giant kelp, of which most are autotrophic and non-vascular organisms that live almost exclusively in aquatic environments.

Autotrophic: ability to convert energy from light (photoautotrophic) or from oxidation of inorganic compounds (chemoautotrophic) to organic material by utilising inorganic carbon (usually CO₂).

Bacteria: constitute a large domain of prokaryotic microorganisms, most of which are heterotrophic and, typically, a few micrometres in length.

Biological pump, the: is driven by the sinking of particulate material -either organic carbon (i.e., dead algal cell) or particulate inorganic carbon (i.e., calcium carbonate from calcifying organisms such as coccolithophores, foraminiferans or pteropods).

Brine skim: a highly saline skim of brine that is formed on the surface of newly formed sea ice.

Calcium carbonate: Exists in six phases, namely, amorphous calcium carbonate, calcium carbonate monohydrate, calcium carbonate hexahydrate (ikaite) and three anhydrous phases: vaterite, aragonite and calcite. In both Arctic and Antarctic sea ice, precipitation of calcium carbonate in the form of ikaite has been observed. At present, it is not clear whether ikaite is the only calcium carbonate phase formed in sea ice. However, precipitation of ikaite in sea ice is an important process as it catalyses chemical processes such as boundary layer ozone depletion events (ODEs) and the formation and subsequent draw-down of CO₂ via brine drainage.

Carbon cycle: is the biogeochemical cycle by which carbon is exchanged among the atmosphere, hydrosphere, lithosphere, cryosphere and pedosphere of the earth.

Carbon dioxide (CO₂): next to water vapour CO₂ is the most abundant greenhouse gas on earth. Most global CO₂ is dissolved in water, and CO₂ reacts with water and forms bicarbonate (HCO₃⁻) and carbonate ions (CO₃²⁻). The concentration of the different ions depends on thermodynamic equilibria that are related to temperature, pH, salinity and pressure. However, at typical sea water conditions, HCO₃⁻ is dominant (86.5 %), whereas CO₂ (0.5 %) and CO₃²⁻ (13 %) are only present in small concentrations.

Cells: are the smallest unit of life that can replicate independently.

Cell membrane: is a biological membrane that separates the interior of all cells from the outside environment (called cell wall). It is made of a lipid bilayer interspersed with proteins, which makes it selectively permeable to ions and organic molecules.

Chlorophyll: a group of green pigments in photosynthetic organisms that traps the energy of sunlight for photosynthesis and exists in several forms of which the most abundant is chlorophyll *a*.

Chlorophyll *a*: a type of chlorophyll that is common and predominant in all oxygen-evolving photosynthetic organisms. It is abbreviated Chl *a*.

Chlorophyta: is a division of green algae.

Ciliates: are a group of protozoans characterized by the presence of hair-like organelles called cilia.

Deep-water masses: water located below the intermediate waters. It generally has low temperatures (2°C) and high salinity (34.9) and, therefore, a high density.

Diatoms: are a major group of algae and are among the most common types of phytoplankton of which most are unicellular. They can exist as colonies and with a cell wall of amorphous silica.

Dimethylsulphoniopropionate (DMSP): is a widely used osmolyte used by microalgae to acclimate to changes in salinity. DMSP is a precursor of dimethylsulphide (DMS), which is a climate-active gas.

Dissolved organic carbon (DOC): are organic molecules of varied origin and composition within aquatic systems. DOC in marine systems is generally a result of decomposition processes from dead organic matter such as plants. DOC is a food supplement supporting the growth of microorganisms and plays an important role in the global carbon cycle through the microbial loop.

Dissolved organic nitrogen (DON): is a mixture of compounds ranging from simple amino acids to complex humic substances.

Exponential growth: Growth of microorganisms whereby the cell number doubles within a fixed time period.

Extracellular polymeric substances (EPS): are high-molecular weight compounds secreted by microorganisms into their environment. EPS can function as cryoprotection, as external reserves of hydrolysable organic compounds, to depress the freezing point and to provide a physical buffer against encroaching ice crystals.

First-year sea ice: is sea ice of not more than one winter's growth. It develops from young ice and has a thickness > 30 cm.

Flagellate: is an organism with one or more organelles called flagella. Flagella-bearing species are common in all algal classes except Cyanophyceae, Rhodophyceae, Phaeophyceae and Bacillariophyceae.

Frost flowers: clusters of saline ice crystals that have a dendritic and branched structure. Frost flowers form at the interface between a warm ice surface and a cold atmosphere at conditions with low surface wind conditions.

Global carbon budget: is the sum of all exchanges (inflows and outflows) of carbon compounds between the earth's carbon reservoirs of the carbon cycle.

Halotolerant: the ability to withstand large changes in salinity.

Heterotrophic: ability to obtain carbon for organic synthesis by metabolising organic material.

Ikaite (CaCO₃ · 6H₂O): is an unstable hexahydrate polymorph of CaCO₃, which begins to precipitate at -2.2°C and dissolves at temperatures above 4°C. Precipitation of ikaite has been confirmed in sea ice from both hemispheres.

In situ: means on site.

Intracellular: occurs or functions within a cell.

Lipid bilayer: is a flat and thin polar membrane that consists of two layers of lipid molecules. This sheet forms a continuous barrier around all cells.

Melt ponds: result from an accumulation of meltwater on sea ice – mainly, due to the melting of snow, but the underlying sea ice cover also contributes to the melt pond formation. Melt ponds absorb solar radiation rather than reflecting it as ice does and, thereby, have a significant influence on the earth's radiation balance.

Membrane fluidity: is the viscosity of the lipid bilayer of a cell membrane that can affect the rotation and diffusion of proteins and, therefore, also affects the function of these molecules. The lipid bilayer has proteins embedded in them, and lipid packing can influence the fluidity of the cell membrane.

Multi-year ice: ice of more than one year's growth.

Osmolytes: are dissolved ion or organic solutes within a cell that prevent osmotic shock by maintaining osmotic pressure within the cell to avoid cell lysis (too much internal pressure) or shrinkage (too little internal pressure).

Osmotic shock: is a sudden change in the solute concentration around a cell that causes a change in the movement of water across its cell membrane. In environments with high concentrations of salts, water is drawn out of the cells. This is avoided by the incorporation of osmolytes.

$p\text{CO}_2$: the partial pressure of CO_2 .

Pelagic: describes organisms that swim or drift in a sea.

Pelagic organisms: are plankton and nekton.

pH: pH of seawater plays an important role in the ocean's carbon cycle. pH measurement in sea water is complicated by its chemical properties, and several distinct pH scales exist, i.e., total scale, sea water scale and free scale.

Photosynthesis: the process by which green plants and some unicellular organisms convert incoming sunlight into organic material from CO_2 and water.

Photosynthetically active radiation (PAR): is the spectral range (wave band) of solar radiation from 400 to 700 nanometres in which photosynthetic organisms are able to use for photosynthesis. PAR is normally quantified as $\mu\text{mol photons m}^{-2} \text{s}^{-1}$.

Polyhydroxyalkanoates (PHA): produced in nature by bacteria to store carbon and energy.

Polynya: is an area of open water surrounded by sea ice. In this area, new sea ice is produced and frequently blown away, thereby allowing new ice to form again and again

Precipitation: formation of a solid from solution by chemical or physical processes.

Proteome: is the entire complement of proteins that are or can be expressed by a cell, tissue or organism.

Psychrophilic organisms: are organisms that have optimal growth rates at temperatures usually below 15°C and cannot grow above 20°C .

Psychrotolerant organisms: are organisms that have optimal growth rates at temperatures above 20°C but are able to tolerate and, for bacteria, grow under cold conditions.

Pycnocline: is a boundary in oceanography separating two water layers of different densities. The formation of a pycnocline may result from changes in salinity or temperature. Because the pycnocline layer is extremely stable, it acts as a barrier for surface processes; and, therefore the changes in salinity and temperature are very small below the pycnocline but are seasonal in surface water.

Respiration: bacteria perform two major functions in the transformation of organic material: 1) they produce new bacterial biomass (bacterial production), and 2) they respire organic carbon to inorganic carbon (bacterial respiration).

Salinity: the total grams of salts in 1 kg of sea water.

Solubility pump, the: is driven by two processes in the ocean: 1) CO_2 solubility strongly related to sea water temperature where CO_2 is more soluble in cold waters, and 2) thermohaline circulation, driven by the formation of cold, dense water masses at high latitudes

Stratification: occurs when water masses with different properties – e.g., of salinity (halocline), density (pycnocline) and temperature (thermocline) – form layers that act as barriers to water mixing and, therefore, create barriers to nutrient-mixing between layers.

Sympagic: describes organisms that live where water exists mostly as a solid, i.e., sea ice.

TA: total alkalinity is related to the charge balance in sea water and in natural sea water at $\text{pH} > 8$ in $\mu\text{mol kg}^{-1}$ of seawater.

TCO_2 : in sea water, CO_2 exists in three inorganic forms: CO_2 (aq), HCO_3^- and CO_3^{2-} . The sum of the concentration of these forms is called total dissolved inorganic carbon, abbreviated TCO_2 , in $\mu\text{mol kg}^{-1}$ of seawater.

1.8 Literature cited

- Alou-Font E, Mundy J-C, Roy S, Gosselin M, Agusti S (2013) Snow cover affects ice algal pigment composition in the coastal Arctic Ocean during spring. *Mar Ecol Prog Ser* 474:89 – 104
- Alvarez-Aviles L, Simpson WR, Douglas TA, Sturm M, Perovich D, Domine F (2008) Frost flower chemical composition during growth and its implications for aerosol production and bromine activation. *J Geophys Res-Atmos* 113:D21304, doi:10.1029/2008JD010277
- Anderson LG, Falck E, Jones EP, Jutterström S, Swift JH (2004) Enhanced uptake of atmospheric CO₂ during freezing of seawater: a field study in Storfjord, Svalbard. *J Geophys Res* 109:C06004, doi:10.1029/2003JC002120
- Arendt KE, Nielsen TG, Rysgaard S, Tønnesson K (2010) Differences in plankton community structure along the Godthåbsfjord, from the Greenland Ice Sheet to offshore waters. *Mar Ecol Prog Ser* 401:49 – 162
- Arendt K, Dutz J, Jónasdóttir SH, Jung-Madsen S, Mortensen J, Møller EF, Nielsen TG (2011) Effects of suspended sediments on copepods feeding in a glacial influenced sub-Arctic fjord. *Jour Plankt Res* 33:1526 – 11537
- Arrigo KR, Dijken GL, Pabi S (2008) Impact of a shrinking Arctic ice cover on marine primary production. *Geophys Res Lett* 35:L19603, doi:10.1029/2008GL035028
- Arrigo KR, Mock T, Lizotte MP (2010) Primary production and sea ice. In: Thomas DN, Dieckmann GS (eds) *Sea ice*, 2nd Edition. Wiley-Blackwell Publishing Oxford, pp 283 – 1326
- Arrigo KR, Perovich DK, Pickart RS, Brown ZW, van Dijken GL, Lowry KE, Mills MM, Palmer MA, Balch WM, Bahr F, Bates NR, Benitez-Nelson C, Bowler B, Brownlee E, Ehn JK, Frey KE, Garley R, Laney SR, Lubelczyk L, Mathis J, Matsuoka A, Mitchell BG, Moore GWK, Ortega-Retuerta E, Pal S, Polashenski CM, Reynolds RA, Schieber B, Sosik HM, Stephens M, Swift JH (2012) Massive Phytoplankton Blooms Under Arctic Sea Ice. *Science* 336:1408 – 11408
- Assmy P, Ehn JK, Fernández-Mendez M, Hop H, Katlein C, Sundfjord A, Bluhm K, Daase M, Engel A, Fransson A, Granskog MA, Hudson SR, Kristiansen S, Nicolaus M, Peeken I, Renner AHH, Spreen G, Tatarek A, Wiktor J (2013) Floating ice-algal aggregates below melting Arctic sea ice. *PLOS* 8:1 – 113
- Assur A (1958) Composition of sea ice and its tensile strength, in Arctic Sea ice Conference Proceedings, pp. 106-138, NAS-NRC Publ. 598, Nat. Academy of Sci., Washington D.C
- Assur A (1960) Composition of sea ice and its tensile strength, Res. Rep. 44:49 pp. U.S. Army Snow Ice and Permafrost Res. Establ., Wilmette, Ill
- Bates NR (2006) Air-sea CO₂ fluxes and the continental shelf pump of carbon in the Chukchi Sea adjacent to the Arctic Ocean. *J Geophys Res* 111:C10013, doi:10.1029/2005JC003083
- Bates NR, Mathis JT (2009) The Arctic Ocean marine carbon cycle: evaluation of air-sea CO₂ exchanges, ocean acidification impacts and potential feedbacks. *Biogeosciences* 6:2433 – 12459
- Bischoff JL, Fitzpatrick JA, Rosenbauer RJ (1993) The solubility and stabilization of ikaite (CaCO₃ · H₂O) from 0° to 25°C: Environmental and paleoclimatic implications for thionolite tufa. *J Geol* 101:21 – 133
- Boetius A, Albrecht S, Bakker K, Bienhold C, Felden J, Fernandez-Mendez M, Hendricks A, Katlein C, Lalande C, Krumpfen T, Nicolaus M, Peeken I, Rabe B, Rogacheva A, Rybakova E, Somavilla R, Wenzhöfer F (2013) Export of algal biomass from the melting Arctic sea ice. *Science* 339:1430 – 11432
- Bowman JP (2008) Genomic analysis of psychrophilic prokaryotes. In: Psychrophiles: from Biodiversity to Biotechnology (Eds. R. Margesin, F. Schinner, J-C. Marx and C. Gerday) Springer-Verlag, Berlin, pp. 265 – 1284
- Bowman JS, Deming JW (2010) Elevated bacterial abundance and exopolymers in saline frost flowers and implications for atmospheric chemistry and microbial dispersal. *Geophys Res Lett* 37:L13501, doi:10.1029/2010GL043020
- Bowman JS, Larosa C, Vogel TM, Deming JW (2013) Selective occurrence of Rhizobiales in frost flowers on the surface of young sea ice near Barrow, Alaska and distribution in the polar marine rare biosphere. *Environ Microbiol Rep* 5: 575 – 1582
- Brent G, Else T, Galley RJ, Lansard B, Barber DG, Brown K, Miller LA, Mucci A, Papakyriakou TN, Tremblay J-E, Rysgaard S (2013) Further observations of a decreasing atmospheric CO₂ uptake capacity in the Canada Basin (Arctic Ocean) due to sea ice loss. *Geophys Res Lett* 40:1132 – 11137, doi:10.1002/grl.50268
- Buchardt B, Israelson C, Seaman P, Stockmann G (2001) Ikaite tufa towers in Ikka Fjord, southwest Greenland: Their formation by mixing of seawater and alkaline spring water. *J Sediment Res* 71:176 – 1189
- Buck KR, Nielsen TG, Hansen BW, Gastrup-Hansen D, Thomsen HA (1998) Infiltration phyto- and protozooplankton assemblages in the annual sea ice of Disko Island, West Greenland, spring 1996. *Polar Biol* 20:377 – 1381
- Cai W-J, Chen L, Chen B, Gao Z, Lee SH, Chen J, Pierrot D, Sullivan K, Wang Y, Hu X, Huang W-J, Zhang Y, Xu S, Murata A, Grebmeier JM, Jones EP, Zhang H (2010) Decrease in the CO₂ uptake capacity in an ice-free Arctic Ocean Basin. *Science* 329:556 – 1559
- Calbet A, Riisgaard K, Saiz E, Stedmon C, Nielsen TG (2011) Phytoplankton growth and microzooplankton grazing along a sub-Arctic fjord (Godthåbsfjord, West Greenland) *Mar Ecol Prog Ser* 442:11 – 122, doi:10.3354/meps09343
- Cameotra SS, Makkar RS (1998) Synthesis of biosurfactants in extreme conditions. *Appl Microbiol Biotechnol* 50: 520 – 1529
- Cavaliere DJ, Parkinson CL (2012) Arctic sea ice variability and trends, 1979 – 2010. *TC* 6: 881-889, doi: 10.5194/tc-6-881 – 12012
- Collins RE, Carpenter SD, Deming JW (2008) Spatial heterogeneity and temporal dynamics of particles and pEPS in Arctic winter sea ice. *J Mar Syst* 74:902 – 1917
- Collins RE, Rocap G, Deming JW (2010) Persistence of bacterial and archaeal communities in sea ice through an Arctic winter. *Environ Microbiol* 12:1828 – 11841

- Collins RE, Deming JW (2011) Abundant dissolved genetic material in Arctic sea ice, Part II: Virus dynamics during autumn freeze-up. *Polar Biol* 34:1831–1841
- Comiso JC (2003) Large-scale characteristics and variability of the global sea ice cover. In: Thomas DN, Dieckmann GS (eds), 1st Edition. *Sea ice: an introduction to its physics, chemistry, biology and geology*. Blackwell Science, Oxford, pp 112–1142
- Comiso JC, Parkinson CL, Gersten R, Stock L (2008) Accelerated decline in the Arctic sea ice cover. *Geophys Res Lett* 35:L01703, doi:10.1029/2007GL031972
- Comiso JC (2012) Large Decadal Decline of the Arctic Multiyear Ice Cover. *J Climate* 25:1176–11193
- Cota GF, Horne EPW (1989) Physical control of arctic ice algal production. *Mar Ecol Prog Ser* 52:111–1121
- Cota GF, Anning JL, Harris LR, Harrison WG, Smith REH (1990) The impact of ice algae on inorganic nutrients in seawater and sea ice in Barrow Strait, NWT, Canada during spring. *Can J Fish Aquat Sci* 47:1402–11415
- Cox GFN, Weeks WF (1974) Salinity variations in sea ice. *J Glaciol* 13:109–1120
- Cox GFN, Weeks WF (1983) Equations for determining the gas and brine volumes in sea-ice samples. *J Glaciol* 29:306–1316
- Crabeck O, Delille B, Thomas DN, Geilfus NX, Rysgaard S, Tison JL (2014) CO₂ and CH₄ in sea ice from a subarctic fjord. *Biogeosciences Discuss* 11:4047–14088, doi:10.5194/bgd-11-4047-2014
- Delille B (2006) Inorganic carbon dynamics and air-ice-sea CO₂ fluxes in the open and coastal waters of the Southern Ocean, PhD thesis, 296 pp. Univ. de Liège, Liège, France.
- Delille B, Jourdain B, Borges AV, Tison J-L, Delille D (2007) Biogas CO₂, O₂, dimethylsulfide dynamics in spring Antarctic fast ice. *Limnol Oceanogr* 52:1367–11379
- Deming J (2010) Sea ice bacteria and viruses. In: Thomas DN, Dieckmann GS (eds) *Sea ice*, 2nd Edition. Wiley-Blackwell Publishing Oxford, pp 247–1282
- Dieckmann GS, Nehrke G, Papadimitriou S, Göttlicher J, Steininger R, Kennedy H, Wolf-Gladrow D, Thomas DN (2008) Calcium carbonate as ikaite crystals in Antarctic sea ice. *Geophys Res Lett* 35:L08501, doi:10.1029/2008GL033540
- Dieckmann GS, Nehrke G, Uhlig C, Göttlicher J, Gerland S, Granskog MA, Thomas DN (2010) Brief communication: ikaite CaCO₃·6H₂O discovered in Arctic sea ice. *TC* 4:227–1230, doi:10.5194/tc-4-227-2010
- Domine F, Taillandier AS, Simpson WR, Severin K (2005) Specific surface area, density and microstructure of frost flowers. *Geophys Res Lett* 32: L13502, doi: 10.1029/2005GL023245
- Douglas TA, Domine F, Barret M, Anastasio C, Beine HJ, Bottenheim J, Grannas A, Houdier S, Netcheva S, Rowland G, Staebler R, Steffen A (2012) Frost flowers growing in the Arctic ocean-atmosphere-sea ice-snow interface: 1. Chemical composition. *J Geophys Res* 117:D00R09, doi: 10.1029/2011JD016460
- Drinkwater MR, Crocker GB (1988) Modelling changes in the dielectric and scattering properties of young snow-covered sea ice at GHz frequencies. *J Glaciol* 34:274–1282
- Eicken H, Lange MA (1989) Development and properties of sea ice in the coastal regime of the Southeastern Weddel Sea. *J Geophys Res-Ocean* 94:8193–18206, doi:10.1029/JC094iC06p08193
- Eicken H (2003) From the microscopic to the macroscopic to the regional scale, growth, microstructure and properties of sea ice. In: Thomas DN, Dieckmann GS (eds), 1st Edition. *Sea ice: an introduction to its physics, chemistry, biology and geology*. Wiley-Blackwell Publishing Oxford, pp 22–181
- Eicken H, Grefell TC, PErovich DK, Richter-Menge JA, Frey K (2004) Hydraulic controls of summer Arctic pack ice albedo. *J Geophys Res-Oceans* 109:C08007, doi:10.1029/2003JC001989
- Eicken H, Dmitrenko I, Tyshko K, Darovskikh A, Dierking W, Blahak U, Groves J, Kassens H (2005) Zonation of the Laptev Sea landfast ice cover and its importance in a frozen estuary. *Global Planet Change* 48: 55–183, doi:10.1016/j.gloplacha.2004.12.005
- Else BGT, Papkyriakou T, Asplin M, Barber D, Galley R, Miller L, Mucci A (2013a) Annual cycle of air-sea CO₂ exchange in an Arctic polynya region. *Glob Biogeochem Cycles* 27, doi:10.1002/gbc.20016
- Else BGT, Galley RJ, Lansard B, Barber DG, Brown K, Miller LA, Mucci A, Papkyriakou TN, Temblay JE, Rysgaard S (2013b) Further observations of a decreasing atmospheric CO₂ uptake capacity in the Canada Basin (Arctic Ocean) due to sea ice loss. *Geophys Res Lett* 40:1132–11137, doi:10.1002/grl.50268
- Else BGT, Papkyriakou TN, Galley RJ, Drennan WM, Miller LA, Mucci A, Thomas H (2011) Wintertime CO₂ fluxes in an Arctic polynya using eddy covariance: evidence of enhanced air-sea gas transfer during ice formation. *J Geophys Res* 116:C00G03, doi: 10.1029/2010JC006760
- Eronen-Rasimus W, Kaartokallio H, Lyra C, Autio C, Autio R, Kuosa H, Dieckmann GS, Thomas DN (2014) Bacterial community dynamics and activity in relation to dissolved organic matter availability during sea ice formation in a mesocosm experiment. *Microbiol* 3:139–1156
- Feller G, Gerday C (2003) Psychrophilic enzymes: hot topics in cold adaptation. *Nat Rev Microbiol* 1: 200–1208
- Fetterer F, Untersteiner N (1998) Observations of melt ponds on Arctic sea ice. *J Geophys Res-Oceans* 103:24821–124835
- Fischer M (2013) Sea ice and the air-sea exchange of CO₂. PhD thesis, University Bremen
- Fischer M, Thomas DN, Krell A, Nehrke G, Göttlicher J, Norman L, Meiners KM, Riaux-Gobin C, Dieckmann GS (2013) Quantification of ikaite in Antarctic sea ice. *Ant Sci* 25:421–1432
- Fransson A, Chierici M, Nojiri Y (2006) Increased net CO₂ outgassing in the upwelling region of the southern Bering Sea in a period of variable marine climate between 1995 and 2001. *J Geophys Res* 111: C08008, 10.1029/2004JC002759
- Fransson A, Chierici M, Nojiri Y (2009) New insights into the spatial variability of the surface water carbon dioxide in varying sea ice conditions in the Arctic Ocean. *Continent shelf Res* 29:1317–11328

- Fransson A, Chierici M, Yager PL, Smidt Jr. Wo (2011) Antarctic sea ice carbon dioxide system and controls. *J Geophys Res* 116:C12035. doi:10.1029/2010JC006844
- Fritsen CH, Ackley SF, Kremer JN, Sullivan CW (1998) Flood-freeze and microalgal dynamics in Antarctic pack ice, in *Antarctic sea ice: Biological processes, interactions and variability*. *Antarct Res Ser* 73:1 – 122
- Garrison DL, Buck KR (1986) Organisms losses during melting: A serious bias in sea ice community studies. *Polar Biol* 6:237 – 239
- Garrison DL, Close AR, Reimnitz E (1990) Microorganisms concentrated by frazil ice: evidence from laboratory experiments and field measurements. In *Sea Ice Properties and Processes* (eds) SF Ackley and WF Weeks, U.S. Army Corps of Engineers, Cold of Engineers, Cold Regions Research and Engineering Laboratory, Monograph 90-1, Pp. 92 – 196
- Geilfus N-X, Garnat G, Papakyriakou T, Tison JL, Else B, Thomas H, Shadwick E, Delille B (2012b) Dynamics of $p\text{CO}_2$ and related air-ice CO_2 fluxes in the Arctic coastal zone (Amundsen Gulf, Beaufort Sea). *J Geophys Res* 117:C00G10, doi:10.1029/2011JC007118
- Geilfus NX, Carnat G, Dieckmann GS, Halden N, Nehrke G, Papakyriakou T, Tison JL, Delille B (2013a) First estimates of the contribution of CaCO_3 precipitation to the release of CO_2 to the atmosphere during young sea ice growth. *J Geophys Res* 118:244 – 1255, doi:10.1029/2012JC007980
- Geilfus NX, Galley RJ, Crabeck O, Papkyriakou T, Landy J, Tison JL, Rysgaard S (2014) Inorganic carbon dynamics of melt pond-covered first year sea ice in the Canadian Arctic. *Biogeosciences Discuss* 11:7485 – 17519, doi: 10.5194/bgd-11-7485-2014
- Gibson J, Trull T (1999) Annual cycle of $f\text{CO}_2$ under sea-ice and in open water in Prydz Bay, East Antarctica. *Mar Chem* 66:187 – 1200
- Gleitz M, Thomas DN (1992) Physiological responses of a small Antarctic diatom (*Chaetoceros* sp.) to simulated environmental constraints associated with sea ice formation. *Mar Ecol Prog Ser* 88:271 – 1278
- Gleitz G, Rutgers VD, Thomas DN, Dieckmann GS, Millero FJ (1995) Comparison of summer and winter inorganic carbon, oxygen and nutrient concentrations in Antarctic sea ice brine. *Mar Chem* 51:81 – 191
- Glud RN, Rysgaard S, Kühl M, Hansen JW (2007) The sea ice in Young Sound: Implications for C cycling. In: *Carbon cycling in Arctic marine Ecosystems: Case study Young Sound*. Chapter 4 p: 62 – 185. Rysgaard S & Glud RN (Eds), *Carbon cycling in Arctic marine Ecosystem: Case study Young Sound*. Meddelsler om Grønland, Bioscience Vol 58. Copenhagen the Commission for Scientific Research in Greenland 2007
- Glud RN, Rysgaard S, Turner G, McGinnis DF, Leakey RJG (2014) Biological and physical-induced oxygen dynamics in melting sea ice of the Fram Strait. *Limnol Oceanogr* 59:1097 – 1111
- Golden K, Ackley SF, Lytle V (1998) The Percolation Phase Transition in Sea Ice. *Science* 282:2238 – 12241, doi:10.1126/science.282.5397.2238
- Golden KM, Eicken H, Heaton L, Miner J, Pringle D, Zhu J (2007) Thermal evolution of permeability and microstructure in sea ice. *Geophys Res Lett* 34:L16501, doi:10.1029/2007GL030447
- Gosselin M, Legendre L, Therriault J-C, Demers S, Rochet M (1986) Physical control of the horizontal patchiness of sea-ice microalgae. *Mar Ecol Prog Ser* 29:289 – 1298
- Gosselin M, Legendre L, Therriault J-C, Demers S (1990) Light and nutrient limitation of sea ice microalgae (Hudson Bay, Canadian Arctic). *J Phycol* 26:220 – 1232
- Gounot, A.M., Russell, N.J., 1999. Physiology of cold-adapted microorganisms. In: Margesin, R., Schinner, F. (Eds.), *Cold-adapted Organisms. Ecology, Physiology, Enzymology and Molecular Biology*. Springer, Berlin, pp. 33 – 155
- Gowing MM, Garrison DL, Gibson AH, Krupp JM, Jeffries MO, Fritsen CH (2004) Bacterial and viral abundance in Ross Sea summer pack ice communities. *Mar Ecol Prog Ser* 279:3 – 112
- Gradinger R, Ikävalko J (1998) Organism incorporation into newly forming Arctic sea ice in the Greenland Sea. *J Plankton Res* 20:871 – 1886
- Gradinger R, Friedrich C, Spindler M (1999) Abundance, biomass and composition of the sea ice biota of the Greenland Sea pack-ice. *Deep-Sea Res Part Li Top Stud Oceanogr* 46:1457 – 11472
- Gradinger R (2009) Sea ice algae: Major contributors to primary production and algal biomass in the Chukchi and Beaufort Seas during May/June 2002. *Deep-Sea Res PT II* 17: 1201 – 11212, doi:10.1016/j.dsr2.2008.10.016
- Grossmann S, Gleitz M (1993) Microbial responses to experimental sea-ice formation: implications for the establishment of Antarctic sea-ice communities. *J Exp Mar Biol Ecol* 173:273 – 1289
- Haas C, Hendricks S, Eicken H, Herber A (2010) Synoptic airborne thickness surveys reveal state of Arctic sea ice cover. *Geophys Res Lett* 37:L09501, doi:10.1029/2010GL042652
- Hansen PJ (2002) The effect of high pH on the growth and survival of marine phytoplankton: implications for species succession. *Aquat Microb Ecol* 28:279 – 1288
- Hare AA, Wang F, Barber D, Geilfus N-X, Galley R, Rysgaard S (2013) pH evolution in sea ice grown at an outdoor experimental facility. *Mar Chem* 154:46 – 164, doi:10.1016/j.marchem.2013.04.007
- Heinesch B, Tison JL, Carnat G, Eicken H, Geilfus N-X, Goosens T, Papakyriakou T, Yernaux M, Delille B (2010) Micrometeorological survey of air-sea ice CO_2 fluxes in arctic coastal waters. In *EGU Genral Assembly, 2 – 17 May, 2010, Vienna, Austria*
- Hinga KR (2002) Effect of pH on coastal marine phytoplankton. *Mar Ecol Prog Ser* 238:281 – 1300
- Horner R, Alexander V (1972) Algal populations in arctic sea ice: an investigation of heterotrophy. *Limnol Oceanogr* 17:454 – 1458
- Horner R, Schrader GC (1982) Relative contributions of ice algae, phytoplankton, and benthic microalgae to primary production in nearshore regions of the Beaufort Sea. *Arctic* 35:485 – 1503
- Horner RA (1985) Ecology of sea ice microalgae. In: Horner RA (Ed.), *Sea Ice Biota*. CRC Press, Boca Raton, FL, pp. 83 – 1103
- Hu Y-B, Wolf-Gladrow DA, Dieckmann GS, Völker C, Nehrke G (2014) A laboratory study of ikaite ($\text{CaCO}_3 \cdot 6\text{H}_2\text{O}$) precipitation as a function of pH, salinity, temperature and phosphate concentration. *Mar Chem* 162:10 – 118

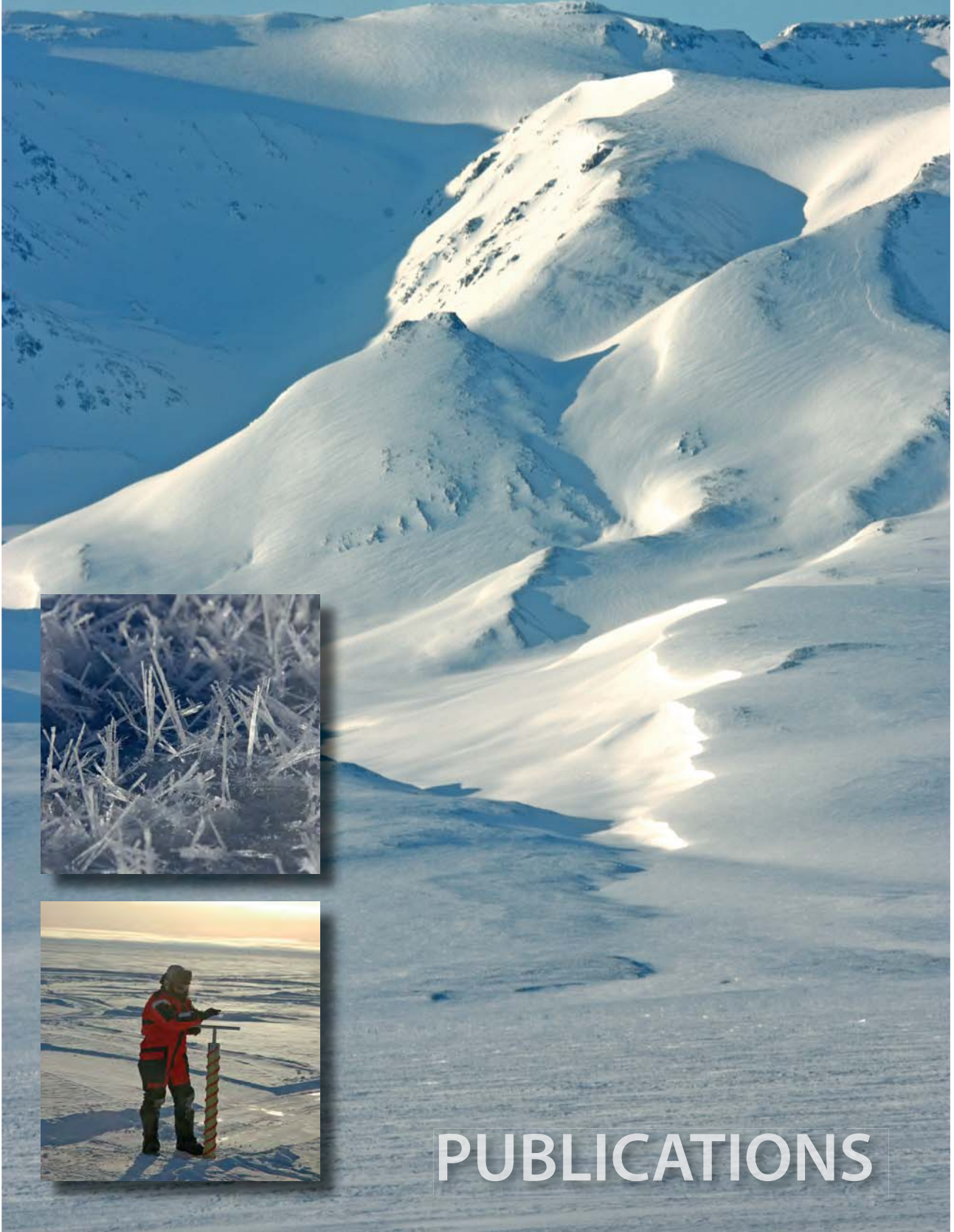
- Huertas IE, Colman B, Espie GS, Lubian LM (2000) Active transport of CO₂ by the three species of marine microalgae. *J Phycol* 36:314 – 1320
- Inall ME, Murray T, Cottier FR, Scharrer K, Boyd TJ, Heyword KJ, Bevan SL (2014) Oceanic heat delivery via Kangerdlugssuaq Fjord to the south-east Greenland ice sheet. *J Geophys Res-Ocean* 119:1 – 115, doi:10.1002/2013JC009295
- Isleifson D, Galley RJ, Barber DG, Landy JC, Komarov AS, Shafai L (2013) A study on the C-band polarimetric scattering and physical characteristics of frost flowers on experimental sea ice. *IEEE Trans Geosci Remote Sensing* 52:1787 – 11798
- Jakobsson, M Grantz A, Kristoffersen Y, Macnab R (2004) Bathymetry and physiography of the Arctic Ocean and its constituent seas. In Stein R & MacDonald RW (eds) *The organic carbon cycle in the Arctic Ocean*. Springer Verlag Berlin Heidelberg New York, pp. 1 – 16
- Jones EP, Coote AR (1981) Oceanic CO₂ produced by the precipitation of CaCO₃ from brines in sea ice. *J Geophys Res* 86: 11041 – 111043, doi:10.1029/JC086iC11p11041
- Juul-Pedersen, Arendt KE, Mortensen J, Blicher M, Søgaard DH, Rysgaard S (submitted) Seasonal and interannual phytoplankton production in a sub-arctic fjord (Godthåbsfjord) connected to the Greenland Ice Sheet. *Mar Ecol Prog Ser*
- Kaartokallio H (2004) Food web components, and physical and chemical properties of Baltic Sea ice. *Mar Ecol Prog Ser* 273:49 – 163
- Kaartokallio H, Kuosa H, Thomas DN, Granskog MA, Kivi K (2006) Biomass, composition and activity of organism assemblages along a salinity gradient in sea ice subjected to river discharge in the Baltic Sea. *Polar Biol* 30:183 – 1197
- Khan SA, Kjær KH, Bevis M, Bamber JL, Wahr J, Kjeldsen KK, Bjørk AA, Korsgaard NJ, Stearns LA, Broeke MR, Liu L, Larsen NK, Muresan LS (2014) Sustained mass loss of the northeast Greenland ice sheet triggered by regional warming. *Nature Climate Change* 4:292 – 1299, doi:10.1038/NCLIMATE2161
- Killawee JA, Fairchild IJ, Tison JL, Janssens L, Lorrain R (1998) Segregation of solutes and gases in experimental freezing of dilute solutions: Implications for natural glacial systems. *Geochim Cosmochim Acta* 62:3637 – 13655
- Korb RE, Saville PJ, Johnston AM, Raven J (1997) Sources of inorganic carbon for photosynthesis by three species of marine diatoms. *J Phycol* 33:433 – 1440
- Krell A, Funck D, Plettner I, John U, Dieckmann G (2007) Regulation of proline metabolism under salt stress in the psychrophilic diatom *Fragilariopsis cylindrus* (Bacillariophyceae). *J Phycol* 43: 753 – 1762
- Kuosa H, Borrmann B, Kivi K, Brandini F (1992) Effects of Antarctic sea ice biota on seeding as studied in aquarium experiments. *Polar Biol* 12:333 – 1339
- Kühl M, Glud RN, Borum J, Roberts R, Rygaard S (2001) Photosynthetic performance of surface-associated algae below sea ice as measured with a pulse-amplitude-modulated (PAM) fluorometer and O₂ microsensors. *Mar Ecol Prog Ser* 223:1 – 114
- Lannuzel D, Schoermann V, Jong JD, Tison J-L, Chou L (2007) Distribution and biogeochemical behaviour of iron in the East Antarctic sea ice. *Mar Chem* 106:18 – 132
- Lavoie D, Denman K, Michel C (2005) Modeling ice algal growth and decline in a seasonally ice-covered region of the Arctic (Resolute Passage, Canadian Archipelago). *J Geophys Res-Ocean* 110: C11009, doi:10.1029/2005JC002922
- Lazzara L, Nardello I, Ermanni C, Mangoni O, Saggiomo V (2007) Light environment and seasonal dynamics of microalgae in the annual sea ice at Terra Nova Bay, Ross Sea, Antarctica. *Antarct Sci* 19: 83 – 192
- Lee SH, Stockwell DA, Joo H-M, Son YB, Kang C-K, Whitledge TE (2012) Phytoplankton production from melting ponds on Arctic sea ice. *J Geophys Res* 117:C04030, doi:10.1029/2011JC007717
- Legendre L, Ackley SF, Dieckmann GS, Gulliksen B, Horner R, Hoshiai T, Melnikov IA, Reeburgh WS, Spindler M, Sullivan CW (1992) Ecology of sea ice biota. *Polar Biol* 12:429 – 1444
- Leu E, Wiktor J, Søreide JE, Berge J, Falk-Petersen S (2010) Increased irradiance reduced food quality of sea ice algae. *Mar Ecol Prog Ser* 411:49 – 160
- Leu E, Søreide JE, Hessen DO, Falk-Pedersen S, Berge J (2011) Consequences of changing sea ice cover for primary production and secondary producers in the European Arctic Shelf seas: Timing, quantity and quality. *Prog Oceanography* 90:18 – 132
- Leu E, Mundy CJ, Assmy P, Campbell K, Gabrielsen TM, Gosselin M, Juul-Pedersen T, Gradinger R (submitted) Arctic spring awakening – steering principles behind the phenology of vernal ice algae blooms
- Long MH, Koopmans D, Berg P, Rysgaard S, Glud RN, Søgaard DH (2012) Oxygen exchange and ice melt measured at the ice-water interface by eddy correlation. *BG* 9:1957 – 11967, doi:10.5194/bg-9-1-2012
- Loose B, Miller LA, Elliott S, Papakyriakou T (2011a) Sea Ice Biogeochemistry and Material Transport Across the Frozen Interface. *Ocean* 24:203 – 1218
- Loose B, Schlosser P, Perovich DK, Ringelberg D, Ho D, Takahashi T, Richter-Menge JA, Reynolds C, McGillis W, Tison JL (2011b) Gas diffusion through columnar laboratory sea ice: implications for mixed-layer ventilation of CO₂ in the seasonal ice zone. *Tellus* 63B:23 – 139, doi:10.1111/j.1600-0889.2010.00506.x
- Lüthje M, Feltham Taylor PD, Worster MG (2006) Modeling the summertime evolution of sea ice melt ponds. *J Geophys Res* 111:C02001, doi:10.1029/2004JC002818
- Lydersen C, Assmy P, Falk-Petersen S, Kohler J, Kovacs KM, Reigstad M, Steen H, Strøm H, Sundfjord A, Varpe Ø, Walczowski W, Weslawski JM, Zajaczkowski M (2014) The importance of tidewater glaciers for marine mammals and seabirds in Svalbard, Norway. *J Mar Syst* 129:452 – 1471
- MacGilchrist GA, Garabato CAN, Tsubouchi T, Bacon S, Torres-Valdés S, Azetsu-Scott K (2014) The Arctic Ocean carbon sink. *Deep-Sea Res I* 86:39 – 155
- Marion GM (2001) Carbonate mineral solubility at low temperatures in the Na-K-Mg-Ca-H-Cl-SO₄-OH-HCO₃-CO₃-CO₂-H₂O system. *Geochim Cosmochimica Acta* 65:1883 – 11896
- Martin S, Drucker R, Fort M (1995) A laboratory study of frost flower growth on the surface of young sea ice. *J Geophys Res* 100:7027 – 17036, doi:10.1029/94JC03243

- Marx JG, Carpenter SD, Deming JW (2009) Production of cryo-protectant extracellular polysaccharide substances (EPS) by the marine psychrophilic bacterium *Colwellia psychrerythraea* strain 34H under extreme conditions. *Can J Microbiol* 55: 63 – 172, doi:10.1139/W08-130
- Miller L, Garnat G, Else B, Sutherland N, Papakyriakou T (2011a) Carbonate system evolution at the Arctic Ocean surface during autumn freeze-up. *J Geophys Res* 116:C00G04, doi:10.1029/2011JC007143
- Miller LA, Papakyriakou TN, Collins RE, Deming JW, Ehn JK, Macdonald RW, Mucci A, Owens O, Raudsepp M, Sutherland N (2011b) Carbon dynamics in sea ice: A winter flux time series. *J Geophys Res* 116:C02028, doi:10.1029/2009JC006058
- Millero FJ (1995) Thermodynamic of the carbon dioxide system in the ocean. *Geochim Cosmochim Acta* 59:661 – 1677
- Mikkelsen DM, Rysgaard S, Glud RN (2008) Microalgal composition and primary production in Arctic sea ice: a seasonal study from Kobbefjord (Kangerluarsunnguaq), West Greenland. *Mar Ecol Prog Ser* 368:65 – 174
- Mikkelsen DM, Witkowski A (2010) Melting sea ice for taxonomic analysis: a comparison of four melting procedures. *Polar Res*, doi:10.1111/j.1751-8369.2010.00162.x
- Mock T, Gradinger R (1999) Determination of Arctic ice algal production with a new in situ incubation technique. *Mar Ecol Prog Ser* 177:15 – 126
- Mortensen J, Lennert K, Bendtsen J, Rysgaard S (2011) Heat sources for glacial melt in a sub-Arctic fjord (Godthåbsfjord) in contact with the Greenland Ice Sheet. *J Geophys Res* 116, C01013, doi:10.1029/2010JC006528
- Mortensen J, Bendtsen J, Motyka RJ, Lennert K, Truffer M, Fahnestock M, Rysgaard S (2013) On the seasonal freshwater stratification in the proximity of fast-flowing tidewater outlet glaciers in a sub-Arctic sill fjord. *J Geophys Res-Oceans* 118:1382 – 11395, doi:10.1002/jgrc.20134
- Mundy CJ, Gosselin M, Ehn J, Gratton Y, Rossnagel A, Barber DG, Martin J, Tremblay J-E, Palmer M, Arrigo KR, Darnis G, Fortier L, Else B, Papakyriakou T (2009) Contribution of under-ice primary production to an ice-edge upwelling phytoplankton bloom in the Canadian Beaufort Sea. *Geophys Res Lett* 36:L17601, doi:10.1029/2009GL038837
- Mundy CJ, Gosselin M, Gratton Y, Brown K, Galindo V, Campbell K, Levasseur M, Barber D, Papakyriakou T, Bélanger S (2013) Role of environmental factors on phytoplankton bloom initiation under landfast sea ice in Resolute Passage, Canada. *Mar Ecol Prog Ser* 497:39 – 149
- Munro DR, Dunbar RB, Mucciarone DA, Arrigo KR, Long MC (2010) Stable isotope composition of dissolved inorganic carbon and particulate organic carbon in sea ice from the Ross Sea, Antarctica. *J Geophys Res-Ocean* 115:C09005, doi:10.1029/2009JC005661
- Nansen F (1906) Northern Waters: Captain Roald Amundsen's oceanographic observations in the Arctic Seas in 1901. In commission by Jacob Dybvad, Christiania.
- Nakaoka S-I, Aoki S, Nakazawa T, Hashida G, Morimoto S, Yamanouchi T, Yoshikawa-Inoue H (2006) Temporal and spatial variations of oceanic $p\text{CO}_2$ and air-sea CO_2 flux in the Greenland Sea and the Barents Sea. *Tellus* 58B:148 – 1161
- Nedashkovsky A, Khvedynich S, Petrovsky T (2009). Alkalinity of sea ice in the High-Latitudinal Arctic according to the surveys performed at North Pole Drifting Station 34 and characterization of the role of the Arctic ice in the CO_2 exchange. *Mar Chem* 49:61 – 169
- Nicolaus M, Haas C, Willmes S (2009) Evolution of first-year and second-year snow properties on sea ice in the Weddell Sea during spring-summer transition. *J Geophys Res-Atmos* 114:1 – 117, doi:10.1029/2008JD011227
- Nicolaus M, Katlein C, Maslanik J, Hendricks S (2012) Changes in Arctic sea ice result in increasing light transmittance and absorption. *Geophys Res Lett* 39:L24501, doi:10.1029/2012GL053738
- Nomura DH, Yoshikawa-Inoue, Toyota T (2006) The effect of sea-ice growth on a air-sea CO_2 flux in a tank experiment. *Tellus B Chem Phys Meteorol* 58:418 – 1426
- Nomura D, Eicken H, Gradinger R, Shirasawa K (2010a) Rapid physically driven inversion of the air-sea ice CO_2 flux in the seasonal land fast ice off Barrow, Alaska after onset of surface melt. *Continental Shelf Res* 30:1998 – 12004, doi:10.1016/j.csr.2010.09.014
- Nomura D, Yoshikawa-Inoue H, Toyota T, Shirasawa K (2010b) Effects of snow, snowmelting and refreezing processes on air-sea ice CO_2 flux. *J Glaciol* 56:262 – 1270
- Nomura D, Granskog MA, Assemy P, Simizu D, Hashida G (2013a) Arctic and Antarctic sea ice acts as a sink for atmospheric CO_2 during periods of snowmelt and surface flooding. *J Geophys Res-Ocean* 118:6511 – 16524, doi:10.1002/2013JC009048
- Nomura D, Assmy P, Nehrke G, Granskog MA, Fischer M, Dieckmann GS, Fransson A, Hu Yubin, Schnetger B (2013b) Characterization of ikaite ($\text{CaCO}_3 \cdot 6\text{H}_2\text{O}$) crystals in first-year Arctic sea ice north of Svalbard. *Annals Glaciology* 62:125 – 1131, doi:10.3189/2013AoG62A034
- Parkinson CL (2000) Variability of Arctic sea ice: The view from space and 18-year record. *Arctic* 53:341 – 1358
- Papadimitriou S, Kennedy H, Kattner G, Dieckmann GS, Thomas DN (2004) Experimental evidence for carbonate precipitation and CO_2 degassing during sea ice formation. *Geochim Cosmochim Acta* 68:1749 – 11761
- Papadimitriou S, Thomas DN, Kennedy H, Haas C, Kuosa H, Krell A, Dieckmann GS (2007) Biogeochemical composition of natural sea ice brines from the Weddell Sea during early austral summer. *Limnol Oceanogr* 52:1809 – 11823
- Papadimitriou S, Thomas D, Kennedy H, Kuosa H, Dieckmann GS (2009) Inorganic carbon removal and isotopic enrichment in Antarctic sea ice gap layers during early austral summer. *Mar Ecol Prog Ser* 386:15 – 127
- Papadimitriou S, Kennedy H, Norman L, Kennedy DP, Dieckmann GS, Thomas DN (2012) The effect of biological activity, CaCO_3 mineral dynamics and CO_2 degassing in the inorganic carbon cycle in sea ice in late winter-early spring in the Weddell Sea, Antarctica. *J Geophys Res* 117:C08011, doi:10.1029/2012JC008058

- Papakyriakou T, Miller L (2011) Springtime CO₂ exchange over seasonal sea ice in the Canadian Arctic Archipelago. *Annals Glaciol* 52:215 – 1224
- Pedersen JTP, Kaufmann LH, Kroon A, Jakobsen BH (2010) The northeast Greenland Sirius Water Polynya dynamics and variability inferred from satellite imagery. *Geografisk Tidsskrift* 110:131 – 1142
- Perovich DK, Richter-Menge JA (1994) Surface characteristics of lead ice. *J Geophys Res Lett* 99:16341 – 116350, doi:10.1029/94JC01194
- Perovich DK (1996) The optical properties of sea ice, *CRREL Monograph*, 96 – 11, 25 pp
- Perovich DK, Jones KF, Light B, Eicken H, Markus T, Stroeve J, Lindsay R (2011) Solar partitioning in a changing Arctic sea-ice cover. *Ann Glaciol* 52:192 – 1196, doi:10.3189/172756411795931543
- Petrich C, Eicken H (2010) Growth, Structure and Properties of sea ice. In: Thomas DN, Dieckmann GS (eds) *sea ice*, 2nd Edition. Wiley-Blackwell Publishing Oxford, pp 23 – 178
- Polashenski C, Perovich D, Courville Z (2012) The mechanisms of sea ice melt pond formation and evolution. *J Geophys Res-Oceans* 117:C01001, doi:10.1029/2011JC007231
- Ralph PJ, Ryan KG, Martin A, Fenton G (2007) Melting out of sea ice causes greater photosynthetic stress than freezing in. *J Phycol* 43: 948 – 1956
- Ramaswamy V, Chanin M-L, Angell J, Barnett J, Gaffen D, Gelman M, Keckhut P, Koshelkov Y, Labitzke K, Lin J-JR, O'Neill A, Nash J, Randel W, Rood R, Shine K, Shiotani M, Swinbank R (2001) Stratospheric temperature trends: Observation and model simulations. *Review Geophys* 39:71 – 1122, doi:10.1029/199RG000065
- Rankin AM, Auld V, Wolff EW (2000) Frost flowers as a source of fractionated sea salt aerosol in the polar regions. *Geophys Res Lett* 27:3469 – 13472
- Rankin AM, Wolff EW, Martin S (2002) Frost flowers: Implications for tropospheric chemistry and ice core interpretation. *J Geophys Res-Atmos* 107:D23, doi:10.1029/2002JD002492
- Raven J (1980) Limits on growth rate. *Nature* 361:209 – 1210
- Reimnitz E, Marincovich L Jr, McCormick M, Briggs WM (1992) Suspension freezing of bottom sediment and biota in the Northwest Passage and implications for Arctic Ocean sedimentation. *Can J Earth Sci* 29:693 – 1703
- Richardson C (1976) Phase relationships in sea ice as a function of temperature. *J Glaciol* 17:507 – 519
- Riedel A, Michel C, Gosselin M, LeBlanc B (2007) Enrichment of nutrients, exopolymeric substances and microorganisms in newly formed sea ice on the Mackenzie Shelf. *Mar Ecol Prog Ser* 342:55 – 67
- Roscoe HK, Brooks B, Jackson AV, Smith MH, Walker SJ, Obbard RW, Wolff EW (2011) Frostflowers in the laboratory: Growth, characteristics, aerosol and the underlying sea ice. *J Geophys Res* 116: D12301, doi:10.1029/20010JD 015144
- Rösel A, Kaleschke L (2012) Exceptional melt pond occurrence in the years 2007 and 2011 on the Arctic sea ice revealed from MODIS satellite data. *J Geophys Res-Oceans* 117: C05018, doi:10.1029/2011JC007869
- Ròzanska M, Poulin M, Gosselin M (2008) Protist entrapment in newly formed sea ice in the coastal Arctic Ocean. *J Mar Sys* 74:887 – 1901
- Ròzanska M, Gosselin M, Poulin M, Wiktor MP, Michel C (2009) Influence of environmental factors on the development of bottom ice protist communities during the winter-spring transition. *Mar Ecol Prog Ser* 386: 43 – 159
- Ryan KG, Ralph PJ, McMinn A (2004) Acclimation of Antarctic bottom-ice algal communities to lowered salinities during melting. *Polar Biol* 27:679 – 186
- Rysgaard S, Kühl M, Glud RN, Hansen JW (2001) Biomass, production and horizontal patchiness of sea ice algae in a high-Arctic fjord (Young Sound, NE Greenland). *Mar Ecol Prog Ser* 223:15 – 26
- Rysgaard S, Glud R (Eds.) (2007) *Carbon cyclin in Arctic marine ecosystem: Case study Young Sound*. Meddr Grønland, Bioscience 58. Copenhagen, the Commision of Scientific Research in Greenland, 214 pp
- Rysgaard S, Glud RN, Sejr MK, Bendtsen J, Christensen PB (2007) Inorganic carbon transport during sea-ice growth and decay: A carbon pump in polar seas. *J Geophys Res* 112:C03016, doi:10.1029/2006JC003572
- Rysgaard S, Arendt K, Frederiksen M. et al. (2008) Nuuk Basic: The Marine Basic Program 2005-2006. In Klitgaard AB, Rasch M and Caning K (eds.), *Nuuk Ecological Research Operations, 1st Annual Report 2008*. Danish Polar Center, Copenhagen
- Rysgaard S, Bendtsen J, Petersen LT, Ramløv J, Glud RN (2009) Increased CO₂ uptake due to sea ice growth and decay in the Nordic Seas. *J Geophys Res* 114:C09011, doi:10.1029/2008JC005088
- Rysgaard S, Bendtsen J, Delille B, Dieckmann GS, Glud RN, Kennedy H, Mortensen J, Papadimitriou S, Thomas DN, Tison JL (2011) Sea ice contribution to the air-sea CO₂ exchange in the Arctic and Southern Oceans. *Tellus B* 63:823 – 830, doi:10.1111/J.1600-0889-2011.005471.x
- Rysgaard S, Glud RN, Lennert K, Cooper M, Halden N, Leaky R, Hawthorne FC, Barber D (2012) Ikaite crystals in melting sea ice – implications for pCO₂ and pH levels in Arctic surface waters. *TC* 6:1015 – 11035, doi:10.5194/tcd-6-015-2012
- Rysgaard S, Wang F, Galley RJ, Grimm R, Notz D, Lemes M, Geilfus NX, Chaulk A, Hare AA, Crabeck O, Else BGT, Campbell K, Sørensen LL, Sievers J, Papakyriakou T (2014) Temporal dynamics of ikaite in experimental sea ice. *TC* 8:1469 – 11478, doi:10.5194/tc-8-1469-2014
- Sabine CL, Feely RA, Gruber N, Key RM, Lee K, Bullister JL, Wanninkhof R, Wong CS, Wallace DWR, Tilbrook B, Millero FJ, Peng T-H, Kozyr A, Ono T, Rios AF (2004) The oceanic sink for anthropogenic CO₂. *Science* 305: 367 – 1371, doi:10.1126/science.1097403
- Sakshaug E (2004) Primary and secondary production in the Arctic seas. In: Stein R, Macdonald RW (eds) *The organic carbon cycle in the Arctic Ocean*, 2nd Edition. Springer-Verlag Berlin Heidelberg. Pp: 57 – 181
- Sejr MK, Krause-Jensen D, Rysgaard S, Sørensen LL, Christensen PB, Glud RN (2011) Air-sea flux of CO₂ in arctic coastal waters influenced by glacial melt water and sea ice. *Tellus B* 63:815 – 1822, doi:10.1111/j.1600-0889.2011.00540.x

- Selleck BW, Carr PF, Jones BG (2007) A review and synthesis of Glendonites (Pseudomorphs after ikaite) with new data. Assessing applicability as recorders of ancient coldwater conditions. *J Sediment Res* 77:980 – 1991
- Semiletov I, Makshtas A, Aksofu SI (2004) Atmospheric CO₂ balance: The role of Arctic sea ice. *Geophys Res Lett* 31:L05121, doi:10.1029/2003GL017996
- Semiletov IP, Pipko II, Repina I, Shakhova NE (2007) Carbonate chemistry dynamics and carbon dioxide fluxes across the atmosphere-ice-water interfaces in the Arctic Ocean: Pacific sector of the Arctic. *J Mar Syst* 66:204 – 1226
- Smith REH, Clement P (1990) Heterotrophic activity and bacterial productivity in assemblages of microbes from Sea ice in the High Arctic. *Polar Biol* 10:351 – 1357
- Stoecker DK, Gustafson DE, Merrell JR, Black MMD, Baier CT (1997) Excystment and growth of chrysophytes and dinoflagellates at low temperatures and high salinities in Antarctic sea-ice. *J Phycol* 33:585 – 1595
- Stroeve J, Holland MM, Meier W, Scambos T, Serreze M (2007) Arctic sea ice decline: faster than forecast. *Geophys Res Lett* 34:L09501, doi:10.1029/2007GL029703
- Stroeve JC, Serreze MC, Holland MM, Kay JE, Malanik J, Barrett AP (2012) The Arctic's rapidly shrinking sea ice cover: a research synthesis. *Climatic Change* 110:1005 – 11027
- Sturm M, Massom RA (2010) Snow and Sea Ice. In Thomas DN and Dieckmann GS, 2nd editors, *Sea Ice*. Blackwell Science, Oxford, pp 153 – 1204
- Style RW, Worster MG (2009) Frost flower formation on sea ice and lake ice. *Geophys Res Letter* 36:L11501, doi:10.1029/2009GL037304
- Sørensen LL, Jensen B, Glud RN, McGinnis DF, Sejr MK, Sievers J, Søgaard DH, Tison JL, Rysgaard S (2014) Parameterization of atmospheric-surface exchange of CO₂ over sea ice. *CD* 8:853 – 1866, doi:10.5194/tc-8-853-2014
- Takahashi T, Sutherland SC, Wanninkhof R, Sweeney C, Feely RA, Chipman DW, Hales B, Friederich G, Chavez F, Sabine C, Watson A, Bakker DCE, Schuster U, Metzl N, Yoshikawa-Inoue H, Ishii M, Midorikawa T, Nojiri Y, Kortzinger A, Steinhoff T, Hoppema M, Olafsson J, Arnarson TS, Tilbrook B, Johannessen T, Olsen A, Bellerby R, Wong S, Delille B, Bates NR, de Baar HJW (2009) Climatological mean and decadal change in surface ocean pCO₂, and net sea-air CO₂ flux over the global oceans. *Deep-Sea Res PT II* 56:554 – 1577, doi:10.1016/J.dsr2.2008.12.009
- Taraldsvik M, Mykkestad SM (2000) The effect of pH on the growth rate, biochemical composition and extracellular carbohydrate production of the marine diatom *Skeletonema costatum*. *Eur J Phycol* 35:189 – 194
- Timco GW, Weeks WF (2010) A review of the engineering properties of sea ice. *Cold Reg Sci Technol* 60:107 – 1129
- Thomas DN, Kennedy H, Kattner G, Gerdes D, Gough C, Dieckmann GS (2001b) Biogeochemistry of platelet ice: its influence on particle flux under fast ice in the Weddell Sea, Antarctica. *Polar Biol* 24:486 – 1496
- Thomas DN, Dieckmann GS (2002) Antarctic sea ice – a habitat for extremophiles. *Science* 95: 641 – 1644, doi:10.1126/science.1063391
- Thomas DN, Papadimitriou S, Michel C (2010) Biogeochemistry of sea ice. In: Thomas DN, Dieckmann GS (eds) *sea ice*, 2nd Edition. Wiley-Blackwell Publishing Oxford, pp 425 – 1469
- Tison J-L, Haas C, Gowing MM, Sleewaegen S (2002) Tank study of physic-chemical controls on gas content and composition during growth of young sea ice. *J Glaciol* 48:177 – 1191
- Untersteiner N (1968) Natural desalination and equilibrium salinity profile of perennial sea ice. *J Geophys Res* 73:1251 – 11257, doi:10.1029/JB073i004p01251
- Vézina AF, Demers S, Laurion I, Sime-Ngando T, Juniper SK, Devine L (1997) Carbon flows through the microbial food web of first-year ice in Resolute Passage (Canadian High Arctic). *J Mar Syst* 11:173 – 1189
- Weeks WF, Ackley (1982) The growth, structure, and properties of sea ice. 117 pp., CRREL Monograph
- Weeks WF (2010) Sea ice structure. In: Weeks WF (eds) *On sea ice*. University of Alaska Press, pp 78 – 1144
- Xie HX, Belanger S, Demers S, Vincent WF, Papakyriakou TN (2009) Photobiogeochemical cycling of carbon monoxide in the southeastern Beaufort Sea in spring and autumn. *Limnol Oceanogr* 54:234 – 1249, doi:10.4319/lo.2009.54.1.0234
- Zemmelink HJ, Delille B, Tison JL, Hintsa EJ, Houghton L, Dacey JWH (2006) CO₂ deposition over the multi-year ice of the western Weddell Sea. *Geophys Res Lett* 33:1 – 14, doi:10.1029/2006GL026320
- Zhou J, Delille B, Eicken H, Vancoppenolle M, Brabant F, Carnat G, Geilfus NX, Papakyriakou T, Heinesch B, Tison JL (2013) Physical and biogeochemical properties in landfast sea ice (Barrow, Alaska): insights on brine and gas dynamics across seasons. *J Geophys Res-Oceans* 118:3172 – 13189

CHAPTER 2



PUBLICATIONS

PAPER I



Photo: Dorte H. Søgaard.

The relative contributions of biological and abiotic processes to carbon dynamics in subarctic sea ice

D.H. Søgaard • D.N. Thomas • S. Rysgaard • R. N. Glud •
L. Norman • H. Kaartokallio • T. Juul-Pedersen • N. X. Geilfus

Polar Biology 36:1761 – 1777, doi: 10.1007/s00300-013-1396-3

The relative contributions of biological and abiotic processes to carbon dynamics in subarctic sea ice

Dorte Haubjerg Sørensen · David N. Thomas · Søren Rysgaard ·
Ronnie Nøhr Glud · Louiza Norman · Hermann Kaartokallio ·
Thomas Juul-Pedersen · Nicolas-Xavier Geilfus

Received: 6 December 2012 / Revised: 9 July 2013 / Accepted: 10 August 2013 / Published online: 4 September 2013
© The Author(s) 2013. This article is published with open access at Springerlink.com

Abstract Knowledge on the relative effects of biological activity and precipitation/dissolution of calcium carbonate (CaCO_3) in influencing the air-ice CO_2 exchange in sea-ice-covered season is currently lacking. Furthermore, the spatial and temporal occurrence of CaCO_3 and other biogeochemical parameters in sea ice are still not well described. Here we investigated autotrophic and heterotrophic activity as well as the precipitation/dissolution of CaCO_3 in subarctic sea ice in South West Greenland. Integrated over the entire ice season (71 days), the sea ice was net autotrophic with a net carbon fixation of 56 mg C m^{-2} , derived from a sea-ice-related gross primary production of 153 mg C m^{-2} and a bacterial carbon demand of 97 mg C m^{-2} . Primary production contributed only marginally to the TCO_2 depletion of the sea ice (7–25 %), which was mainly controlled by physical export by brine drainage and CaCO_3 precipitation. The net biological production could only explain 4 % of this sea-ice-driven CO_2 uptake. Abiotic processes contributed to an air-sea CO_2 uptake of $1.5 \text{ mmol m}^{-2} \text{ sea ice day}^{-1}$, and

dissolution of CaCO_3 increased the air-sea CO_2 uptake by 36 % compared to a theoretical estimate of melting CaCO_3 -free sea ice. There was a considerable spatial and temporal variability of CaCO_3 and the other biogeochemical parameters measured (dissolved organic and inorganic nutrients).

Keywords Subarctic · Sea ice · Spatial variability · CaCO_3 · Net biological production · DOC and DON

Introduction

Sea ice has previously been considered to be an impermeable barrier to gas exchange, and global climate models do not include CO_2 exchange with the oceans during periods of closed ice cover (Tison et al. 2002; Loose et al. 2011; Rysgaard et al. 2011). However, recent observations of gas exchange using both tower-based micrometeorological approaches and chamber sampling indicate that

D. H. Sørensen (✉) · S. Rysgaard · R. N. Glud ·
T. Juul-Pedersen
Greenland Climate Research Centre (C/O Greenland
Institute of Natural Resources), Kivioq 2, Box 570,
3900 Nuuk, Greenland
e-mail: doso@natur.gl

D. H. Sørensen · R. N. Glud
University of Southern Denmark, Campusvej 55,
5230 Odense M, Denmark

D. N. Thomas · L. Norman
School of Ocean Sciences, Bangor University,
Menai Bridge, Anglesey LL59 5AB, UK

D. N. Thomas · H. Kaartokallio
Finnish Environment Institute, Marine Research Centre,
Erik Palmenin Aukio 1, 00560 Helsinki, Finland

D. N. Thomas · S. Rysgaard
Arctic Research Centre, Aarhus University, C.F. Møllers Allé 8,
bldg. 1110, 8000 Aarhus C, Denmark

S. Rysgaard · N.-X. Geilfus
Centre for Earth Observation Science, CHR Faculty
of Environment Earth and Resources, University of Manitoba,
499 Wallace Building, Winnipeg, MB R3T 2N2, Canada

R. N. Glud
Scottish Association for Marine Science, Scottish Marine
Institute, Oban, UK

uptake and degassing of CO₂ does occur over sea ice (Semiletov et al. 2004; Zemmeling et al. 2006; Delille et al. 2007; Nomura et al. 2010; Miller et al. 2011; Papakyriakou and Miller 2011; Geilfus et al. 2012). In addition, the recognition that there are extensive and active microorganism communities within sea ice, and the finding of the sea-ice-driven carbon pump (Rysgaard et al. 2007), has changed this general perception. Sea ice is now considered to be an active component in the biogeochemical cycling of carbon in ice-covered waters.

During winter, as sea ice grows, salts are partly rejected from the sea ice and partly trapped within the sea ice structure, concentrated into brine pockets, tubes, and channels (Weeks and Ackley 1986; Petrich and Eicken 2010). As the temperature decreases, brine salinity and concentration of solutes and gases increase in brine, and the resulting brine $p\text{CO}_2$ is furthermore, strongly influenced by brine drainage and CaCO₃ precipitation (Papadimitriou et al. 2007, 2012; Rysgaard et al. 2011, 2012).

Brine drainage from sea ice causes the formation of highly saline dense cold water that sinks to deeper layers and contributes to the global ocean circulation. Furthermore, brine drainage may also change the $p\text{CO}_2$ concentrations below sea ice by releasing dissolved gasses and solutes into the water column (Gibson and Trull 1999; Semiletov et al. 2004, 2007; Delille 2006). CaCO₃ precipitation can occur in sea ice due to the changes in the mineral-liquid thermodynamic equilibrium (Marion 2001). Ikaite, a hexahydrate polymorph of calcium carbonate (CaCO₃·6H₂O), begins to precipitate at −2.2 °C and has been found in both Antarctic and Arctic sea ice (Dieckmann et al. 2008, 2010; Rysgaard et al. 2012, 2013; Fischer et al. 2013; Geilfus et al. 2013). CO₂ is expelled more efficiently from the ice than total alkalinity (TA), because alkalinity is trapped in ikaite crystals within the interstices between the ice crystals and sea ice becomes enriched in TA (Rysgaard et al. 2013). Studies in the Arctic suggest that, due to brine drainage, CO₂ and TCO₂ can be transported below the pycnocline and, subsequently, incorporated into intermediate and deep-water masses (Rysgaard et al. 2007, 2011). A combination of the transport of CO₂, TCO₂, and meltwater from sea ice will lead to a decrease in surface $p\text{CO}_2$ with a corresponding increase in the air–sea CO₂ flux.

During spring, when the sea ice melts, dissolution of CaCO₃ (Nedashkovsky et al. 2009), autotrophic assimilation of CO₂ (Søgaard et al. 2010), and dilution of brine by melting sea ice are all processes that can decrease the $p\text{CO}_2$ of the brines and, ultimately, of the surface waters (Geilfus et al. 2012). This will result in a lowering of the surface seawater CO₂, thereby causing an increase in the air–sea flux of CO₂ (Rysgaard et al. 2011, 2012). However, the significance of CaCO₃ precipitation/dissolution in sea ice

on the air–sea flux of CO₂ depends on the sea ice permeability, the timing and location of CaCO₃ precipitation, the rate of CaCO₃ precipitation, and the fate of the CaCO₃ (Delille 2006).

Another potential process in sea ice that could counteract an atmospheric CO₂ draw-down is heterotrophic respiration releasing CO₂ (Deming 2010; Søgaard et al. 2010).

The understanding of sea ice CO₂ dynamics and whether or not the polar regions are, or will be, a source or a sink for CO₂ exchange is of fundamental importance for understanding global air–ocean CO₂ dynamics. Several studies have focused on the spatial heterogeneity of sea ice algae and/or bacteria, as well as key biogeochemical parameters (Gosselin et al. 1986; Eicken et al. 1991; Rysgaard et al. 2001; Granskog et al. 2005; Steffens et al. 2006; Mikkelsen et al. 2008; Søgaard et al. 2010; Fischer et al. 2013). However, to date, few attempts have been made to investigate the spatial and temporal variability of CaCO₃ and the relationship between CaCO₃ precipitation and other biogeochemical parameters.

Factors affecting the precipitation, growth, and dissolution of CaCO₃ crystals in natural sea ice are still poorly understood (Rysgaard et al. 2012). However, it has been shown that orthophosphate can inhibit the crystallization of the anhydrous forms of CaCO₃ (Bischoff et al. 1993; Lin and Singer 2006) but does not interact with ikaite (Bischoff et al. 1993; Buchardt et al. 2001). Furthermore, high concentrations of dissolved organic matter (DOM) can inhibit CaCO₃ precipitation in natural environments (Berner et al. 1978; Zullig and Morse 1988). Since sea ice is known to have high concentrations of both DOM and phosphate, especially associated with high biological activity (Thomas et al. 2010), it is pertinent to study these together with CaCO₃ dynamics in ice.

The objectives of this study were (1) to investigate the factors that control the spatial and temporal distribution of CaCO₃, dissolved organic carbon and nitrogen (DOC, DON), TCO₂, TA, inorganic nutrients, bulk salinity, and temperature as well as primary and bacterial productivity in subarctic first-year sea ice, (2) to discuss the potentially synergy between these parameters, and (3) to understand how they can affect the sea ice CO₂ system.

Materials and methods

Sampling was conducted from February 17 to May 1, 2010, on first-year fast ice in Kapisigdlit Bight (60 km to the SW of Nuuk), SW Greenland (64°26'N 50°13'W; Fig. 1). During this period, sea ice thickness gradually reduced from the maximum thickness of 81 cm until it completely melted. A maximum snow thickness of 7 cm was measured



Fig. 1 Map showing the sea ice area in Kapisiglit in SW Greenland and the temporal development and spatial variability sampling stations

in March. The water column in the Kapisiglit Bight was fully mixed and the salinity under the sea ice varied between 33 and 33.5. The water depth under the sea ice was 30–40 meter. More details on the oceanographic conditions in the Godthåbsfjord are provided by Mortensen et al. (2011).

Two sampling designs were used:

1. Spatial variability was investigated over a perpendicular x - y transect covering 0.07 km^2 that was investigated on March 11 and April 8, 2010 (See Fig. 1 for location of these). The parameters sampled in this part of the work were CaCO_3 , dissolved organic carbon and nitrogen (DOC, DON), inorganic nutrients (PO_4^{3-} , Si(OH)_4 , NO_2^- , NO_3^- , and NH_4^+), temperature, salinity, and snow and sea ice thickness.
2. The temporal development of CaCO_3 , TCO_2 , TA, inorganic nutrients, DOC, DON, primary production, bacteria production, bulk salinity, snow and sea ice thickness, and temperature was also investigated at a single location in the study area (Fig. 1) every 2–3 weeks from February to May 2010 (i.e. 17 February, 10, 11, 12 and 15 March, 8 April and 1 May).

Spatial variability

In both of the transect surveys (i.e., March 11 and April 8, 2010), 25 sea ice cores were taken along a 266-m-long perpendicular x - y transect. The cores were collected at

distances of 0, 0.2, 0.4, 0.6, 0.8, 1, 3, 9, 20, 42, 64, 128, and 266 m in both x and y directions. At each sampling point, a sea ice core was collected using a MARK II coring system (Kovacs Enterprises Ltd) and an overlying snow sample was collected using a small shovel. The air temperature was measured 2 m above the snow, and vertical profiles of temperatures within the ice were measured using a calibrated thermometer (Testo®). Sea ice temperature measurements were complemented by a custom-built string of thermistors that were frozen into the sea ice from 11 March until 8 April. The thermistor string data were recorded every 6 h at a spatial resolution of 4 cm.

The retrieved ice cores were cut into 12 cm sections with a stainless steel saw and placed in plastic containers and transported back to the laboratory in dark thermo-insulated boxes. Sea ice and snow samples were slowly melted in the dark at $3 \pm 1 \text{ }^\circ\text{C}$, which took between 2 and 3 days. We measured all the parameters in all sea ice sections. However, we only report data from the top and bottom section as they are the most important.

To determine the amount of CaCO_3 within the ice and snow, between 300 and 500 ml of melted ice or snow was divided into three subsamples and filtered ($3 \pm 1 \text{ }^\circ\text{C}$) through pre-combusted ($450 \text{ }^\circ\text{C}$, 6 h) Whatman® GF/F filters. The exact volume of the filtered meltwater was measured. The filters were transferred to tubes (12 ml Extainer®) containing $20 \mu\text{l}$ HgCl_2 (5 % w/v, saturated solution) to avoid microbial activity during storage and 12 ml deionized water with a known TCO_2 concentration. The tubes were then spiked with $300 \mu\text{l}$ of 8.5 %

phosphoric acid to convert CaCO_3 on the filters to CO_2 , and after coulometric analysis (Johnson et al. 1993) of CO_2 the CaCO_3 concentration was calculated.

At each sampling occasion, samples from different ice depth horizons were inspected under the microscope to check for the presence of microorganisms with calcium carbonate external structures such as coccolithophores and foraminifers. These inspections showed that no microorganisms with calcium carbonate external structures were present in any of the samples.

The remaining meltwater was filtered through 25-mm Whatman® GD/X disposable syringe filters (pore size 0.45 μm). A subsample of the filtrate was transferred to pre-combusted glass vials; 100 μl of 85 % phosphoric acid was added; and the vials were frozen for later analyses of DOC. The remaining filtrate was transferred to pre-combusted (450 °C, 6 h) and alkali-washed glass vials and frozen for later analysis of DON, PO_4^{3-} , NO_3^- , NO_2^- , Si(OH)_4 , and NH_4^+ . The DOC, DON, and nutrient samples were frozen at -19 °C until analysis. DOC was measured by high-temperature catalytic oxidation, using a MQ 1001 TOC Analyzer (Qian and Mopper 1996). The concentrations of NO_3^- , NO_2^- , PO_4^{3-} , and Si(OH)_4 were determined by standard colorimetric methods (Grasshoff et al. 1983) as adapted for flow injection analysis (FIA) on a LACHAT Instruments Quick-Chem 8000 autoanalyzer (Hales et al. 2004). The PO_4^{3-} samples from the first sampling was contaminated, and therefore we did not include them. The concentration of NH_4^+ was determined with the fluorometric method of Holmes et al. (1999) using a HITACHI F2000 fluorescence spectrophotometer. The concentration of DON was determined by subtraction of the concentration of DIN ($\text{DIN} = [\text{NO}_3^-] + [\text{NO}_2^-] + [\text{NH}_4^+]$) from that of the total dissolved nitrogen determined by FIA on the LACHAT autoanalyzer, using online peroxodisulphate oxidation coupled with UV radiation at pH 9.0 and 100 °C (Kroon 1993).

The conductivity of the melted sea ice sections was measured (Thermo Orion 3-star with an Orion 013610MD conductivity cell), and values were converted to bulk salinity (Grasshoff et al. 1983). The brine volumes of the original sea ice samples were calculated from the measured bulk salinity and temperature and a fixed density of 0.917 g cm^{-3} according to Leppäranta and Manninen (1988) for temperatures >-2 °C and according to Cox and Weeks (1983) for temperatures <-2 °C.

Spatial autocorrelation (Legendre and Legendre 1998) was used to analyze the correlation of the horizontal and vertical distribution of CaCO_3 concentration, DOC, DON, inorganic nutrients, temperature, and salinity as well as the snow and sea ice thickness. Autocorrelation was estimated by Moran's I coefficients (Moran 1950; Legendre and Legendre 1998). This coefficient was calculated for each of the following intervals along the transect (classes of

distance): 0–0.25, 0.25–0.50, 0.50–1.5, 1.5–2.5, 2.5–5.0, 5.0–10, 10–50, 100–150, 150–200, 200–250, and >250 m. The autocorrelation coefficients estimated by the Moran's I coefficient were tested for significance according to the method described in Legendre and Legendre (1998). A 2-tailed test of significance was used. Positive (+) indicates positive autocorrelation (correlation) and negative (–) indicates negative autocorrelation. A zero (0) value indicates a random spatial pattern. We applied a significance level of $P < 0.05$. Pearson's correlation was used to find the correlation between the parameters. Furthermore, a full factorial generalized linear model (GLM) including time, depth, and position as explanatory variables, which was reduced based on Akaike's Information Criterion (AIC), was applied. The same model was applied for several dependent variables: position (horizontal), depth (vertical), and time on CaCO_3 concentration, bulk salinity, DOC, and DON.

Temporal development

On each of the 7 sampling occasions for the temporal study, triplicate ice cores and environmental parameters were collected from a defined area (5 m^2), and samples were processed as described above.

Primary production was measured (Søgaard et al. 2010) on 4 occasions (i.e. 17 February, 11 March, 8 April, and 1 May). In short, primary production was determined on melted sea ice samples (melted within 48 h in the dark at 3 ± 1 °C). The potential primary production in the sea ice at different sea ice depths (i.e. 12 cm sections) was measured in the laboratory cold room at 3 irradiances (72, 50, 14 $\mu\text{mol photons m}^{-2} \text{s}^{-1}$) and corrected with one dark incubation, using the $\text{H}^{14}\text{CO}_3^-$ incubation technique (incubation time was 5 h). The potential primary production measured in the laboratory at different sea ice depths was plotted against the three laboratory light intensities 42, 21, and 9 $\mu\text{mol photon m}^{-2} \text{s}^{-1}$ and fitted to the following function described by Platt et al. (1980)

$$\text{PP}(\mu\text{g C l}^{-1} \text{ h}^{-1}) = P_m \left[1 - \exp\left(\frac{-\alpha E_{\text{PAR}}}{P_m}\right) \right] \quad (1)$$

where PP is the primary production, P_m ($\mu\text{g C l}^{-1} \text{ h}^{-1}$) is the maximum photosynthetic rate at light saturation, α ($\mu\text{g C m}^{-2} \text{s}^{-1} \mu\text{mol photons}^{-1} \text{l}^{-1} \text{ h}^{-1}$) is the initial slope of the light curve, and E_{PAR} ($\mu\text{mol photons m}^{-2} \text{s}^{-1}$) is the laboratory irradiance. The photoadaptation index, E_k ($\mu\text{mol photons m}^{-2} \text{s}^{-1}$), was calculated as P_m/α .

In situ down-welling irradiance was measured at ground level (Kipp & Zonen pyrometer, CM21, spectrum range of 305–2,800 nm) once every 5 min, and hourly averages were provided by Asiaq (Greenland Survey). Hourly down-welling irradiance was converted into hourly

photosynthetically active radiation (PAR; light spectrum 300–700 nm) after intercalibration ($R^2 = 0.99$, $P < 0.001$, $n = 133$) with a Li-Cor quantum 2 pi sensor connected to a LI-1400 data logger (Li-Cor Biosciences®). The in situ hourly PAR irradiance was calculated at different depths, depending on sea ice and snow thickness, using the attenuation coefficients measured during the sea ice season.

In situ primary production was calculated for each hour at different sea ice depths using hourly in situ PAR irradiance (Eq. 1). Total daily (24 h) in situ primary production was calculated as the sum of hourly in situ primary production for each depth. The depth-integrated net primary production was calculated using trapezoid integration.

Light attenuation of the sea ice samples was measured with a Li-Cor quantum 2 pi sensor connected to a LI-1400 data logger (Li-Cor Biosciences®) in a dark, temperature-regulated room (at in situ temperatures to avoid brine loss) using a fiber lamp with a spectrum close to natural sunlight (15 V, 150 W, fiber-optic tungsten–halogen bulb). The sensor was placed under the sea ice section and the fiber lamp was placed above. Light attenuation was measured in this way for each sea ice section. We assume depth-independent attenuation in the sea ice. To measure light attenuation of the snow cover, we gently removed the snow and placed the sensor on the ice surface and then we placed the snow on top of the sensor. Thus, down-welling irradiance was measured directly above and below the snow (Søgaard et al. 2010).

The bacterial production procedures employed (i.e., 17 February, 11 March, 8 April, and 1 May) have been described by Søgaard et al. (2010), except those between 13 and 16 March, when the measurements were made using an ice-crushing method described by Kaartokallio (2004) and Kaartokallio et al. (2007). The two methods used for bacterial production measurements yield comparable results (the mean values from March using the ice-crushing method were $2.4 \mu\text{g C l}^{-1} \text{ day}^{-1}$ and the mean values from April using the melting sea ice approach were $2.5 \mu\text{g C l}^{-1} \text{ day}^{-1}$).

Bacterial production in melted sea ice samples was determined by measuring the incorporation of [^3H] thymidine into DNA. Triplicate samples (volume = 0.01 L) were incubated in darkness at $3 \pm 1 \text{ }^\circ\text{C}$ with 10 nmol l^{-1} of labeled [^3H] thymidine (New England Nuclear®, specific activity $10.1 \text{ Ci mmol}^{-1}$). Trichloroacetic acid (TCA)-treated controls were made to measure the abiotic adsorption. At the end of incubation period ($T = 6 \text{ h}$), 1 ml of 50 % cold TCA was added to all the samples. The samples were filtered and counted using a liquid scintillation analyzer (TricCarb 2800, PerkinElmer®).

For the ice-crushing method, samples were prepared by crushing each intact 5 to 10 cm ice core section, first using a spike tool, and then grinding ice chunks in an electrical

ice cube crusher. Approximately 10 ml of crushed ice was placed in a scintillation vial and weighed. To ensure even distribution of labeled substrate, 2–4 ml of sterile-filtered ($0.2 \mu\text{m}$ minisart filters, Sartorius®) seawater was added to the scintillation vials. All ice-processing work was done in a cold on-deck laboratory at near-zero temperature. Two aliquots and a formaldehyde-killed absorption blank were amended with [methyl- ^3H] thymidine (New England Nuclear®; specific activity 20 Ci mmol^{-1}). Concentrations of 20 nmol l^{-1} for thymidine were used for all samples. Samples were incubated in the dark at $-0.2 \text{ }^\circ\text{C}$ in a seawater/ice-crush bath for 17–18 h and incubation stopped with the addition of $200 \mu\text{l}$ of 37 % sterile-filtered formaldehyde. Samples were processed using standard cold-TCA extraction and filtration procedure (using Advantec® MFS $0.2 \mu\text{m}$ MCE filters). A Wallac Win-Spectral 1414 counter (PerkinElmer®) and InstaGel (PerkinElmer®) cocktail were used for scintillation counting.

For both methods, the bacterial carbon production was calculated, using the conversion factors presented in Smith and Clement (1990).

Bacterial carbon demand (BCD) for growth was calculated as:

$$\text{BCD}(\mu\text{g C l}^{-1} \text{ h}^{-1}) = \frac{\text{BP}}{\text{BGE}} \quad (2)$$

where BP is the bacteria production and BGE is a bacterial growth efficiency estimate of 0.5 measured in polar oceans (Rivkin and Legendre 2001).

To investigate the temporal distribution of TCO_2 and TA, an additional sea ice core was collected on each sampling occasion. The core was cut into 12-cm sections and placed in laminated transparent NEN/PE plastic bags (Hansen et al. 2000) fitted with a gas-tight Tygon tube and a valve for sampling. These sections were brought back to the laboratory cold room ($3 \pm 1 \text{ }^\circ\text{C}$). Cold ($1 \text{ }^\circ\text{C}$) deionized water of known weight and TA and TCO_2 concentration was added (10–30 ml) to each NEN/PE bag (Hansen et al. 2000). The bags were closed, and excess air quickly extracted through the valve. Then, the ice was melted ($<48 \text{ h}$) in the dark. Gas bubbles released from the melting sea ice were transferred to tubes (12 ml Exetainer®). Sea ice meltwater was likewise transferred to similar tubes containing $20 \mu\text{l}$ HgCl_2 (5 % w/v saturated solution; Rysgaard and Glud 2004). Standard methods of analysis were used: TCO_2 concentrations were measured on a coulometer, TA by potentiometric titration (Haraldsson et al. 1997), and gaseous O_2 , CO_2 , N_2 by gas chromatography (SRI 8610C; FID/TCD detector; Lee et al. 2005).

A Wilcoxon rank sum test was used to test whether CaCO_3 concentration was significantly differently distributed within the sea ice. We applied a significance level of 95 %.

Following the bulk determination of TCO_2 and TA, the bulk $p\text{CO}_2$ and pH (on the total scale) were computed using the temperature and salinity conditions in the field and a standard set of carbonate system equations (See Rysgaard et al. 2013), excluding nutrients, with the CO2SYS program of Lewis and Wallace (2012). We used the equilibrium constants of Mehrbach et al. (1973), refitted by Dickson and Millero (1987, 1989). We assumed a conservative behavior of CO_2 dissociation constants at subzero temperatures since Marion (2001) and Delille et al. (2007) suggested that a thermodynamic constant relevant for the carbonate system can be assumed to be valid at subzero temperatures.

Results

Figure 1 shows a map of the investigated sea ice area with the different sampling stations in Kapisigdlit, SW Greenland (Fig. 1).

The air temperature during the study period ranged from $-17\text{ }^\circ\text{C}$ in February to $+16\text{ }^\circ\text{C}$ in May just before the sea ice break-up (Fig. 2). Temperatures within the snow and sea ice varied from -6.0 ± 0.1 to $0 \pm 0.02\text{ }^\circ\text{C}$, with minimum temperatures measured in February and March, followed by a gradual increase to maximum values in late April (Fig. 3a).

The bulk salinity of the sea ice samples varied from 1.7 to 6 (Fig. 3b). The brine volume varied from 5 to 32 % at the top of the sea ice and from 12 to 40 % at the bottom of the sea ice (Fig. 3c), an indication that the ice was permeable for most of the study (Golden et al. 1998). In April, when air temperatures varied between -2 and $+16\text{ }^\circ\text{C}$, the ice began to melt, which resulted in high relative brine volumes and low bulk salinities (Fig. 3b, c).

Spatial variability

Moran's I (Table 1) was used to estimate the spatial autocorrelation within the datasets collected for the two

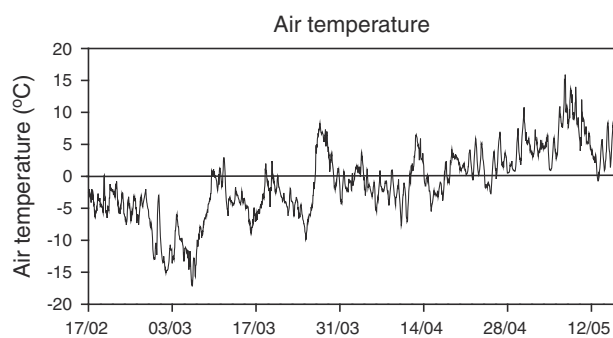


Fig. 2 Meteorological data on air temperature ($^\circ\text{C}$) at the Asiaq meteorological station in Kapisigdlit

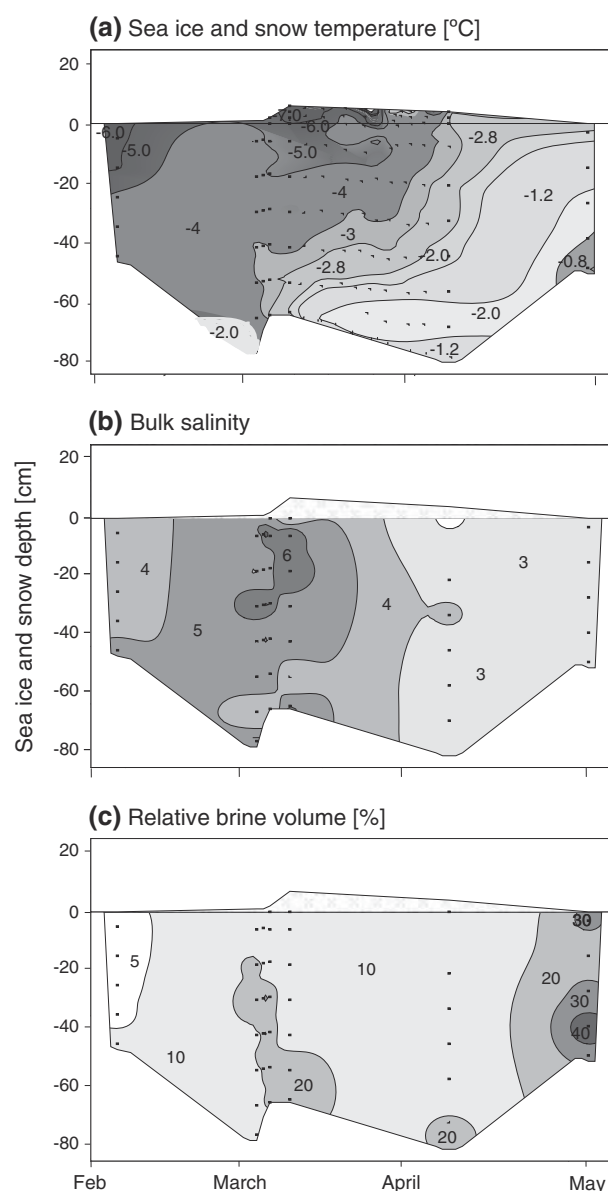


Fig. 3 Temporal development in (a) sea ice and snow temperature [$^\circ\text{C}$] N.B. The temperature data collected from retrieved ice cores are supplemented by thermistor string data from 11 March until 8 April, (b) bulk salinity, (c) relative brine volume fraction [%]. The black dots represent triplicate measurements

transect samplings in March and April. All parameters had a random spatial distribution pattern with no apparent patches, indicating that the distribution of the parameters investigated was highly heterogeneous on the scale of meters to hundreds of meters (Table 1).

Despite this heterogeneity, there was evidence of a correlation between several parameters: CaCO_3 had significant correlation with PO_4^{3-} , bulk salinity, $\text{Si}(\text{OH})_4$ and NO_3^- . CaCO_3 and DON were significantly correlated (negative) only during the second sampling. There was no

Table 1 Moran’s I as a function of distance class (m) between sites for CaCO₃, bulk salinity, DOC, DON, NH₄⁺, NO₂⁻, NO₃⁻, Si(OH)₄ and PO₄³⁻ in snow (S), top sea ice (T) and bottom sea ice (B). First sampling period was on March 11 and second sampling

period was on April 8, 2010. Positive (+) indicates positive autocorrelation (correlation) or negative (-) negative autocorrelation (dispersion). A zero value indicates a random spatial pattern

First sampling																											
Distance class (m)	CaCO ₃			Bulk salinity			DOC			DON			NH ₄ ⁺			NO ₂ ⁻			NO ₃ ⁻			Si(OH) ₄					
	S	T	B	S	T	B	S	T	B	S	T	B	S	T	B	S	T	B	S	T	B	S	T	B			
0.25	0	0	0	0	0	0	0	0	0	0	0	0	0	0	0	0	0	0	0	0	0	0	0				
0.5	0	0	0	0	-	0	0	0	0	0	0	0	0	0	0	0	0	0	0	0	0	0	0				
1.0	0	0	0	0	-	-	0	0	0	0	-	0	0	0	0	0	0	0	-	-	-	0	0				
2.5	0	0	0	-	0	0	0	0	0	+	+	0	-	0	0	-	+	+	+	+	0	0	-	0			
5.0	0	0	0	0	-	0	0	0	0	0	-	0	0	0	0	0	0	0	0	0	0	-	0	0			
10	0	0	0	-	0	0	0	0	0	0	0	0	0	0	0	0	0	0	0	0	0	0	0	0			
50	0	0	0	0	0	0	0	0	0	0	0	0	-	0	0	0	-	0	0	0	0	0	0	0			
100	0	0	0	0	0	0	0	0	0	-	0	-	0	0	0	0	0	0	0	0	0	0	0	0			
200	0	0	0	0	0	0	0	0	0	-	0	0	0	0	0	0	0	0	0	0	0	0	-	0			
250	-	0	0	0	+	0	0	0	0	-	0	0	+	0	0	0	0	0	-	0	0	0	0	0			
>250	-	0	0	0	0	0	0	0	0	0	0	0	0	0	0	0	0	0	0	0	0	0	0	0			
Second sampling																											
Distance class (m)	CaCO ₃			Bulk salinity			DOC			DON			NH ₄ ⁺			NO ₂ ⁻			NO ₃ ⁻			Si(OH) ₄			PO ₄ ³⁻		
	S	T	B	S	T	B	S	T	B	S	T	B	S	T	B	S	T	B	S	T	B	S	T	B	S	T	B
0.25	0	0	0	0	0	0	0	0	0	0	0	0	0	0	0	0	0	-	0	0	0	0	0	0	0		
0.5	0	0	0	0	0	0	0	-	0	0	-	0	0	0	0	0	0	0	0	0	0	0	0	0	0		
1.0	0	0	0	0	-	0	0	0	0	0	0	0	0	0	0	-	-	0	0	-	0	0	0	0	0		
2.5	+	-	0	+	+	+	0	+	0	-	0	0	-	0	+	0	0	0	+	0	0	0	0	0	0		
5.0	0	0	0	0	0	0	0	0	0	0	0	0	0	0	0	0	0	-	-	0	0	-	0	0	+	0	0
10	0	0	0	0	0	0	0	0	0	0	0	0	0	0	0	0	+	0	0	0	0	0	0	0	0	0	0
50	0	0	0	0	0	0	0	0	0	0	0	0	0	0	0	0	-	0	0	0	0	0	0	0	0	0	0
100	0	0	0	0	0	0	0	-	0	0	0	0	0	0	-	0	0	0	0	0	0	0	0	0	0	-	0
200	0	0	0	0	0	0	0	0	0	0	0	0	0	0	0	0	0	0	0	0	0	0	0	0	0	0	0
250	0	0	-	0	0	0	0	+	0	0	0	0	0	0	0	0	0	+	0	-	-	0	0	0	0	0	0
>250	0	0	0	0	0	0	0	0	0	0	0	0	0	0	0	0	0	0	0	0	0	0	0	0	0	0	0

correlation between CaCO₃ and DOC, NH₄⁺, NO₂⁻, and temperature (Table 2).

A GLM where depth (vertical), time, and position (horizontal) as explanatory variables is used to test whether there was a significant effect on several dependent variables: CaCO₃, bulk salinity, DOC, and DON. The GLM test was applied on the datasets collected for the two transect samplings in March and April. There was a significant effect of depth for all the parameters. The significant effect of depth was largely dependent on the time of sampling for CaCO₃ ($F_{5,261} = 15.9784, P < 0.001$), bulk salinity ($F_{5,248} = 5.6322 P < 0.001$), and DON ($F_{5,239} = 3.6861 P < 0.001$) (data not shown). Furthermore, when the two studies in March and April were compared, a significant effect of time was found for bulk salinity, DOC, and DON (Table 3). No significant effect of position

(horizontal) was found for CaCO₃, bulk salinity, and DON (Table 3).

Temporal distribution

In the temporal survey, there were no vertical differences in TCO₂ and TA (Fig. 4), although the concentrations of TCO₂ and TA decreased with time (Fig. 4). The highest TCO₂ and TA concentrations were measured in February (293 ± 6.1 and $410 \pm 40 \mu\text{mol kg}^{-1}$ in melted sea ice), which decreased to 181 ± 1.3 and $190 \pm 1.2 \mu\text{mol kg}^{-1}$ in melted sea ice in the beginning of May, respectively (Fig. 4). However, high concentrations of TA and TCO₂ were also measured in April (Fig. 4). No small-scale variability was observed for TCO₂ and TA concentrations.

Table 2 Pairwise comparison of CaCO₃, bulk salinity, temperature, DOC, DON, NH₄⁺, NO₂⁻, NO₃⁻, Si(OH)₄ and PO₄³⁻. (–) indicates significantly negative (–) and (+) indicates significantly positive (+)

	CaCO ₃		bulk salinity		temperature		DOC		DON		NH ₄ ⁺		NO ₂ ⁻		NO ₃ ⁻		Si(OH) ₄		PO ₄ ³⁻		
	1	2	1	2	1	2	1	2	1	2	1	2	1	2	1	2	1	2	1	2	
CaCO ₃																					
bulk salinity	-	-																			
temperature																	
DOC															
DON													
NH ₄ ⁺											
NO ₂ ⁻	+	+					
NO ₃ ⁻	+	+	.	.	+	+	+	.	+	.	.					
Si(OH) ₄	.	.	.	+	+
PO ₄ ³⁻

correlated variables (Pearsons) at a 5 % significance level. First sampling period was in March and second sampling period in April 2010

In the water column, the highest TCO₂ concentration, of $2,101 \pm 7.7 \mu\text{mol kg}^{-1}$, was measured in February, which decreased to $2,085 \pm 27 \mu\text{mol kg}^{-1}$ in May (Fig. 4). The highest TA concentration of $2,253 \pm 2.5 \mu\text{mol kg}^{-1}$ was measured in May and the lowest of $2,220 \pm 2.2 \mu\text{mol kg}^{-1}$ in March (Fig. 4).

The average TA:TCO₂ ratio within the sea ice was >1 during February (average 1.25) and March (average 1.20), and higher than that in the water column (Fig. 4). The highest TA:TCO₂ ratio (1.75) was calculated for the uppermost horizons of the sea ice in April. In April, the average ratio was 1.32, while the value in the beginning of May was 1.1.

The CaCO₃ concentrations varied vertically within the ice cores: in February the highest concentration of $2.4 \pm 0.4 \mu\text{mol CaCO}_3 \text{ l}^{-1}$ was measured in the upper most layer of the sea ice (Wilcoxon rank sum test; $P < 0.05$; Fig. 5). Conversely, just before ice break-up in early May, the highest CaCO₃ concentration of $4.4 \pm 0.1 \mu\text{mol CaCO}_3 \text{ l}^{-1}$ was measured in the lowermost ice horizon (Wilcoxon rank sum test; $P < 0.05$; Fig. 5). In March and April, CaCO₃ was evenly distributed within the sea ice with an average concentration of $1.8 \pm 0.40 \mu\text{mol CaCO}_3 \text{ l}^{-1}$ in March and $2.0 \pm 0.30 \mu\text{mol CaCO}_3 \text{ l}^{-1}$ in April (Wilcoxon rank sum test; $P > 0.05$). No small-scale variability was observed for CaCO₃ concentration in the sea ice (Fig. 5). CaCO₃ concentrations in the snow decreased throughout the

sea ice season: from $5.2 \pm 1.5 \mu\text{mol CaCO}_3 \text{ l}^{-1}$ in February to $3.0 \pm 1.5 \mu\text{mol CaCO}_3 \text{ l}^{-1}$ in April (Fig. 5). Sediment traps were deployed under the sea ice during the study period but no CaCO₃ crystals were found (data not shown).

The DOC concentrations increased over time with a maximum concentration of $160 \mu\text{mol l}^{-1}$ being measured in May in the bottommost layer of the ice (Fig. 6). DON concentrations did not vary vertically within the sea ice during winter. However, in April and May, when the sea ice began to melt, the DON concentrations increased, and maximum DON values of $15 \mu\text{mol l}^{-1}$ were measured in the bottommost part of the sea ice (Fig. 6). The DOC:DON ratios ranged from 5 to 20 (average 12).

The highest volume-specific primary production (bulk) of $25 \mu\text{g C l}^{-1} \text{ day}^{-1}$ was measured in March in the bottom of the sea ice (Fig. 6). Bacterial carbon demand varied vertically within the sea ice, with maximum values measured in the top and bottom section of the sea ice in March and May (Fig. 6). In February and April, the maximum BCD was measured in the internal sea ice layers. The highest BCD of $5.8 \mu\text{g C l}^{-1} \text{ day}^{-1}$ was estimated in the bottommost sections of the sea ice in March.

Bulk nutrient concentrations for each sampling date were plotted as a function of bulk salinity and compared with the expected dilution line (Clarke and Ackley 1984). To calculate the dilution line, we used the average nutrient concentration and salinity measured at 17 February, 11

Table 3 Results from a GLM model where depth, time, and position as explanatory variables were used to test whether there was a significant effect on several dependent variables: CaCO₃, bulk salinity, DOC, and DON

Variable	Position		Time		Depth	
CaCO ₃	$F_{24,261} = 1.2685$	$P = 0.19$	$F_{1,261} = 2.6087$	$P = 0.11$	$F_{5,261} = 53.7673$	$P < 0.001$
Bulk salinity	$F_{24,248} = 0.8054$	$P = 0.73$	$F_{1,248} = 18.4728$	$P < 0.001$	$F_{5,248} = 14.2994$	$P < 0.001$
DOC	$F_{24,217} = 2.13$	$P < 0.001$	$F_{1,217} = 224.6497$	$P < 0.001$	$F_{5,217} = 3.1986$	$P < 0.001$
DON	$F_{24,239} = 0.5919$	$P = 0.94$	$F_{1,239} = 162.4025$	$P < 0.001$	$F_{5,239} = 6.6925$	$P < 0.001$

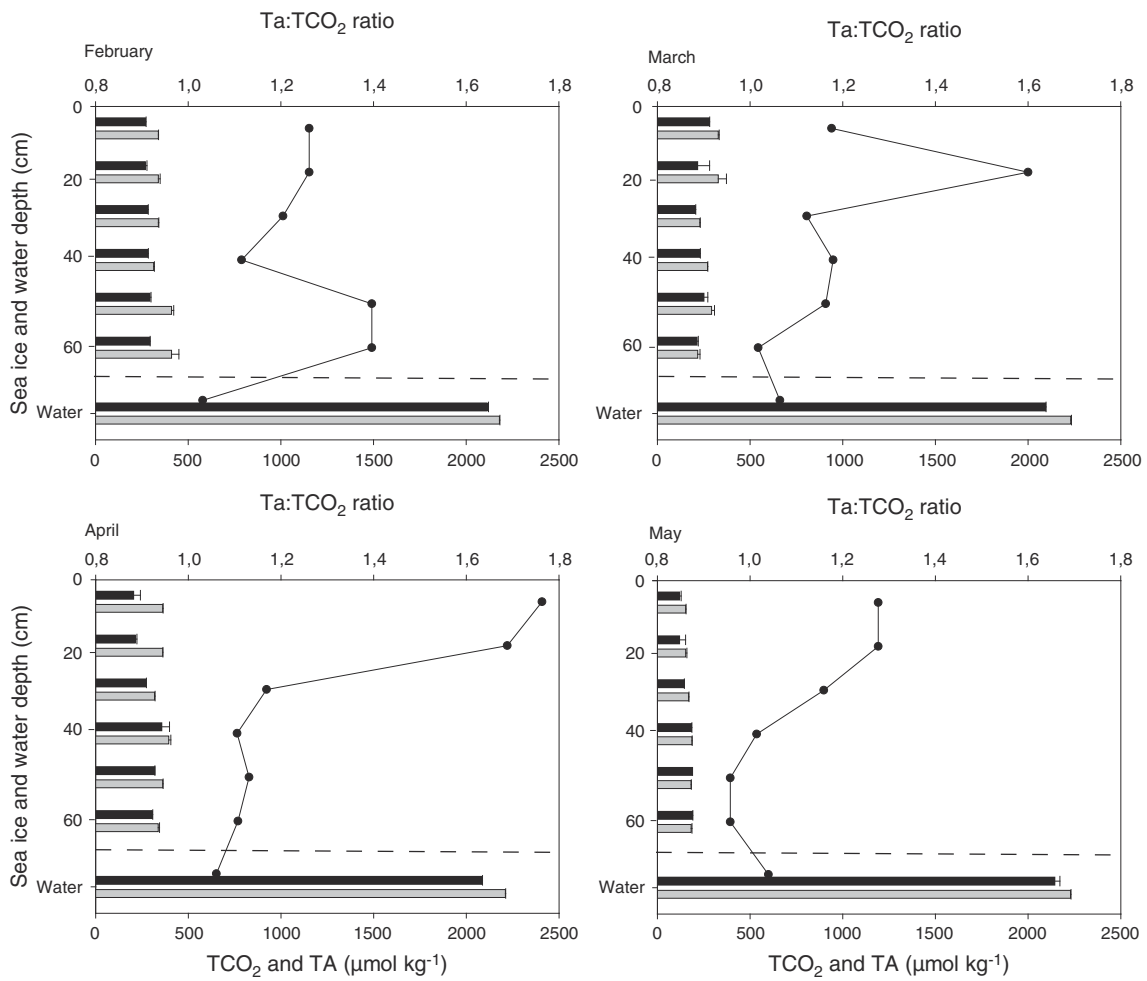


Fig. 4 Temporal development of the vertical concentration profiles of TCO₂ (black bars) and TA (gray bars) and the TA:TCO₂ ratio (circles) in bulk melted sea ice during the 2010 sea ice season. Note

that TCO₂ and TA below 60 cm are water column values. Horizontal dotted line represents the sea ice–water column interface. Data points represent treatment mean ± SE (n = 3)

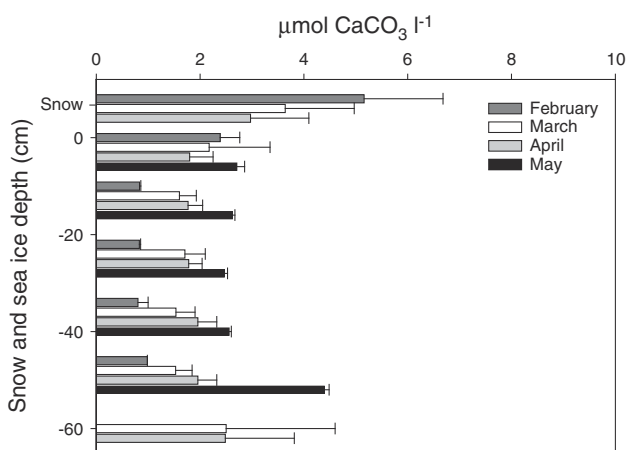


Fig. 5 Temporal development of the CaCO₃ concentration [μmol CaCO₃ l⁻¹] in bulk sea ice and snow in February, March, April, and May 2010

March, 8 April, and 1 May in the water column (i.e. 0–10 m; PO₄³⁻ = 0.94 μmol l⁻¹, Si(OH)₄ = 7.0 μmol l⁻¹, NO₂⁻ + NO₃⁻ = 8.6 μmol l⁻¹, NH₄⁺ = 0.28 μmol l⁻¹, DOC = 62.6 μmol l⁻¹, DON = 1.2 μmol l⁻¹ and a average salinity of 33). If values are below the line, depletion of nutrients has taken place, and if above the dilution line production, or net-deposition, of the solute has occurred. Plots of salinity versus PO₄³⁻, Si(OH)₄, NO₂⁻ + NO₃⁻, NH₄⁺, DOC, and DON in sea ice were generally all above the dilution line implying accumulation of nutrients and organic matter within the ice (Fig. 7a–f). However, depletion of PO₄³⁻ was observed in February and March. Furthermore, NO₂⁻ + NO₃⁻ was depleted in April and May.

There was a negative correlation between PO₄³⁻ and CaCO₃ and Si(OH)₄ and CaCO₃, while a positive correlation was observed between NO₃⁻ and CaCO₃ (Table 2).

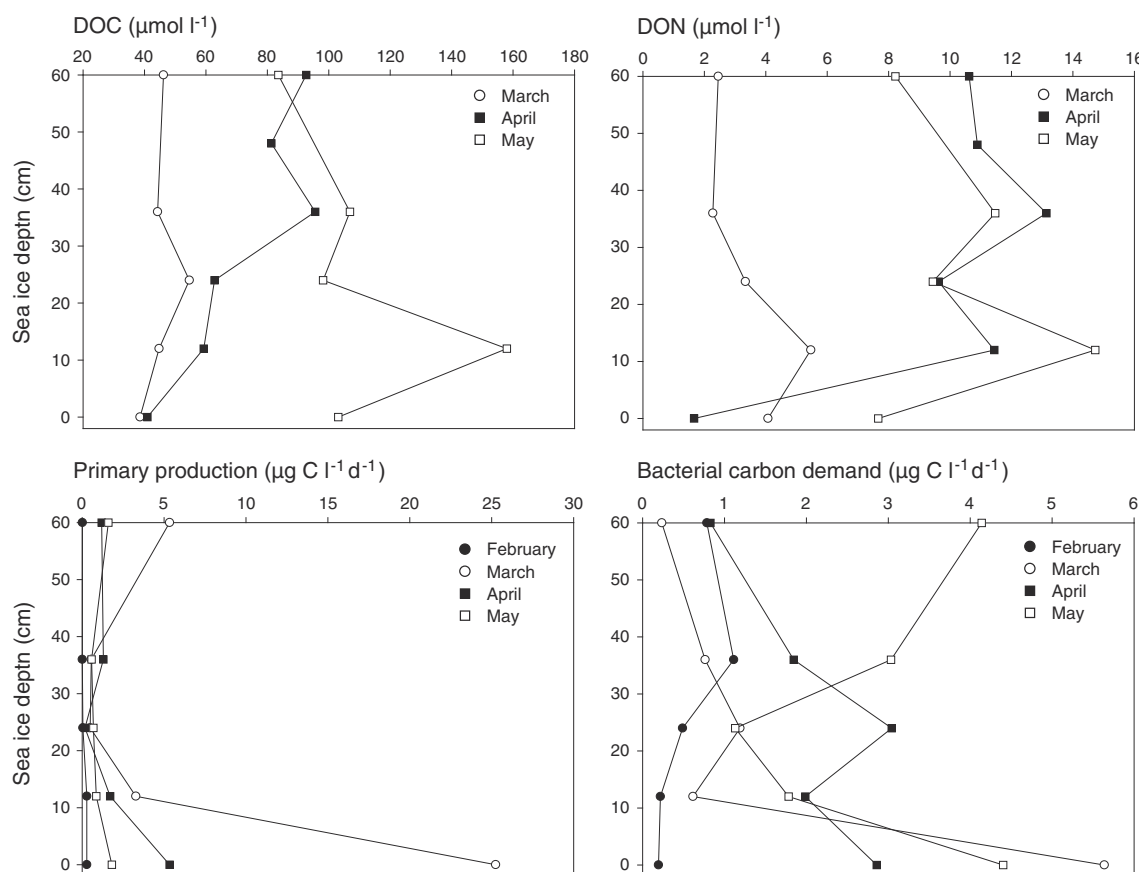


Fig. 6 Vertical profiles of DOC, DON, primary production, and bacterial carbon demand in bulk sea ice in February to May. N.B. there were no data available on the vertical profiles of DOC and DON in February

Figure 8 shows nTA and $nTCO_2$ (TA and TCO_2 value being normalized to a salinity of 33 to remove correlation to salinity) relationships in seawater samples and bulk ice samples. The different lines represent the theoretical effects of precipitation–dissolution of $CaCO_3$, CO_2 release–uptake and photosynthesis–respiration on the ratio $nTCO_2:nTA$. The precipitation of $CaCO_3$ decreases both TCO_2 and TA in a ratio of 2:1. An exchange of CO_2 has no impact on TA, while TCO_2 will be affected. Biological activity has an almost negligible effect on TA, with a ratio $TA:TCO_2 = -0.16$ (Zeebe and Wolf-Gladrow 2001). Considering that sea ice was formed from seawater with a known $TA:TCO_2$ ratio (Fig. 4), we are able to decipher which process took place in the ice: in February and March, the sea ice samples were aligned on the theoretical line for $CaCO_3$ precipitation (Fig. 8). In April and May, the ice samples were well aligned (slope 0.75; $R^2 = 0.86$) between the theoretical trend for $CaCO_3$ precipitation/dissolution and the one for CO_2 release/uptake (Fig. 8). In April two sea ice samples were aligned on the theoretical line for $CaCO_3$ dissolution. This implies that both $CaCO_3$ precipitation/dissolution and CO_2 release/uptake had occurred in the ice.

Discussion

Biological activity

A maximum BCD of $5.8 \mu g C l^{-1} day^{-1}$ (Fig. 6) was estimated, which is low compared with maximum rates of $27 \mu g C l^{-1} day^{-1}$ estimated in the neighboring fjord Malene Bight in April 2008 (60 km to the SW from the present study site; Sjøgaard et al. 2010).

Pairwise correlations between primary production and BCD revealed significant positive relationships. Furthermore, accumulation of DOC was observed (Fig. 6e–f) as well as DOC/DON ratios ranging from 5 to 20 indicating a probable production of carbon-rich extracellular polymeric substances (EPS) by the sea ice algae and bacteria (Underwood et al. 2010; Krembs et al. 2011; Juhl et al. 2011). Correlation between primary production and BCD, high DOC/DON ratio and accumulation of DOC points to there being a low-quality substrate resulting in a low bacteria production. Previous studies have shown that EPS is a low-quality substrate for heterotrophic bacteria (Pomeroy and William 2001), which might explain the low BCD and the observed DOC accumulation (Fig. 6). However, several

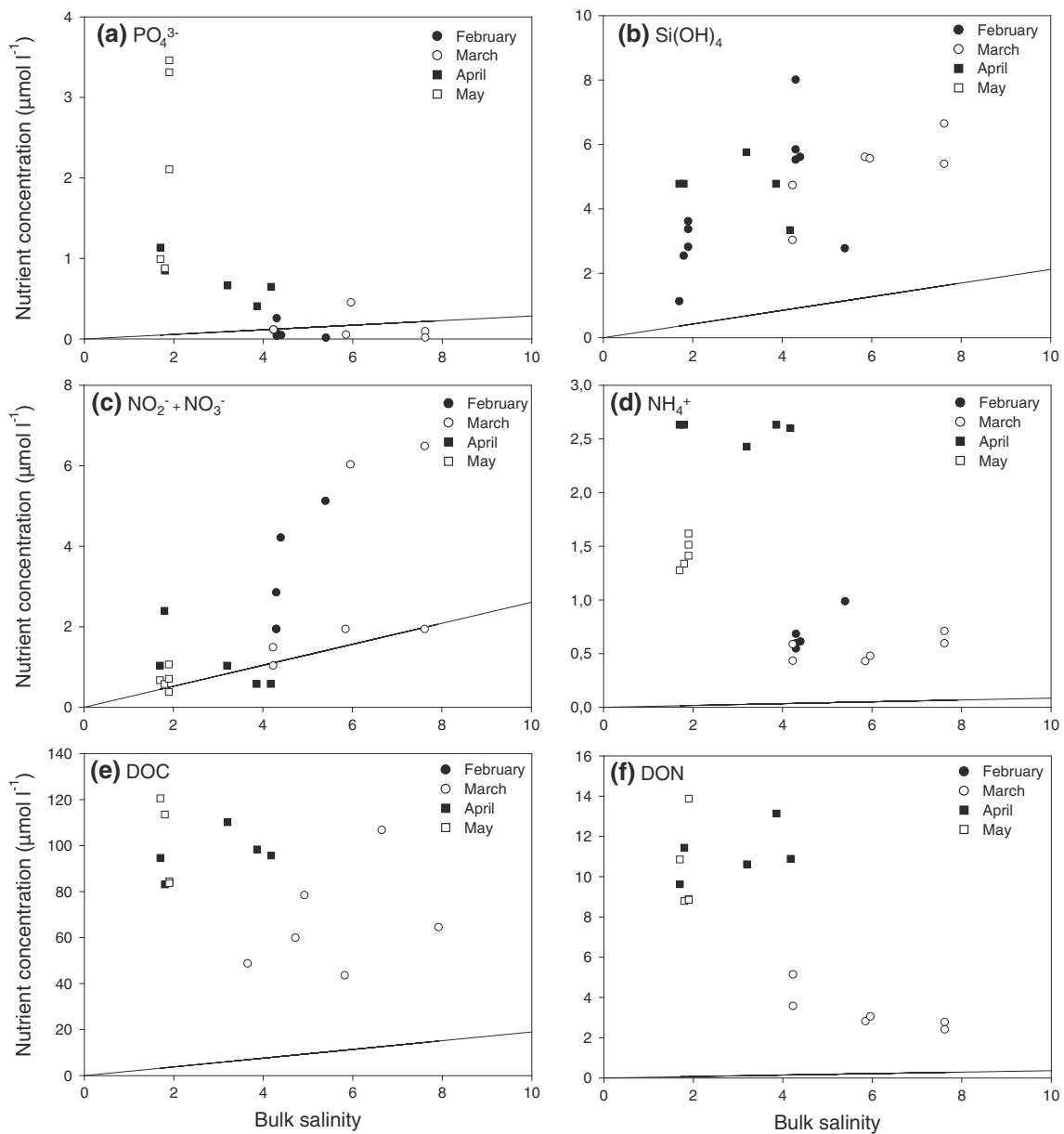


Fig. 7 Temporal development of (a) PO_4^{3-} , (b) $\text{Si}(\text{OH})_4$, (c) $\text{NO}_2^- + \text{NO}_3^-$, (d) NH_4^+ , (e) DOC, and (f) DON concentrations versus bulk salinity in sea ice from February to May. The *solid line*

indicates the expected dilution line predicted from salinity and nutrient concentrations in seawater (0–10 m, average salinity of 33 under the sea ice)

studies suggest the opposite that EPS serve as high-quality substrate for bacteria (e.g. Junge et al. 2004; Meiners et al. 2008).

Another explanation for the low BCD might be the value for bacterial growth efficiency used. We used a bacterial growth efficiency of 0.50 (Rivkin and Legendre 2001). However, growth efficiency is an inverse function of temperature, and small changes in temperature would influence growth efficiency (~2.5 % decrease in growth efficiency per 1 °C increase) and thereby the BCD (Rivkin and Legendre 2001). Using a lower growth efficiency (<0.15; e.g. Middelboe et al. 2012), the seasonal net

autotrophic sea ice would change to a net heterotrophic sea ice, which compares to result found by Long et al. (2011) in Kapisigdlit Bight in March 2010. Thereby the biological activity would not contribute to the atmospheric CO_2 uptake at all. However, we believe the use of a growth efficiency of 0.50 to be most valid since it also agrees with the growth efficiency of 0.41 measured by Kuparinen et al. (2011) and Del Giorgio and Cole (1998).

The highest estimates of primary production (Fig. 6) were measured in the bottom ice horizons in March. Average rates of sea ice algal primary production during March ($4.03 \text{ mg C m}^{-2} \text{ day}^{-1}$) are at the lower end of the

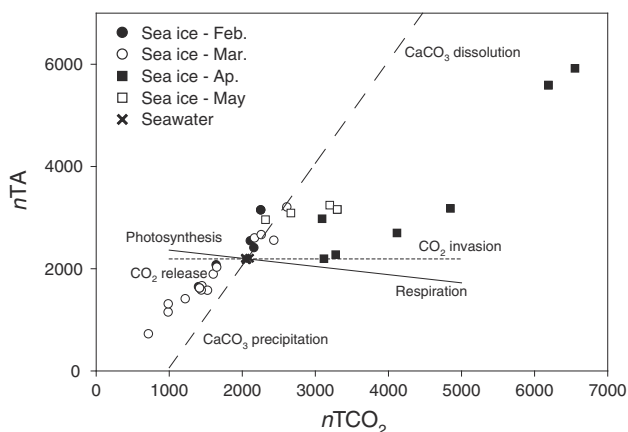


Fig. 8 $nTA:nTCO_2$ (values normalized to a salinity of 33) relationship in seawater samples and bulk ice samples from February to May. The different lines represent the theoretical evolution of $TCO_2:TA$ following precipitation/dissolution of calcium carbonate (dashed line), a release or uptake of $CO_2(g)$ (dotted line) and impact of biology (solid line)

scale for values reported from the Arctic ($0.2\text{--}463\text{ mg C m}^{-2}\text{ day}^{-1}$; Arrigo et al. 2010 and references therein). A decrease in TCO_2 was measured in the bottommost ice at the time of the algae growth, suggesting that primary production was responsible for the decrease in TCO_2 (Figs. 4, 6). However, the average net biological production in the bottom of the sea ice in March was only $1.6\text{ }\mu\text{mol C day}^{-1}$ (Fig. 6) and the average TCO_2 loss in the bottom of the sea ice in March was $6.4\text{ }\mu\text{mol day}^{-1}$, indicating that processes other than primary production influence the inorganic carbon dynamics in the sea ice.

TCO_2 in sea ice is controlled by primary production and respiration by both autotrophic and heterotrophic organisms, $CaCO_3$ precipitation/dissolution, and CO_2 release/uptake. The magnitude of the primary production and thus the potential role of the production in controlling the sea ice inorganic carbon cycle depend primarily on light availability and the size of the inorganic nutrient pool (Papadimitriou et al. 2012). The highest light attenuation coefficient of 12 m^{-1} was measured in March in the snow, corresponding to coefficients reported in snow cover in both the Arctic and Antarctic (Thomas 1963; Weller and Schwerdtfeger 1967; Sogaard et al. 2010). High snow reflection causes low light conditions in the sea ice. However, the highest primary production was found in the bottom of the sea ice in March (Fig. 6), where the light availability was low compared to spring, indicating that light was not the main factor controlling the primary production. However, the low primary production in the bottom of the sea ice after March suggests that the sea ice algae were nutrient-limited late in the sea ice season. Assuming that nutrient uptake by the ice algae follows the Redfield-Brzezinski ratio of 106C:16N:15Si:1P (from

Redfield et al. 1963; Brzezinski 1985), then the nitrogen (N:P ratio <2) and silicate (Si:P ratio <6) appear to have limited the sea ice algal primary production in April and May, while phosphate was found at relatively higher concentrations. This is supported by the nutrient-salinity plot for $NO_2^- + NO_3^-$ in Fig. 7, which indicates depletion of $NO_2^- + NO_3^-$ at the end of the sea ice season. A further factor known to influence the sea ice algal communities is grazing (Gradinger et al. 1999; Bluhm et al. 2010); however, grazing was not measured during the present study.

$CaCO_3$ precipitation

The observed $CaCO_3$ formation was expected (Anderson and Jones 1985; Marion 2001; Papadimitriou et al. 2004) and is consistent with the elevated $TA:TCO_2$ ratios (Fig. 4). We measured much lower TCO_2 and TA concentrations within the sea ice compared to concentrations found in the underlying seawater (average $TA:TCO_2$ ratio = 1.06 in seawater; Fig. 4). Likewise, we found elevated $TA:TCO_2$ ratios in the sea ice with a maximum of 1.75, as compared to the underlying seawater (Fig. 4). However, the $TA:TCO_2$ ratios found in the sea ice in the present study are low compared to values found in other sea ice studies (Rysgaard et al. 2007, 2012; Papadimitriou et al. 2012; Geilfus et al. 2012; Rysgaard et al. 2013).

Ikaite precipitation is favored by near-freezing temperature, alkaline condition, and elevated phosphate concentrations ($>5\text{ }\mu\text{mol l}^{-1}$; Bischoff et al. 1993; Buchardt et al. 2001; Selleck et al. 2007).

In this study, bulk phosphate concentrations between 0.2 and $3.1\text{ }\mu\text{mol l}^{-1}$ were measured in the sea ice, and therefore, the brine phosphate concentrations were occasionally above $5\text{ }\mu\text{mol l}^{-1}$. Furthermore, the phosphate concentrations observed in present study were 5–20 times higher than concentrations found in previous studies in the Arctic (e.g. Krembs et al. 2002; Mikkelsen et al. 2008; Sogaard et al. 2010). Sea ice temperatures during our study ranged from -6 to $0\text{ }^\circ\text{C}$, which is the temperature where ikaite will form. Alkalinity condition was also satisfied as a C-shaped pH profile with high pH (>9) in surface, and bottom sea ice layers, and slightly lower pH conditions (8.5) in the internal sea ice layers were calculated for February, using temperature and bulk salinity (Fig. 3), TA and TCO_2 concentrations (see “Materials and methods” section; Fig. 4). A C-shaped pH profile was also observed in a recent study on experimental sea ice (Hare et al. 2013).

In the early part of the study, we measured the highest $CaCO_3$ concentrations in the surface of the sea ice, and the concentrations decreased with depth (Fig. 5). This is similar to that described by Geilfus et al. (2013) and Rysgaard et al. (2013).

However, just before the ice break-up, the highest CaCO_3 concentration was measured in bottom of the sea ice (Fig. 5). This high CaCO_3 concentration might be due to a migration of the crystals through the brine channels network or could result from the effects of surface flooding and/or gravity drainage. The average brine salinity was 67 in February, 39 in March, and 27 in April; thus, gravity drainage was only possible in February and March. A negative correlation between CaCO_3 concentration and bulk salinity was evident (Table 2), which also suggests that the highest CaCO_3 concentrations were found in the sea ice with low bulk salinities, i.e., in the bottom of the sea ice and/or in summer sea ice.

The concentration of CaCO_3 in the sea ice was 2.13 g m^{-2} (Fig. 5), which compares with values from Antarctic sea ice of 0.3 to 3.0 g m^{-2} (Dieckmann et al. 2008) and 0.1 to 6.5 g m^{-2} found in the top 10 cm of Antarctic sea ice (Fischer et al. 2013). However, these values are one order of magnitude lower than measurements in Arctic ice by Rysgaard et al. (2012, 2013).

Assuming that sea ice is formed from surface seawater with a TA:TCO₂ ratio of 1, the TA:TCO₂ ratio of 1.1–1.75 observed in the sea ice could be generated by a CaCO_3 concentration of 25–120 $\mu\text{mol CaCO}_3 \text{ l}^{-1}$. The calculated CaCO_3 concentrations are between 6 and 25 times higher than our measured CaCO_3 concentrations. However, the highest calculated CaCO_3 concentration compares with surface concentrations of 160–240 $\mu\text{mol CaCO}_3 \text{ l}^{-1}$ melted sea ice reported in the Fram Strait (Rysgaard et al. 2012). The reason for this difference is not clear but could be associated with the melting procedures used. We assume that ikaite does not dissolve if the temperature is maintained below 4 °C, but ikaite could dissolve according to: $\text{CaCO}_3 \cdot 6\text{H}_2\text{O} + \text{CO}_2 \leftrightarrow \text{Ca}^{2+} + 2\text{HCO}_3^- + 5\text{H}_2\text{O}$ in the meltwater being in contact with atmospheric CO_2 during the melting procedure. Another explanation could be that not all the changes in TA originate from CaCO_3 precipitation, and so the TA concentration is higher than CaCO_3 concentration.

The snow contained relatively high amounts of CaCO_3 , which has also been found in Antarctic snow overlying sea ice (Fischer et al. 2013). The mass of CaCO_3 found in the snow ranged from 0.12 to 0.30 g m^{-2} (Fig. 5), which is 7 times lower than the values measured in the sea ice. An explanation for the occurrence of CaCO_3 in the snow could be the upward brine expulsion, which builds up a high salinity layer on top of the ice. Subsequently, when temperature decreases, some salts may reach their solubility threshold and begin to precipitate (Geilfus et al. 2013).

The strong horizontal, vertical, and temporal variability in CaCO_3 concentration suggests that CaCO_3 concentration is influenced by variability in several inherent sea ice properties. We found a strong correlation between CaCO_3 concentrations and bulk salinity, and inorganic nutrients

(Table 2). Pairwise correlations between all measured parameters revealed a negative relationship between CaCO_3 concentration and DON in the second sampling period (Table 2), which may be due to the adverse effect of high DOM concentrations on the CaCO_3 precipitation (Berner et al. 1978; Zullig and Morse 1988).

There was no clear correlation between CaCO_3 and temperature (Table 2), which was unexpected as it is a key variable controlling CaCO_3 release/uptake and the precipitation of CaCO_3 (Papadimitriou et al. 2004). However, a similar lack of correlation was also observed in a study on Antarctic sea ice (Papadimitriou et al. 2012). This is probably because the measured temperature was not in equilibrium with the temperature conditions that led to the precipitation in the first place.

There was no effect of position for CaCO_3 concentrations, DON, and bulk salinity, indicating that the parameters were homogeneously distributed in the sea ice (Table 3). However, Moran's I indicates that the parameters were highly heterogeneous on the scale of meters to hundreds of meters (Table 1). Fischer et al. (2013) also found high spatial variability for CaCO_3 concentration, and high spatial variability has also been observed for other sea ice biochemical and biological properties (Rysgaard et al. 2001; Granskog et al. 2005; Steffens et al. 2006; Sogaard et al. 2010). This clearly emphasizes the importance of seasonal and spatial studies and replicate sampling when collecting sea ice biogeochemical samples.

Effects of CaCO_3 precipitation/dissolution and biological activity on CO_2 dynamics

The changes in the TA:TCO₂ ratio were to a large extent explained by CaCO_3 precipitation and CO_2 release/uptake from the ice (Fig. 8). This observation compares with studies by Munro et al. (2010), Fransson et al. (2011), Rysgaard et al. (2012), Papadimitriou et al. (2012), and Geilfus et al. (2012), in which most of the depletion in TCO₂ was explained by processes other than biological activity. Furthermore, there was no correlation between CaCO_3 and primary production or BCD, which suggests that CaCO_3 precipitation and/or dissolution is not significantly influenced by microbial activity.

The relative effects of biological activity and precipitation/dissolution of CaCO_3 in influencing the air–sea CO_2 exchange in sea ice can be estimated from measurements during the entire sea-ice-covered season. Using a carbon-to-Chl *a* ratio of 20–40 for sea ice algae (Arrigo et al. 2010), an estimate of primary production of 220–540 mg C m^{-2} (data not shown) was calculated, which was low compared to the integrated CaCO_3 concentration of $2,130 \text{ mg m}^{-2}$ (Fig. 5). Furthermore, the

integrated gross primary production of 153 mg C m^{-2} recorded was also relatively low compared to the integrated CaCO_3 concentration. Thus, contribution of primary production to TCO_2 depletion was minor (7–25 %) compared to the contribution of CaCO_3 precipitation (Fig. 8).

The primary production measured in this study might be a conservative estimate. Assuming that between 10 and 61 % of the carbon fixed by photosynthesis was released as DOC (Passow et al. 1994; Chen and Wangersky 1996; Malinsky-Rushansky and Legrand 1996; Gosselin et al. 1997; Riedel et al. 2008), the average primary production in this study of $0.19 \mu\text{mol C l}^{-1} \text{ day}^{-1}$ is equivalent to a DOC accumulation of $0.02\text{--}0.11 \mu\text{mol l}^{-1} \text{ day}^{-1}$. The average DOC concentration in the sea ice was $75 \mu\text{mol l}^{-1}$ (Fig. 6), which is much higher than the expected DOC accumulation calculated from the primary production. If the primary production is a conservative estimate, the contribution to the changes in TCO_2 and TA by the net biological production might be higher.

However, a recent study with high primary production showed that only 10–20 % of the changes in TCO_2 could be explained by net biological production (Fransson et al. 2011). In another study by Rysgaard et al. (2012), abiotic processes including CaCO_3 dissolution accounted for between 88 and 98 % of the air–sea CO_2 uptake, indicating that the contribution of primary production was relatively low.

Assuming that all CaCO_3 dissolved within the sea ice or in the mixed layer, melting a 0.4-m-thick sea ice cover (temperature: $-1.1 \text{ }^\circ\text{C}$, bulk salinity: 4.4, TA: $291 \mu\text{mol kg}^{-1}$, and TCO_2 : $238 \mu\text{mol kg}^{-1}$) into a 20-m-thick mixed water layer (temperature: $0 \text{ }^\circ\text{C}$, salinity: 33, TA: $2,239 \mu\text{mol kg}^{-1}$, TCO_2 : $2,109 \mu\text{mol kg}^{-1}$) from Figs. 3 and 4 would result in a 1.5 ppm decrease in $p\text{CO}_2$ per week. Assuming that no CaCO_3 precipitates (e.g. TA and TCO_2 are both $291 \mu\text{mol kg}^{-1}$), the resultant $p\text{CO}_2$ decrease would be 0.9 ppm per week. Using average conditions during the field campaign (Fig. 4), this corresponds to an air–sea CO_2 uptake of $1.5 \text{ mmol m}^{-2} \text{ sea ice day}^{-1}$ (with CaCO_3) and $1.1 \text{ mmol m}^{-2} \text{ sea ice day}^{-1}$ (without CaCO_3). Therefore, dissolution of CaCO_3 increased the air–sea CO_2 uptake by 36 % as compared with CaCO_3 -free sea ice. Furthermore, the abiotic sea-ice-driven CO_2 is higher than the net biological production of $0.07 \text{ mmol m}^{-2} \text{ day}^{-1}$ (which accounts for 4 % of CO_2 uptake, Fig. 6); and, therefore we conclude that the abiotic processes, including CaCO_3 dissolution and CO_2 uptake, played a more important role than the net biological production in the sea ice for the air–sea CO_2 dynamics during this period.

Comparing the sea-ice-driven CO_2 uptake with a recent study by Rysgaard et al. (2012), the uptake found in the present study is sevenfold lower. Furthermore, the amount of CaCO_3 found in the present study is low compared to

other studies (Dieckmann et al. 2008; Rysgaard et al. 2012; Fischer et al. 2013). Our study was performed in subarctic sea ice exposed to higher seasonal air temperatures than the aforementioned studies, which might explain the lower CaCO_3 concentrations and, hence, the lower sea-ice-driven CO_2 uptake.

Conclusion

Abiotic processes contributed to an air–sea CO_2 uptake of $1.5 \text{ mmol m}^{-2} \text{ sea ice day}^{-1}$ and dissolution of CaCO_3 increased the air–sea CO_2 uptake by 36 % as compared to a theoretical assessment of melting CaCO_3 -free sea ice. Furthermore, primary production only contributed marginally to TCO_2 depletion of the sea ice (7–25 %), which was mainly controlled by physical export via brine drainage and CaCO_3 precipitation/dissolution. The net biological production could only explain 4 % of the sea-ice-driven CO_2 uptake. These estimates must be considered with the caveat that for all of the parameters investigated, their distribution in the ice was highly heterogeneous. Furthermore, there was considerable temporal variability for all parameters.

Acknowledgments We thank Paul Batty, Rasmus Hedeholm, and Michael R. Schröder for assistance in the field and in the laboratory. Furthermore, we would like to thank Asiaq (Greenland Survey) for the meteorological data provided. The study received financial support from the Greenland Climate Research Centre, and DHS was financially supported by the Commission for Scientific Research in Greenland (KVUG). David Thomas and Louiza Norman are grateful to the Royal Society and NERC for support for their participation in the work. DT and Hermanni Kaartokallio are also grateful to the Academy of Finland (FiDiPro) for the support that enabled their participation. Søren Rysgaard acknowledges the Canada Excellence Research Chair (CERC) program.

Open Access This article is distributed under the terms of the Creative Commons Attribution License which permits any use, distribution, and reproduction in any medium, provided the original author(s) and the source are credited.

References

- Anderson LG, Jones EP (1985) Measurements of total alkalinity, calcium and sulphate in natural sea ice. *J Geophys Res* 90:9194–9198
- Arrigo KR, Mock T, Lizotte MP (2010) Primary production and sea ice. In: Thomas DN, Dieckmann GS (eds) *Sea ice*, 2nd edn. Wiley-Blackwell Publishing, Oxford, pp 283–326
- Berner R, Westrich JT, Graber R, Smits J, Martens C (1978) Inhibition of aragonite precipitation from supersaturated seawater. *Am J Sci* 278:816–837
- Bischoff JL, Fitzpatrick JA, Rosenbauer RJ (1993) The solubility and stabilization of ikaite ($\text{CaCO}_3 \cdot \text{H}_2\text{O}$) from 0° to 25°C : environmental and paleoclimatic implications for thiolite tufa. *J Geol* 101:21–33

- Bluhm BA, Gradinger RR, Schnack-Schiel SB (2010) Sea ice meio- and macrofauna. In: Thomas DN, Dieckmann GS (eds) *Sea ice*, 2nd edn. Wiley-Blackwell Publishing, Oxford, pp 357–393
- Brzezinski MA (1985) The Si:C:N ratio of marine diatoms: interspecific variability and the effect of some environmental variables. *J Phycol* 21:347–357
- Buchardt B, Israelson C, Seaman P, Stockmann G (2001) Ikaite tufa towers in Ikka Fjord, southwest Greenland: their formation by mixing of seawater and alkaline spring water. *J Sediment Res* 71:176–189
- Chen WH, Wangersky PJ (1996) Production of dissolved organic carbon in phytoplankton cultures as measured by high temperature catalytic oxidation and ultraviolet photo-oxidation methods. *J Plankton Res* 18:1201–1211
- Clarke DB, Ackley SF (1984) Sea ice structure and biological activity in the Antarctic marginal ice zone. *J Geophys Res* 89:2087–2096
- Cox GFN, Weeks WF (1983) Equations for determining the gas and brine volumes in sea-ice samples. *J Glaciol* 29:306–316
- Del Giorgio PA, Cole JJ (1998) Bacterial growth efficiency in natural aquatic systems. *Annu Rev Ecol Syst* 29:503–541
- Delille B (2006) Inorganic carbon dynamics and air-ice-sea CO₂ fluxes in the open and coastal waters of the Southern Ocean. University of Liège, Liège, p 297
- Delille B, Jourdain B, Borges AV, Tison JP, Delille D (2007) Biogas (CO₂, O₂, dimethylsulfide) dynamics in spring Antarctic fast ice. *Limnol Oceanogr* 52:1367–1379. doi:10.4319/lo.2007.52.4.1367
- Deming J (2010) Sea ice bacteria and viruses. In: Thomas DN, Dieckmann GS (eds) *Sea ice*, 2nd edn. Wiley-Blackwell Publishing, Oxford, pp 267–302
- Dickson AG, Millero FJ (1987) A comparison of the equilibrium constants for the dissociation of carbonic acid in seawater media. *Deep-Sea Res* 34:1733–1743
- Dickson AG, Millero FJ (1989) Corrigenda. *Deep-Sea Res* 36:983
- Dieckmann GS, Nehrke G, Papadimitriou S, Göttlicher J, Steininger R, Kennedy H, Wolf-Gladrow D, Thomas DN (2008) Calcium carbonate as ikaite crystals in Antarctic sea ice. *Geophys Res Lett*. doi:10.1029/2008GL033540
- Dieckmann GS, Nehrke G, Uhlig J, Göttlicher J, Gerland S, Granskog MA, Thomas DN (2010) Brief communication: ikaite (CaCO₃ × H₂O) discovered in Arctic sea ice. *Cryosphere Discuss* 4:153–161
- Eicken H, Lange MA, Dieckmann GS (1991) Spatial variability of sea-ice properties in the northwestern Weddell Sea. *J Geophys Res* 96:603. doi:10.1029/91JC00546
- Fischer M, Thomas DN, Krell A, Nehrke G, Göttlicher J, Norman L, Meiners KM, Riaux-Gobin C, Dieckmann GS (2013) Quantification of ikaite in Antarctic sea ice. *Antarct Sci* 25:421–432
- Fransson A, Chierici M, Yager PL, Smidt WO Jr (2011) Antarctic sea ice carbon dioxide system and controls. *J Geophys Res* 116:C12035. doi:10.1029/2010JC006844
- Geilfus NX, Carnat G, Papakyriakou T, Tison JL, Else B, Thomas H, Shadwick E, Delille B (2012) Dynamics of pCO₂ and related air-ice CO₂ fluxes in the Arctic coastal zone (Amundsen Gulf, Beaufort Sea). *J Geophys Res* 117:C00G10. doi:10.1029/2011JC007118
- Geilfus NX, Carnat G, Dieckmann GS, Halden N, Nehrke G, Papakyriakou T, Tison JL, Delille B (2013) First estimates of the contribution of CaCO₃ precipitation to the release of CO₂ to the atmosphere during young sea ice growth. *J Geophys Res* 118:244–255. doi:10.1029/2012JC007980
- Gibson JAE, Trull TW (1999) Annual cycle of fCO₂ under sea-ice and in open water in Prydz Bay, East Antarctica. *Mar Chem* 66:187–200. doi:10.1016/S0304-4203(99)00040-7
- Golden KM, Ackley SF, Lytle VI (1998) The percolation phase transition in sea ice. *Science* 282:2238–2241. doi:10.1126/science.282.5397.2238
- Gosselin M, Legendre L, Therriault JC, Demers S, Rochet M (1986) Physical control of the horizontal patchiness of sea ice microalgae. *Mar Ecol Prog Ser* 29:289–298
- Gosselin M, Levasseur M, Wheeler PA, Horner RA, Booth BC (1997) New measurements of phytoplankton and ice algal production in the Arctic Ocean. *Deep Sea Res Part II* 44:1623–1644
- Gradinger R, Friedrich C, Spindler M (1999) Abundance, biomass and composition of the sea ice biota of the Greenland Sea pack ice. *Deep Sea Res Part 2* 46:1457–1472
- Granskog MA, Kaartokallio H, Kuosa H, Thomas DN, Ehn J, Sonninen E (2005) Scales of horizontal patchiness in chlorophyll a, chemical and physical properties of landfast sea ice in the Gulf and Finland (Baltic Sea). *Polar Biol* 28:276–283
- Grasshoff K, Erhardt M, Kremling K (1983) *Methods of seawater analysis*, 2nd revised and extended version. Verlag Chemie, Weinheim, Deerfield Beach, Florida, Basel
- Hales B, Van Geen A, Takahashi T (2004) High-frequency measurement of seawater chemistry: flow-injection analysis of macronutrients. *Limnol Oceanogr Methods* 2:91–101
- Hansen JW, Thamdrup B, Jørgensen BB (2000) Anoxic incubation of sediment in gas-tight plastic bags: a method for biogeochemical process studies. *Mar Ecol Prog Ser* 208:273–282
- Haraldsson C, Anderson LG, Hasselöv M, Hult S, Olsson K (1997) Rapid, high-precision potentiometric titration of alkalinity in ocean and sediment pore water. *Deep Sea Res Part I* 44:2031–2044
- Hare AA, Wang F, Barber D, Geilfus N-X, Galley R, Rysgaard S (2013) pH evolution in sea ice grown at an outdoor experimental facility. *Mar Chem* 154:46–64. doi:10.1016/j.marchem.2013.04.007
- Holmes RM, Aminot A, Kérouel R, Hooker BA, Peterson BJ (1999) A simple and precise method for measuring ammonium in marine and freshwater ecosystem. *Can J Fish Aquat Sci* 56:1801–1808
- Johnson KM, Wills KD, Butler DB, Johnson WK, Wong CS (1993) Coulometric total carbon dioxide analysis for marine studies. Maximizing the performance of an automated gas extraction system and coulometric detector. *Mar Chem* 44:167–187. doi:10.1016/0304-4203(93)90201-X
- Juhl AR, Krembs C, Meiners K (2011) Seasonal development and differential retention of ice algae and other organic fractions from Arctic sea ice. *Mar Ecol Prog Ser* 436:1–16
- Junge K, Eicken H, Deming JW (2004) Bacterial activity at –2 to –20°C in Arctic wintertime sea ice. *Appl Environ Microbiol* 70:550–557. doi:10.1128/AEM.70.1.550-557.2004
- Kaartokallio H (2004) Food web components, and physical and chemical properties of Baltic Sea ice. *Mar Ecol Prog Ser* 273:49–63
- Kaartokallio H, Kuosa H, Thomas DN, Granskog MA, Kivi K (2007) Changes in biomass, composition and activity of organism assemblages along a salinity gradient in sea ice subjected to river discharge. *Polar Biol* 30:186–197
- Krembs C, Eicken H, Junge K, Deming JW (2002) High concentrations of exopolymeric substances in Arctic winter sea ice: implications for the polar ocean carbon cycle and cryoprotection of diatoms. *Deep Sea Res Part 1* 49:2163–2181
- Krembs C, Eicken H, Deming JW (2011) Exopolymer alteration of physical properties of sea ice and implications for ice habitability and biogeochemistry in a warmer Arctic. *Proc Natl Acad Sci USA* 108:3653–3658
- Kroon H (1993) Determination of nitrogen in water: comparison of continuous flow method with on-line UV digestion with the original Kjeldahl Method. *Anal Chem Acta* 276:287–293
- Kuparinen J, Autio R, Kaartokallio H (2011) Sea ice bacterial growth rate, growth efficiency and preference for inorganic nitrogen sources in the Baltic Sea. *Polar Biol* 34:1361–1373

- Lazar B, Loya Y (1991) Bioerosion of coral reefs—a chemical approach. *Limnol Oceanogr* 36:377–383. doi:10.4319/lo.1991.36.2.0377
- Lee H-F, Yang TF, Lan TF (2005) Fumarolic gas composition of the Tatum Volcano Group, Northern Taiwan. *TAO* 16:843–864
- Legendre P, Legendre L (1998) Developments in environmental ecology, 20. Numerical ecology, 2nd English ed. Elsevier Science BV, Amsterdam
- Leppäranta M, Manninen T (1988) The brine and gas content of sea ice with attention to low salinities and high temperatures. Finnish Inst. Marine Res. Internal report, p 14
- Lewis E, Wallace D (2012) The program CO2SYS.EXE can be downloaded at: <http://cdiac.esd.ornl.gov/oceans/co2prntnbk.html>, 2012
- Lin YP, Singer PC (2006) Inhibition of calcite precipitation by orthophosphate: speciation and thermodynamic considerations. *Geochimica Cosmochim Acta* 70:2530–2539
- Long MH, Koopman D, Berg P, Rysgaard S, Glud RN, Søgaard DH (2011) Oxygen exchange and ice melt measured at the ice-water interface by eddy correlation. *Biogeosci Discuss* 8: 11255–11284. doi:10.5194/bgd-8-11255-2011
- Loose B, Miller LA, Elliott S, Papakyriakou T (2011) Sea ice biogeochemistry and material transport across the frozen interface. *Ocean* 24:203–218
- Malinsky-Rushansky NZ, Legrand C (1996) Excretion of dissolved organic carbon by phytoplankton of different sizes and subsequent bacterial uptake. *Mar Ecol Prog Ser* 132:249–255
- Marion GM (2001) Carbonate mineral solubility at low temperatures in the Na–K–Mg–Ca–H–Cl–SO₄–OH–HCO₃–CO₃–CO₂–H₂O system. *Geochim Cosmochim Acta* 65:1883–1896
- Mehrbach C, Culbertson H, Hawley JE, Pytkowicz RM (1973) Measurement of the apparent dissociation constants of carbonic acid in seawater at atmospheric pressure. *Limnol Oceanogr* 18:897–907
- Meiners K, Krembs C, Gradinger R (2008) Exopolymer particles: microbial hotspots of enhanced bacterial activity in Arctic fast ice (Chukchi Sea). *Aquat Microb Ecol* 52:195–207
- Middelboe M, Glud RN, Sejr MK (2012) Bacterial carbon cycling in a subarctic fjord: a seasonal study on microbial activity, growth efficiency, and virus-induced mortality in Kobbefjord, Greenland. *Limnol Oceanogr* 57:1732–1742
- Mikkelsen DM, Rysgaard S, Glud RN (2008) Microalgal composition and primary production in Arctic sea ice: a seasonal study from Kobbefjord (Kangerluarsunnguaq), West Greenland. *Mar Ecol Prog Ser* 368:65–74
- Miller L, Papkyriakou TEC, Deming J, Ehn J, Macdonald R, Mucci A, Owens O, Raudsepp M, Sutherland N (2011) Carbon dynamics in sea ice: a winter flux time series. *J Geophys Res* 116. doi:10.1029/2009JC006058
- Moran PAP (1950) Notes on continuous stochastic phenomena. *Biometrika* 37:17–23
- Mortensen J, Lennert K, Bendtsen J, Rysgaard S (2011) Heat sources for glacial melt in a sub-Arctic fjord (Godthåbsfjord) in contact with the Greenland Ice Sheet. *J Geophys Res* 116:c01013. doi:10.1029/2010JC006528
- Munro DR, Dunbar RB, Mucciarone DA, Arrigo KR, Long MC (2010) Stable isotope composition of dissolved inorganic carbon and particulate organic carbon in sea ice from the Ross Sea, Antarctica. *J Geophys Res Ocean* 115:C09005. doi:10.1029/2009JC005661
- Nedashkovsky AP, Khvedynich SV, Petovsky TV (2009) Alkalinity of sea ice in the high-latitude arctic according to the surveys performed at north pole drifting station 34 and characterization of the role of the arctic in the CO₂ exchange. *Mar Chem* 49:55–63. doi:10.1134/s000143700901007x
- Nomura D, Eicken H, Gradinger R, Shirasawa K (2010) Rapid physically driven inversion of the air-sea ice CO₂ flux in the seasonal landfast ice off Barrow, Alaska after onset surface melt. *Cont Shelf Res* 30:1998–2004
- Notz D, Worster MG (2009) Desalination processes of sea ice revisited. *J Geophys Res* 114:1–10. doi:10.1029/2008JC004885
- Papadimitriou S, Kennedy H, Kattner G, Dieckmann GS, Thomas DN (2004) Experimental evidence for carbonate precipitation and CO₂ degassing during sea ice formation. *Geochim Cosmochim Acta* 68:1749–1761
- Papadimitriou S, Thomas DN, Kennedy H, Haas C, Kuosa H, Krell A, Dieckmann GS (2007) Biogeochemical composition of natural sea ice brines from the Weddell Sea during early austral summer. *Limnol Oceanogr* 52:1809–1823
- Papadimitriou S, Kennedy H, Norman L, Kennedy DP, Dieckmann GS, Thomas DN (2012) The effect of biological activity, CaCO₃ mineral dynamics and CO₂ degassing in the inorganic carbon cycle in sea ice in late winter-early spring in the Weddell Sea, Antarctica. *J Geophys Res* 117:C08011. doi:10.1029/2012JC008058
- Papakyriakou T, Miller L (2011) Springtime CO₂ exchange over seasonal sea ice in the Canadian Arctic Archipelago. *Ann Glaciol* 52:1–10
- Passow U, Alldredge AL, Logan BE (1994) The role of particulate carbohydrate exudates in the flocculation of diatoms blooms. *Deep Sea Res I* 41:335–357
- Petrich C, Eicken H (2010) Growth, structure and properties of sea ice. In: Thomas DN, Dieckmann GS (eds) *Sea ice*, 2nd edn. Wiley-Blackwell Publishing, Oxford, pp 425–469
- Platt T, Gallegos CL, Harrison WG (1980) Photoinhibition of photosynthesis in natural assemblages of marine phytoplankton. *J Mar Res* 38:687–701
- Pomeroy LR, William JW (2001) Temperature and substrate as interactive limiting factors for marine heterotrophic bacteria. *Aquat Microbiol Ecol* 23:187–204
- Qian J, Mopper K (1996) Automated high-performance, high-temperature combustion total organic carbon analyzer. *Anal Chem* 68:3090–3097. doi:10.1021/AC960370Z
- Redfield AC, Ketchum BH, Richards FA (1963) The influence of organisms on the composition of seawater. In: Hill MN (ed) *The composition of sea-water and comparative and descriptive oceanography*. Wiley-Intersciences, New York, pp 26–87
- Riedel A, Michel C, Gosselin M, LeBlanc B (2008) Winter–spring dynamics in sea-ice carbon cycling in the coastal Arctic Ocean. *J Mar Syst* 74:918–932
- Rivkin RB, Legendre L (2001) Biogenic carbon cycling in the upper ocean: effects of microbial respiration. *Science* 291:2398–2400
- Rysgaard S, Glud RN (2004) Anaerobic N₂ production in Arctic sea ice. *Limnol Oceanogr* 49:86–94
- Rysgaard S, Kuhl M, Glud RN, Hansen JW (2001) Biomass, production and horizontal patchiness of sea ice algae in a high-Arctic fjord (Young Sound, NE Greenland). *Mar Ecol Prog Ser* 223:15–26
- Rysgaard S, Glud RN, Sejr MK, Bendtsen J, Christensen PB (2007) Inorganic carbon transport during sea-ice growth and decay: a carbon pump in polar seas. *J Geophys Res* 112:111–118
- Rysgaard S, Bendtsen J, Delille B, Dieckmann GS, Glud RN, Kennedy H, Mortensen J, Papadimitriou S, Thomas DN, Tison JL (2011) Sea ice contribution to the air-sea CO₂ exchange in the Arctic and Southern Oceans. *Tellus Ser B* 63:823–830. doi:10.1111/j.1600-0889-2011.005471.x
- Rysgaard S, Glud RN, Lennert K, Cooper M, Halden N, Leaky R, Hawthorne FC, Barber D (2012) Ikaite crystals in melting sea ice—implications for pCO₂ and pH levels in Arctic surface waters. *Cryosphere* 6:1015–1035. doi:10.5194/tcd-6-015-2012

- Rysgaard S, Søgaard DH, Cooper M, Pućko M, Lennert K, Papakyriakou TN, Wang F, Geilfus NX, Glud RN, Ehn J, McGinnis DF, Attard K, Sievers J, Deming JW, Barber D (2013) Ikaite crystal distribution in winter sea ice and implications for CO₂ system dynamics. *Cryosphere* 7:707–718. doi:10.5194/tc-7-707-2013
- Selleck BW, Carr PF, Jones BG (2007) A review and synthesis of Glendonites (Pseudomorphs after ikaite) with new data. Assessing applicability as recorders of ancient coldwater conditions. *J Sediment Res* 77:980–991
- Semiletov I, Makshtas A, Syun-Ichi A (2004) Atmospheric CO₂ balance: the role of Arctic sea ice. *Geophys Res Lett* 31:L05121. doi:10.1029/2003GL017996
- Semiletov IP, Pipko I, Repina I, Shakhova NE (2007) Carbonate chemistry dynamics and carbon dioxide fluxes across the atmosphere-ice water interfaces in the Arctic Ocean: Pacific sector of the Arctic. *J Mar Syst* 66:204–226. doi:10.1016/j.jmarsys.2006.05.012
- Smith REH, Clement P (1990) Heterotrophic activity and bacterial productivity in assemblages of microbes from Sea ice in the high Arctic. *Polar Biol* 10:351–357
- Søgaard DH, Kristensen M, Rysgaard S, Glud RN, Hansen PJ, Hilligsøe KM (2010) Autotrophic and heterotrophic activity in Arctic first-year sea ice: seasonal study from Malene Bight, SW Greenland. *Mar Ecol Prog Ser* 419:31–45
- Steffens M, Granskog MA, Kaartokallio H, Kuosa H, Luodekari K, Papadimitriou S, Thomas DN (2006) Spatial variation of biogeochemical properties of landfast sea ice in the Gulf of Bothnia, Baltic Sea. *Ann Glaciol* 44:80–87
- Thomas CW (1963) On the transfer of visible radiation through sea ice and snow. *J Glaciol* 4:481–484
- Thomas DN, Papadimitriou S, Michel C (2010) Biogeochemistry of sea ice. In: Thomas DN, Dieckmann GS (eds) *Sea ice*, 2nd edn. Wiley-Blackwell Publishing, Oxford, pp 425–469
- Tison J-L, Haas C, Gowing MM, Sleewaegen S (2002) Tank study of physico-chemical controls on gas content and composition during growth of young sea ice. *J Glaciol*. doi:10.3189/172756502781831377
- Underwood GJC, Fietz S, Papadimitriou S, Thomas DN, Dieckmann GS (2010) Distribution and composition of dissolved extracellular polymeric substances (EPS) in Antarctic sea ice. *Mar Ecol Prog Ser* 404:1–19
- Weeks WF, Ackley SF (1986) The growth, structure and properties of sea ice, Chapter 1 of *The Geophysics of Sea Ice*, NATO ASI Series, Series B, Physics Vol. ed. N. Untersteiner, Plenum Press, NY
- Weller G, Schwerdtfeger P (1967) Radiation penetration in Antarctic plateau and sea ice. *Polar Meteorol World Meteorol Org Tech Note* 87:120–141
- Zeebe RE, Wolf-Gladrow D (2001) *CO₂ in seawater: equilibrium, kinetics, isotopes*. Elsevier, Amsterdam
- Zemmelink HJ, Delille B, Tison JL, Hintsä EJ, Houghton L, Dacey JW (2006) CO₂ deposition over the multi-year ice of the western Weddell Sea. *Geophys Res Lett* 33:L13606. doi:10.1029/2006GL026320
- Zullig JJ, Morse JW (1988) Interaction of organic acids with carbonate mineral surfaces in seawater and related solutions: I. Fatty acid adsorption. *Geochim Cosmochim Acta* 52:1667–1678

PAPER II

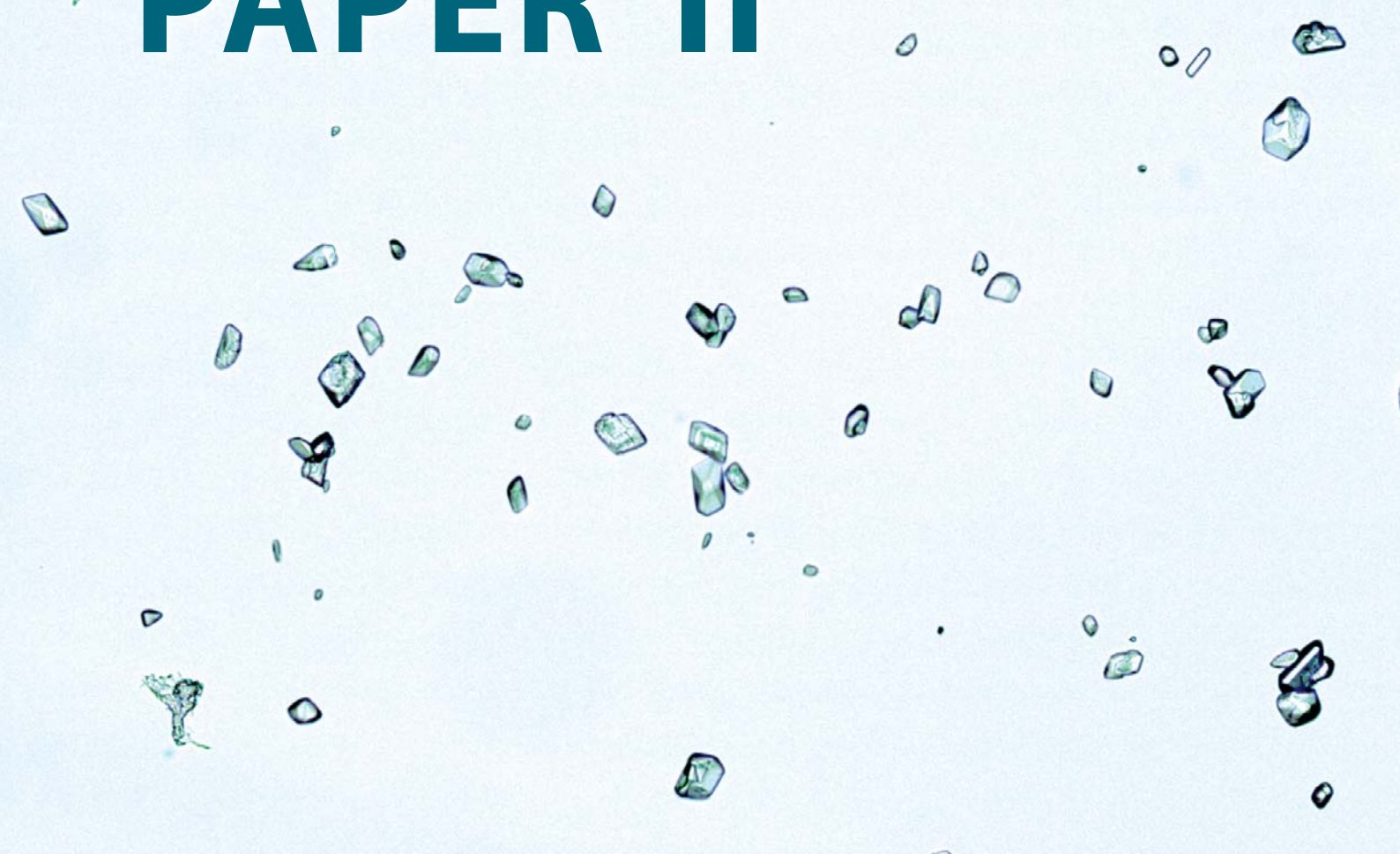


Photo: Søren Rysgaard.

Ikaite crystal distribution in winter sea ice and implications for CO₂ system dynamics

S. Rysgaard • D. H. Søgaard • M. Cooper • M. Pućko • K. Lennert
• T. N. Papakyriakou • F. Wang • N. X. Geilfus • R. N. Glud • J. Ehn
• D. F. McGinnis • K. Attard • J. Sievers • J. W. Deming • D. Barber

The Cryosphere 7:707 – 718, doi: 10.5194/tc-7-707-2013



Ikaite crystal distribution in winter sea ice and implications for CO₂ system dynamics

S. Rysgaard^{1,2,3,4}, D. H. Sogaard^{3,6}, M. Cooper², M. Pućko¹, K. Lennert³, T. N. Papakyriakou¹, F. Wang^{1,5}, N. X. Geilfus¹, R. N. Glud^{3,6,7}, J. Ehn¹, D. F. McGinnis⁶, K. Attard^{3,6}, J. Sievers⁴, J. W. Deming⁸, and D. Barber¹

¹Centre for Earth Observation Science, Department of Environment and Geography, University of Manitoba, Winnipeg, MB R3T 2N2, Canada

²Department of Geological Sciences, University of Manitoba, Winnipeg, MB R3T 2N2, Canada

³Greenland Climate Research Centre, Greenland Institute of Natural Resources, 3900 Nuuk, Greenland

⁴Arctic Research Centre, Aarhus University, 8000 Aarhus, Denmark

⁵Department of Chemistry, University of Manitoba, Winnipeg, MB R3T 2N2, Canada

⁶University of Southern Denmark and NordCEE, Odense M, Denmark

⁷Scottish Association for Marine Science, Oban, UK

⁸University of Washington, School of Oceanography, Seattle, WA, USA

Correspondence to: S. Rysgaard (soeren.rysgaard@ad.umanitoba.ca)

Received: 18 November 2012 – Published in The Cryosphere Discuss.: 6 December 2012

Revised: 30 March 2013 – Accepted: 2 April 2013 – Published: 23 April 2013

Abstract. The precipitation of ikaite (CaCO₃·6H₂O) in polar sea ice is critical to the efficiency of the sea ice-driven carbon pump and potentially important to the global carbon cycle, yet the spatial and temporal occurrence of ikaite within the ice is poorly known. We report unique observations of ikaite in unmelted ice and vertical profiles of ikaite abundance and concentration in sea ice for the crucial season of winter. Ice was examined from two locations: a 1 m thick land-fast ice site and a 0.3 m thick polynya site, both in the Young Sound area (74° N, 20° W) of NE Greenland. Ikaite crystals, ranging in size from a few μm to 700 μm, were observed to concentrate in the interstices between the ice platelets in both granular and columnar sea ice. In vertical sea ice profiles from both locations, ikaite concentration determined from image analysis, decreased with depth from surface-ice values of 700–900 μmol kg⁻¹ ice (~25 × 10⁶ crystals kg⁻¹) to values of 100–200 μmol kg⁻¹ ice (1–7 × 10⁶ crystals kg⁻¹) near the sea ice–water interface, all of which are much higher (4–10 times) than those reported in the few previous studies. Direct measurements of total alkalinity (TA) in surface layers fell within the same range as ikaite concentration, whereas TA concentrations in the lower half of the sea ice were twice as high. This depth-related discrepancy suggests interior ice processes where ikaite crystals form in surface sea ice layers

and partly dissolve in layers below. Melting of sea ice and dissolution of observed concentrations of ikaite would result in meltwater with a *p*CO₂ of <15 μatm. This value is far below atmospheric values of 390 μatm and surface water concentrations of 315 μatm. Hence, the meltwater increases the potential for seawater uptake of CO₂.

1 Introduction

As sea ice forms from seawater, dissolved salts are trapped in interstitial liquid brine inclusions. Because phase equilibrium must be maintained between these inclusions and the surrounding ice, the brine becomes increasingly concentrated as temperatures decrease. Solid salts begin to precipitate out of solution, starting with ikaite (CaCO₃·6H₂O) at –2.2 °C, mirabilite (NaSO₄·10H₂O) at –8.2 °C and hydrohalite (NaCl·2H₂O) at –23 °C (Assur, 1960). The mineral ikaite was recently discovered in springtime sea ice in both hemispheres (Dieckmann et al., 2008, 2010). Ikaite crystals appeared to be present throughout the sea ice, but with larger crystals and higher abundance in surface layers (Dieckmann et al., 2010; Rysgaard et al., 2012; Geilfus et al., 2013). Ikaite crystals of various sizes and morphologies have been isolated

from sea ice. They range in size from a few μm to large mm-size crystals; all are highly transparent with rounded rhombic morphology and show uniform extinction under crossed polarized light, suggesting simple, single well-crystalline crystals. The specific conditions promoting ikaite precipitation in sea ice are poorly understood, but if precipitation occurs during the ice-growing season in the porous lower sea ice layer, where the brine volume is greater than 5 % (Weeks and Ackley, 1986; Golden et al., 1998, 2007; Ehn et al., 2007), then the resulting CO_2 -enriched brine will exchange with seawater via gravity drainage (Notz and Worster, 2009). Earlier work has led to the suggestion that ikaite crystals may remain trapped within the skeletal layer where they act as a store of TA, becoming a source of excess TA to the ocean water upon subsequent mineral dissolution during summer melt (Nedashkovsky et al., 2009; Rysgaard et al., 2011). This excess would lower the partial pressure of CO_2 ($p\text{CO}_2$) of surface waters affected by melting sea ice and cause an increase in the air–sea CO_2 flux.

At this point, the spatial and temporal occurrence of ikaite precipitates within sea ice is poorly constrained. There is urgency for increasing the knowledge base, given that the precipitation of CaCO_3 is implicated in many processes of global significance, including the sea ice-driven carbon pump and global carbon cycle (Delille et al., 2007; Rysgaard et al., 2007, 2011; Papadimitriou et al., 2012) and pH conditions (acidification) in surface waters (Rysgaard et al., 2012; Hare et al., 2013). Quantification of CaCO_3 crystals in sea ice in the few previous studies has been made on melted samples assuming that ikaite will not dissolve if temperature is maintained below 4°C . In principle, however, dissolution may also be related to the reaction of ikaite with CO_2 in the meltwater or with the atmosphere during the melting procedure, which can last for days at low temperature allowing the possibility of changing pH in the surroundings of the ikaite crystal and underestimation of ikaite concentration. Examining ikaite in such melted samples also makes it impossible to evaluate spatial distribution within the sea ice matrix on the micrometer to millimeter scale and determine whether or not the mineral is entrapped in the ice crystal lattice and thus separated from the solution.

Precipitation of ikaite in standard seawater conditions is described by



Brine drainage from sea ice is expected to result in a removal of dissolved CO_2 along with salts. If precipitated ikaite crystals become trapped within sea ice interstices, then the reaction in Eq. (1) is pushed to the right in brine, providing further potential for CaCO_3 growth. Over time, the concentration of trapped ikaite crystals could increase. Here we provide novel tests of these ideas during crucial winter conditions by examining ikaite in intact (unmelted) natural sea ice and determining detailed vertical ikaite distributions in the sea ice from two locations in Young Sound (northeast

Greenland). Combined with other measurements and model calculations, the results allow us to relate sea ice formation and melt to the observed $p\text{CO}_2$ conditions in surface waters, and hence, the air–sea CO_2 flux.

2 Methods

2.1 Study site and sampling

Sampling was performed at two locations in the Young Sound area (74°N , 20°W : Rysgaard and Glud, 2007), NE Greenland, in March 2012 (Fig. 1). The land-fast ice station, ICE I ($74^\circ 18.5764' \text{N}$, $20^\circ 18.2749' \text{W}$), was in the fjord with 110–115 cm thick sea ice covered by 70 cm of snow. Freeboard at ICE I was negative, e.g. when a hole was drilled through the ice, the ice surface flooded. However, at sites without drilled holes, we did not observe flooding during our experiment and there was a distinct snow–ice interface. On top of the ice of ICE I, about 8 cm of slush snow at the snow–ice interface was observed. The new-ice station, POLY I ($74^\circ 13.905' \text{N}$, $20^\circ 07.701' \text{W}$), was situated in a polynya region about 3 km off the sharp land-fast ice edge, where sea ice regularly breaks up in winter. At the time of sampling, POLY I was 15–30 cm thick and covered by 17 cm of snow. At POLY I there was negative freeboard too – with about 2 cm of slush snow at the snow–ice interface. At POLY I the snow was denser up to ~ 8 cm from the ice interface, then a bit lighter (newer snow) above. Air temperature during sampling ranged from -20 to -25°C . The polynya site is representative of thin Arctic sea ice, whereas the ICE I location is representative of fjord ice in the Arctic where there is a large source of winter precipitation (snow). Snow was very dry and very cold (unlike Antarctic ice). There was also no surface flooding. ICE I is typical of sea ice in fjords or where large moisture sources are available to the Arctic winter climate system.

Sea ice cores were extracted using a MARK II coring system (Kovacs Enterprises). Vertical temperature profiles were measured with a thermometer (Testo Orion 3-star with an Orion 013610MD conductivity cell) in the center of the cores immediately after coring. Sea ice was then cut into 5–10 cm sections, kept cold and brought to the field laboratory within 1 h for processing. In the 20°C laboratory, sea ice sections were melted for measurement of bulk salinity with a conductivity probe (Thermo Orion 3-star with an Orion 013610MD conductivity cell, UK) calibrated against a 15N KCL solution at 20°C . Brine volume in sea ice was calculated according to Cox and Weeks (1983) and Leppäranta and Manninen (1988). Brine salinity was calculated from the measured sea ice temperatures and freezing point of seawater (Unesco, 1978).

Although there was a lot of snow on the thick fast ice in the fjord there was not natural flooding of the surface. When we installed ocean instruments (drilling through the ice) we

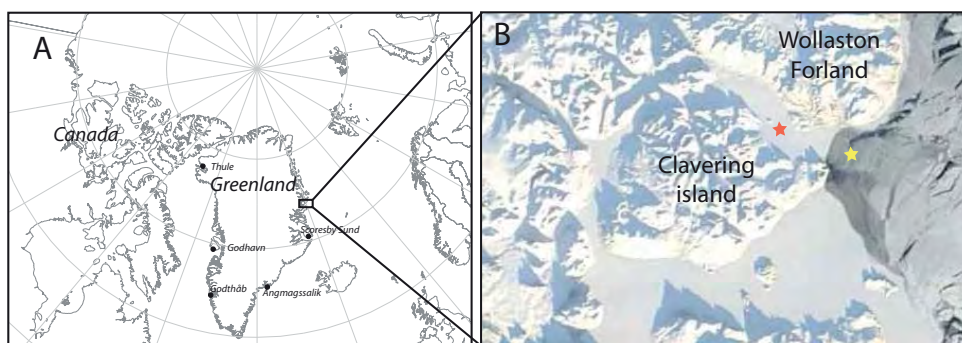


Fig. 1. Study site. (A) Greenland showing the study area (box) and (B) the Young Sound fjord between Wollaston Forland and Clavering Island. Sea ice coring sites for the land-fast ice location (ICE I) is shown as a red star and the polynya coring site (POLY I) as a yellow star. The satellite image showing land-fast ice in the fjord and thin ice–open water conditions in the polynya outside the fjord is from early March 2012.

created some artificial flooding. A widely distributed snow-ice interface survey, however, showed that flooding was limited to only the area immediately surrounding the installed instruments. The same was the case for the Polynya site.

2.2 Analysis

In the cold laboratory (-20 to -25 °C), corresponding sea ice cores were cut into vertical thick sections ($10\text{ cm} \times 6\text{ cm} \times 1\text{ cm}$) and horizontal thick sections ($6\text{ cm} \times 6\text{ cm} \times 1\text{ cm}$), then mounted onto slightly warmed glass plates and thinned to 1–3 mm thickness using a microtome (Leica SM 2010R). Each section was then photographed (Nikon D70) using polarized filters to document ice texture. Subsequently, each thin section was inspected under a stereomicroscope (Leica M125 equipped with a Leica DFC 295 camera and Leica Application Suite ver. 4.0.0. software) to document the vertical and horizontal position of ikaite crystals in sea ice.

To document the abundance and concentrations of ikaite crystals in sea ice, 20–90 mg of sea ice were cut off, using a stainless steel knife, at three random places within each 5–10 cm sea ice section. These subsamples were weighed and placed onto a glass slide that rested on a chilled aluminum block with a 1 cm central viewing hole, then brought into the 20 °C laboratory. There they were inspected intact under a microscope (Leica DMiL LED) under 100–400 magnification as they were also allowed to melt. A few seconds after the sea ice had melted the first image was taken (same camera and software as described above). This image was used to document the amount and concentration of ikaite crystals (further details given below). After 2–5 min the second image was taken and compared with the first one. If crystals were dissolving, they were assumed to be ikaite. Three random samples, each covering 1.07 mm^2 of the counting area, were imaged in this fashion. The area of the melted sea ice sample was determined after thawing to calculate the counted area

to total area ratio. Ikaite crystals and other precipitates were observed to settle to the glass slide rapidly after ice crystal melt due to their high density. In total, three 20–90 mg sea ice sub-samples were processed from each sea ice section in triplicates, resulting in 9 replicate images for each 5–10 cm vertical sea ice section.

The abundance and concentrations of crystals were calculated from the images using the software ImageJ (1.45 s). Individual images were brightness/contrast adjusted prior to binary file conversion. A “close-function” routine then ensured that crystals were closed before “filling-holes” with black. An “analyze” routine was then applied to count the crystals and analyze their area relative to counting area. This ratio was multiplied by the area of the melted ice subsample. For concentration estimates of ikaite a cubic form was assumed for the mineral. Ikaite concentration in sea ice was calculated from its volume, density (1.78 g cm^{-3}), molar weight (208.18 g mol^{-1}), and weight of subsample and converted into $\mu\text{mol kg}^{-1}$ melted sea ice units.

A sea ice core (entire core) from each site was kept at -20 °C for three weeks and brought to the x-ray laboratory at the Department of Geological Sciences at the University of Manitoba, Canada. There, 20–90 mg subsamples of sea ice were cut randomly from each sea ice section (5–10 cm vertical sections) and mounted onto a cold glass slide resting on a chilled aluminum block containing a 1 cm central viewing hole. The crystals were first examined with a polarized light microscope to assess their optical properties and then mounted for x-ray study using a stereo binocular microscope. Ikaite crystals were selected from each 10 cm section of the sea ice cores from both ICE I and POLY I, dragged across the cold glass slide using a metal probe and immersed into a drop of special purpose sampling oil that restricted sublimation. Each crystal was then scooped up with a low x-ray scattering micro-loop and instantly transferred to the nitrogen cold stream (-10 °C) on the x-ray diffraction instrument with a magnetic coupling goniometer head. The

x-ray diffraction instrument consisted of a Bruker D8 three-circle diffractometer equipped with a rotating anode generator (MoK α X-radiation), multi-layer optics, APEX-II CCD detector, and an Oxford 700 Series liquid-N Cryostream. The intensities of more than 100 reflections were harvested from six frame series (each spanning 15° in either ω or φ) collected to 60° 2θ using 0.6 s per 1° frame with a crystal-to-detector distance of 5 cm. In total, 12 crystals (one from all ice layers investigated from both ICE I and POLY I) were identified through successful indexing of observed x-ray diffraction maxima onto known characteristic unit cells.

To determine TA and total dissolved inorganic carbon (TCO_2) concentrations in sea ice, three sea ice cores were cut into 5–10 cm sections and brought to the field laboratory. Here, the ice segment was placed immediately in a gas-tight laminated (Nylon, ethylene vinyl alcohol, and polyethylene) plastic bag (Hansen et al., 2000) fitted with a 50 cm gas-tight Tygon tube and a valve for sampling. The weight of the bag containing the sea ice sample was recorded. Cold (1 °C) deionized water (25–50 mL) of known weight and TA and TCO_2 concentration was added. The plastic bag was closed immediately and excess air and deionized water quickly removed through the valve and weighed. The weight of the deionized water accounted for <5 % of the sea ice weight. This processed sea ice was subsequently melted, and the meltwater mixture transferred to a gas-tight vial (12 ml Ex-tainer, Labco High Wycombe, UK). Any $CaCO_3$ crystals present in these ice core sections are expected to have dissolved during sample processing and, thus, be included in the measured TA and TCO_2 concentrations. Standard methods of analysis were used: TCO_2 concentrations were measured on a coulometer (Johnson et al., 1987), TA by potentiometric titration (Haraldsson et al., 1997), and gaseous CO_2 by gas chromatography. Routine analysis of Certified Reference Materials (provided by A. G. Dickson, Scripps Institution of Oceanography) verified that TCO_2 and TA concentrations ($n = 3$) could be analyzed within $\pm 1 \mu\text{mol kg}^{-1}$ and $\pm 4 \mu\text{mol kg}^{-1}$, respectively. Bulk concentrations of TA and TCO_2 in the sea ice (C_i) were calculated as $C_i = [(C_m W_m - C_a W_a) / W_i]$, where C_m is the TA or TCO_2 concentration in the meltwater mixture, W_m is the weight of the meltwater mixture, C_a is the TA or TCO_2 concentration in the deionized water, W_a is the weight of the deionized water, and W_i is the weight of the sea ice (Rysgaard et al., 2008).

Following the bulk determination of TCO_2 and TA, the bulk pCO_2 and pH (on the total scale) were computed using the temperature and salinity conditions in the field and a standard set of carbonate system equations, excluding nutrients, with the CO2SYS program of Lewis and Wallace (2012). We used the equilibrium constants of Mehrbach et al. (1973) refitted by Dickson and Millero (1987, 1989).

In summary, triplicate cores were collected 18, 20 and 24 March for snow and ice thickness determination, ice temperatures and bulk ice salt concentrations. Measurements were performed on the same cores. Triplicate separate cores

were sampled for determination of TCO_2 and TA concentrations. Ice texture, density and photo documentation of ikaite location in intact ice corers were performed on triplicate separate cores (ICE I, 17 March: POLY I, 20 March). Ikaite image analysis for concentration determination was done on three separate cores collected 18, 20 and 24 March. X-ray diffraction analyses were performed on a separate core collected 24 March. Samples for bulk salt, TA, TCO_2 , ikaite crystal abundance and concentration were processed immediately in the field laboratory. Crystals for ikaite determination on x-ray were kept frozen (-20°C) until analysis a month later. Photo documentation showed that ikaite crystal morphology did not change due to storage. Thus, prolonged freezing period prior analysis should not affect the results obtained. However, it is important that preservation of TA, TCO_2 and quantification of ikaite is done in the field. These samples should not be stored at low temperatures before analysis as $CaCO_3$ could be produced during the storage.

2.3 FREZCHEM modeling

The production of ikaite in the sea ice cores was modeled by FREZCHEM (version 10), an equilibrium chemical thermodynamic model parameterized for concentrated solutions (up to 20 mol kg^{-1} (H_2O)) and sub-zero temperatures (to -70°C) (Marion et al., 2010). The model uses the Pitzer approach correcting for activity coefficients of solutes in concentrated solutions. Our calculation was done by following the freezing process of seawater with the same chemical composition as the local seawater under the local pCO_2 values; the thermodynamic constants used were the default values provided with the model. It should be noted that FREZCHEM modeling is based on the assumption that chemical species in the sea ice environment (ice, brine, and air) have reached thermodynamic equilibrium, and that most of the thermodynamic constants used in the model were extrapolated to low temperatures rather than being directly determined experimentally. Nevertheless, the model has shown promising applications in exploring cold geochemical processes associated with seawater freezing among many others (Marion et al., 1999, 2010).

3 Results

Sea ice covered the fjord on our arrival, but there was a polynya outside the fjord with a distinct ice edge running across the fjord between Wollaston Forland and Clavering Island (Fig. 1). Several freezing and opening incidents were observed in this area from satellite images prior to our arrival; however, due to low temperatures of -20°C to -36°C and calm conditions, the polynya began to re-freeze prior to our sampling. Due to the insulating effect of the thick (70 cm) snow cover at ICE I, our land-fast station in the fjord, sea ice surface temperature was relatively warm, -10°C ,

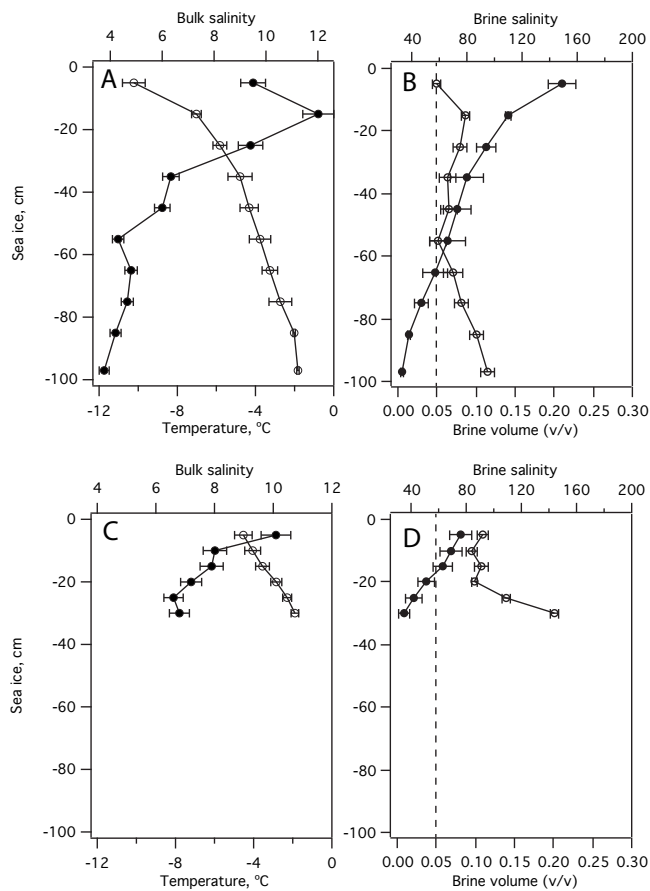


Fig. 2. Vertical profiles of sea ice features. (A) Temperature (—○) and bulk salinity (—●) and (B) brine volume (—○) and brine salinity (—●) at ICE I. (C) Temperature (—○) and bulk salinity (—●) and (D) brine volume (—○) and brine salinity (—●) at POLY I. Vertical dotted line represents the brine volume where sea ice becomes permeable.

with a gradient to -2°C towards the sea ice–water interface (Fig. 2a). Bulk salinities ranged from 10–12 in the top layers to 4 at the bottom. Calculated brine volumes ranged from less than 5% in surface layers to 12% near the bottom (Fig. 2b); brine salinities, from 150 in the surface sea ice to 33 near the water column. At POLY I, our new-ice station in the polynya where snow cover was thinner (17 cm), surface sea ice temperature was only -5°C (Fig. 2c) due to the rapid freezing with concurrent heat release and proximity to the water column (thin ice of 15–30 cm). Bulk salinities ranged from 10 in surface ice layers to 7 in the lower ice layers (Fig. 2c). Given high bulk salinities and temperatures, brine volumes ranged from 10% in the top layers to 20% in the lower ice layers; brine salinities were lower at ICE I, ranging from 78 at the surface to 33 near the water column (Fig. 2d).

The upper 35 cm of sea ice at ICE I was composed of polygonal granular ice, formed through percolation and re-freezing of brine and seawater into snow, i.e. snow ice (Fig. 3a). The snow ice formation was likely promoted by

negative freeboard. The fact that we do not observe flooding is probably due to low temperatures (brine or seawater quickly refreezes in the cold snow). Daily images with automatic camera systems (MarinBasis Program, c/o Greenland Institute of Natural Resources) show that sea ice started to form locally outside the fjord in early October, and that those ice floes drifted into the fjord and consolidated with local ice to form a uniform ice cover that persisted through our study. Thus, the top layers of ice at ICE I may have been produced outside the fjord. The ice layer from 35–112 cm consisted of columnar sea ice (Fig. 3d). Microscopic examination of different vertical and horizontal ice thin sections showed the presence of ikaite crystals throughout the ice column (Fig. 3b, c and e, f). Ikaite crystals were located in the interstices between the ice platelets.

The sea ice at POLY I was less than one week old when first sampled. The upper 5 cm of the ice consisted of orbicular granular ice crystals, followed by transitional granular/columnar texture from 5 to 12 cm (Fig. 4a). This uppermost layer closely resembles the disc-like granular ice observed in nilas (Ehn et al., 2007) and may be related to freezing of brine expelled to the sea ice surface. The transition into mainly columnar-like sea ice occurred at around 10–12 cm from the surface and continued to the sea ice–water interface (29 cm); however, the disorderly structure implies intrusion of frazil ice and platelet ice forms, and thus supercooling at the ice–ocean interface was a significant factor in determining the ice structure. Similarly to ICE I, microscopic examination of thin ice sections from POLY I revealed the presence of ikaite crystals throughout the ice column (Fig. 4b, c and e, f). Ikaite crystals were again observed primarily in the interstices between the ice platelets.

Ikaite crystals become easily visible when the sea ice melts. As an example from POLY I, 19 crystals were observed a few seconds after melting 50 mg of randomly subsampled sea ice (10–20 cm section; Fig. 5a and b). Allowing the crystals to dissolve for a few minutes before taking another image allowed us to identify ikaite crystals (as the ones that had dissolved; Fig. 5c). In this case, the crystal area covered 0.48% of the counting area.

At ICE I, the number of ikaite crystal per kg of melted ice ranged from $\sim 25 \times 10^6 \text{ kg}^{-1}$ in the upper layers to $\sim 1 \times 10^6 \text{ kg}^{-1}$ near the ice–water interface (Fig. 6a). At POLY I, similar ikaite abundances were observed in upper ice layers, whereas abundances near the water column reached $\sim 7 \times 10^6 \text{ kg}^{-1}$ (Fig. 6b). The molar concentration of ikaite per kg melted ice at ICE I decreased with depth from surface values of $900 \mu\text{mol kg}^{-1}$ to $100 \mu\text{mol kg}^{-1}$ near the ice–water interface. At POLY I, the highest concentrations ($700 \mu\text{mol kg}^{-1}$) were observed at 5–10 cm from the ice surface, decreasing to $\sim 200 \mu\text{mol kg}^{-1}$ near the water column.

The crystals (a few μm to $700 \mu\text{m}$ in size) observed in the sea ice were highly transparent with a rhombic morphology and showed uniform extinction under cross-polarized

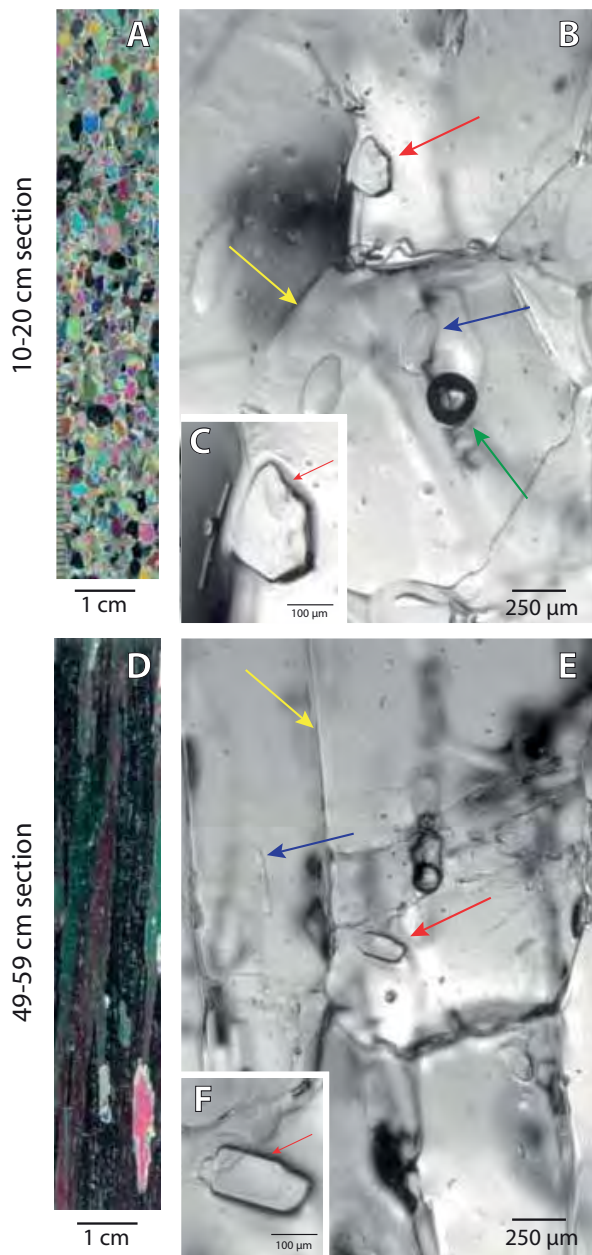


Fig. 3. Images of sea ice with ikaite crystals, from ICE I. (A, D) Sea ice texture (polarized light); (B, E) microscopic images of sea ice. Yellow arrows point to ice crystal borders, blue arrows to brine pockets, green arrows to air bubbles and red arrows to ikaite crystals. (C, F) Ikaite crystals at higher magnification. (A), (B) and (C) from 10–20 cm section; (D), (E) and (F) from 49–59 cm section.

light, suggesting that they were simple single crystals. All x-ray reflections fitted well to a monoclinic C-centered cell with refined cell parameters shown in Table 1. From the general shape, optical properties and unit-cell determination, the crystals examined were ikaite (Hesse and Küppers, 1983). The crystals identified as ikaite had a very distinct

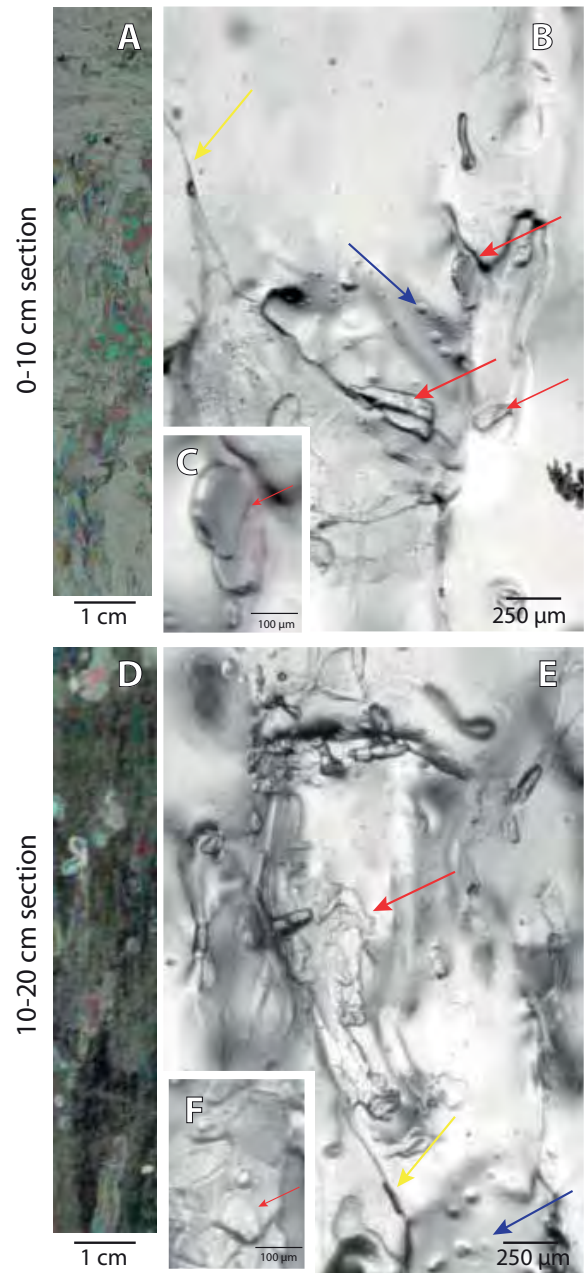


Fig. 4. Images of sea ice with ikaite crystals, from POLY I. (A, D) Sea ice texture (polarized light); (B, E) microscopic image of sea ice. Yellow arrows point to ice crystal borders, blue arrows to brine pockets, and red arrows to ikaite crystals. (C, F) Ikaite crystals at higher magnification. (A), (B) and (C) from 0–10 cm section; (D), (E) and (F) from 10–20 cm section.

morphology, and were easily recognized with two significant variations: the more common thicker rhombs (Fig. 7a) and rather rare thinner plates (Fig. 7b). Whereas ikaite crystals in intact sea ice sometimes were assembled in aggregates such as the ones illustrated in Fig. 4e and f, they consisted mostly of isolated rhombic forms and thin plates as observed under

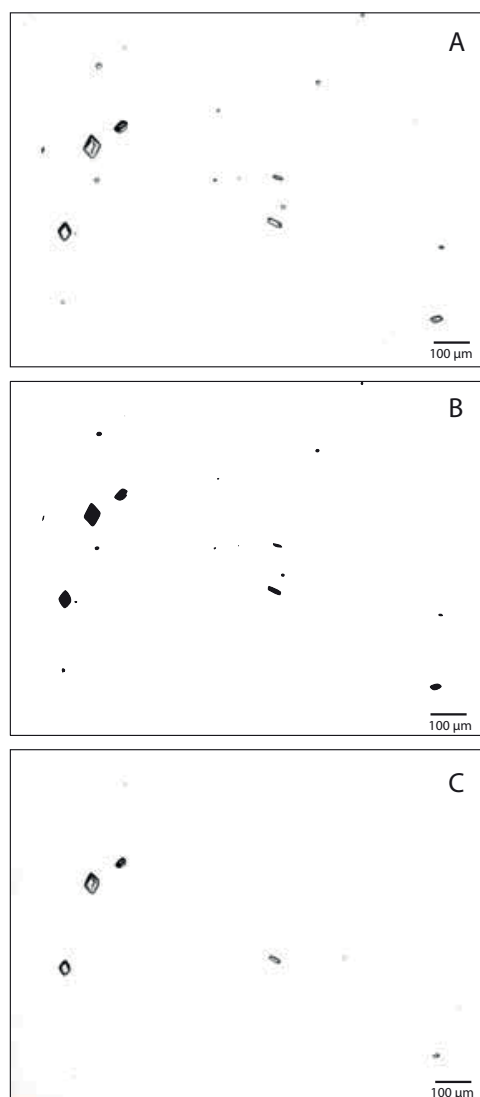


Fig. 5. Microscopic images of ikaite crystals (A) a few seconds after melting 50 mg sea ice (10–20 cm section) from POLY I. Image represents a very small fraction (2 μg) of the sample. (B) Software (ImageJ 1.45 s) processing of image A to find the number (19) and area (0.48 % of counting area) of the crystals. (C) Image taken after 2 min showing that crystals are dissolving.

the microscope immediately after ice platelets had melted (Fig. 5).

Surface TA concentrations of 600–800 $\mu\text{mol kg}^{-1}$ melted sea ice were measured at ICE I, with decreasing concentrations to 380 $\mu\text{mol kg}^{-1}$ melted sea ice in ice layers close to the water column (Fig. 8a). $T\text{CO}_2$ values at ICE I had similar vertical distribution with lower concentrations. At POLY I site, TA values were measured at $\sim 800 \mu\text{mol kg}^{-1}$ melted sea ice near the surface, and decreased to $\sim 500 \mu\text{mol kg}^{-1}$ melted sea ice near the water column. As at ICE I, the vertical $T\text{CO}_2$ concentrations at POLY I were similar to TA, but with lower values.

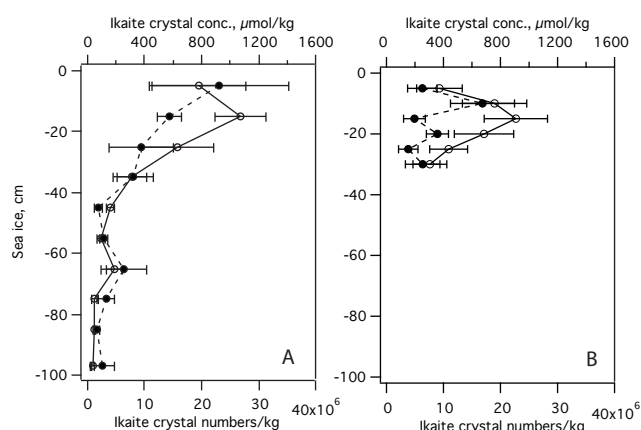


Fig. 6. Vertical distribution of ikaite crystals determined from image analysis. Abundance of crystals (–o–) and concentration of ikaite (–●–) at ICE I (A) and POLY I (B).

4 Discussion

4.1 Spatial and temporal variability of ikaite occurrence and concentration

Ikaite concentrations from this study are higher than those reported previously: 10 times higher than those measured in spring sea ice from Antarctica (Dieckmann et al., 2008), and 4 times higher than in surface summer ice from Fram Strait (160–240 $\mu\text{mol kg}^{-1}$ melted sea ice; Rysgaard et al., 2012). The differences may be explained in part by differences in quantification procedure, as our study is unique in employing immediate analysis in the field without prolonged melting. The higher values we report may also reflect real differences between sites and seasons, as we present results for winter sea ice, while other studies were conducted in spring and summer with melt already apparent. As a result, a fraction of ikaite crystals in the previous studies may already have been dissolved due to ice warming and melting or lost via brine drainage. In addition, ikaite crystals were observed in the week-old POLY I sea ice and even within 1 hour in frost flowers and thin ice in an artificially opened lead (data to be presented elsewhere). This observation indicates dynamic conditions of ikaite formation even on short timescales. Understanding the dynamics of those processes is an important objective for future studies. Here, we note that higher concentrations of ikaite in surface sea ice are predicted by the FREZCHEM model (Marion et al., 2010). Assuming that a standard seawater ($S = 35$, $[\text{Na}^+] = 0.4861$, $[\text{K}^+] = 0.01058$, $[\text{Ca}^{2+}] = 0.01065$, $[\text{Mg}^{2+}] = 0.05475$, $[\text{Cl}^-] = 0.56664$, $[\text{SO}_4^{2-}] = 0.02927$, $[\text{HCO}_3^-] = 0.0023$; ions concentration unit: mole kg^{-1} water) freezes in an open system with $p\text{CO}_2 = 320 \mu\text{atm}$, the FREZCHEM model predicts an ikaite concentration of up to 620 $\mu\text{mol kg}^{-1}$ sea ice in the cold surface layer of ICE I, decreasing exponentially downwards (Fig. 9). Both the concentration range

Table 1. X-ray diffraction data. Refined unit-cell parameters for ikaite crystals identified by x-ray diffraction analysis. () = Standard deviation, R = rhombs, TP = thin plate.

ICE I Section						
cm		$a(\text{\AA})$	$b(\text{\AA})$	$c(\text{\AA})$	$\beta(^{\circ})$	$V(\text{\AA}^3)$
0–10	R	8.808(2)	8.313(2)	11.031(2)	110.59(1)	756.1(8)
10–20	R	8.820(2)	8.330(2)	11.050(3)	110.57(2)	761.7(4)
20–30	TP	8.823(3)	8.326(3)	11.049(4)	110.64(2)	759.6(7)
30–40	R	8.813(2)	8.312(2)	11.034(3)	110.60(1)	756.7(4)
40–50	R	8.817(3)	8.312(2)	11.027(3)	110.58(2)	756.6(5)
50–60	R	8.812(2)	8.311(1)	11.040(2)	110.58(1)	756.9(6)
60–70	R	8.831(3)	8.320(2)	11.047(3)	110.55(2)	760.1(6)
70–80	R	8.812(2)	8.318(2)	11.031(3)	110.56(2)	757.0(8)
80–90	R	8.819(2)	8.315(2)	11.025(3)	110.57(2)	758.3(5)
90–100	TP	8.820(2)	8.323(2)	11.049(2)	110.64(1)	759.2(5)

POLY I Section						
cm		$a(\text{\AA})$	$b(\text{\AA})$	$c(\text{\AA})$	$\beta(^{\circ})$	$V(\text{\AA}^3)$
0–10	TP	8.816(3)	8.333(2)	11.043(3)	110.68(2)	759.1(6)
10–20	TP	8.810(1)	8.320(1)	11.033(1)	110.58(1)	757.1(2)

and distribution pattern agreed well with the empirical data at ICE I. Although the FREZCHEM modeling assumes that the system reaches thermodynamic equilibrium and is always open to a constant $p\text{CO}_2$, assumptions that are not fulfilled under natural conditions, the modeling results nevertheless support the observation that ikaite concentration increases with decreasing temperature. Seasonally variable ikaite concentration, with highest values in winter, is thus expected.

It is a key point as to exactly where the crystals are located. If they are in the brine channels then they can potentially move with the circulation of brine as the temperatures change internally in the ice. If they are isolated from larger brine networks and are located at the interstices then they may remain trapped in the ice as convection occurs. This will make a big difference on the exchange through winter and well into spring. Our images document that ikaite crystals are located between the interstices of the sea ice matrix between the pure ice platelets. As they are particles they can be trapped between the small interstitial pore spaces and therefore retained in the ice. In contrast, solutes and gases (CO_2), as well as organic particles including microorganisms (Junge et al., 2001; Krembs et al., 2011), can be transported within the brine system. It was possible to see brine motion in the microscope as small particles and air bubbles moved between the interstices of ice platelets. Increasing the temperature by a few degrees significantly accelerated the transport velocity. The TA: bulk salinity ratio in sea ice was 84 ± 4 (ICE I) and 78 ± 0.8 (POLY I) as compared with the water column 67 ± 3 (ICE I) and 61 ± 0.2 (POLY I). Thus, the higher TA-S ratio in sea ice than in seawater shows that CaCO_3 release adds a

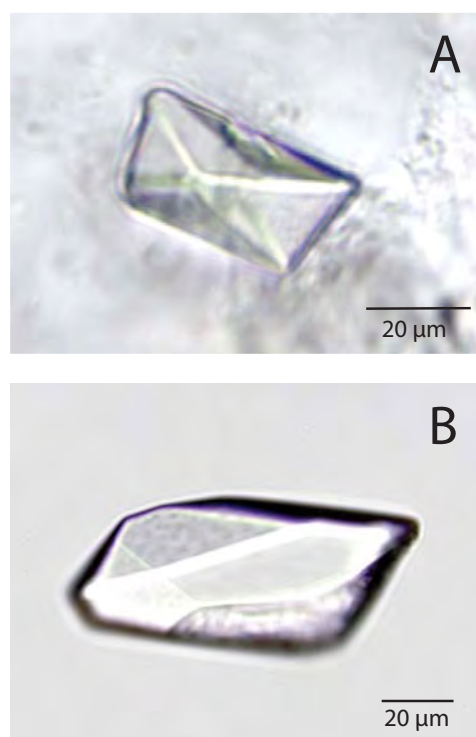


Fig. 7. Two most common forms of ikaite in freezing sea ice. (A) rhombs, (B) thin plates.

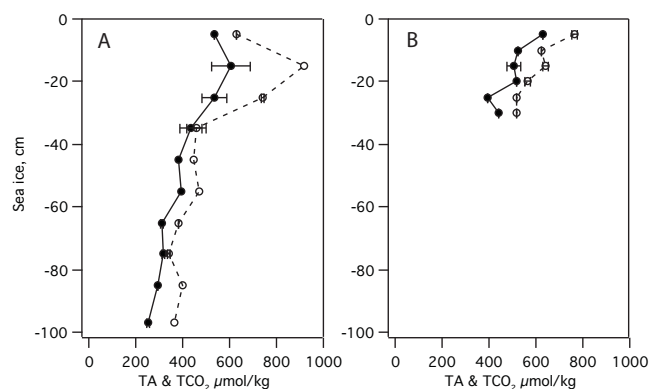


Fig. 8. Vertical profiles of concentration of total alkalinity (–o–) and dissolved inorganic carbon (–●–) in (A) at ICE I and (B) at POLY I.

further alkalinity contribution to the simple melt of ice. These observations confirm previous hypotheses (Rysgaard et al., 2007, 2009, 2011) that ikaite crystals are trapped within the sea ice matrix, whereas CO_2 released through ikaite production (Eq. 1) and dissolved within the brine can be lost from the sea ice. As a result, CaCO_3 stores twice as much TA as $T\text{CO}_2$, hence TA of the meltwater increases relative to $T\text{CO}_2$ in sea ice. When ikaite crystals dissolve during sea ice melt, surface water $p\text{CO}_2$ will decrease. This is important as low

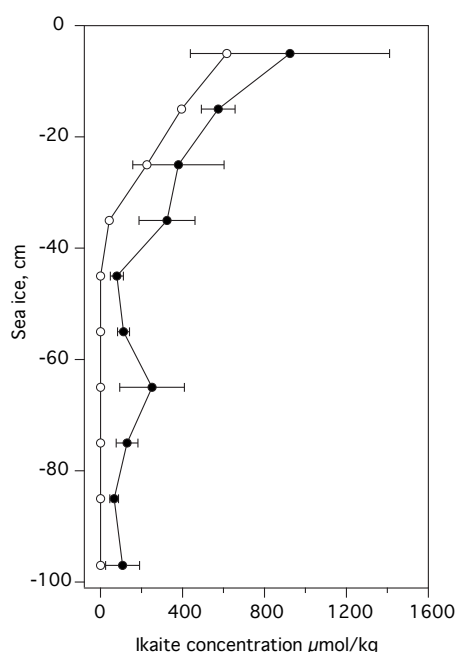


Fig. 9. Vertical profiles of ikaite concentration. Measured (●) and FREZCHEM calculated (○) at ICE I.

$p\text{CO}_2$ values in surface waters will lead to a large CO_2 flux from the atmosphere into the ocean.

Bulk TA concentrations in surface ice layers (including ikaite crystals) were within the same range as ikaite concentrations, implying that most of TA is present in the crystal form of ikaite and, thus, trapped within the surface sea ice matrix. In contrast, bulk TA concentrations were higher than ikaite crystal concentrations in the internal and bottom layer of the sea ice at both stations, implying that not all TA in the lower ice layers originate from ikaite crystals. One explanation for this finding invokes dissolution or reduced growth rate of ikaite in interior ice layers due to exposure to excess CO_2 originating from cold upper ice layers, where elevated brine concentrations of Ca^{2+} and HCO_3^- are higher due to lower brine volumes. The CO_2 released in upper ice could be transported to interior ice layers by downward brine drainage. Low pH conditions in interior ice layers have recently been reported for experimental sea ice (Hare et al., 2013). Here, vertical pH profiles for bulk ice, as measured at near-freezing temperatures, revealed a consistent C-shaped pattern during columnar ice growth, with the highest pH values (>9) in both the exterior (top and bottom) ice sections and lowest pH (~ 7) in the interior ice sections (Hare et al., 2013). Calculating the vertical pH profile at ICE I, using temperature and bulk salinity (Fig. 2) and TA and $T\text{CO}_2$ conditions (Fig. 8) from our winter ice study, yielded a similar C-shaped pH profile with high pH (>9) in surface and bottom ice layers, and lower pH (~ 8) in interior layers. At POLY I, a C-shaped pH profile was also estimated, although

the pH values in exterior layers were slightly lower (~ 8.5). The sum of these findings suggests that downward transport of pH equivalents could be responsible for dissolving ikaite in the interior ice layers.

Another mechanism that could affect the dissolution/precipitation dynamics of trapped ikaite crystals involves convective solutes (Worster and Wettlaufer, 1997) ensuring contact between the interior brine system and the underlying water column. CO_2 -enriched brine can exchange with seawater via gravity drainage (Notz and Worster, 2009) if the brine volume is above 5% to allow vertical ice permeability (Cox and Weeks, 1975; Notz and Worster, 2009). In this study, brine volume fractions were above 5% in the lower 50 cm of sea ice at ICE I, and throughout the ice column at POLY I. Thus, the increase in pH in the sea ice layers close to the water column could be caused by replenishment of brine with surface seawater (pH 8.1–8.3).

4.2 Role of ikaite in seawater CO_2 system and gas exchange

The observation that ikaite crystals are trapped within the sea ice matrix, while CO_2 dissolved in the brine through ikaite production (Eq. 1) can be mobile (lost from the ice with brine), means that ikaite crystal formation increases the amount of CO_2 available for export beyond that attributed solely to the solubility effect. The implication is that, in an open system, TA is preferentially stored in the sea ice as ikaite, raising the buffering capacity of sea ice (and surface water) upon melting and subsequent crystal dissolution. With trapped ikaite crystals, ice melt will therefore lead to both lower surface water salinity and $p\text{CO}_2$. As the low $p\text{CO}_2$ meltwater remains at the ocean surface due to density stratification gradient, CO_2 flux from the atmosphere to the surface will be enhanced (Rysgaard et al., 2012). Based on data from this study, the melting of sea ice (salinity from Fig. 2, TA and $T\text{CO}_2$ from Fig. 8) at 0°C and dissolution of observed concentrations of ikaite (Fig. 6) would result in meltwater with a $p\text{CO}_2$ of $<15 \mu\text{atm}$ at both sites. This value is far below atmospheric values of $390 \mu\text{atm}$ and surface water concentrations of $315 \mu\text{atm}$ measured in this study. Hence, the meltwater can increase the air–sea CO_2 uptake.

During ice growth, $p\text{CO}_2$ in the brine system will increase and reduce pH in interior ice layers. In the surface ice layer, released CO_2 may escape to the atmosphere or be transported to deeper ice layers by downward brine drainage. Few measurements of air–sea CO_2 fluxes have been reported for winter conditions. Geilfus et al. (2012) detected no CO_2 release for ice surface temperatures below -10°C , instead observing a small negative flux (into the sea ice) of $0.23 \text{ mmol m}^{-2} \text{ d}^{-1}$ over sea ice in the Amundsen Gulf, Beaufort Sea. Miller et al. (2011) measured fluctuating CO_2 fluxes over sea ice with strong downward fluxes in February in the Southern Beaufort Sea. Sejr et al. (2011) observed that 99% of $T\text{CO}_2$ in newly forming ice over drilled holes

in meter thick sea ice was rejected to the underlying seawater in Young Sound, Greenland. The suggestion that most of the CO₂ released through ikaite crystal formation will sink towards the seawater in dense brine is consistent with these several findings.

The fate of CO₂ expelled from the sea ice to seawater remains unclear. Dense brine production in the polynya region (Anderson et al., 2004) may provide a mechanism to deliver CO₂ below the mixed layer, making ikaite production in sea ice a “carbon pump” that removes CO₂ from the surface ocean to deeper water layers (Rysgaard et al., 2009, 2011). Low-density ice meltwater remaining at the surface will facilitate atmospheric CO₂ deposition as a result of ikaite dissolution. An air–sea CO₂ flux of $-10.6 \text{ mmol m}^{-2} \text{ d}^{-1}$ has been reported during spring and summer for the region previously (Rysgaard et al., 2012).

Geilfus et al. (2012) calculated, based on the carbon chemistry in the sea ice brine in equilibrium partitioning with the atmosphere, that melting of a 1.3 m thick sea ice cover within one month in the Beaufort Sea could lead to CO₂ fluxes ranging from -1.2 to $-3.1 \text{ mmol m}^{-2} \text{ d}^{-1}$, which are comparable to CO₂ fluxes measured over melt ponds. At ICE I, we calculated the potential influence of melting the entire ice cover into a 20 m thick mixed layer (typical for summer conditions at this location) on the CO₂ flux in the region, using the measured ice carbon chemistry (salinity of 6.5, TA of $516 \text{ } \mu\text{mol kg}^{-1}$, $T\text{CO}_2$ of $406 \text{ } \mu\text{mol kg}^{-1}$, and average temperature of 0 °C) and the initial mixed layer characteristics (average temperature of 0 °C, salinity of 31.7, TA of $2276 \text{ } \mu\text{mol kg}^{-1}$, and $T\text{CO}_2$ of $2101 \text{ } \mu\text{mol kg}^{-1}$). The resultant conditions in a 20 m mixed layer (temperature of 0 °C, salinity of 30.4, TA of $2184 \text{ } \mu\text{mol kg}^{-1}$, and $T\text{CO}_2$ of $2013 \text{ } \mu\text{mol kg}^{-1}$) would cause a $14 \text{ } \mu\text{atm}$ decrease in $p\text{CO}_2$. Assuming the melt occurs over one month, the resultant air–sea CO₂ flux to return to pre-melt conditions would be $-5.9 \text{ mmol m}^{-2} \text{ d}^{-1}$, which falls within the range reported previously.

This calculation is based on a single melt event and does not account for the numerous cycles of sea ice growth and melt characteristic of polynya systems (Tamura and Ohshima, 2011; Drucker et al., 2011). The polynya formation at POLY I is predominantly governed by mechanical forcing caused by northerly gales; it has been classified as a wind-driven shelf water system (Pedersen et al., 2010), where sea ice formation is continuous and rejection of CO₂ to deeper water layer with dense brine occurs (Anderson et al., 2004). Ikaite crystals trapped in the forming sea ice will be exported with the ice to melt elsewhere. Such polynya systems are thus likely to export CO₂ to depth effectively. Based on results presented here, enhanced ice production in winter polynyas would add considerable amounts of TA to the surface waters in the form of ikaite crystals from sea ice, lowering surface water $p\text{CO}_2$ upon ice melt and crystal dissolution, and increasing the potential for seawater uptake of CO₂.

An interesting observation in the polynya region we have studied (Sejr et al., 2011; Papakyriakou et al., 2013) is that the $p\text{CO}_2$ levels in the water column are very low, gradually increasing with depth from surface values of $315 \text{ } \mu\text{atm}$ to $360 \text{ } \mu\text{atm}$ at 80 m. During the present study, the average $p\text{CO}_2$ concentration of the upper 20 m water column was $335 \text{ } \mu\text{atm}$ compared to $390 \text{ } \mu\text{atm}$ in the atmosphere. As melting 1 m of sea ice will reduce $p\text{CO}_2$ levels by $14 \text{ } \mu\text{atm}$ in a 20 m water column according to the calculations above, $\sim 4 \text{ m}$ of sea ice would need to melt locally to explain the low $p\text{CO}_2$ concentrations in the water column. In polynya areas the sea ice production is usually much greater than indicated by the annual sea ice thickness due to the continued production of ice (McLaren, 2006). The local ice production at POLY I is thus likely responsible for much more larger ice growth than the April–May ice thickness of 1.4–1.6 m usually observed at ICE I (Rysgaard and Glud, 2007). Furthermore, the study site is located on the NE Greenland Sea shelf where large amounts of sea ice exported from the Arctic Ocean through Fram Strait subsequently melt during southward transport toward the Denmark Strait (Vinje, 2001). Sea ice containing ikaite crystals as observed in the present study may well explain a large part of the low $p\text{CO}_2$ levels in the upper part of the water column due to melting of sea ice from previous summer/autumn in the area. Biological CO₂ fixation will also contribute to the atmospheric draw-down, but constraining this factor is beyond the scope of the present study. The current work nevertheless supports previous model calculations from the area estimating that melting of sea ice exported from the Arctic Ocean into the East Greenland current and the Nordic Seas greatly increases the seasonal and regional CO₂ uptake in the area (Rysgaard et al., 2009). More work is required to determine how applicable our results are to other regions of the Arctic (or Antarctic), given the variable nature of CaCO₃ among the few available ikaite studies (above references) and the seasonal nature of $p\text{CO}_2$ in ice-free Arctic systems (Mucci et al., 2010; Cai et al., 2010).

5 Conclusions

We report unique observations of ikaite in unmelted ice and vertical profiles of ikaite abundance and concentration in sea ice for the crucial season of winter. Ikaite crystals, ranging in size from a few μm to $700 \mu\text{m}$, were observed to concentrate in the interstices between the ice platelets in both granular and columnar sea ice. Their concentration decreased with depth from surface-ice values of $700\text{--}900 \text{ } \mu\text{mol kg}^{-1}$ ice ($\sim 25 \times 10^6$ crystals kg^{-1}) to values of $100\text{--}200 \text{ } \mu\text{mol kg}^{-1}$ ice ($1\text{--}7 \times 10^6$ crystals kg^{-1}) near the ice–water interface, all of which are much higher (4–10 times) than those reported in the few previous studies. Direct measurements of TA in surface layers fell within the same range as ikaite concentration, whereas TA concentrations in

interior and bottom layers were twice as high. This depth-related discrepancy suggests interior ice processes where ikaite crystals form in surface sea ice layers and partly dissolve in internal ice layers. The result is a C-shaped pH profile with high pH (>9) in surface and bottom ice layers, and lower pH (~8) in interior layers. Based on results presented here, enhanced ice production in winter polynyas would add considerable amounts of TA to the surface waters in the form of ikaite crystals from sea ice, lowering surface water $p\text{CO}_2$ upon ice melt and crystal dissolution, and increasing the potential for seawater uptake of CO_2 in regions downstream where the ice melts.

Acknowledgements. The study received financial support from Canada Excellence Research Chair (CERC) program, the Danish Agency for Science, Technology and Innovation, the Arctic Research Centre at Aarhus University, the Commission for Scientific Research in Greenland. J. W. D. acknowledges support from OPP RAPID award from the US National Science Foundation. Egon Frandsen, Ivali Lennert and Bruce Johnson are thanked for outstanding assistance in the field.

Edited by: R. Lindsay

References

- Anderson, L. G., Falck, E., Jones, E. P., Jutterström, S., and Swift, J. H.: Enhanced uptake of atmospheric CO_2 during freezing of seawater: A field study in Storfjorden, Svalbard, *J. Geophys. Res.*, 109, C06004, doi:10.1029/2003JC002120, 2004.
- Assur, A.: Composition of sea ice and its tensile strength, SIPRE Research Report 44, 1960.
- Cai, W.-J., Chen, L., Chen, B., Gao, Z., Lee, S. H., Chen, J., Pierrot, D., Sullivan, K., Wang, Y., Hu, X., Huang, W.-J., Zhang, Y., Xu, S., Murata, A., Grebmeier, J. M., Jones, E. P., and Zhang, H.: Decrease in the CO_2 Uptake Capacity in an Ice-Free Arctic Ocean Basin, *Science*, 329, 556–559, doi:10.1126/science.1189338, 2010.
- Cox, G. F. N. and Weeks, W. F.: Brine drainage and initial salt entrapment in sodium chloride ice, *CRREL Res. Rep.* 345, US Army Cold Reg. Res. and Eng. Lab., Hanover, N.H., 1975.
- Cox, G. F. N. and Weeks, W. F.: Equations for determining the gas and brine volumes in sea ice samples, *J. Glaciol.*, 29, 306–316, 1983.
- Delille, B., Jourdain, B., Borges, A. V., Tison, J.-P., and Delille, D.: Biogas (CO_2 , O_2 , dimethylsulfide) dynamics in spring Antarctic fast ice, *Limnol. Oceanogr.*, 52, 1367–1379, doi:10.4319/lo.2007.52.4.1367, 2007.
- Dickson, A. G. and Millero, F. J.: A comparison of the equilibrium constants for the dissociation of carbonic acid in seawater media, *Deep-Sea Res.*, 34, 1733–1743, 1987.
- Dickson, A. G. and Millero, F. J.: Corrigenda, *Deep-Sea Res.*, 36, p. 983, 1989.
- Dieckmann, G. S., Nehrke, G., Papadimitriou, S., Göttlicher, J., Steinger, R., Kennedy, H., Wolf-Gladrow, D., and Thomas, S. N.: Calcium carbonate as ikaite crystals in Antarctic sea ice, *Geophys. Res. Lett.*, 35, L08501, doi:10.1029/2008GL033540, 2008.
- Dieckmann, G. S., Nehrke, G., Uhlig, C., Göttlicher, J., Gerland, S., Granskog, M. A., and Thomas, D. N.: Brief Communication: Ikaite ($\text{CaCO}_3 \cdot 6\text{H}_2\text{O}$) discovered in Arctic sea ice, *The Cryosphere*, 4, 227–230, doi:10.5194/tc-4-227-2010, 2010.
- Drucker, R., Martin, S., and Kwok, R.: Sea ice production and export from coastal polynyas in the Weddell and Ross Seas, *Geophys. Res. Lett.*, 38, L17502, doi:10.1029/2011GL048668, 2011.
- Ehn, J. K., Hwang, B. J., Galley, R., and Barber D. G.: Investigations of newly formed sea ice in the Cape Bathurst polynya: 1. Structural, physical, and optical properties, *J. Geophys. Res.*, 112, C05002, doi:10.1029/2006JC003702, 2007.
- Geilfus, N.-X., Carnat, G., Papakyriakou, T., Tison, J.-L., Else, B., Thomas, H., Shadwick, E., and Delille, B.: Dynamics of $p\text{CO}_2$ and related air-sea CO_2 fluxes in the Arctic coastal zone (Amundsen Gulf, Beaufort Sea), *J. Geophys. Res.*, 117, C00G10, doi:10.1029/2011JC007118, 2012.
- Geilfus, N.-X., Carnat, G., Dieckman, G. S., Halden, N., Nehrke, G., Papakyriakou, T., Tison, J.-L., and Delille, B.: First estimates of the contribution of CaCO_3 precipitation to the release of CO_2 to the atmosphere during young sea ice growth, *J. Geophys. Res. Ocean*, 118, 1–12, doi:10.1029/2012JC007980, 2013.
- Golden, K. M., Ackley, S. F., and Lytle, V. I.: The percolation phase transition in sea ice, *Science*, 282, 2238–2241, 1998.
- Golden, K. M., Eicken, H., Heaton, A. L., Miner, J., Pringle, D. J., and Zhu, J.: Thermal evolution of permeability and microstructure in sea ice, *Geophys. Res. Lett.* 34, L16501, doi:10.1029/2007GL030447, 2007.
- Hansen, J. W., Thamdrup, B., and Jørgensen, B. B.: Anoxic incubation of sediment in gas tight plastic bags: A method for biogeochemical process studies, *Mar. Ecol. Prog. Ser.*, 208, 273–282, 2000.
- Haraldsson, C., Anderson, L. G., Hasselöv, M., Hult, S., and Olsson, K.: Rapid, high-precision potentiometric titration of alkalinity in ocean and sediment pore water, *Deep-Sea Res. Pt. I*, 44, 2031–2044, 1997.
- Hare, A. A., Wang, F., Barber, D., Geilfus, N.-X., Galley, R., and Rysgaard, S.: pH evolution in sea ice grown at an outdoor experimental facility, *Mar. Chem.*, in press, 2013.
- Hesse, K. F. and Küppers, H.: Refinement of the structure of Ikaite, $\text{CaCO}_3 \cdot 6\text{H}_2\text{O}$, *Z. Kristallographie*, 163, 227–231, 1983.
- Johnson, K. M., Sieburth, J. M., Williams, P. J., and Brändström, L.: Coulometric total carbon dioxide analysis for marine studies: Automation and calibration, *Mar. Chem.*, 21, 117–133, 1987.
- Junge, K., Krembs, C., Deming, J., Stierle, A., and Eicken, H.: A microscopic approach to investigate bacteria under in situ conditions in sea-ice samples. *Ann. Glaciol.*, 33, 304–310, 2001.
- Krembs, C., Eicken, H., and Deming, J. W.: Exopolymer alteration of physical properties of sea ice and implications for ice habitability and biogeochemistry in a warmer Arctic, *Proc. Natl. Acad. Sci., USA*, 108, 3653–3658, 2011.
- Leppäranta, M. and Manninen, T.: The brine and gas content of sea ice with attention to low salinities and high temperatures, Finnish Institute of Marine Research Internal Report, Helsinki, Finland, 15 pp., 1988.
- Lewis, E. and Wallace D.: The program $\text{CO}_2\text{SYS.EXE}$ can be downloaded at: <http://cdiac.esd.ornl.gov/oceans/co2prtrnbk.html> (last access: 24 September 2012), 2012.
- Marion, G. M., Farren, R. E., and Komrowski, A. J.: Alternative pathways for seawater freezing, *Cold Reg. Sci. Technol.*, 29,

- 259–266, 1999.
- Marion, G. M., Mironenko, M. V., and Roberts, M. W.: FREZCHEM: A geochemical model for cold aqueous solutions, *Comput. Geosci.*, 36, 10–15, 2010.
- McLaren, A. J., Banks, H. T., Durman, C. F., Gregory, J. M., Johns, T. C., Keen, A. B., Ridley, J. K., Roberts, M. J., Lipscomb, W. H., Connolley, W. M., and Laxon, S. W.: Evaluation of the sea ice simulation in a new coupled atmospheric-ocean climate model (HadGEM1), *J. Geophys. Res.*, 111, C12014, doi:10.1029/2005JC003033, 2006.
- Mehrbach, C., Culberson, H., Hawley, J. E., and Pytkowicz, R. M.: Measurement of the apparent dissociation constants of carbonic acid in seawater at atmospheric pressure, *Limnol. Oceanogr.*, 18, 897–907, 1973.
- Miller, L. A., Papakyriakou, T. N., Collins, R. E., Deming, J. W., Ehn, J., Macdonald, R. W., Mucci, A., Owens, O., Raudsepp, M., and Sutherland, N.: Carbon dynamics in sea ice: A winter flux time series, *J. Geophys. Res.*, 116, C02028, doi:10.1029/2009JC006058, 2011.
- Mucci, A., B. Lansard, L. A. Miller, and Papakyriakou, T. N.: CO₂ fluxes across the air-sea interface in the southeastern Beaufort Sea: Ice-free period, *J. Geophys. Res.*, 115, C04003, doi:10.1029/2009JC005330, 2010.
- Nedashkovsky, A. P., Khvedynich, S. V., and Petovsky, T. V.: Alkalinity of sea ice in the high-latitude arctic according to the surveys performed at north pole drifting station 34 and characterization of the role of the arctic in the CO₂ exchange, *Oceanology*, 49, 55–63, doi:10.1134/s000143700901007x, 2009.
- Notz, D. and Worster, M. G.: Desalination processes of sea ice revisited, *J. Geophys. Res.*, 114, C05006, doi:10.1029/2008JC004885, 2009.
- Papadimitriou, S., Kennedy, H., Norman, L., Kennedy, D. P., Dieckmann, G. S., and Thomas, D. T.: The effect of biological activity, CaCO₃ mineral dynamics, and CO₂ degassing in the inorganic carbon cycle in sea ice in late winter-early spring in the Weddell Sea, Antarctica, *J. Geophys. Res.*, 117, C08011, doi:10.1029/2012JC008058, 2012.
- Papakyriakou, T. N., Rysgaard, S., Geilfus, N. X., Pucko, M., Glud, R. N., Sej, M. K., and Barber, D.: Seasonal variation in the carbon budget of a sea-ice dominated fjord system: Young Sound, Greenland, in preparation, 2013.
- Pedersen, J. T. P., Kaufmann, L. H., Kroon, A., and Jakobsen, B. H.: The northeast Greenland Sirius Water Polynya dynamics and variability inferred from satellite imagery, *Geogr. Tidsskr.*, 110, 131–142, 2010.
- Rysgaard, S. and Glud, R. N.: Carbon cycling in Arctic marine ecosystems: Case study – Young Sound, Medd Greenland, *Bio-science*, 58, 216 pp., 2007.
- Rysgaard, S., Glud, R. N., Sej, M. K., Bendtsen, J., and Christensen, P. B.: Inorganic carbon transport during sea ice growth and decay: a carbon pump in polar seas, *J. Geophys. Res.*, 112, C03016, doi:10.1029/2006JC003572, 2007.
- Rysgaard, S., Glud, R. N., Sej, M. K., Blicher, M. E., and Stahl, H. J.: Denitrification activity and oxygen dynamics in Arctic sea ice, *Polar Biol.*, 31, 527–537, 2008.
- Rysgaard, S., Bendtsen, J. B., Pedersen, L. T., Ramløv, H., and Glud, R. N.: Increased CO₂ uptake due to sea-ice growth and decay in the Nordic Seas, *J. Geophys. Res.*, 114, C09011, doi:10.1029/2008JC005088, 2009.
- Rysgaard, S., Bendtsen, J., Delille, B., Dieckmann, G., Glud, R. N., Kennedy, H., Mortensen, J., Papadimitriou, S., Thomas, D., and Tison, J.-L.: Sea ice contribution to air-sea CO₂ exchange in the Arctic and Southern Oceans, *Tellus B*, 63, 823–830, doi:10.1111/j.1600-0889.2011.00571.x, 2011.
- Rysgaard, S., Glud, R. N., Lennert, K., Cooper, M., Halden, N., Leakey, R. J. G., Hawthorne, F. C., and Barber, D.: Ikaite crystals in melting sea ice – implications for pCO₂ and pH levels in Arctic surface waters, *The Cryosphere*, 6, 901–908, doi:10.5194/tc-6-901-2012, 2012.
- Sej, M. K., Krause-Jensen, D., Rysgaard, S., Sørensen, L. L., Christensen, P. B., and Glud, R. N.: Air-sea flux of CO₂ in arctic coastal waters influenced by glacial melt water and sea ice, *Tellus B*, 63, 815–822, doi:10.1111/j.1600-0889.2011.00540.x, 2011.
- Tamura, T. and Ohshima, K. I.: Mapping of sea ice production in the Arctic coastal polynyas, *J. Geophys. Res.*, 116, C07030, doi:10.1029/2010JC006586, 2011.
- Unesco tech. papers in the marine science no. 28. Eight report. Joint panel on oceanographic tables and standards, Annex 6: Freezing point of seawater, edited by: Millero, F. J., 29–35, 1978.
- Vinje, T.: Fram Strait ice fluxes and atmospheric circulation: 1950–2000, *J. Climate*, 14, 3508–3517, 2001.
- Weeks, W. F. and Ackley, S. F.: The growth, structure and properties of sea ice, in: *The Geophysics of Sea Ice*, edited by: Untersteiner, N., Plenum, New York, 1986.
- Worster, M. G. and Wettlaufer, J. S.: Natural convection, solute trapping, and channel formation during solidification of seawater, *J. Phys. Chem. B*, 101, 6132–6136, 1997.

PAPER III

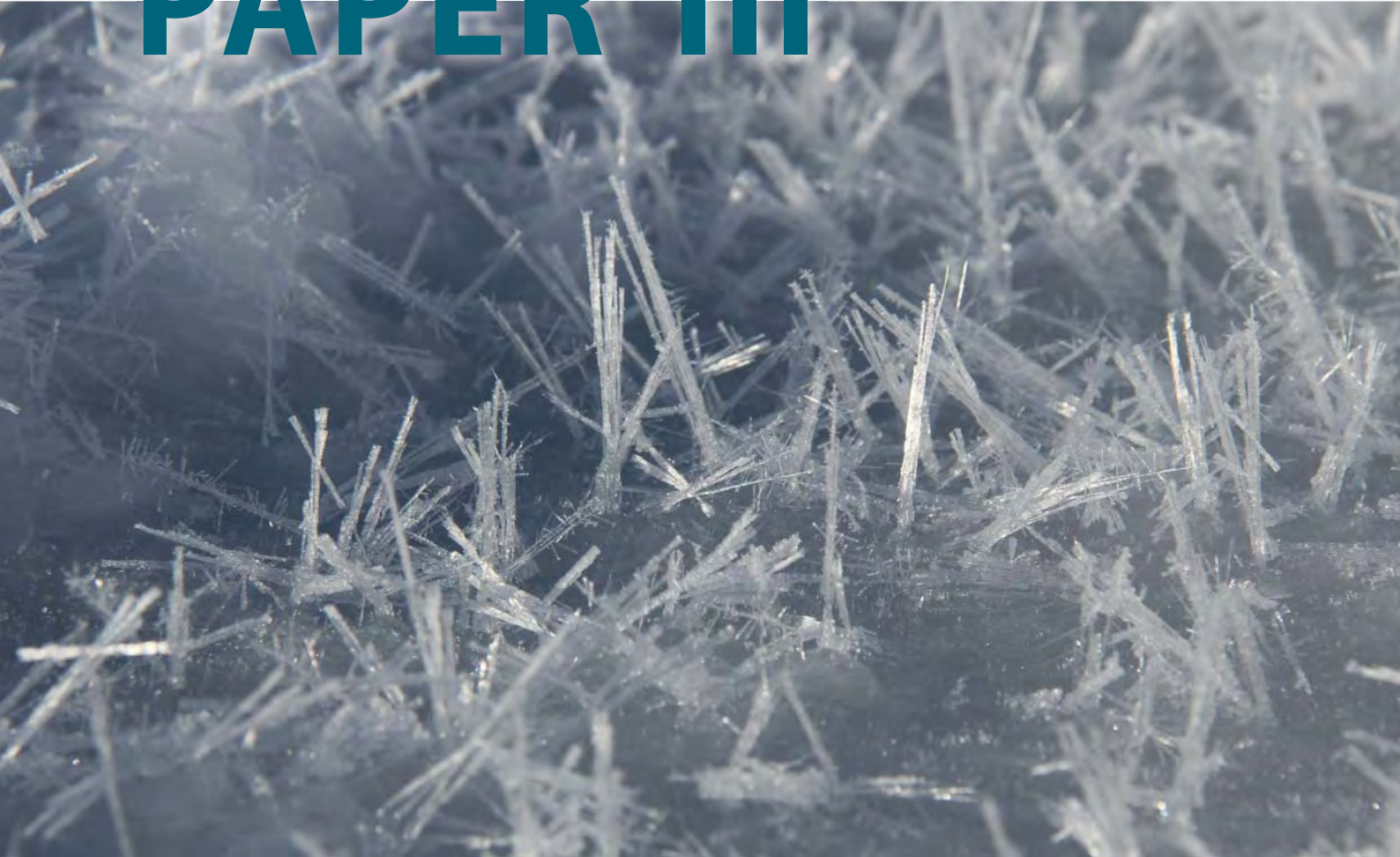


Photo: David Barber.

Frost flowers on young Arctic sea ice: The climatic, chemical and microbial significance of an emerging ice type

D.G. Barber • J.K. Ehn • M. Pućko • S. Rysgaard • J.W. Deming •
J.S. Bowman • T. Papakyriakou • R.J. Galley • D.H. Sjøgaard

Accepted

Frost flowers on young Arctic sea ice: The climatic, chemical and microbial significance of an emerging ice type

D.G. Barber^{1*}, J.K. Ehn¹, M. Pučko¹, S. Rysgaard^{1,2,3}, J.W. Deming⁴, J.S. Bowman⁴, T. Papakyriakou¹, R.J. Galley¹ and D.H. Sørensen^{2,3,5}

¹Centre for Earth Observation Science, Clayton H. Riddell Faculty of Environment, Earth, and Resources, University of Manitoba, Winnipeg, MB R3T 2N2, Canada

²Greenland Institute of Natural Resources, Greenland Climate Research Centre, Nuuk 3900, Greenland

³Arctic Research Centre, Aarhus University, DK-8000 Århus, Denmark

⁴School of Oceanography, University of Washington, Seattle, USA

⁵University of Southern Denmark, Campusvej 55, 5230 Odense M, Denmark

*corresponding author (david.barber@umanitoba.ca)

Abstract

Ongoing changes in Arctic sea ice are increasing the spatial and temporal range of young sea ice types over which frost flowers can occur, yet the significance of frost flowers to ocean-sea ice-atmosphere exchange processes remains poorly understood. Frost flowers form when moisture from seawater becomes available to a cold atmosphere and surface winds are low, allowing for supersaturation of the near-surface boundary layer. Ice grown in a pond cut in young ice at the mouth of Young Sound, NE Greenland, in March 2012, showed that expanding frost flower clusters began forming as soon as the ice formed. The new ice and frost flowers dramatically changed the radiative and thermal environment. The frost flowers were about 5°C colder than the brine surface, with an approximately linear temperature gradient from their base to their upper tips. Salinity and $\delta^{18}\text{O}$ values indicated that frost flowers originated primarily from the surface brine skim. Ikaite crystals were observed to form within an hour in both frost flowers and the thin pond ice. Average ikaite concentrations were 1013 $\mu\text{mol kg}^{-1}$ in frost flowers and 1061 $\mu\text{mol kg}^{-1}$ in the surface slush layer. Chamber flux measurements confirmed an efflux of CO_2 at the brine-wetted sea ice surface, in line with expectations from the brine chemistry. Bacteria concentrations generally increased with salinity in frost flowers and the surface slush layer. Bacterial densities and taxa indicated that a selective process occurred at the ice surface and confirmed the general pattern of primary oceanic origin versus negligible atmospheric deposition.

Introduction

New and young sea ice forms are becoming a more prevalent feature in the Arctic as the icescape transitions from one dominated by multi-year ice to one of primarily first-year sea ice [Kwok, 2007; Maslanik *et al.*, 2011; Barber *et al.*, 2012]. The physical, geochemical, and energy balance characteristics of these surfaces are poorly understood, as are the processes that govern their role in climate, ecology, and biogeochemistry-related processes across the ocean-sea ice-atmosphere (OSA) interface. Because of later fall freeze-up and increased dynamic opening of thinner and more mobile pack ice in winter, the areal extent and periodicity of frost flowers on sea ice are expected to increase [Isleifson *et al.*, 2013].

Frost flowers are relatively short-lived clusters of ice crystals that form dendritic and branched structures at the interface between a warm ice surface and a cold atmosphere and that are found almost exclusively on new and young ice [Perovich and Richter-Menge, 1994]. Frost flowers can form either from atmospheric deposition of water vapor onto the ice surface or through sublimation or evaporation of warm ice into a cold atmospheric boundary layer (Domine *et al.*, 2005). Key processes governing frost flower formation include gradients in temperature and relative humidity between the ice surface and the lower boundary layer of the atmosphere, as described in Style and Worster [2009] hereinafter the SW model. According to the SW model, frost flowers grow as a result of local super-saturation of air directly above the ice surface, when the warmer ice surface sublimates and/or evaporates water into the much colder atmosphere. Calm weather allows for the condition of near surface supersaturation to persist, enabling frost flower formation [e.g. Perovich and Richter-Menge, 1994; Martin *et al.*, 1996]. During the initial hours of sea ice growth, the presence of a highly saline (ca. 100) skim of brine on the surface of sea ice is consistently observed [e.g. Drinkwater and Crocker, 1988; Wensnahan *et al.*, 1993]. This brine skim is typically 1–2 mm thick and results from upward migration of brine as the brine pockets within the ice constrict during growth [Martin *et al.*, 1995]. The presence of a brine-wetted ice surface appears to be an important element in frost flower formation either as a source of warm water for evaporation [Roscoe *et al.*, 2011] or a source of brine that can then be wicked up into the already formed frost flowers [Martin *et al.*, 1995; Style and Worster, 2009].

As a result of their formation mechanism and later integration into the overlying snow on sea ice, frost flowers present a unique way for the ocean and sea ice to interact chemically with the atmosphere. During winter and spring in polar regions, frost flowers represent a potential source of aerosols, containing for example sea salts and organic particles, which can interact chemically across the OSA [Perovich and Richter-Menge, 1994; Rankin *et al.*, 2000, 2002; Rankin and Wolff, 2003; Alvarez-Aviles *et al.*, 2008; Bowman and Deming, 2010; Shaw *et al.*,

2010]. Xu *et al.* [2013] quantified both the magnitude and uncertainty in the cloud radiative forcing due to these aerosols and concluded they may play a small but important role in cloud radiative forcing. Sea salts also affect bromine exchange in the winter months [Wagenbach *et al.*, 1998; Alvarez-Aviles *et al.*, 2008] as they form over leads given saline frost flowers contain elevated concentrations of seawater ions, including bromine concentration three times greater than in seawater [Rankin *et al.*, 2002]. It is therefore argued that frost flowers are a potential source of atmospheric bromine, which is connected to polar tropospheric ozone depletion [Rankin *et al.*, 2002; Alvarez-Aviles *et al.* 2008; Nghiem *et al.*, 2012]. Atmospheric mercury depletion events occur episodically during Arctic spring. Chemical reactions involving reactive halogens periodically oxidize gaseous elemental mercury in the atmosphere; products of this oxidation, including reactive gaseous mercury and mercury bound to particles are deposited onto Arctic spring snow packs. Frost flowers are thought also to be a source of these halogens [Rankin *et al.*, 2002]. Douglas *et al.* [2005] and Sherman *et al.* [2012] showed that frost flowers contain high concentrations of mercury that may have been scavenged as a result of the high halogen concentrations that frost flowers exhibit. During their life spans, frost flowers may retain atmospheric mercury, along with other chemical constituents, from depletion events until incorporated into the snowpack upon frost flower collapse. Frost flowers thus present a potential pathway for atmospheric mercury to the sea ice and ocean below [Sherman *et al.*, 2012].

Previous studies have shown that CaCO₃ in the form of ikaite can precipitate in frost flowers [Geilfus *et al.*, 2013], thus frost flowers have the potential to augment air-sea cycling of CO₂ given CO₂ is released/assimilated on formation/dissolution of the carbonate mineral. However, field measurements of CaCO₃ precipitation in frost flowers and associated brine skim in high Arctic is currently lacking [Geilfus *et al.*, 2013].

There is also field evidence that frost flowers are a cryospheric microbial habitat. Bowman and Deming [2010] showed that bacterial abundance correlated strongly with salinity in both frost flowers and the brine skim formed on sea ice, meaning that bacterial abundance in these salty features was elevated compared to the sea ice on which the frost flowers had formed. Concentrations of extracellular polysaccharide substances (EPS) were also elevated in the frost flowers and brine skim. No evidence was obtained to suggest that bacteria were preferentially enriched or depleted with respect to salinity in frost flowers or the underlying brine skim [Bowman and Deming, 2010], but recent work implicated a selective process at the OSA interface in the detection of a distinctive bacterial community in the frost flowers [Bowman *et al.*, 2013] with the genetic potential to participate in key biogeochemical cycles involving mercury, dimethylsulfide and halocarbons [Bowman *et al.*, 2014]. Frost flower bacteria may also constitute a portion of the organic particles found in the aerosols of polar regions [Bowman and Deming, 2010].

Our objectives are to investigate the physical, radiative and thermal environment of frost flowers on new sea ice grown in a winter polynya off the NE coast of Greenland. We seek to understand the climate forcing on the formation of these flowers and in particular to examine the processes that create and drive their growth and deterioration. We then examine the potential role of frost flowers in geochemical exchange across the OSA interface and as a microbial habitat. More specifically we address the following interrelated research questions:

1. What are the climatic and geophysical forcing conditions associated with frost flower formation and development? (Climate Forcing)
2. How did the above conditions affect vapor diffusion processes and temperatures across the young ice surface and can we determine if atmospheric deposition or sea ice sublimation/evaporation or brine wicking dominated frost flower formation? (Frost Flower Formation)
3. How does the concentration of salt in the ice surface and frost flowers affect the carbonate chemistry of the sea ice and the exchange of CO₂ across the OSA interface? (Gas Exchange)
4. Can bacterial measurements across the OSA interface over time help to inform the frost flower formation process and the suitability of these unique physical and biogeochemical environments as habitats for microbes? (Microbial Habitat)

Methods

A multinational, multidisciplinary field program was coordinated through the University of Manitoba's Canada Excellence Research Chair (CERC) at the Danish/Greenlandic field station, Daneborg. The station is located in the Young Sound fjord on the NE coast of Greenland (Figure 1). General de-

scription of the Daneborg field site and the winter carbonate chemistry cycle in the fjord are found elsewhere [Rysgaard and Glud, 2007; Rysgaard et al., 2013].

The thin-ice station, POLY I (74°13.905'N 20°07.701'W, 29-30 cm thick on 22 March, snow-covered with varying thickness), was situated in a recurrent winter polynya region about 3 km off the landfast ice edge. An area of ~5 × 7 m was opened near POLY I at 16:00 GMT on 22 March to expose the ocean to the atmosphere (hereinafter referred to as the 'pond' site). The opening of the pond was done using a hand-held ice saw by cutting smaller segments that then were pushed to the side underneath the ice cover. A time-lapse camera was installed at the pond site to document the development of frost flowers as the ice formed *in situ*. Half of the pond was reopened on 24 March at 15:00 GMT; i.e., after about 47 h of the initial pond opening. At this time, the initial ice was ~12 cm thick. The recurrent polynya at this location will occur as open water (as evidenced by satellite imagery just prior to our arrival) or with a young ice cover (like we experienced); frost flowers are known to occur regularly on this polynya ice (Rysgaard and Glud, 2007).

Components of the surface energy balance were acquired using purpose-built meteorological stations located in proximity to the pond site over the period spanning this experiment. Wind speed and direction were measured at the heights of 3.8 m and 3.1 m using sonic anemometers (Gill® Windmaster Pro and Metek®, model uSonic-3). Incoming and reflected short-wave, and incoming and emitted longwave radiation were measured at the station (over a snow surface) using a four component net radiometer (Kipp & Zonen®, model CNR4) at a height of 1.5 m. Air temperature and relative humidity were measured using a HMP45C probe (Vaisala®) installed in radiation shields at a height of 1.6 m.

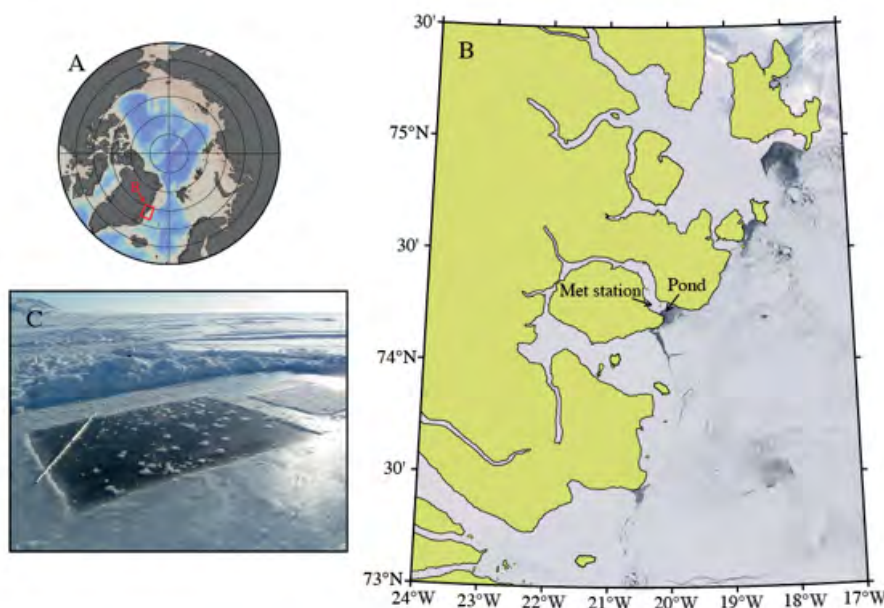


Figure 1. Daneborg field station at the NE Greenland coast (A) showing the location of the Young Sound fjord (B) and the newly formed ice in the polynya at the mouth of the fjord where the frost flower 'pond' was constructed (C).

Downwelling incident scalar irradiance and transmitted scalar irradiance over 400–700 nm wavelength range was measured at 1-min intervals at the pond site using MDS-L photosynthetically available radiation (PAR) sensors (Alec Electronics Co. Ltd). The surface reference PAR sensor was shielded from the upwelling component of the radiation and installed next to the pond. Two other PAR sensors were installed at the air-water interface and at 30-cm depth in the pond by attaching them to a string hanging from a horizontal aluminum pole that extended across the northern pond corner (Figure 1C).

To fill gaps between measured ice thicknesses (H) and surface temperatures ($T_{surface}$), we used the hourly averaged air temperatures (T_{air}) from the meteorological station as input in an analytical ice growth model [Maykut 1986]:

$$-\rho_{ice} L \frac{dH}{dt} = k_{ice} \left(\frac{T_{surface} - T_{sw}}{H} \right) + F_w, \quad (1)$$

where $\rho_{ice} = 920 \text{ kg m}^{-3}$ is the assumed density of sea ice which was kept constant, $L = 333.5 \text{ J g}^{-1}$ the latent heat of fusion, $k_{ice} = 1.8465 \text{ J m}^{-1} \text{ s}^{-1} \text{ K}^{-1}$ thermal conductivity of sea ice with a salinity of 8 and temperature of -5°C , $T_{sw} = -1.7^\circ\text{C}$ the temperature of the underlying seawater, $F_w = 0 \text{ W m}^{-2}$ is ocean heat flux, and

$$T_{surface} = \frac{k_{ice} T_{sw} + c_t T_{air} H}{k_{ice} + c_t H} \quad (2)$$

The calculation of $T_{surface}$ relied on a surface-to-air heat transfer coefficient C_r , which was found by matching to observed ice thicknesses and surface temperatures. The best match to observations were obtained by keeping C_r at $140 \text{ J cm}^{-1} \text{ day}^{-1} \text{ K}^{-1}$ for the first 7 cm of ice growth and then reducing it to $110 \text{ J cm}^{-1} \text{ day}^{-1} \text{ K}^{-1}$ for the remainder. These values are notably smaller than the $C_r = 209 \text{ J cm}^{-1} \text{ day}^{-1} \text{ K}^{-1}$ derived by Maykut [1986], reflecting the large temperature difference between the warm ice surface and the atmosphere in this thin ice environment.

The upwelling longwave radiation LW_u was not measured above the pond ice but calculated from $T_{surface}$ (for a bare frost flower free surface) using the Stefan-Boltzmann law with an emissivity of 0.985. Surface and interior brine salinities were then estimated assuming a linear temperature profile from $T_{surface}$ to T_{sw} and using the equation for the freezing point of seawater following Fofonoff and Millard [UNESCO 1983].

Data on the Infrared Temperature (IR) of the ice and frost flower surfaces were collected with a FLIR systems SC660 thermal camera (Wilsonville, OR, USA). The IR camera uses an uncooled microbolometer over the spectral range of 7.5 to 13.0 μm . Thermal images were stored as calibrated 32-bit floating point data over a 640 by 480 image plane. Calibration of the FLIR was conducted with an external black body and using an internal camera calibration system. System specifications were verified through a series of calibration tests conducted daily. The system was capable of an average $\pm 0.1^\circ\text{C}$

precision over the range of thermal conditions encountered; absolute calibration was not tested but FLIR indicates it to be $< 1\%$. Additional measurements of the bare ice surface temperature were taken with a handheld digital thermometer (Traceable, model 4000, Control Company, USA).

Throughout this manuscript we discuss the effects of the brine skim but sampled the ‘surface slush layer’, which contains the brine and the uppermost ice grains of the young ice, or the lowermost grains of the frost flower base, or potentially some snow that might have settled on top of the brine skim. Brine skim is a liquid with both its salinity and temperature controlled by the fact that it has to remain above its freezing point to exist as a liquid, while the surface slush additionally contains (salt-free) ice crystals and possibly precipitated salts. Our results show a significant difference between the salinity of the surface brine skim (calculated) versus the bulk salinity of the slush layer. Frost flower and surface slush layer samples for salinity and $\delta^{18}\text{O}$ analysis were collected with a sharp metal spatula, put into plastic bags, and melted at room temperature prior to analysis. Samples of sea ice brine for salinity and $\delta^{18}\text{O}$ were collected from the top part of the ice by scraping an approximate 2-cm deep hole in the surface after the removal of frost flowers and the surface slush layer, allowing the interior sea ice brine to accumulate for a few minutes, then collecting it with a plastic syringe. Sea ice was sampled with a 9-cm diameter ice corer (Mark II coring system, Kovacs Enterprises, Lebanon, USA). After extraction, ice cores were imaged thermally using the aforementioned FLIR camera, cut into layers, placed in tightly closed containers, and returned to the laboratory to melt at room temperature. The salinity of the melted frost flowers, surface slush layer, sea ice, and brine samples was calculated from conductivity and temperature using a HACH SENSION5 portable conductivity meter (Hach, Loveland, USA (± 0.01)) calibrated against a 15N KCl solution at 20°C . Samples for oxygen isotope composition were transferred into glass vials tightly capped with polyseal closures and parafilm. Analysis was performed on a Picarro Isotopic Water Analyzer, L2120-I (Picarro, Sunnyvale, USA) equipped with a PAL autosampler (Leap Technologies, Carrboro, USA). Details of the method can be found elsewhere [e.g., Versteegh *et al.*, 2012]. Results are expressed in standard $\delta^{18}\text{O}$ notation with the V-SMOW standard as a reference value. Agreement between triple consecutive injections of the same sample was within $\pm 0.1 \%$. The $\delta^{18}\text{O}$ signal of frost flowers of atmospheric origin was assumed to be that of freshly fallen snow; the $\delta^{18}\text{O}$ signature of frost flowers of brine origin was calculated from $\delta^{18}\text{O}$ measured in brine using a fractionation value of $+2.6$ [Macdonald *et al.*, 1995].

In the cold laboratory (-25 to -20°C), corresponding sea ice cores were cut into vertical sections ($10 \times 6 \times 1 \text{ cm}$) and horizontal sections ($6 \times 6 \times 1 \text{ cm}$), which then were mounted onto slightly warmed glass plates, cooled until frozen onto the plates, and thinned to 1–2 mm thickness using a microtome (Leica® SM 2010R) and a wood plane [e.g., Ehn *et al.*, 2007]. Each of these, so called thin sections, was then photographed

(Nikon® D70) between cross-polarized filters to document ice texture. Subsequently, each thin section was inspected (in the field) under a stereomicroscope (Leica® M125 equipped with a Leica® DFC 295 camera and Leica® Application Suite ver. 4.0.0. software) to document the vertical and horizontal position of ikaite crystals in sea ice.

Samples of ikaite from the pond site were kept at -20°C for three weeks and brought to the x-ray laboratory at the Department of Geological Sciences at the University of Manitoba, Canada. There, subsamples of sea ice and frost flowers were mounted onto a cold glass slide resting on a chilled aluminum block containing a 1-cm central viewing hole. The crystals were first examined with a polarized light microscope to assess their optical properties and then mounted for x-ray study using a stereo binocular microscope. The x-ray diffraction instrument consisted of a Bruker D8 three-circle diffractometer equipped with a rotating anode generator (MoK α X-radiation), multi-layer optics, APEX-II CCD detector, and an Oxford 700 Series liquid-N Cryostream. The intensities of more than 100 reflections were harvested from six frame series (each spanning 15° in either ω or ϕ) collected to $60^{\circ} 2\theta$ using 0.6s per 1° frame with a crystal-to-detector distance of 5 cm. Further details on the ikaite sampling are provided elsewhere [Rysgaard *et al.*, 2013].

The surface diffusive flux of CO₂ associated with the re-freezing pond was sampled both in the presence and absence of frost flowers using an automated chamber flux system (LI-COR®, model LI-8100) equipped with a 20-cm (diameter) survey chamber. As part of the post-processing procedure, the CO₂ concentration time series associated with each sample was screened, after which the fluxes were calculated using the LI-8100A data analysis software.

Frost flowers for microbial analyses were removed from the pond site into sterile 1-L plastic bags using an ethanol-rinsed spatula. A second scraping over the same surface area yielded the corresponding, operationally defined brine skim; i.e., the surface slush layer. Samples of sea ice were also collected, as described above, along with samples of seawater and snow from the surrounding area. Samples of frost flowers, the underlying surface slush layer, and snow were melted directly over the shortest period possible (always < 12 h, with sample temperature remaining at $\leq 0^{\circ}\text{C}$), while sea ice samples were melted into sterile 0.2- μm filtered brine according to the isohaline approach described by Ewert *et al.* [2013]. Immediately upon melting, samples were fixed with 0.2 μm -filtered formaldehyde to a final concentration of 2% and stored in the cold and dark until total bacterial (total prokaryotic) abundance was determined using epifluorescence microscopy, as in Bowman and Deming [2010]; virus-like particles (VLP) were enumerated on a subset of samples, according to Wells and Deming [2006]. Particulate and dissolved extracellular polysaccharide substances (pEPS and dEPS) were quantified using the phenol sulfuric acid assay, as in Krembs *et al.* [2011]

and Ewert *et al.* [2013]. Salinities of samples used for these bacterial and EPS analyses were determined by refractometer.

To determine the dominant members of the bacterial community, DNA was extracted from the different sample types for amplification and sequencing of the 16S rRNA gene using the phenol-chloroform method (as in Bowman *et al.* [2013]); one patch of frost flowers was sampled to obtain the upper centimeter portions separately from the basal portions. The V3-V5 region of the 16S rRNA gene was amplified using primers 357F and 926R for 30 cycles. An aliquot of the amplified material, along with positive and negative controls, was visualized on a gel to insure proper fragment length. Amplicons were purified using the GeneJet Purification Kit (Fermentas) and submitted to the Tufts University Sequencing Center, where amplicons underwent a second round amplification for 10 cycles using bar-coded primers 517F and 967R. Second round amplicons were gel-purified prior to library construction. Sequencing was conducted on the 454 FLX platform (Roche) using Titanium chemistry. Read processing and classification using Mothur [Schloss *et al.*, 2009] followed Bowman *et al.* [2012] except that the Greengenes reference taxonomy was used for classification (available at the Mothur website, http://www.mothur.org/wiki/Greengenes-formatted_databases); sequence data are available under NCBI accession number SRP038953). Brine and Milli-Q blanks were processed along with the environmental samples. Operational taxonomic units (OTUs, defined at the level of 97 % similarity) found in the blanks were removed from the environmental samples prior to downstream analysis. OTUs that classified as chloroplasts were also removed, assuming these reads to be derived primarily from chloroplasts [although see Diez *et al.*, 2001; Waleron *et al.*, 2007; Cottrell and Kirchman, 2009; and Bowman *et al.*, 2012]. Similarity in community composition between samples was assessed by randomly sampling to the depth of the shallowest sample (1,367 reads), calculating the relative abundance of the 25 most abundant OTUs, and applying hierarchical clustering to samples using the complete linkage method through the *vegdist* and *hclust* functions as implemented by the *heatmap* function in R [Oksanen *et al.*, 2013].

Results and Discussion

Climate Forcing

The climate at the Daneborg site was typical of conditions experienced in mid-winter in the Young Sound region of NE Greenland [Rysgaard and Glud, 2007]. Air masses are influenced by the proximal Greenland ice sheet. Storms are generated through the interface of warm, moist air masses, associated with the open water areas of the marginal ice zones surrounding Greenland, interacting with the cold dry air masses associated with the ice cap.

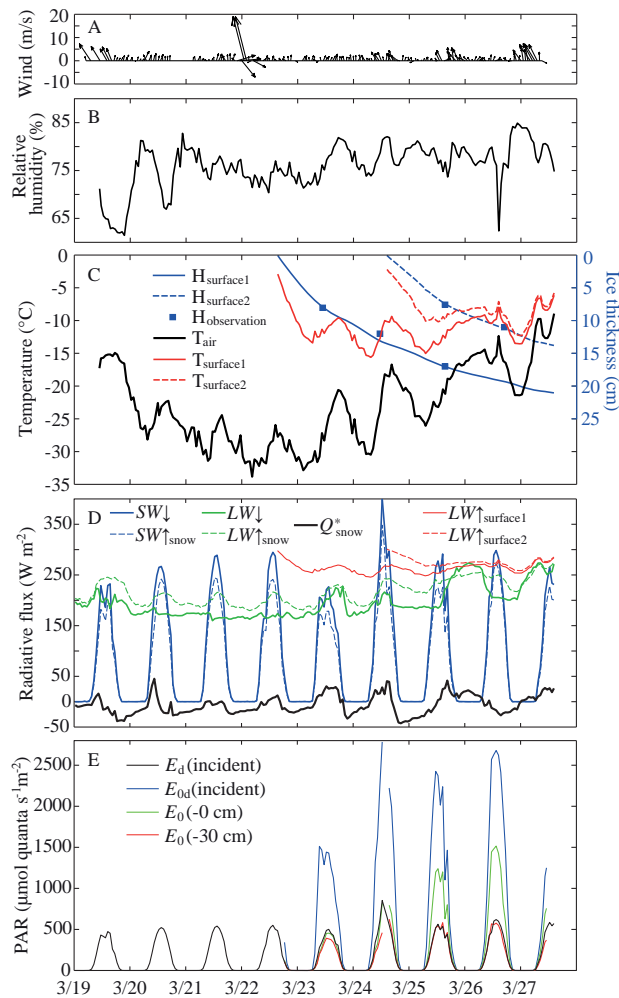


Figure 2. Surface energy balance conditions during the frost flower growing experiment at the pond site: (A) wind (the length of arrows corresponds to wind speed; angle of the arrows corresponds to wind direction with northward wind pointing upward); (B) relative humidity; (C) air temperature (T_{air}) measured at the meteorological station, ice thickness observations ($H_{\text{observation}}$), and calculated ice thicknesses (H_{surface}) and surface ice temperatures (T_{surface}) where subscripts with 1 and 2 denote values for the initially opened and reopened portions of the pond, respectively; (D) shortwave (SW), longwave (LW) and net (Q^*) radiative flux where the subscripts denote the surface type (1, 2, or snow), arrows either downwelling or upwelling; and (E) PAR (E) where subscript 0 is for scalar irradiance and d is for downwelling.

Figure 2 summarizes the salient data from the ‘pond’ met station. After a brief period of $>10 \text{ m s}^{-1}$ winds prior to the opening of the frost flower pool on 22 March, wind speeds remained between 1 and 3 m s^{-1} during the first 2 days of the ice-growth experiment. This period was followed by 3 days of variable winds generally between 1 m s^{-1} and 5 m s^{-1} , reaching about 8 m s^{-1} briefly around noon on 27 March (Figure 2A). These initial low wind speeds are thought necessary for frost flower formation as turbulence during higher wind speeds ($>5 \text{ m s}^{-1}$) destroys the near-surface supersaturated layer [Style and Worster, 2009].

To allow a direct comparison with results from Style and Worster [2009] the measured relative humidity reported here is with respect to water surfaces (as output from sensor) with no correction for ice surfaces [see Andreas *et al.*, 2002]. During the growth experiment, relative humidity remained between 70 and 85% (Figure 2B). We note three rapid drops in the relative humidity on March 20, 21 and 26 below a smaller running mean largely dominated by diurnal fluctuations due to changing air temperature.

Air temperature at the start of the experiment was around -26°C and dropped to -32°C , the lowest during the experiment, in the early hours of 23 March (Figure 2C). Air temperatures showed an increasing trend during the experiment, reaching as high as -10°C on 27 March, and underwent diurnal cycling which was interrupted for the night between 25 and 26 March due to the presence of cloud cover (note period of increased downwelling longwave radiation during 26 March in Figure 2D). The corresponding ice surface temperature, calculated using Eq. (2), rapidly decreased to -10°C about 8 hours after the initial opening of the pond (T_{surface1} in Figure 2C) in response to the cold air temperature and ice thickness growth to 4 cm thickness (H_{surface1}). The decrease to -10°C took 17 hours for the pond portion reopened around 15:00 on 24 March (T_{surface2} in Figure 2C), reflecting the effect of prevailing warmer air temperatures and ice thickness growth to 5 cm (H_{surface2}). After the initial decreases, the surface temperatures remained between -15 and -6°C for both surfaces until the end of the experiment when (calculated) ice thicknesses had reached 20 cm for H_{surface1} and 13 cm for H_{surface2} (Figure 2C).

Scalar irradiance over PAR wavelengths was measured on the side of the pond that was reopened (Figure 1C; Figure 2E). Thus, PAR was measured initially in ice that grew rapidly to about 12 cm and, for the latter part of the experiment, in ice that grew more slowly to 13 cm (Figure 2C). For both ice-growth phases, scalar PAR at about 30 cm below surface followed closely the values recorded by the cosine-corrected downwelling PAR at the meteorological tower. The near interface PAR, however, differed between the two cases due both to how the surfaces evolved (full frost flower coverage vs. patchy coverage) and to differences in where the sensor was located relative to the ice surface (top of sensor located about 5 mm below ice surface vs. top of sensor at surface). These differences resulted in notably higher interface PAR values during the second growth phase and illustrate the importance of near-surface properties and frost flowers on light transmission through thin ice. The observed PAR levels that reached values $> 500 \text{ } \mu\text{mol quanta s}^{-1} \text{ m}^{-2}$ are more than sufficient to support primary production [e.g., Köhl *et al.*, 2001]. This result may have ecosystem implications, considering the much larger spatial expanse of young, frost flower-covered sea ice in March in the Arctic (e.g., thousands of square kilometers in the Southern Beaufort Sea in February–April of 2013; http://www.youtube.com/watch?v=KXjb6MRj_5U).

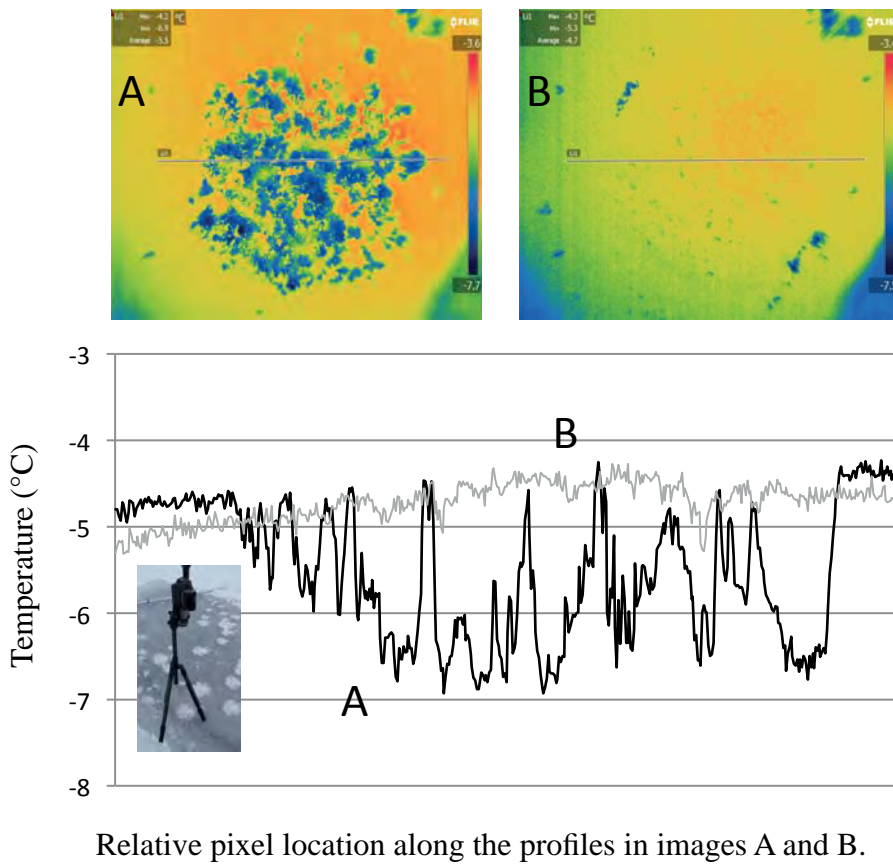


Figure 3. Thermal IR temperature of young ice showing the temperatures for a cluster of frost flowers (A) and after this cluster was removed (B). Profiles in the color FLIR images are plotted from left to right according to the profile line location at A and B (23 March 2013). Larger and more mature flowers in the cluster have a lower surface temperature. Ice surface temperatures dropped by about 0.25°C due to the removal of the frost flowers.

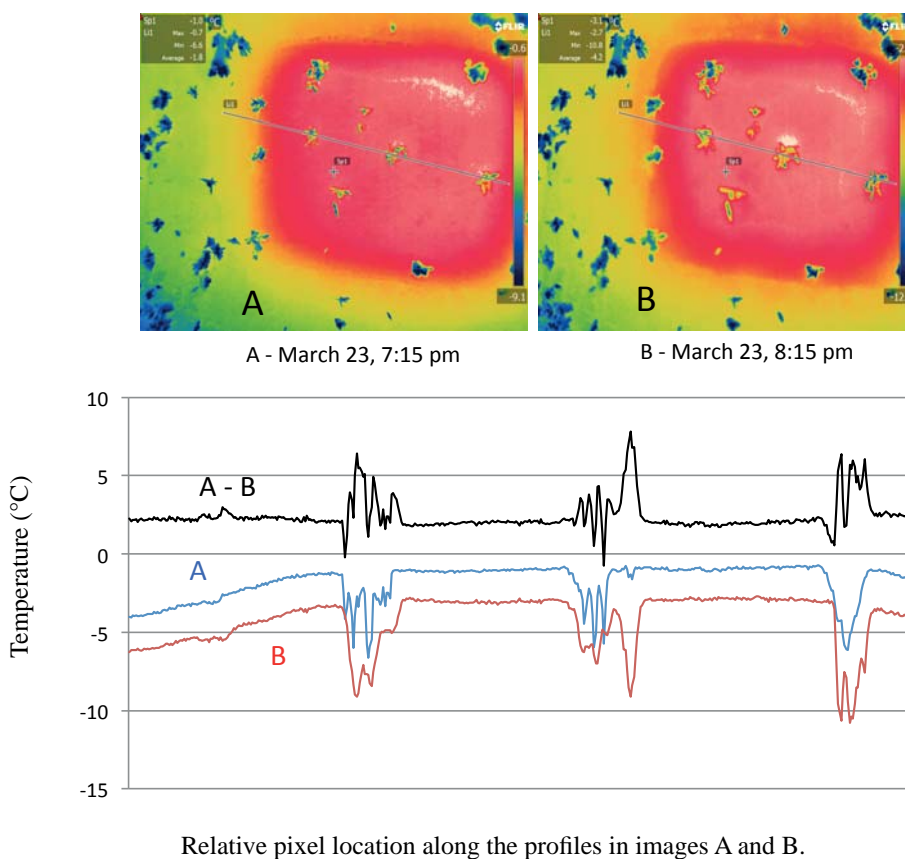


Figure 4. Thermal IR temperature of young ice showing the temperatures of the ice surface relative to that of three frost flowers. Profiles in the color FLIR images are plotted from left to right according to the profile line location at A (23 March, 19:15 GMT, ~27 hours from freeze-up) and B (23 March, 20:15 GMT, ~28 hours from freeze-up). The different lines illustrate the change in ice surface temperature that occurred during 1 hour relative to the change in the size and temperature of three frost flowers.

A patch of mature frost flowers was imaged with a FLIR camera to ascertain the thermal field conditions of the frost flower-covered and bare ice surface (Figure 3A and B, respectively). A patch of frost flowers radiated out from the initial node of

frost flower formation (Figure 3A). The patch consisted of mature frost flowers extending > 1 cm (vertically) into the boundary layer. Top portions of the frost flowers were at a temperature of ~ -7°C, ice surface temperature was ~ -4.5°C, and air

temperature was $\sim -27^\circ\text{C}$. After frost flower removal, the ice surface temperature decreased by $\sim 0.25^\circ\text{C}$ due to direct contact with the cold air just above the growing ice (Figure 3B). On average we found a difference between flower tops and brine skim of about 5°C with a range of $\pm 1^\circ\text{C}$ based on data shown in Figures 3 and 4 and data not shown.

The temperature fields associated with the growth of individual frost flowers were recorded with the FLIR camera by cutting and removing a small section of the ice, then allowing the ice to re-freeze. A one-hour time lapse between images of three growing frost flowers (compare Figure 4A and B) shows the thermal effect of the frost flower formation on the surface ice field and the effect of thickening sea ice on the surface field temperature (Figure 4C). The average relative difference in the profile lines in Figure 4A and B illustrates the difference in ice surface temperature (A-B) of about 2.5°C created by ice growth alone. The three flowers in the thermal IR image frame grew 0.5 cm over 1 hour, which resulted in a temperature difference of $\sim 2.5^\circ\text{C}$ (absolute difference in temperature between 19:15 and 20:15 GMT on 23 March). The greatest temperature differences correspond to the large frost flowers projecting the furthest into the atmospheric boundary layer.

The lower surface temperatures of the frost flowers dampen longwave radiation loss by between $\sim 10 \text{ Wm}^{-2}$ ($\sim 3.6\%$) and $\sim 20 \text{ Wm}^{-2}$ ($\sim 8\%$) relative to background sea ice and brine skim (observed $\Delta T_{\text{surface}} = -25$ and -5°C , respectively). To place the effect in context, the change in longwave emission associated with frost flower formation relative to background brine-wetted sea ice is between 50% and 60% of reported wintertime sensible heat loss from newly formed grease ice (Table 1 in *Else et al.* [2011]), and hence a significant proportion of the heat budget of the youngest forms of sea ice.

Frost flower formation

The first frost flowers were recorded at 16:15 GMT on 22 March (very small white nodules, Figure 5A), after only 15 minutes from when the pond was initially opened. Initial frost flowers formed as distinct nodules in the very young ice, and then expanded from their initial nucleation sites radially outwards in all directions. Frost flowers grew significantly overnight; by the next morning they exhibited a patchy distribution with 9/10 of the pond surface covered. Frost flowers were well formed by about 12 hours into the experiment and exhibited a typical branched structure at maximum growth (Figure 5C).

Table 1. Measurements of $\delta^{18}\text{O}$, S, T, and v_b in samples of sea ice, brine, fresh snow, frost flower and the surface slush layer throughout the duration of the frost flower growth experiment.

		$\delta^{18}\text{O} \pm \text{SD} [\text{‰}]$	S \pm SD	T [$^\circ\text{C}$]	v_b [%]
Brine		-4.9 ± 0.7	88.8		
Fresh snow		-24.6 ± 0.4	0.0		
Ice 19h	0.0-2.5 cm	-1.6 ± 0.1	10.4	-8.7	8.0
	2.5-5.0 cm	-1.9 ± 0.5	11.2	-5.4	14.1
	5.0-8.0 cm	-1.2 ± 0.3	8.7	-2.1	23.9
Ice 26h	0.0-2.0 cm				
	2.0-5.0 cm		7.6	-5.3	6.6
	5.0-8.0 cm		8.6	-2.2	17.7
	8.0-11.0 cm		9.2	-1.8	23.6
	11.0-14.0 cm		6.6	-1.8	16.8
	14.0-17.0 cm		9.5	-1.7	25.9
Frost flowers	19h	-0.8 ± 0.3	125.1	-12.7	43.8
	26h	-1.6 ± 0.3	94.9 ± 13.8	-7.8	56.6
	46h	-2.1 ± 0.3	90.9 ± 10.1	-7.1	58.9
	46h (tops)	-4.0 ± 0.2	92.2 ± 16.5		
	46h (bottoms)	-0.1 ± 0.4	89.6 ± 3.8	-7.1	58.9
	70h	-4.4 ± 1.2	87.0 ± 9.7		
	90h	-4.4 ± 0.3	64.4		
	90h (tops)	-7.7	50.2		
	90h (middles)	-4.6 ± 0.4	78.8		
	90h (bottoms)	-0.9 ± 0.3	64.1		
	114h	-4.3 ± 0.1	77.4		
Surface slush layer	19h	-0.1 ± 0.5	48.2	-10.3	22.7
	26h	-0.9 ± 0.4	66.2 ± 7.6		
	46h	2.1 ± 0.9	77.4 ± 19.1	-8.7	41.7
	70h	-0.4 ± 0.5	72.7 ± 11.0		
	90h	-0.4 ± 0.0	52.9		
	114h	-1.3 ± 0.5	72.3		

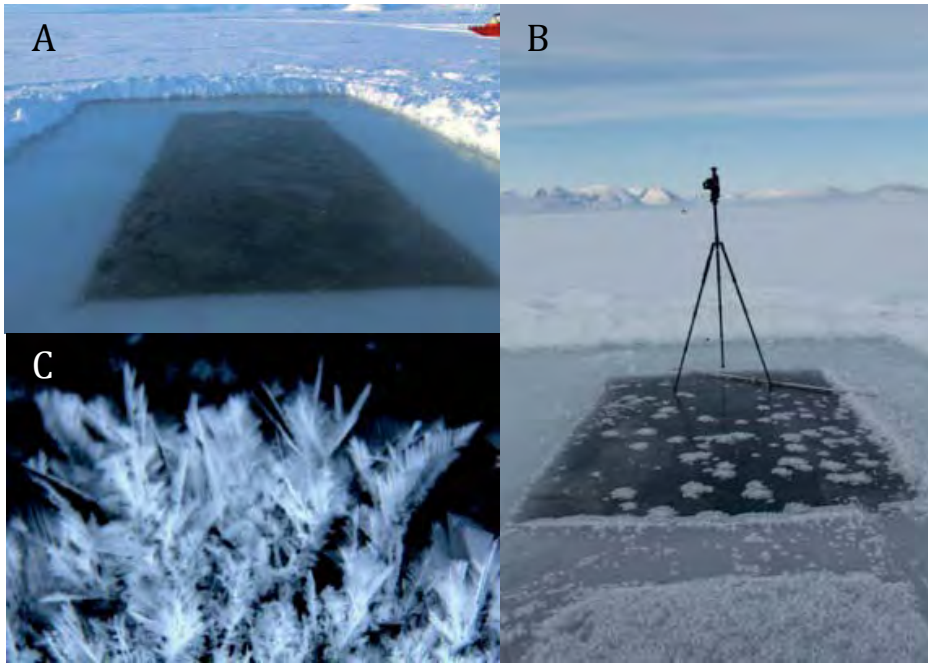


Figure 5. Examples of frost flowers grown at the pond. (A) The first evidence of frost flower formation (see small white dots within the black rectangle) at ~ 3 hours into the experiment (ice < 1 cm thick; 22 March 19:00 GMT); (B) a patchy frost flower coverage on the re-opened pond half after ~ 24 hours of growth (ice < 10 cm thick). Foreground shows the mature frost flower field on the initially grown ice (~ 17 cm thick); and (C) a close-up image of a typical frost flower structure at ~ 48 hours into the experiment.

Over the course of the second night, the initially patchy coverage evolved into a relatively homogeneous cover (lower part of Figure 5B). A brine skim formed very early in the growth cycle of the new ice. This brine skim is often seen on young growing ice and is the result of brine being ejected upwards during ice growth. When the frost flowers form, this brine skim can provide both a vapor source (for frost flower growth) and brine for salt migration into the frost flowers. Work on chemical composition of frost flowers corroborates this basic process of microstructure development [Alvarez-Aviles *et al.*, 2008]. In what follows we discuss the effects of the brine skim, recognizing along the way that what we sampled was the ‘surface slush layer’, as defined above.

The environmental conditions of frost flower formation during the experiment were placed in the context of the six regimes hypothesized in the SW model based on relative humidity of the atmosphere and temperature difference between the atmosphere and the ice surface (Figure 6; the numbering I-VI follows that

of *Style and Worster* [2009]). Evaporation into vs. condensation from a supersaturated atmosphere (relative humidity > 100%) is characterized by regimes I and II, respectively. Regimes III to VI are for exchanges with an undersaturated atmosphere. Condensation from the air occurs at the surface in III-IV, while evaporation from the surface occurs in V-VI. Regimes V and VI distinguish between undersaturated vs. supersaturated water vapor conditions in the near-surface layer, as determined by the Clausius–Clapeyron equation. In both V and VI, the source of water vapor in the layer directly above the sea ice comes from evaporation or sublimation from the sea ice surface rather than from deposition from the cold atmosphere. For most of the experiment, pond surface conditions remained within regime VI with a brief transition into regime V after about 84 hours of the initial pond opening (Figure 6). *Style and Worster* [2009] observed that larger values of supersaturation, depicted by conditions to the left of the dash-dotted curve in Figure 6, were required for frost flower formation to occur. Our observations closely corroborate this finding.

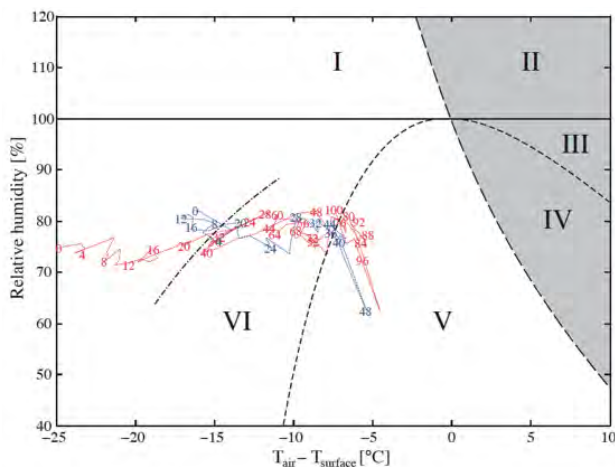


Figure 6. The relative differences in humidity and temperature during the pond experiment set in the context of environmental conditions under which different condensation, evaporation and sublimation processes occur, following *Style and Worster* [2009]. Red (first opening) and blue (second opening) colored numbers indicate the time (hours) elapsed in 4-hour intervals from the start of freeze-up (i.e., from 22 March at 16:00 GMT and 24 March at 15:00 GMT, respectively); their locations show the prevailing conditions at the time. Roman numerals I through VI are the categorical conditions under which various vapor-temperature differentials create various features: frost flower, rime, fog, dew, etc. The dashed and dash-dotted lines are redrawn from *Style and Worster* [2009, Figures 3-4], while the adjacent solid lines are obtained using the same equations but the temperatures observed during the pond experiment.

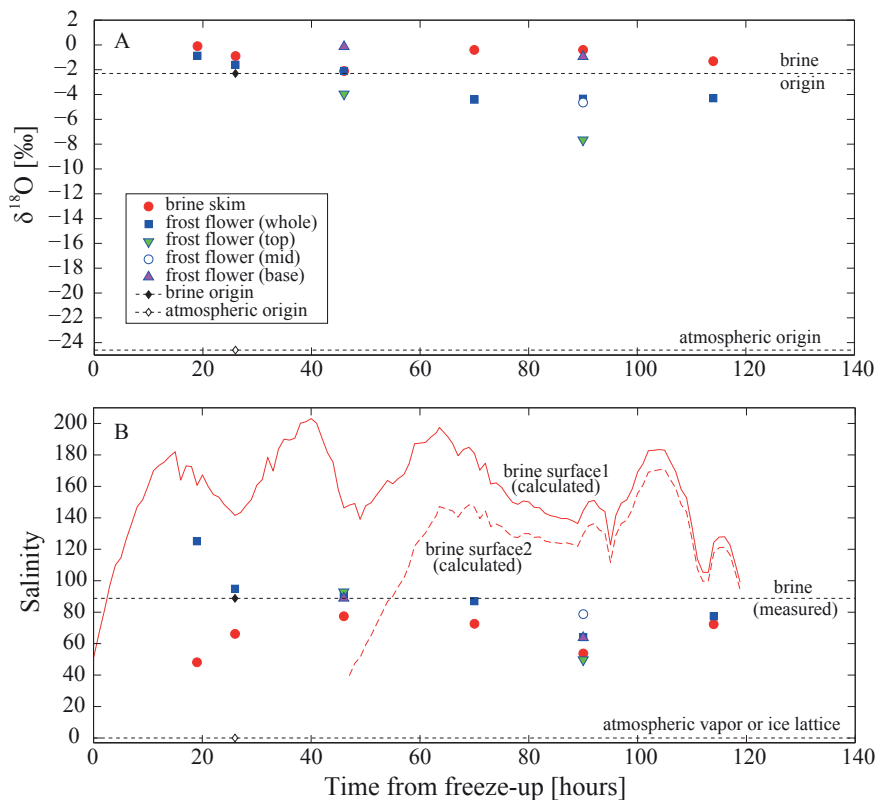


Figure 7. Temporal evolution of $\delta^{18}\text{O}$ (A) and salinity (B) in frost flowers and surface slush layer over the duration of the frost flower growing experiment that started 16:00 GMT on 22 March.

In the literature, there is still a debate as to whether frost flowers form due to deposition of atmospheric water vapor onto the ice surface or sublimation or evaporation of the warm ice surface into the atmospheric boundary layer. Measured $\delta^{18}\text{O}$ values of frost flowers from 19 to 114 hours after freeze-up suggest that the frost flowers were composed primarily of brine (Figure 7A). Fresh (19-h) unsectioned frost flowers had a $\delta^{18}\text{O}$ value of $-0.8 \pm 0.3\text{‰}$ which was similar to the signature of the surface slush layer ($-0.1 \pm 0.5\text{‰}$) and decreased gradually with time to $-4.3 \pm 0.1\text{‰}$ after 114 hours from freeze-up (Table 1), pointing to the influence of secondary atmospheric deposition either from vapor or from blowing snow ($\delta^{18}\text{O}$ value of $-24.6 \pm 0.4\text{‰}$) during later stages of the experiment. Influence of that secondary atmospheric deposition is particularly pronounced in the top sections of frost flowers, while bottom sections remained composed almost exclusively of brine (Figure 7A). Results presented here are generally in agreement with similar studies on Arctic leads [Douglas *et al.*, 2005] and over large open water expanse formations of young frost flower covered sea ice [Douglas *et al.*, 2012].

Initial salinities of frost flowers were much higher than those measured in the surface slush layer (Figure 7B), strongly supporting the brine origin of frost flowers revealed by the $\delta^{18}\text{O}$ signature analysis (and further corroborated by the bacterial results; see below). The low temperatures of the frost flowers (Figure 3) and, perhaps more importantly, the direct contact of brine with the atmosphere allowing for high evaporation rates, suggest that precipitated salts must be present [Assur, 1960], possibly explaining the high salinities of melted frost flowers. Only after 46 hours of the experiment, when a $\delta^{18}\text{O}$ atmos-

pheric signature began to appear in the frost flowers and the collected brine skim had a higher salinity, did the frost flower salinities approach those measured for the brine skim. Previous work has shown that brine can be wicked up into frost flowers from a high-density brine skim, both *in situ* [Perovich and Richter-Menge, 1994] and in laboratory experiments [Martin *et al.*, 1995; Roscoe *et al.*, 2011] and sea ice mesocosm experiments [Isleifson *et al.*, 2012]. Lack of data prior to 19 hours after freeze-up in our experiment prevents a definitive determination of initial ice-surface origin, but formation of nucleating nodules from frozen brine and/or precipitated salts seems plausible as: 1) atmospheric temperatures were below the temperature of freezing for brine with the maximum modeled salinity of ~ 200 ($\sim -10^\circ\text{C}$; Figure 7B), potentially allowing for the precipitation of salts to occur after cooling of brine to $< -5^\circ\text{C}$ [Light *et al.*, 2003]; and 2) initial salinities of frost flowers were much higher than those measured in the surface slush layer within the range of modeled salinities of the liquid brine in the top 5 cm of ice (Figure 8).

Brine skim temperatures (Figure 2C) calculated using Eq. (2) agreed well with measured surface slush layer temperatures (Table 1). The salinity of the brine in the surface slush layer could then be estimated using seawater freezing-point relationships [Fofonff and Millard, 1983]. The differences in salinity among the samples then allowed estimates of the brine volume within the surface slush layer, calculated as: 31, 49, 54, 41, 37, and 59% at 19, 26, 46, 70, 90 and 114 hours, respectively, into the ice-growth experiment. Furthermore, assuming that the brine from the brine skim wicks into the frost flower and forms part of its structure, we estimated the rela-

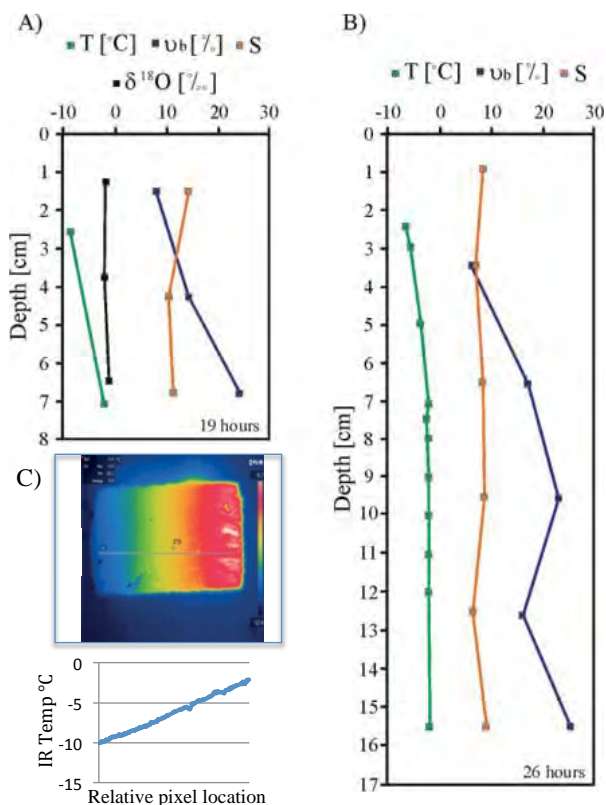


Figure 8. Temperature, salinity, brine volume fraction (v_b) and $\delta^{18}\text{O}$ profiles in sea ice during the frost flower growing experiment after 19 (A) and 26 (B) hours from freeze-up. Thermal IR image of small scale temperature of a sea ice core extract from the pond site at 26 hours into the experiment (coincident with temperature probe measurements in B).

tive proportions of the sampled frost flowers that were formed through brine wicking versus vapor deposition: for the above six sampling occasions, wicked brine composed about 81, 70, 64, 49, 45, and 63%, respectively, of the mass of the frost flowers. This exercise illustrates the important role of brine wicking, not only in transferring salt (and organic matter, including bacteria), but also in bringing water to the frost flowers. Over the course of the ice-growth experiment there was a general decrease in the brine-wicked fraction and consequent increase in deposition from vapor, a pattern entirely consistent with the $\delta^{18}\text{O}$ signature analysis that also suggested a temporal increase in the atmospheric fraction (see above). Despite internal consistency, this approach to estimating the composition of frost flowers could not account for possible changes in brine salinities over the course of the frost flower formation process, for example due to evaporation or sublimation.

Gas Exchange

The climate forcing and resulting frost flower formation concentrate brine in the upper layer of the ice and within the frost flowers. This brine concentration affects the carbonate chemistry of the sea ice and thus gas exchanges across the OSA interface, specifically through the influence of ikaite formation.

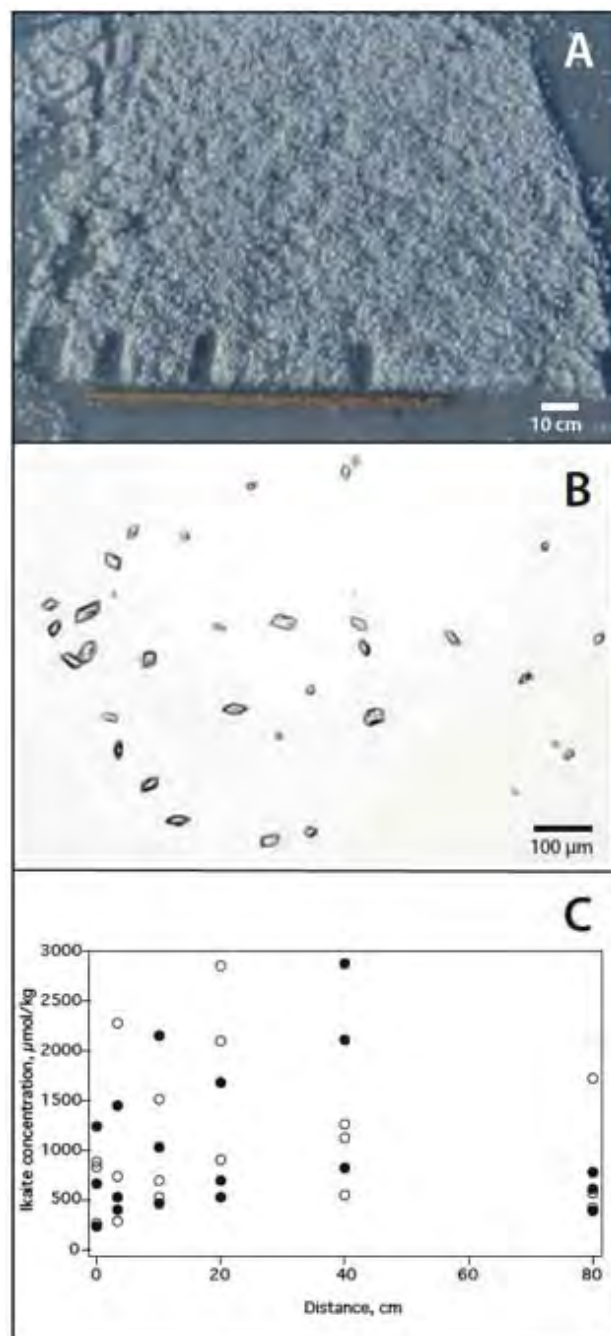


Figure 9. Frost flowers at the pond during sampling of ikaite crystals for characterization and quantification. (A) Frost flower field with marks after sampling at different centimeter distances in the lower part of the image above the ruler. (B) Example of ikaite crystals just after ice crystals in the sample had melted. (C) Ikaite concentrations in frost flowers (filled circles) and surface slush layer (empty circles).

Ikaite crystal concentrations in frost flowers and brine skim were characterized and quantified by sampling at different times and distances (centimeter-scale) in the newly frozen pond (Figure 9A). Within 1 hour ikaite crystals were observed to form in both the thin ice and the frost flowers, indicating the short-term dynamic conditions of ikaite formation. Ikaite crystals become easily visible when sea ice is melted. For example, 39 crystals were observed in a 3 μg subsample a few seconds after melt-

ing 58 mg of new frost flowers (Figure 9B). This image represents a very small fraction (3 μg) of the sample. In this case, the crystals covered 1.5% of the counting area, corresponding to an ikaite concentration of 2150 $\mu\text{mol kg}^{-1}$. The crystals observed in the sea ice ranged in size (maximum dimension) from a few micrometers to 200 μm , were highly transparent with a rhombic morphology, and showed uniform extinction under cross-polarized light, suggesting that they were simple single crystals. All x-ray reflections fit well to a monoclinic C-centered cell with $a(\text{\AA}) = 8.816(3)$, $b(\text{\AA}) = 8.333(2)$, $c(\text{\AA}) = 11.043(3)$, $\beta(^{\circ}) = 110.68(2)$, and $V(\text{\AA}^3) = 759.1(6)$. From the general shape, optical properties and unit-cell determination, the crystals examined were ikaite [Hesse and Küppers, 1983]. Average ikaite concentrations in the frost flowers were 1013 $\mu\text{mol kg}^{-1}$ (± 632 , standard deviation) and in the surface slush layer, 1061 $\mu\text{mol kg}^{-1}$ (± 736 , standard deviation) (Figure 9C). The highest concentration of ikaite was observed in the sea ice column [Rysgaard *et al.*, 2013]. The surface slush layer and frost flowers represented a thin low-density layer on top of the ice with a strikingly high abundance of ikaite crystals (e.g., compared to Geilfus *et al.* [2013]), yet accounted for only 5% of the total ikaite in the ice column [Rysgaard *et al.*, 2013]. Formation of ikaite in surface ice layers, however, can lead to a CO_2 flux from the ice into the atmosphere.

Due to logistical constraints we were only able to sample the surface CO_2 flux at the pond on March 23 and 24. Sampling was performed on ice thickness of approximately 10 and 13 cm, respectively (Figure 2C), with ice surface temperatures between -10 and -13°C . Air temperature ranged between -21.5 and -19°C during sampling. Chamber flux measurements confirmed an expected efflux of CO_2 at the brine-wetted sea ice surface ($3.35 \pm 0.86 \text{ mmol m}^{-2} \text{ day}^{-1}$, $n = 8$), but there was no discernible difference in this efflux if frost flowers were within the chamber footprint ($3.02 \pm 0.76 \text{ mmol m}^{-2} \text{ day}^{-1}$, $n = 4$) or not ($3.67 \pm 1.99 \text{ mmol m}^{-2} \text{ day}^{-1}$, $n = 4$). These results may not be unexpected given the small difference in ikaite concentration between the frost flowers and surrounding brine skim. Few studies exist against which to compare our results. Fluxes are consistent in sign, but generally smaller than chamber flux measurements reported by Geilfus *et al.* [2013] over young, landfast sea ice near Barrow, AK. They observed an average efflux of $6.7 \text{ mmol m}^{-2} \text{ day}^{-1}$ (4.2 to $9.6 \text{ mmol m}^{-2} \text{ day}^{-1}$) based on four measurements over ice that was thicker (20 cm), covered with older frost flowers, and marginally colder (ice surface temperature of -14.2°C) relative to the newer ice in our pond experiment. Ignoring possible differences in sea ice organic carbon composition between sites, the larger efflux of CO_2 at the Barrow site is possibly the result of colder near-surface temperature. On cooling, pCO_2 in the brine system of sea ice tends to increase, given the likelihood of ikaite production, and because gases are generally less soluble in stronger electrolyte solutions (e.g., Thomas *et al.*, 2010). Given that the brine volume was $> 5\%$ throughout their sea ice profile, outgassing could occur along a brine-to-air pCO_2 gradient.

Microbial Habitat

In general, the higher the salinity of the frost flower (or brine skim) sample, the greater its bacterial content according to Bowman and Deming [2010], whose data support the view that bacteria in sea ice brine are transported upwards as the brine wicks into frost flowers. In our pond experiment, the highest concentrations of bacteria were again observed in the saltiest features (in rank order, on a melt-volume basis): $1.56\text{--}4.46 \times 10^5 \text{ cells ml}^{-1}$ ($n = 32$) in frost flowers and the surface slush layer, compared to $1.10\text{--}2.11 \times 10^5 \text{ ml}^{-1}$ ($n = 7$) in seawater, $6.58\text{--}7.85 \times 10^4 \text{ ml}^{-1}$ ($n = 2$) in young sea ice, and only $133\text{--}353 \text{ ml}^{-1}$ ($n = 2$) in freshly deposited snow (which had no detectable salinity by refractometer). An atmospheric source of bacteria (represented by fresh snow samples) to the frost flowers and brine skim at the pond was thus negligible, including even for aging frost flowers showing signs by $\delta^{18}\text{O}$ analysis of atmospheric ice-crystal deposition (Figure 7). The contribution of vapor-derived ice to frost flowers, however, represents an unavoidable dilution (upon sample melting) of the true bacterial density in the habitable brine volume fraction of these structures. Although estimates of this dilution factor could be made in a few cases, comparing bacterial abundance across the data set required scaling numbers to melted sample volume.

Earlier short-term laboratory and mesocosm experiments to evaluate bacterial content as a function of frost flower age have not been definitive [Bowman and Deming, 2010; Aslam *et al.*, 2012], but this field experiment clearly revealed highest concentrations of bacteria early in the growth phase of these briny ice structures (Figure 10) when salinity was also highest. Frost

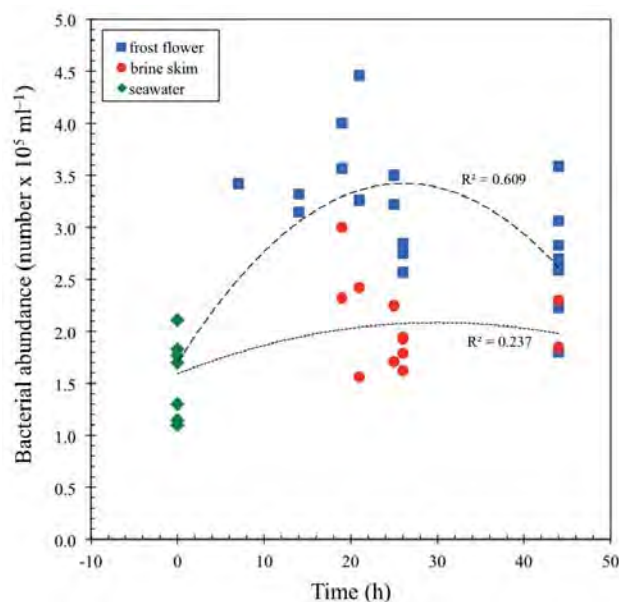


Figure 10. Bacterial abundance in frost flowers (blue squares) and surface slush layer (red circles) over time since opening the experimental pond, with abundance in seawater (green diamonds) representing time zero. The first three values for frost flowers derive from the second opening of the pond. Second-order polynomials were fit to the data primarily to help visualize the different apparent time-course trajectories for frost flowers ($R^2 = 0.609$) and surface slush layer ($R = 0.237$).

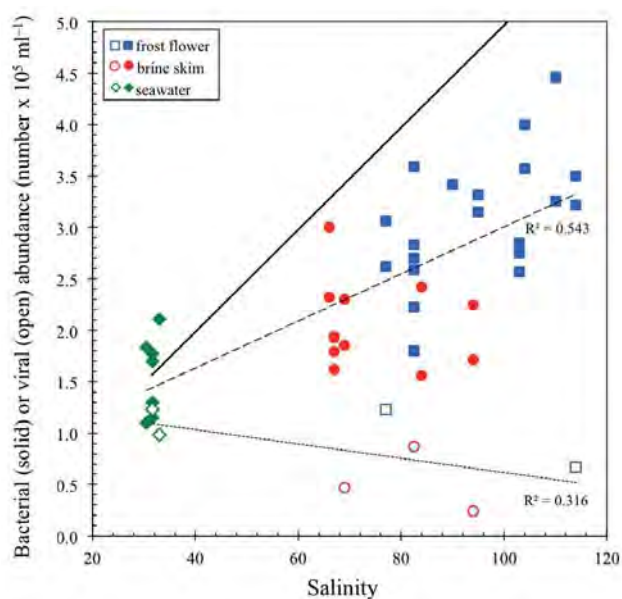


Figure 11. Abundance of bacteria (solid symbols) and viral-like particles (VLP, open symbols) in frost flowers (blue squares), the surface slush layer (red circles) and seawater (green diamonds) as a function of sample salinity. The calculated dilution curve (solid line) assumes that seawater bacteria after incorporation into sea ice brine behave as passive particles, concentrating or diluting in synchrony with dissolved salts. The data for frost flower, surface slush layer and seawater bacterial abundance are fit to a linear regression (dashed line, $R^2 = 0.543$, $n = 40$), as are the VLP data (dotted line with negative slope, $R^2 = 0.316$, $n = 7$). If the difference between the bacterial dilution and regression lines were due to virally mediated mortality, then VLP abundance would be higher than bacterial abundance and the slope of the VLP line would be positive and steeper than the slope for the bacterial regression.

flowers that were ≤ 26 hours old always harbored more bacteria than the underlying slush layer sampled at the same time, as evident from Figure 10 and from a comparison of mean values \pm SD: $3.30 \pm 0.525 \times 10^5 \text{ ml}^{-1}$ for frost flowers (range of $2.57\text{--}4.46 \times 10^5 \text{ ml}^{-1}$, $n = 13$); and $2.05 \pm 0.446 \times 10^5 \text{ ml}^{-1}$ for the slush layer (range of $1.56\text{--}3.00 \times 10^5 \text{ ml}^{-1}$, $n = 6$). Older frost flowers (44 hours) continued to support relatively high bacterial abundance (mean of $2.68 \pm 0.532 \times 10^5 \text{ ml}^{-1}$, range of $1.80\text{--}3.59 \times 10^5 \text{ ml}^{-1}$, $n = 8$), but distinguishing abundance in frost flowers from that in the slush layer (represented by only two samples) was not possible. The apparent decrease in bacterial abundance in frost flowers as they aged (Figure 10) may be due to a number of factors, including the effective dilution of bacteria in the frost flower mass by vapor deposition over time, in which case no true change in bacterial abundance (derived from brine wicked into the frost flowers) may have occurred. Other considerations include possible brine drainage or bacterial mortality in the older frost flowers. There is $\delta^{18}\text{O}$ evidence for dilution by vapor deposition, but brine drainage is speculative and bacterial mortality in frost flowers is difficult to distinguish from bacterial retention in the underlying ice. In prior studies of young sea ice and upper winter sea ice [Collins *et al.*, 2008; 2011] if bacterial mortality was detected, it was attributed to vi-

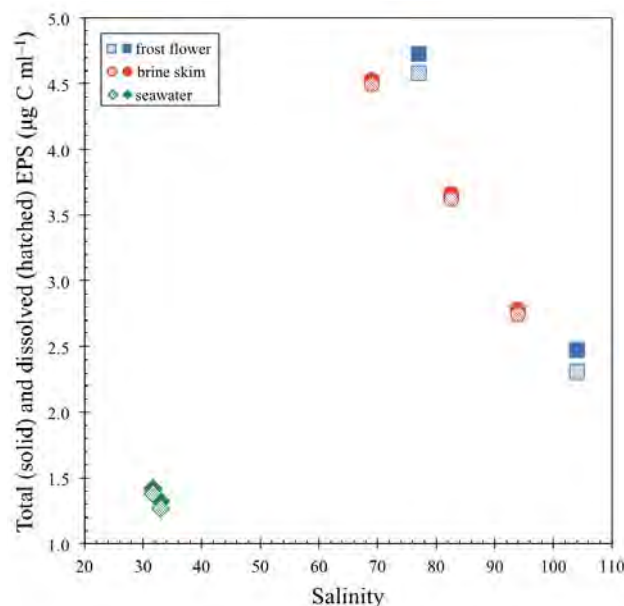


Figure 12. Concentration of total EPS (filled symbols) and dissolved EPS (dEPS, hatched symbols) in seawater (green diamonds), the surface slush layer (red circles), and frost flowers (blue squares) as a function of sample salinity. The saltiest samples are the youngest samples (19 hours for frost flowers, 25 hours for the slush layer) and the freshest samples are the oldest samples (44 hours); i.e., EPS values in these samples are not only higher than in seawater but also appear to have increased over time.

ral lysis. In this study, viral densities were too low ($0.245\text{--}1.23 \times 10^5 \text{ ml}^{-1}$, $n = 7$; Figure 11) to indicate bacterial mortality by this mechanism, nor was evidence of cell death (“ghost” cells or cell debris) apparent during microscopic analyses. Overall, it appears that bacteria wicked into frost flowers survive conditions encountered as the frost flowers age.

A mechanism to explain bacterial survival under the challenging conditions that characterize winter saline frost flowers is the production of EPS. EPS are considered to be extracellular cryoprotectants and likely osmoprotectants for microbes encased in winter sea ice [Ewert and Deming, 2013], where particulate EPS (pEPS) production has been documented at temperatures as low as -27°C and corresponding brine salinities as high as 220 [Krembs *et al.*, 2002; Collins *et al.*, 2008]. In this study, EPS occurred predominantly in the form of dissolved EPS (93–99% of total EPS) and appeared to increase in both frost flowers and the surface slush layer over time (Figure 12), suggesting a possible response by live bacteria transported upwards from sea ice [as in Ewert *et al.*, 2013] into the more extreme conditions at the ice surface and centimeter heights reached by frost flowers (Figure 3). Although our EPS data set is small, the highest amount of total EPS was detected in the oldest (44-day) frost flowers sampled, and the highest percentage of pEPS in frost flowers, compared to other sample types (Figure 12). Overall, the amount of EPS detected in frost flower and surface slush samples (range of $2.31\text{--}4.58 \mu\text{g C ml}^{-1}$; $n = 5$) falls at the upper end of reported EPS values for

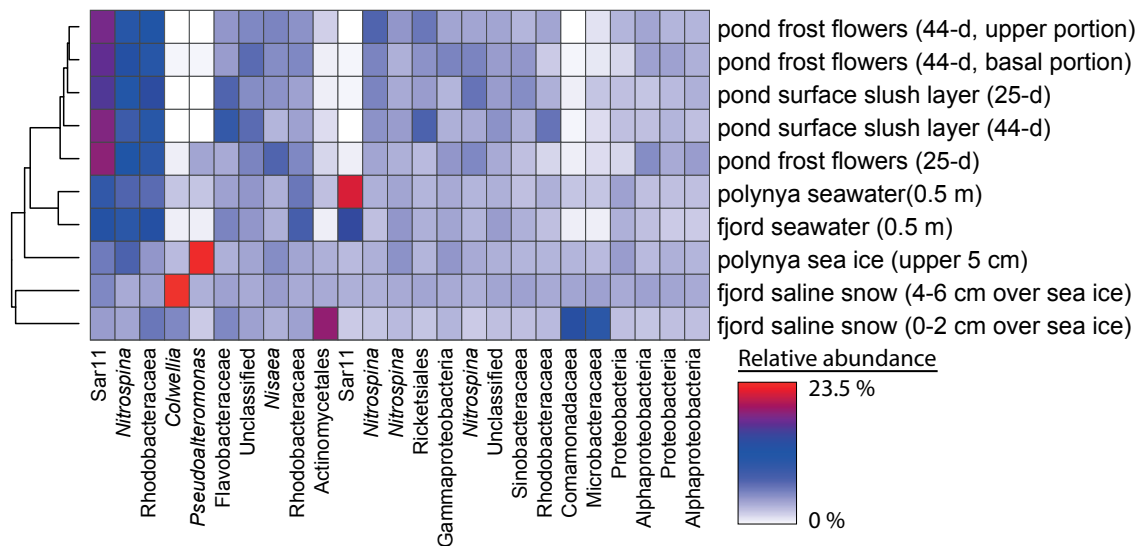


Figure 13. Sample similarity evaluated by bacterial community structure among the 25 most abundant operational taxonomic units (OTUs) as distributed in each of the different sample types. OTU identifications are to the most resolved taxonomic level. Hierarchical clustering of samples is shown by the dendrogram along the y-axis. White indicates low values (min = 0 % of total community); red indicates high values (max = 23.5 % of total community). The upper and basal portions of the same 44-day frost flower patch are the most closely related, dominated by the same members of the SAR11 clade (OTU0025) and the genus *Nitrospina* (OTU0032). All frost flower and surface slush layer samples cluster together at a higher level. Seawater samples, which also cluster together and are dominated by a different member of the SAR11 clade (OTU0054), are more closely related to the frost flower and surface slush samples than to the other sample types.

Arctic or Antarctic sea ice [Underwood *et al.*, 2013; Ewert *et al.*, 2013], though lower than those reported for frost flowers on young sea ice near Barrow, Alaska [Bowman and Deming, 2010], a more biologically productive region in general than Young Sound [Krembs *et al.*, 2011; Bowman *et al.*, 2014].

Relating bacterial abundance and salinity in frost flowers and the underlying slush layer (Figure 11) reinforced the positive correlation observed earlier by Bowman and Deming [2010] based on collections from other Arctic locations and from artificially grown frost flowers. With the availability of seawater data (missing from Bowman and Deming [2010]), a theoretical dilution (or concentration) curve could be calculated (Figure 11) to represent the concentration of bacteria expected in frost flowers had the bacteria moved as passive particles in synchrony with dissolved salts. Regression analysis of the frost flower and surface slush data with the seawater data ($y = 0.0229x + 0.719$, $R^2 = 0.543$, $n = 40$) indicated a discrepancy in the transport of bacteria relative to salts during upward movement of brine into frost flowers (compare slopes of the dilution and regression lines; Figure 11). Although most bacteria were still traveling with the brine all the way into the uppermost segments of frost flowers, and completely in one case (Figure 11), a portion present in seawater prior to freezing was not delivered to the new ice surface or wicked into the frost flowers. Bacterial mortality (and recovery) following entrainment into young sea ice has been deduced from earlier ice-core studies [Grossman and Dieckmann, 1994; Collins *et al.*, 2011b], as has selective bacterial retention in the ice during brine expulsion to the surface

[Ewert *et al.*, 2013; Bowman *et al.*, 2013]. This unique field experiment allowed not only confirmation that some bacteria are not delivered to the young OSA interface but also that the majority delivered into the slush layer and frost flowers persist for days in these more extreme environments, highlighting them as promising natural laboratories for the study of microbial extremophiles. Measuring microbial activity in these environments was not possible during this study, but the temperatures and salinities involved are already known to permit bacterial activity [Junge *et al.*, 2004; Ewert and Deming, 2014]. The regression equation obtained for the relationship between bacterial abundance and salinity (Figure 11) may also facilitate inclusion of frost flower bacteria into aerosol models for this region [e.g., Shaw *et al.*, 2010; Xu *et al.*, 2013].

Complementing this salinity-based analysis of bacterial delivery into brine skim and frost flowers on the surface of young ice are comparative analyses of the most abundant bacterial taxa found in the different types of samples in the study area (Figure 13). Strong similarities were observed among all frost flower and surface slush communities, with no marked distinction by age or extension into the atmosphere (upper versus basal segments of the frost flowers). Together the frost flower and slush communities clustered separately from those detected in underlying seawater, and even further from those in other sample types. All sample types had in common the presence of members of the genus *Nitrospina*, known for nitrification, but seawater was clearly dominated by a member of the oligotrophic bacterial clade known as SAR11, in keeping with the

oligotrophic status of this fjord. A different member of the SAR11 clade dominated in frost flowers and the surface slush layer. A member of the genus *Colwellia*, known for cold adaptation, appeared in seawater and dominated in polynya sea ice but was virtually undetected in the saltier frost flower and brine skim communities, consistent with the limited salt tolerance expressed by *Colwellia* species in culture [Marx *et al.*, 2009; Ewert *et al.*, 2014]. Although DNA results from sea ice directly underlying the frost flowers were not obtained due to technical problems, the available results on community composition are consistent with the salinity-based analysis of total bacterial numbers in that both point to a selective process occurring between seawater freezing and frost flower formation on the surface of the ice, as well as persistence of those delivered to frost flowers over the period of the pond experiment. Bowman *et al.* [2013] reached a similar conclusion regarding selection of bacterial communities in frost flowers near Barrow, Alaska, although the dominant taxa there (members of the Rhizobiales) reflect the different nature of that coastal environment in terms of greater biological productivity and coastal erosion [as discussed in Bowman *et al.*, 2014].

Conclusions

The greater presence of young sea ice formations in the Arctic increases both the spatial coverage and temporal range within which frost flowers occur. At our field site frost flowers formed when open water became available to a very cold atmosphere and surface wind conditions were low, allowing for supersaturation of the near-surface boundary layer. The formation of the young ice and its frost flower-covered surface dramatically changed the PAR and thermal environment of this young OSA interface. A large and contiguous area of frost flowers reduced PAR transmission until it closely resembled a thin snow cover on the sea ice.

Thermally, frost flowers also affected energy exchange across this interface. The frost flowers themselves were 5°C colder than the brine surface, with a temperature gradient that was approximately linear from the base to the upper tip of the frost flowers. Larger (older) flowers, which protruded further into the atmospheric boundary layer, were both colder and lower in brine volume – reaching maximum temperatures that were about 7°C colder than at the base. Our results suggest that expansive frost flower coverage will raise both net longwave and net all-wave radiation. Net radiation and the heat budget will also depend, however, on associated changes to surface albedo and air-ice sensible heating in the presence of frost flowers. Regarding net radiation, frost flowers will only affect the shortwave budget during a small part of the annual cycle (i.e., when solar insolation is a factor in the surface radiation budget). As sensible heating responds to the air-surface temperature difference, a greater loss of heat is expected for

surfaces free of frost flowers during the cold season. A more detailed assessment (beyond the scope of this contribution) of the response of the surface heat budget to frost flowers is underway using these and other data.

Modeling of frost flower formation at our study site indicates that our observations match well with the processes suggested by Style and Worster [2009]. For most of the experiment the pond surface conditions remained within regime VI, with a brief transition into regime V, where these two regimes distinguish between unsaturated vs. supersaturated water vapor conditions in the near-surface boundary layer into which the frost flowers grew. In both regimes the source of the water vapor in the layer immediately above the sea ice resulted from evaporation/sublimation of brine at the sea ice surface rather than from the cold unsaturated atmosphere.

Measured $\delta^{18}\text{O}$ values of frost flowers for several hours after freeze-up further support that the frost flowers originated primarily from the surface brine skim. The youngest unsectioned frost flowers had a mean $\delta^{18}\text{O}$ value of $-0.8 \pm 0.3\text{‰}$, which was similar to the surface slush signature ($-0.1 \pm 0.5\text{‰}$) and decreased gradually with time to $-4.3 \pm 0.1\text{‰}$ after 114 hours from freeze-up. Based on our direct temperature and salinity measurements, 50–80% of the frost flower mass was formed from brine wicked from the surface of the ice, while 20–50% of the water vapor in the layer directly above the sea ice originated from evaporation of brine in the brine skim.

The climate forcing, and response of this ice surface to the formation of frost flowers, is seen as a key aspect of inorganic carbon processes operating at this interface. Ikaite crystals were observed to form within 1 hour in frost flowers at our site, and to high concentrations; the average ikaite concentration in frost flowers was $1013 \mu\text{mol kg}^{-1}$ (632, standard deviation) and in the surface slush layer, $1061 \mu\text{mol kg}^{-1}$ (736, standard deviation). Given the difference in density of these surface features, however, the highest amount of ikaite was observed in the sea ice. Chamber flux measurements confirmed an efflux of CO_2 at the brine-wetted sea ice surface, though there appeared to be no difference in the CO_2 flux if frost flowers were within the chamber footprint, pointing to the overriding importance of the brine skim in this context, for it covers the entire ice surface whereas frost flowers can be patchy.

The microbial results supported our physical analysis of brine migration processes within the brine skim and the associated surface slush layer. The highest concentrations of bacteria were observed in the saltiest features (in rank order, on a melt-volume basis). Consistent with the $\delta^{18}\text{O}$ analyses, an atmospheric source of bacteria (represented by fresh snow samples) to the frost flowers and brine skim at the pond was negligible, including for aging frost flowers showing signs of atmospheric ice-crystal deposition. Young frost flowers consistently harbored more bacteria than the underlying slush layer.

Analysis of a dilution curve confirmed the expected concentration of bacteria in frost flowers, assuming that bacteria move as passive particles in synchrony with dissolved salts during the freezing process. The difference between the slopes of dilution and regression curves, however, suggests that a portion of the bacteria were either retained in the ice during upward brine expulsion or progressively lost during freezing. Converging lines of evidence favored the former explanation. The temporal aspect of our experiment enabled the observation that the selected majority of bacteria, delivered with brine to the ice surface and wicked into frost flowers, persisted there for the duration of the experiment, showing these environments to be promising natural laboratories for the study of microbial extremophiles and their potential roles in biogeochemical exchanges across the OSA.

As we move forward into a warmer Arctic we can expect increased dynamics of the mobile ice creating periods when a warm ocean will be exposed to a cold atmosphere, allowing for the creation of expansive frost flower-covered young ice surfaces. We have shown that the geophysical, thermal and radiative transfer of these young ice types can have significant impacts on exchange processes across the OSA interface. We have also shown that the exchange of CO₂ across this interface can be affected by ikaite geochemistry and that brine-rich features on the surface of new ice may be providing a selective habitat for microbes. The overarching biogeochemical consequences of this emerging icescape appear to require continued scientific attention.

Acknowledgments

This project is a contribution to the Arctic Science Partnership (ASP) and to the ArcticNet Networks of Centres of Excellence (NCE). Funding was provided by the Canada Excellence Research Chair (CERC) and Canada Research Chair (CRC) programs; the Natural Sciences and Engineering Research Council (NSERC); the Canada Foundation for Innovation (CFI); the US National Science Foundation (award OPP-ARC1205152) and Walters Endowed Professorship (J.W.D.); and a US EPA Star Fellowship (J.S.B.). D.H.S. was supported financially by the commission for scientific Research in Greenland (KVUG). We thank E. Frandsen, R. Glud, B. Johnston, I. Lennert, K. Lennert, and J. Sievers for field support and S. Carpenter and E. Firth for microbial data analysis. To obtain the data set used in this work, please contact the corresponding author (david.barber@umanitoba.ca). This paper is dedicated to Dr. Klaus Hochheim, who tragically lost his life while doing sea ice research in the Canadian Arctic in September, 2013.

Literature Cited

- Alvarez-Aviles, L., W.R. Simpson, T.A. Douglas, M. Sturm, D. Perovich, and F. Domine (2008), Frost flower chemical composition during growth and its implications for aerosol production and bromine activation, *J. Geophys. Res.*, 113, D21304, doi:10.1029/2008JD010277
- Andreas, E.L., P.S. Guest, P.-O. G. Persson, C.W. Fairall, T.W. Horst, R.E. Moritz and S.R. Semmer (2002), Near-surface water vapour over polar sea ice is always near ice saturation. *J. Geophys. Res.*, 107, (C10), 8033, doi: 10.1029/2000JC000411.
- Aslam, S., G. Underwood, H. Kaartokallio, L. Norman, R. Autio, M. Fischer, et al. (2012), Dissolved extracellular polymeric substances (dEPS) dynamics and bacterial growth during sea ice formation in an ice tank study, *Pol. Biol.*, 35, 661–676.
- Assur, A. (1960), Composition of sea ice and its tensile strength, SIPRE Research Report, 44.
- Barber, D.G., M.G. Asplin, T. Papakyriakou, L. Miller, B. Else, J. Ioacozza, C.J. Mundy, M. Gosslin, N. Asselin, S. Ferguson, J. Lukovich, G. Stern, A. Gaden, M. Pucko, and F. Wang (2012), Consequences of change and variability in sea ice on marine ecosystem and biogeochemical processes during the 2007–2009 Canadian International Polar Year Program, *Climatic Change*, doi:10.1007/s10584-012-0482-9.
- Barber, D.G., R. Galley, M.G. Asplin, R. De Abreu, K. Warner, M. Pučko, M. Gupta, S. Prinsenberg, and S. Julien (2009), Perennial pack ice in the southern Beaufort Sea was not as it appeared in the summer of 2009, *Geophys. Res. Lett.*, 36, L24501, doi:10.1029/2009GL041434.
- Bowman, J.S., and J.W. Deming (2010), Elevated bacterial abundance and exopolymers in saline frost flowers and implications for atmospheric chemistry and microbial dispersal, *Geophys. Res. Lett.*, 37, L13501, doi: 10.1029/2010GL043020.
- Bowman, J.S., S. Rasmussen, N. Blom, J.W. Deming, S. Rysgaard, and T. Scheritz-Ponten (2012), Microbial community structure of Arctic multiyear sea ice and surface seawater by 454 sequencing of the 16S RNA gene, *ISME*, 6, 11–20, doi:10.1038/ismej.2011.76.
- Bowman, J.S., C. Larose, T. Vogel, and J.W. Deming (2013), Selective occurrence of *Rhizobium* spp., widely distributed bacterial members of the polar marine rare biosphere, in frost flowers on the surface of young sea ice near Barrow, Alaska, *Environ. Microbiol.*, 5, 575–582, doi:10.1111/1758-2229.12047.
- Bowman, J.S., C.T. Berthiaume, E.V. Armbrust, and J.W. Deming (2014), The genetic potential for key biogeochemical processes in Arctic frost flowers and young sea ice revealed by metagenomic analysis, *FEMS Microbiol. Ecol.* DOI: 10.1111/1574-6941.12331
- Collins, R.E., and J.W. Deming (2011a), Abundant dissolved genetic material in Arctic sea ice, Part I: Extracellular DNA, *Pol. Biol.*, 34, 1819–1830, doi:10.1007/s00300-011-1041-y.
- Collins, R.E., and J.W. Deming (2011b), Abundant dissolved genetic material in Arctic sea ice, Part II: Virus dynamics during autumn freeze-up, *Pol. Biol.*, 34, 1831–1841, doi:10.1007/s00300-011-1008-z.

- Collins, R.E., S.D. Carpenter, and J.W. Deming (2008), Spatial heterogeneity and temporal dynamics of particles, bacteria, and pEPS in Arctic winter sea ice, *J. Mar. Systems*, 74, 902–917, doi:10.1016/j.jmarsys.2007.09.005.
- Cottrell, M. T., and D.L. Kirchman (2009), Photoheterotrophic microbes in the Arctic Ocean in summer and winter, *Appl. Environ. Microbiol.*, 75(15), 4958–4966.
- Díez, B., B. Bergman, C. Pedrós-Alió, M. Antó, and P. Snoeijs (2012), High cyanobacterial nifH gene diversity in Arctic seawater and sea ice brine, *Environ. Microbiol. Rep.*, 4, 360–366.
- Domine, F., A.S. Taillandier, W.R. Simpson and K. Severin (2005), Specific surface area, density and microstructure of frost flowers, *Geophys. Res. Lett.*, 32, L13502, doi: 10.1029/2005GL023245.
- Douglas, T.A., M. Sturm, W.R. Simpson, S. Brooks, S.E. Lindberg, and D.K. Perovich (2005), Elevated mercury measured in snow and frost flowers near Arctic sea ice leads, *Geophys. Res. Lett.*, 32, L04502, doi: 10.1029/2004GL022132.
- Douglas, T.A., F. Domine, M. Barret, C. Anastasio, H.J. Beine, J. Bottenheim, A. Grannas, S. Houdier, S. Netcheva, G. Rowland, R. Staebler, and A. Steffen (2012), Frost flowers growing in the Arctic ocean-atmosphere-sea ice- snow interface: 1. Chemical composition, *J. Geophys. Res.*, 117, D00R09, doi: 10.1029/2011JD016460.
- Drinkwater, M.R., and G.B. Crocker (1988), Modelling changes in the dielectric and scattering properties of young snow-covered sea ice at GHz frequencies, *J. Glaciol.*, 34, 274–282.
- Ehn, J. K., B. J. Hwang, R. Galley, and D. G. Barber (2007), Investigations of newly formed sea ice in the Cape Bathurst polynya: 1. Structural, physical and optical properties, *J. Geophys. Res.*, 112, C05002, doi:10.1029/2006JC003702.
- Ewert, M., and J.W. Deming (2013), Sea ice microorganisms: Environmental constraints and extracellular responses, *Biology*, 2, 603–628, doi:10.3390/biology2020603.
- Ewert, M., and J.W. Deming (2014), Bacterial responses to fluctuations and extremes in temperature and brine salinity at the surface of Arctic winter sea ice, *FEMS Microbiol. Ecol.* doi: 10.1111/1574-6941.12363.
- Ewert, M., S.D. Carpenter, J. Colangelo-Lillis, and J.W. Deming (2013), Bacterial and extracellular polysaccharide content of brine-wetted snow over Arctic winter first-year sea ice, *J. Geophys. Res.*, 118, 1–10, doi:10.1002/jgrc.20055.
- Fofonoff, P., and R. C. Millard Jr. (1983), Algorithms for computation of fundamental properties of seawater, *Unesco Tech. Pap. in Mar. Sci.*, 44, 53 pp.
- Geilfus, N.-X., G. Carnat, G.S. Dieckmann, N. Halden, G. Nehrke, T. Papakyriakou, J.-L. Tison, and B. Delille (2013), First estimates of the contribution of CaCO₃ precipitation to the release of CO₂ to the atmosphere during sea ice growth, *J. Geophys. Res.*, 118, 244–255, doi:10.1029/2012J007980
- Hesse, K. F. and H. Küppers (1983), Refinement of the structure of Ikaite, CaCO₃·6H₂O, *Zeitschrift für Kristallographie* 163, 227–231.
- Isleifson, R. J. Galley, D.G. Barber, J. Landy, A. Komarov, L. Shafai (2013), A study on the C-band polarimetric scattering and physical characteristics of frost flowers on experimental sea ice. *IEEE Trans. Geosci. Remote Sensing*, vol.52, no.3, pp.1787,1798, doi: 10.1109/TGRS.2013.2255060.
- Junge, K., H. Eicken, and J.W. Deming (2004), Bacterial activity at –2 to –20°C in Arctic wintertime sea ice, *Appl. Environ. Microbiol.*, 70, 550–557.
- Krembs, C., H. Eicken, and J.W. Deming (2011), Exopolymer alteration of physical properties of sea ice and implications for ice habitability and biogeochemistry in a warmer Arctic, *US Proc. Natl. Acad. Sci.*, 108(9), 3653–3658.
- Krembs, C., J.W. Deming, K. Junge, and H. Eicken (2002), High concentrations of exopolymeric substances in wintertime sea ice: Implications for the polar ocean carbon cycle and cryoprotection of diatoms, *Deep-Sea Res. I*, 49, 2163–2181.
- Kwok, R. (2007), Near zero replenishment of the Arctic multiyear sea ice cover at the end of 2005 summer, *Geophys. Res. Lett.*, 34, L05501, doi: 10.1029/2006GL028737.
- Kwok, R. and G.F. Cunningham (2010), Contribution of melt in the Beaufort Sea to the decline in Arctic multiyear sea ice coverage: 1983–2009, *Geophys. Res. Lett.*, 37, L20501, doi: 10.1029/2010GL044678.
- Kühl, M., R.N. Glud, J. Borum, R. Roberts, and S. Rysgaard (2001), Photosynthetic performance of surface associated algal below sea ice as measured with pulse amplitude modulated (PAM) fluorometer and O₂ microsensors, *Mar. Ecol. Progr. Ser.*, 223, 1–14.
- Magono, C., and C.W. Lee (1966), Meteorological classification of natural snow crystals, *J. Fac. Sci. Hokkaido Univ., Ser. VII*, 2, 321–335.
- Martin, S., R. Drucker, and M. Fort (1995), A laboratory study of frost flower growth on the surface of young sea ice, *J. Geophys. Res.*, 100, 7027–7036.
- Martin, S., Y. Yu, and R. Drucker (1996), The temperature dependence of frost flower growth on laboratory sea ice and the effect of the flowers on infrared observations of the surface, *J. Geophys. Res.*, 101, 12111–12125.
- Marx, J.G., S.D. Carpenter, and J.W. Deming (2009), Production of cryoprotectant extracellular polysaccharide substances (EPS) by the marine psychrophilic bacterium *Colwellia psychrerythraea* strain 34H under extreme conditions, *Can. J. Microbiol.*, 55, 63–72.
- Maslanik, J.A., C. Fowler, J. Stroeve, S. Drobot, J. Zwally, D. Yi, and W. Emery (2007), A younger, thinner Arctic ice cover: Increased potential for rapid, extensive sea-ice loss. *Geophys. Res. Lett.*, 34, L24501, doi: 10.1029/2007GL032043.
- Maslanik, J.A., J. Stroeve, C. Fowler, and W. Emery (2011), Distribution and trends in Arctic sea ice age through spring 2011, *Geophys. Res. Lett.*, 38, L13502, doi: 10.1029/2011GL047735.
- Nghiem, S.V.V., I.G.G. Rigor, A. Richter, J.P.P. Burrows, P.B.B. Shepson, J.W. Bottenheim, D.G. Barber, A. Steffen, J.R. Latonas, F. Wang, G.A. Stern, P. Clemente-Colon, S. Martin, D.K. K. Hall, L. Kaleschke, P.J. Tackett, G. Neumann, and M.G.G. Asplin (2012), Field and satellite observations of the formation and distribution of Arctic atmospheric bromine above a rejuvenated sea ice cover, *J. Geophys. Res.*, doi:10.1029/2011JD016268.

- Oksanen, J., F.G. Blanchet, R. Kindt, P. Legendre, P.R. Minchin, et al. (2012), vegan: Community Ecology Package, R package version 2.0-5.
- Perovich, D.K., and J.A. Richter-Menge (1994), Surface characteristics of lead ice, *J. Geophys. Res.*, 99(C8), 16,341-16,350, doi:10.1029/94JC01194.
- Rankin, A.M., V. Auld, and E.W. Wolff (2000), Frost flowers as a source of fractionated sea salt aerosol in the polar regions, *Geophys. Res. Lett.*, 27(21), 3469-3472, doi:10.1029/2000GL011771.
- Rankin, A.M., E.W. Wolff and S. Martin (2002), Frost flowers: Implications for tropospheric chemistry and ice core interpretation, *J. Geophys. Res.*, 107, 4683, 2002.
- Rankin, A.M. and E.W. Wolff (2003), A year-long record of size-segregated aerosol composition at Halley, Antarctica, *J. Geophys. Res.*, 108, 4775.
- Roscoe, H.K., B. Brooks, A.V. Jackson, M.H. Smith, S.J. Walker, R.W. Obbard and E.W. Wolff (2011), Frost flowers in the laboratory: Growth, characteristics, aerosol and the underlying sea ice, *J. Geophys. Res.*, 116, D12301, doi: 10.1029/2010JD015144.
- Rysgaard, S. and R.N. Glud (2007), Carbon cycling in Arctic marine ecosystems: Case study – Young Sound, *Medd Greenland, Bioscience* vol 58, 216 pp.
- Rysgaard, S., D.H. Sjøgaard, M. Cooper, M. Pućko, K. Lennert, T.N. Papakyriakou, F. Wang, N.X. Geilfus, R.N. Glud, J. Ehn, D.F. McGinnis, K. Attard, J. Sievers, J.W. Deming, and D. Barber (2013), Ikaite crystal distribution in winter sea ice and implications for CO₂ system dynamics, *The Cryosphere*, 7, 707–718, doi:10.5194/tc-7-707-2013.
- Schloss, P.D., S.L. Westcott, T. Ryabin, J.R. Hall, M. Hartmann, et al. (2009), Introducing mothur: open-source, platform-independent, community-supported software for describing and comparing microbial communities, *Appl. Environ. Microbiol.*, 75, 7537–7541.
- Shaw, P.M., L.M. Russell, A. Jefferson, and P.K. Quinn (2010), Arctic organic aerosol measurements show particles from mixed combustion in spring haze and from frost flowers in winter, *Geophys. Res. Lett.*, 37, L10803, doi: 10.1029/2010GL042831.
- Sherman, L.S., J.D. Blum, T.A. Douglas, and A. Steffen (2012), Frost flowers growing in the Arctic ocean-atmosphere-sea ice-snow interface: 2. Mercury exchange between the atmosphere, snow, and frost flowers, *J. Geophys. Res.*, 117, D00R10, doi: 10.1029/2011JD016186.
- Style, R.W. and M.G. Worster (2009), Frost flower formation on sea ice and lake ice, *Geophys. Res. Lett.*, 36, L11501, doi: 10.1029/2009GL037304.
- Underwood, G.J.C., S.N. Aslam, C. Michel, A. Niemi, L. Norman, K.M. Meiners, J. Laybourn-Parry, H. Paterson, and D.N. Thomas (2013), Broad-scale predictability of carbohydrate and exopolymers in Antarctic and Arctic sea ice, *US Proc. Natl. Acad. Sci.*, 110(39), 15734–15739.
- Wagenbach, D., F. Ducroz, R. Mulvaney, L. Keck, A. Minikin, M. Legrand, J.S. Hall, and E.W. Wolff (1988), Seasalt aerosol in coastal Antarctic regions, *J. Geophys. Res.*, 103, doi:10.1029/97JD01804.
- Waleron, M., K. Waleron, W.F. Vincent, et al. (2007), Allochthonous inputs of riverine picocyanobacteria to coastal waters in the Arctic Ocean, *FEMS Microbiol. Ecol.*, 59, 356–365.
- Wells, L.E., and J.W. Deming (2006), Modeled and measured dynamics of viruses in Arctic winter sea-ice brines, *Environ. Microbiol.*, 8(6), 1115–1121.
- Wensnahan, M.R., T.C. Grenfell, D.P. Winebrenner, and G.A. Maykut (1993), Observations and theoretical studies of microwave emission from thin saline ice, *J. Geophys. Res.*, 98, 8531–8545.
- Xu, L., L.M. Russell, R.C. Somerville, and P.K. Quinn (2013), Frost flower aerosol effects on Arctic wintertime longwave cloud radiative forcing, *J. Geophys. Res. – Atmos.*, 118(23), doi:10.1002/2013JD020554.

PAPER IV



Photo: Michael S. Schröder.

Autotrophic and heterotrophic activity in Arctic first-year sea ice: seasonal study from Malene Bight, SW Greenland

D.H. Søgaard • M. Kristensen • S. Rysgaard • R.N. Glud •
P.J. Hansen • K.M Hilligsøe

Marine Ecology Progress Series 419:31 – 45, doi: 10.3354/meps08845



Autotrophic and heterotrophic activity in Arctic first-year sea ice: seasonal study from Malene Bight, SW Greenland

Dorte Haubjerg Søgaard^{1,2,*}, Morten Kristensen^{1,2}, Søren Rysgaard¹,
Ronnie Nøhr Glud^{1,4}, Per Juel Hansen², Karen Marie Hilligsøe³

¹Greenland Climate Research Centre (c/o Greenland Institute of Natural Resources), Kivioq 2, Box 570, 3900 Nuuk, Greenland

²University of Copenhagen, Marine Biological Laboratory, Strandpromenaden 5, 3000 Helsingør, Denmark

³Aarhus University, Department of Biological Sciences, Ny Munkegade 114-116, 8000 Århus C, Denmark

⁴Present address: The Scottish Association for Marine Science, Oban, Argyll PA37 1QA, Scotland, UK

ABSTRACT: We present a study of autotrophic and heterotrophic activities of Arctic sea ice (Malene Bight, SW Greenland) as measured by 2 different approaches: (1) standard incubation techniques ($H^{14}CO_3^-$ and $[^3H]$ thymidine incubation) on sea ice cores brought to the laboratory and (2) cores incubated *in situ* in plastic bags with subsequent melting and measurements of changes in total O_2 concentrations. The standard incubations showed that the annual succession followed a distinctive pattern, with a low, almost balancing heterotrophic and autotrophic activity during February and March. This period was followed by an algal bloom in late March and April, leading to a net autotrophic community. During February and March, the oxygen level in the bag incubations remained constant, validating the low balanced heterotrophic and autotrophic activity. As the autotrophic activity exceeded the heterotrophic activity in late March and April, it resulted in a significant net oxygen accumulation in the bag incubations. Integrated over the entire season, the sea ice of Malene Bight was net autotrophic with an annual net carbon fixation of 220 mg C m^{-2} , reflecting the net result of a sea ice-related gross primary production of 350 mg C m^{-2} and concurrent bacterial carbon demand of 130 mg C m^{-2} . Converting the O_2 net exchange of the bag incubations into carbon turnover estimated an annual net carbon fixation of $1700 \pm 760 \text{ mg C m}^{-2}$ (mean \pm SD), which was higher than the annual net carbon fixation quantified in the standard incubations.

KEY WORDS: Sea ice · Primary production · Bacterial carbon demand · Net autotrophic activity · Net heterotrophic activity · Attenuation coefficients

Resale or republication not permitted without written consent of the publisher

INTRODUCTION

Sea ice provides a low-temperature habitat for diverse communities of microorganisms including viruses, bacteria and heterotrophic (e.g. flagellates and ciliates) and autotrophic protists (e.g. diatoms) (Kaartokallio et al. 2006). During sea ice formation, microorganisms, inorganic solutes and solids can be incorporated into the ice and accumulate to concentrations higher than that in the underlying seawater (Reimnitz et al. 1992, Grossmann & Gleitz 1993, Gradinger & Ikävalko 1998). Organisms incorporated into sea ice are challenged with

changes in space, light availability, salinity, nutrients, dissolved inorganic carbon (DIC) and O_2 concentration, temperature and pH (Gradinger & Ikävalko 1998). Especially, light availability within the sea ice has a major influence on the sea ice algal biomass and production (Cota & Horne 1989, Rysgaard et al. 2001).

Sea ice algae constitute an important component of sympagic communities and have been extensively studied in Arctic sea ice (e.g. Horner & Schrader 1982, Gosselin et al. 1997, Glud et al. 2007, Mikkelsen et al. 2008). The sea ice algae represent an important food source for metazoan grazers, and photosynthetic prod-

*Email: doso@natur.gl

ucts or entrained organic material can lead to elevated bacteria abundance and production within the sea ice (Smith et al. 1989, Krembs et al. 2002, Meiners et al. 2003, Riedel et al. 2007).

Several previous studies have shown that heterotrophic bacteria are active and abundant in Arctic sea ice (Bunch & Harland 1990, Smith & Clement 1990, Brinkmeyer et al. 2003, Lizotte 2003, Kaartokallio 2004), but studies on spatial and seasonal variations are few (Smith et al. 1989, Gradinger and Zhang 1997).

Sea ice represents a partially interconnected network of brine-filled channels comprising 1 to 30% of the sea ice volume (e.g. Weeks & Ackley 1986). The degree of interconnection of the brine enclosures is generally enhanced with increasing temperature, and the potential accumulation of sea ice algae therefore increases towards the polar spring. The significance of heterotrophic processes typically increases during late bloom and postbloom situations close to spring thaw (Vézina et al. 1997, Kaartokallio 2004). In addition to biologically mediated dynamics, thaw and freezing processes induce extensive dynamics in solute and gas distribution (Glud et al. 2002). Consequently, the sea ice matrix is highly heterogeneous and dynamic, and quantification of *in situ* algae and bacterial productivity represent a true challenge.

The overall objective of this investigation was to describe the dynamics of autotrophic and heterotrophic activity in first-year sea ice. We measured autotrophic and heterotrophic activity of intact sea ice cores under *in situ* conditions in bag incubations, and measurements were compared with primary production and bacterial carbon demand as measured in the laboratory by standard $\text{H}^{14}\text{CO}_3^-$ and $[^3\text{H}]$ thymidine incubations under well-defined conditions.

MATERIALS AND METHODS

Measurements were conducted on first-year land-fast sea ice in Malene Bight in the vicinity of Nuuk, SW Greenland (64° 82' N, 51° 42' W). Sampling was performed at 1 to 2 wk intervals from 1 February to 14 April 2008. During that period, sea ice thickness varied between 0 and 62 cm, while snow cover ranged between 0 and 28 cm. The net aerobic activity of an enclosed sea ice community was followed *in situ* by determining the O_2 concentrations in sea ice cores sealed in plastic bags and placed under natural snow cover, hereafter referred to as 'bag incubations'. These measurements were supplemented with standard measurements of temperature, salinity, irradiance attenuation in snow and ice, nutrient concentrations (phosphate, PO_4^{3-} ; nitrate and nitrite, $\text{NO}_3^- + \text{NO}_2^-$; silicic acid, $\text{Si}(\text{OH})_4$; and ammonium, NH_4^+), chlorophyll *a* (chl *a*)

concentrations, sea ice algal productivity and bacterial carbon demand during each sampling campaign, the latter being referred to as 'standard incubations'.

On 15 February and 19 March, 10 sea ice cores were collected using a MARK II coring system (Kovacs Enterprises). Cores were cut into 2 sections of equal length (ca. 22 cm), i.e. top half and bottom half, which were brought back to the laboratory in black plastic bags within 1 h of sampling. In a laboratory cold room ($3 \pm 1^\circ\text{C}$), core sections were placed in laminated transparent NEN/PE plastic bags (Hansen et al. 2000) fitted with a gas-tight Tygon tube and a valve for sampling.

Artificial seawater (salinity of 33) with a known O_2 concentration was added (10 to 30 ml) to the NEN/PE bags (Hansen et al. 2000). The bags were closed, and excess air quickly extracted through the valve. The top and bottom halves of a single ice core (i.e. the contents of one pair of bags) were melted within 48 h in darkness ($3 \pm 1^\circ\text{C}$). Gas bubbles released from the melting sea ice were subsequently transferred to 12 ml Exetainer tubes (Labco) containing 20 μl HgCl_2 (5% w/v, saturated solution). The gas bubbles were analysed for gaseous O_2 by gas chromatography in a flame ionization detector and thermal conductivity detector (FID/TCD, SRI model 8610C). The melted water was also transferred to Exetainer tubes for O_2 measurements. Dissolved O_2 in the melted sea ice was measured by Winkler titration (Grasshoff et al. 1983). The remaining 9 sea ice cores in plastic bags were transferred to the drilled holes at the sea ice sampling site within 2 h, and the *in situ* snow cover above the cores was re-established. The sea ice cores, i.e. top and bottom halves, were sampled at 1 to 2 wk intervals to determine the O_2 bulk concentration of the sea ice.

Permeability of the NEN/PE bags was quantified by adding artificial seawater (salinity of 33) to 9 plastic bags containing a gas-tight valve for sampling (Hansen et al. 2000). The bags were spiked with HgCl_2 (200 μl of a 5% solution per liter seawater) to prevent biological activity during the incubation. The water was then flushed with N_2 gas until the O_2 concentration in the bags reached 50% of atmospheric saturation. The valves in the bags were then closed ensuring that no gas phase was left inside the 1 l bag. Three bags were incubated at -20°C , 3 bags at 3°C and 3 bags at 20°C for 7 d. Initially the O_2 concentration was measured in all bags. After the incubation, O_2 samples were collected and measured as described previously. Ice formation in the bags (-20°C experiment) led to bubble formation and the O_2 concentration was therefore calculated as the sum of O_2 in gas and water. The maximum O_2 flux across the plastic bags was calculated from the O_2 concentration change between initial and final readings to $0.48 \pm 0.20 \mu\text{mol O}_2 \text{ l}^{-1} \text{ d}^{-1}$ (mean \pm SD). This put a lower limit on the activity that can be

resolved by this procedure and may compromise overall net activity at low biomass. In reality the permeability at the incubation temperature (−5 to 0°C) was significantly less than our maximum value.

O₂ bulk concentration in the sea ice (C_i) was calculated as:

$$C_i = \frac{C_m W_m + C_a W_a}{W_i} \quad (1)$$

where C_m is the O₂ concentration in the melted sea ice (gas bubble + melted sea ice), W_m is the weight of the melted sea ice, C_a is the O₂ concentration in the artificial sea water, W_a is the weight of the artificial sea water, and W_i is the weight of the sea ice (Rysgaard & Glud 2004).

The season was divided into Series 1 and Series 2. Series 1 consisted of 10 cores, which were incubated on 15 February and were individually collected for analysis from 15 February to 25 March. Series 2 consisted of another 10 cores incubated on 19 March and were individually collected for analysis from 19 March to 11 April. Linear regression was performed on each of the 4 series (i.e. top half and bottom half of cores in Series 1 and Series 2). The slope of the regression line was tested in all 4 series by means of Student's *t*-test.

On each of the 7 sampling occasions, triplicate ice cores were collected using a MARK II coring system. The 3 sea ice cores were cut into sections using a stainless steel handsaw, and vertical temperature profiles were measured in drilled holes to the centre of each section using a thermometer (Testo thermometer). Downwelling irradiance was measured directly above and below the snow with a data logger (LI-1400, Li-Cor Biosciences). In addition, air temperature was measured 2 m above the snow, and snow and sea ice thicknesses were determined using a measuring stick. The sea ice sections were placed in plastic containers in a dark insulated transport box (Thermobox) and brought back to the laboratory. Light attenuation of the sea ice samples was measured with a LI-1400 data logger in a dark thermally regulated room using a fibre lamp with a spectrum close to natural sunlight (15 V, 150 W, fibre-optic tungsten-halogen bulb). The LI-1400 data logger was placed under the sea ice section and the fibre lamp was placed above. Light attenuation was measured this way for each sea ice section. All sea ice samples were melted within 48 h for analysis of nutrients, salinity, chl *a*, primary production and bacterial carbon demand analysis at 3 ± 1°C in darkness.

The melted sea ice was filtered onto 25 mm GF/F filters (Whatman) for chl *a* analysis. The filters were extracted for 18 h in 96% ethanol (Jespersen & Christoffersen 1987) and analysed fluorometrically (Turner TD-700 fluorometer, Turner Designs) before and after addition of 200 µl of a 1 M HCl solution. The fluorometer was calibrated against a pure chl *a* standard

(Turner Designs). The remaining filtered sea ice was frozen (−18°C) for later analysis of PO₄^{3−}, NO₃[−] + NO₂[−], Si(OH)₄ and NH₄⁺. Concentrations of NO₃[−] + NO₂[−] were measured by vanadium chloride reduction (Braman & Hendrix 1989). Concentrations of Si(OH)₄ and PO₄^{3−} were determined by spectrophotometric analysis (Strickland & Parsons 1972, Grasshoff et al. 1983). Concentrations of NH₄⁺ were determined by a fluorometric method (Holmes et al. 1999). The lower detection limit for the nutrient measurements were 0.002 µmol l^{−1} for PO₄^{3−}, 0.5 µmol l^{−1} for NO₃[−] + NO₂[−], 0.002 µmol l^{−1} for Si(OH)₄ and 0.10 µmol l^{−1} for NH₄⁺ (lower detection limit is calculated using the *t*-value of 2.99 corresponding to a 99% confidence interval with *df* = 7). Conductivity of the melted sea ice sections was measured using a conductivity cell (Thermo Orion 3-star with an Orion 013610MD conductivity cell) and converted to bulk salinity (Grasshoff et al. 1983). Sea ice brine salinity was calculated as a function of temperature (Cox & Weeks 1983) and the brine volume as a function of bulk salinity, density and temperature. Brine volume was calculated according to Leppäranta & Manninen (1988) for temperatures greater than −2°C and according to Cox & Weeks (1983) for temperatures less than −2°C.

Primary production was determined in melted (melted within 48 h in dark conditions at 3 ± 1°C) sea ice water at 3 light intensities (42, 21 and 9 µmol photons m^{−2} s^{−1}) and corrected with one dark incubation using the H¹⁴CO₃[−] incubation technique (Steeman-Nielsen 1952). The sea ice samples were melted and subsequently acclimatised at 20 µmol photons m^{−2} s^{−1} for a few hours (> 2 h). Then the sea ice samples were poured into 120 ml gastight glass bottles and 4 µCi of H¹⁴CO₃[−] were added to each bottle. The bottles were incubated on a plankton wheel at 1 rpm for 5 h at 3 ± 1°C at the different light intensities. Illumination was provided by cool white fluorescent lamps with a spectrum close to natural sunlight (Master TL-D 36W/840, Phillips) and irradiance was measured using a LI-1400 data logger. Incubations were terminated by adding 200 µl of 5% ZnCl₂ and subsequently filtered onto 25 mm GF/F filters (Whatman). The filters were placed in scintillation vials containing 200 µl 1 M HCl to remove labelled, unfixed inorganic carbon, and then extracted in scintillation liquid (PerkinElmer Ultima Gold) for 22 h and counted using a liquid scintillation analyser (Tricarb 2800 TR, PerkinElmer). Dissolved inorganic carbon (DIC) concentrations in melted sea ice were measured on a CO₂ coulometer as described by Rysgaard & Glud (2004). After liquid scintillation counting, counts were converted to potential primary production (under photoinhibition) (PP_i, µg C l^{−1} h^{−1}) as:

$$PP_i = \frac{DPM_{activity} \cdot DIC_{sea\ ice} \cdot F_{discr} \cdot M_c}{DPM_{added} \cdot t_{inc}} \quad (2)$$

where $DPM_{activity}$ is the ^{14}C assimilated carbon corrected for assimilated carbon in the dark (disintegrations per minute [dpm] on filter), $DIC_{sea\ ice}$ is dissolved inorganic carbon in melted sea ice ($\sim 450 \mu\text{mol l}^{-1}$), $F_{discr} = 1.05$ is the discrimination factor of algae assimilation of $^{12}CO_2$ and $^{14}CO_2$, M_c is the molar mass of carbon (12.01 g mol^{-1}), DPM_{added} is the specific activity of the ^{14}C labelled medium (dpm ml^{-1}) in which cells were labelled, and t_{inc} is the incubation time (5 h).

The potential primary production (under no photoinhibition) (PP, $\mu\text{g C l}^{-1} \text{ h}^{-1}$) measured in the laboratory at different sea ice depths was plotted against the 3 laboratory light intensities, 42, 21 and $9 \mu\text{mol photons m}^{-2} \text{ s}^{-1}$, and fitted to the following function described by Platt et al. (1980):

$$PP = \frac{P_m}{1 + \exp\left(-\frac{E_{PAR}}{P_m}\right)} \quad (3)$$

where P_m ($\mu\text{g C l}^{-1} \text{ h}^{-1}$) is the maximum photosynthetic rate at light saturation, $\frac{P_m}{1 + \exp\left(-\frac{E_{PAR}}{P_m}\right)}$ ($\mu\text{g C m}^{-2} \text{ s} \mu\text{mol photons}^{-1} \text{ l}^{-1} \text{ h}^{-1}$) is the initial slope of the light curve and E_{PAR} ($\mu\text{mol photons m}^{-2} \text{ s}^{-1}$) is the laboratory irradiance. The photo-adaptation index, E_k ($\mu\text{mol photons m}^{-2} \text{ s}^{-1}$) was calculated as $P_m / \frac{P_m}{1 + \exp\left(-\frac{E_{PAR}}{P_m}\right)}$.

In situ downwelling irradiance was measured at ground level with a pyrometer (Kipp & Zonen, model CM21, spectrum range of 305 to 2800 nm) once every 5 min, and hourly averages were provided by Asiaq (Greenland Survey). Hourly downwelling irradiance was converted into hourly photosynthetically active radiation (PAR) (light spectrum, 300 to 700 nm) after intercalibration ($r^2 = 0.99$, $p < 0.001$, $n = 133$) with a LI-1400 data logger (Li-Cor). The *in situ* hourly PAR irradiance was calculated at different depths, depending on sea ice and snow thickness, using the attenuation coefficients measured during the sea ice season.

In situ primary production was calculated for each hour at different sea ice depths using hourly *in situ* PAR irradiance (see Eq. 3). Total daily (24 h) *in situ* primary production was calculated as the sum of hourly *in situ* primary production for each depth. The depth-integrated net primary production was calculated using trapezoid integration.

Bacteria production in melted sea ice samples was determined by measuring the incorporation of [^3H]thymidine into DNA. Triplicate subsamples (volume, $V_{\text{filt}} = 0.01 \text{ l}$) were incubated in darkness at $3 \pm 1^\circ\text{C}$ with 10 nM of labelled [^3H]thymidine (New England Nuclear, specific activity, $10.1 \text{ Ci mmol}^{-1}$). Trichloroacetic acid (TCA)-killed controls were made to measure the abiotic adsorption. At the end of the incubation period ($t_{inc} = 6 \text{ h}$), 1 ml of 50% cold TCA was added to all the subsamples (Fuhrman & Azam 1982). Subsamples of [^3H]thymidine were stored at $3 \pm 1^\circ\text{C}$ in scintillation vials until filtration. Subsamples were fil-

tered through 25 mm mixed cellulose ester filters (pore size $0.2 \mu\text{m}$, Advantec MSF) and the filters were placed in scintillation vials. Scintillation vials were rinsed with 5 ml of 5% cold TCA. Subsequently, filters were rinsed 7 times with 1 ml of cold 5% TCA and then extracted in scintillation liquid (Ultima Gold, Perkin-Elmer) for 22 h and counted using a liquid scintillation analyser (Tricarb 2800, Perkin-Elmer).

Bacteria production (BP, $\mu\text{g C l}^{-1} \text{ h}^{-1}$) was calculated as:

$$BP = \frac{DPM_{\text{sample}}}{SA} \frac{N_{\text{cells}}}{t_{inc}} \frac{N_c}{V_{\text{filt}}} \frac{M_c}{V_{\text{filt}}} \quad (4)$$

where DPM_{sample} is the average dpm for the live treatment subtracted from the average dpm for the TCA-killed controls, N_{cells} is the conversion factor ($2.09 \cdot 10^{18} \text{ cells mol}^{-1} \text{ } ^3\text{H}$), according to Smith & Clement

1990), t_{inc} is the incubation period ($t_{inc} = 6 \text{ h}$), V_{filt} is the

volume of the subsamples ($V_{\text{filt}} = 0.01 \text{ l}$), M_c is the molecular mass of carbon and SA is the specific activity of the thymidine solution ($2.24 \cdot 10^{16} \text{ dpm mol}^{-1}$).

$N_c = 5.7 \cdot 10^{-8} \mu\text{g C cell}^{-1}$ is calculated as:

$$N_c = \frac{\text{Cell}_{\text{size}} \cdot C_{\text{factor}}}{1000000} \quad (5)$$

where $\text{Cell}_{\text{size}}$ is the average bacteria cell size ($0.473 \mu\text{m}^3$) (Smith & Clement 1990), and C_{factor} is the factor used to convert cell volume to carbon ($0.12 \text{ pg C } \mu\text{m}^{-3}$) according to Smith & Clement (1990).

Bacterial carbon demand (BCD, $\mu\text{g C l}^{-1} \text{ h}^{-1}$) was calculated as:

$$BCD = \frac{BP}{BGE} \quad (6)$$

where BP is the bacteria production and BGE is the bacterial growth efficiency of 0.5 according to Rivkin & Legendre (2001). To extrapolate bacterial carbon demand to daily *in situ* carbon demand we assumed that the respiration was light-independent (multiply by 24). The depth-integrated bacterial carbon demand was calculated using trapezoid integration.

On 23 February, 10 sea ice cores were collected along a 10 m long section to investigate the spatial (horizontal and vertical) variability of the biotic conditions (chl *a*, primary production and bacterial carbon demand) and the abiotic conditions (sea ice temperature, bulk salinity and brine volume) in the sea ice. The 10 sea ice cores were collected close to the plastic bag incubations at 1 m intervals. The cores were cut into 2 sections, i.e. top and bottom halves, and brought back to the laboratory in a dark Thermobox for further analysis as described.

To extend the evaluation of spatial variability, a large-scale investigation of horizontal variability was conducted on 29 February. Fifty-two sea ice cores were collected along a 367 m long transect to investigate the

heterogeneity of chl *a*, sea ice temperature, brine salinity and brine volume in the bottom of the sea ice. The snow and sea ice thickness was measured as described previously. Four sea ice cores were sampled at 20 cm intervals at position 1 m. The first core was cut vertically into 2 pieces at every sampling position. Sea ice cores were collected at distances of 1, 3, 5, 7, 9, 20, 31, 42, 53, 64, 165, 266 and ca. 367 m. All the ice cores were brought back to the laboratory in a dark Thermo box for determination of brine salinity, volume and chl *a* concentration as described.

Spatial autocorrelation (Legendre & Legendre 1998) was used to analyse the horizontal distribution of chl *a*, sea ice temperature, bulk salinity, snow thickness and sea ice thickness. We assume that the variability along one line is the same as along a perpendicular line. The autocorrelation was estimated by Moran's *I* coefficients (Moran 1950, Legendre & Legendre 1998). This coefficient was calculated for each of the following intervals along the transect (distance classes): 0 to

0.50 m, 0.50 to 1.5 m, 1.5 to 2.5 m, 2.5 to 5.5 m, 5.5 to 10.5 m, 10.5 to 20.5 m, 20.5 to 50.5 m, 50.5 to 100.5 m and >100.5 m. The autocorrelation coefficients estimated by Moran's *I* coefficient were tested for significance according to the method described in Legendre & Legendre (1998). A 2-tailed test of significance was used. The null hypothesis of random spatial distribution was rejected at the specified level of significance when an individual autocorrelation coefficient exceeded a critical value (positive or negative). A significance level of $p < 0.05$ was used.

RESULTS

Abiotic parameters

Temperatures within the snow cover varied from -13 to 0°C and the sea ice temperature from -5 to 0°C (Fig. 1a). Minimum temperatures of the sea ice were

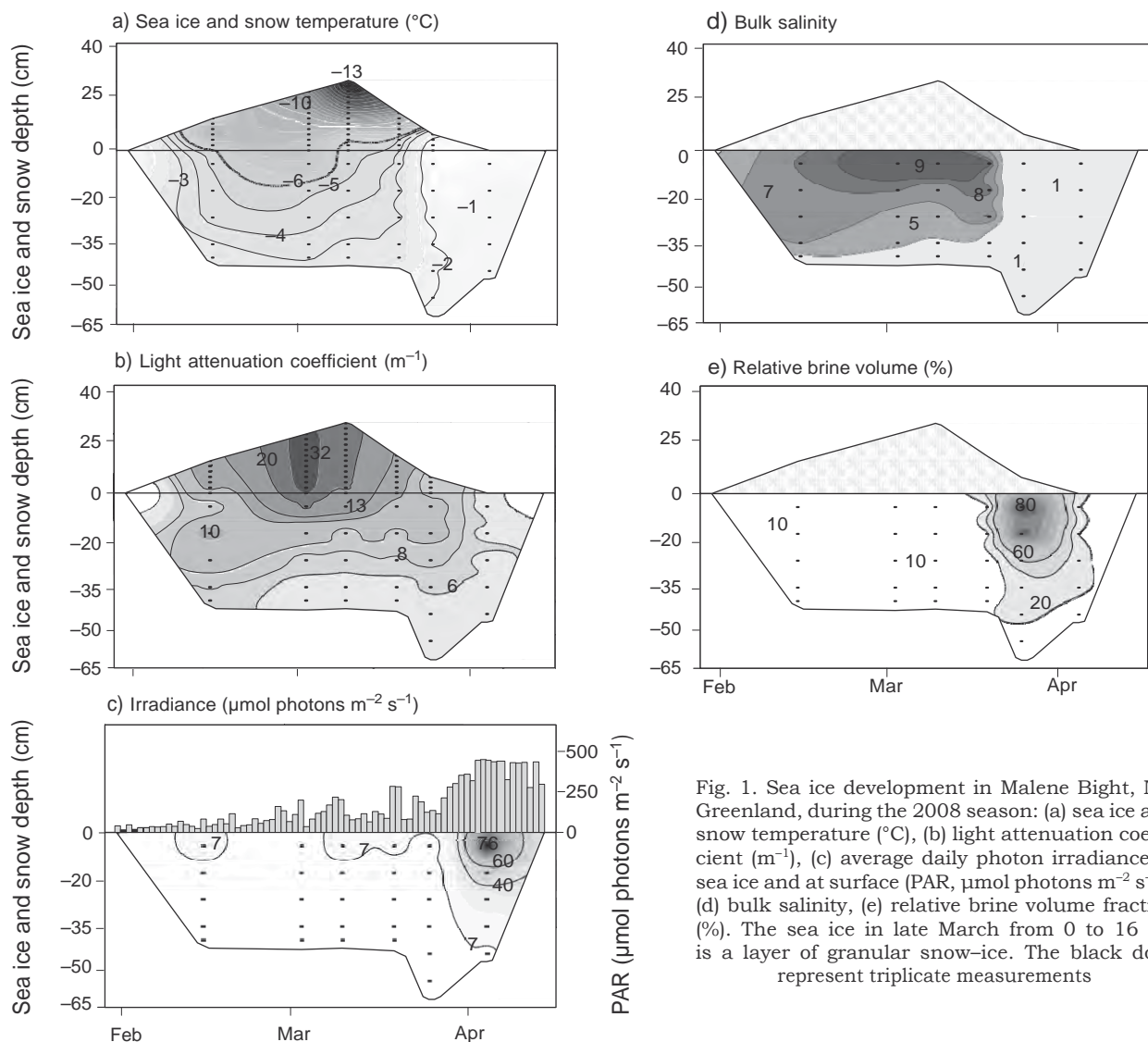


Fig. 1. Sea ice development in Malene Bight, NW Greenland, during the 2008 season: (a) sea ice and snow temperature ($^{\circ}\text{C}$), (b) light attenuation coefficient (m^{-1}), (c) average daily photon irradiance in sea ice and at surface (PAR, $\mu\text{mol photons m}^{-2} \text{s}^{-1}$), (d) bulk salinity, (e) relative brine volume fraction (%). The sea ice in late March from 0 to 16 cm is a layer of granular snow-ice. The black dots represent triplicate measurements

observed in February, after which the temperature gradually increased to maximum values just before sea ice break-up in mid-April. The high light reflectance and scatter from the snow cover caused strong light attenuation throughout the sea ice season, with average attenuation coefficients of $K_{\text{snow}} = 23 \text{ m}^{-1}$ and $K_{\text{ice}} = 8 \text{ m}^{-1}$ (Fig. 1b). Early in the sea ice season, irradiance at the bottom of the sea ice was low (0.03 to $0.15 \mu\text{mol photons m}^{-2} \text{ s}^{-1}$) (Fig. 1c). Light availability increased along with increasing day length and declining snow cover, reaching a maximum downwelling irradiance of $76 \mu\text{mol photons m}^{-2} \text{ s}^{-1}$ in the uppermost sea ice section and $7 \mu\text{mol photons m}^{-2} \text{ s}^{-1}$ in the bottom on April 4.

The bulk salinity decreased over time with a maximum salinity of 9 in early March and a minimum salinity of 1 from late March and onward (Fig. 1d). Bulk salinity varied vertically within sea ice cores during winter, with lower values encountered in the bottom sea ice from mid-February until late March. From 25 March to 4 April, bulk salinity was lowest in the uppermost part of the sea ice. The relative brine volume increased throughout the sea ice season, with a maximum in late March in the uppermost section of

the sea ice (Fig. 1e). In late March melting from the top of the sea ice was initiated, which resulted in high relative brine volumes and low bulk salinities in the uppermost part of the sea ice. During this period air temperatures varied between 0 and 7°C .

Nutrient parameters

Bulk PO_4^{3-} concentration was initially 0.05 to $0.20 \mu\text{mol l}^{-1}$ (Fig. 2a), and increased to a maximum of $0.70 \mu\text{mol l}^{-1}$ in March but subsequently decreased to $0.05 \mu\text{mol l}^{-1}$ in April. Bulk Si(OH)_4 concentration remained constant between 1.8 and $2.3 \mu\text{mol l}^{-1}$ in the sea ice from February to late March with lowest values encountered at the bottom of the sea ice. In late March, Si(OH)_4 concentration decreased rapidly to below $1.4 \mu\text{mol l}^{-1}$ (Fig. 2b). The initial bulk concentration of $\text{NO}_3^- + \text{NO}_2^-$ was $3.2 \mu\text{mol l}^{-1}$ at the top and $2.0 \mu\text{mol l}^{-1}$ at the bottom of the sea ice (Fig. 2c) and decreased throughout the season, reaching a minimum of $1.5 \mu\text{mol l}^{-1}$ in April. The initial bulk concentration of NH_4^+ was $4.0 \mu\text{mol l}^{-1}$ at the top and bottom of the sea ice. During the sea ice season the NH_4^+ concentration

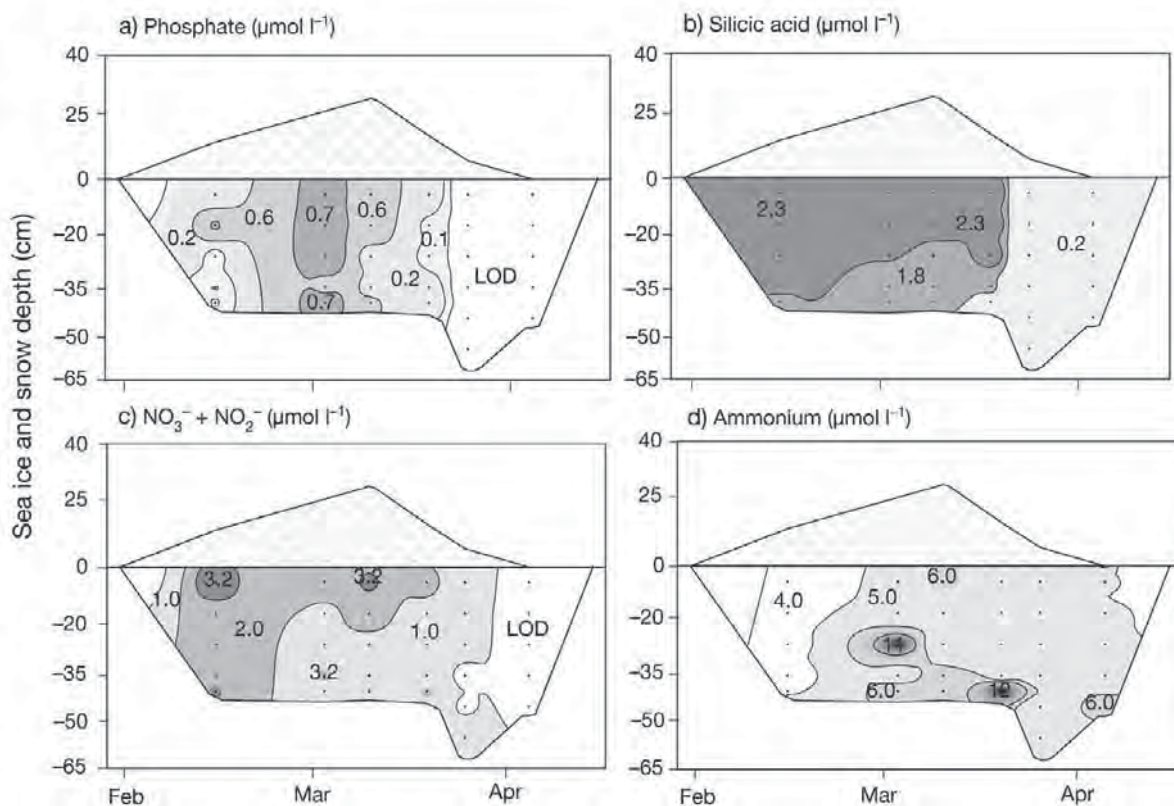


Fig. 2. Nutrient concentration ($\mu\text{mol l}^{-1}$) in bulk sea ice: (a) phosphate, (b) silicic acid, (c) $\text{NO}_3^- + \text{NO}_2^-$, (d) ammonium. LOD is lower limit of detection, which is calculated using the t -value of 2.99 corresponding to a 99% confidence interval with $df = 7$. The black dots represent triplicate measurements

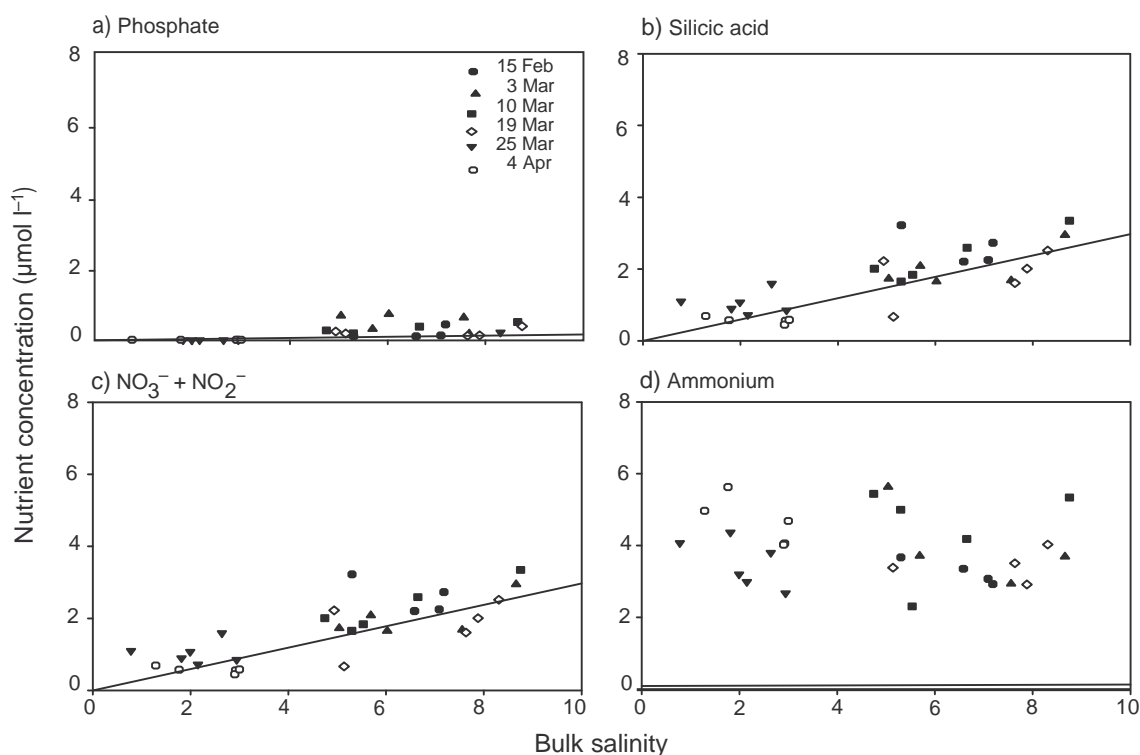


Fig. 3. Concentrations of (a) phosphate, (b) silicic acid, (c) $\text{NO}_3^- + \text{NO}_2^-$ and (d) ammonium versus bulk salinity in sea ice. The solid line indicates the expected dilution line predicted from salinity and nutrient concentrations in seawater (0 to 10 m depth, salinity of 33). See 'Results: Nutrient parameters' for explanation

increased, reaching values of 6 to 12 $\mu\text{mol l}^{-1}$ at the bottom of the sea ice and 5.0 to 6.0 $\mu\text{mol l}^{-1}$ at the top of the sea ice (Fig. 2d).

Bulk nutrient concentrations for each sampling date were plotted as a function of bulk salinity and compared with the expected dilution line (according to Clarke & Ackley 1984). If values were below the line, depletion of nutrients occurred in the sea ice. If values were above the dilution line, production or net deposition of the solute took place. Plots of salinity- PO_4 , salinity-Si(OH) $_4$, salinity- $\text{NO}_3^- + \text{NO}_2^-$ and salinity- NH_4 in sea ice were generally all above the dilution line (Fig. 3), but most explicitly for NH_4 , which clearly accumulated within the sea ice (Fig. 3d).

Biotic parameters

Sea ice profiles of the algal biomass, expressed as chl a , showed that the highest bulk concentration in the lower 15 cm of the sea ice cores was 2.80 $\mu\text{g l}^{-1}$ on 25 March (Fig. 4a). Subsequently, the algal biomass in the lower 15 cm of the sea ice cores decreased rapidly reaching a value of 1.50 $\mu\text{g l}^{-1}$ in April.

Sea ice primary production integrated for the sea ice profile increased throughout winter from 0.09 $\text{mg C m}^{-2} \text{d}^{-1}$ (15 February) to 12.60 $\text{mg C m}^{-2} \text{d}^{-1}$ (4 April) (Fig. 4b). The highest volume-specific primary produc-

tion (bulk) of 40 $\mu\text{g C l}^{-1} \text{d}^{-1}$ was encountered in the middle part of the sea ice profile in April.

The highest sea ice bacterial carbon demand of 27 $\mu\text{g C l}^{-1} \text{d}^{-1}$ was encountered in the central ice at the onset of the melting period (Fig. 4c). However, a single peak of 9.00 $\mu\text{g C l}^{-1} \text{d}^{-1}$ was observed on 10 March in the upper 10 cm section of the sea ice.

Depth integration of the activity reflected low autotrophic and heterotrophic productivity during winter, followed by a slightly net heterotrophic period in late February and March. Finally, a net autotrophic period was observed from late March until the end of the study period (Fig. 5). Integrated over the entire measuring season (i.e. from 15 February to 14 April) the sea ice of Malene Bight was net autotrophic. An annual net carbon fixation of 220 mg C m^{-2} was calculated by subtracting the net result of a sea ice-related gross primary production of 350 mg C m^{-2} from the bacterial carbon demand of 130 mg C m^{-2} .

Bag incubations

Oxygen levels during February and March indicated a low net oxygen accumulation in the top sea ice cores of $0.50 \pm 3.00 \mu\text{mol O}_2 \text{l}^{-1} \text{d}^{-1}$ (mean \pm SD) and in the bottom sea ice cores of $1.30 \pm 5.00 \mu\text{mol O}_2 \text{l}^{-1} \text{d}^{-1}$. However, none of these values were significantly different from

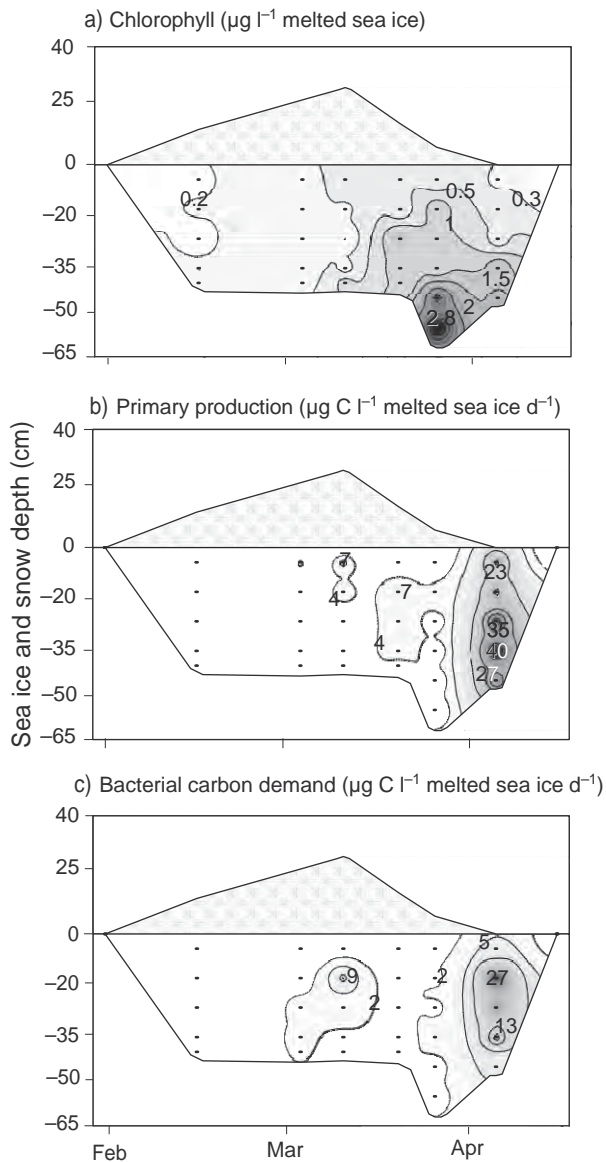


Fig. 4. (a) Chl *a* concentrations ($\mu\text{g chl } a \text{ l}^{-1}$) in bulk sea ice. (b) Primary production ($\mu\text{g C l}^{-1}$ melted sea ice d^{-1}). (c) Bacterial carbon demand ($\mu\text{g C l}^{-1}$ melted sea ice d^{-1}) calculated according to Rivkin & Legendre (2001). The black dots represent triplicate measurements

zero ($p > 0.05$) (Fig. 6). Autotrophic activity exceeded heterotrophic activity in late March and April, resulting in a significantly high net oxygen accumulation in the bottom sea ice cores of $6.30 \pm 2.30 \mu\text{mol O}_2 \text{ l}^{-1} \text{ d}^{-1}$ ($p < 0.01$) whereas no significant oxygen accumulation ($0.80 \pm 3.50 \mu\text{mol O}_2 \text{ l}^{-1} \text{ d}^{-1}$) was observed in the top sea ice cores.

Assuming a photosynthetic quotient of 1.00 CO_2 evolved per O_2 consumed, a net annual carbon fixation of $1700 \pm 760 \text{ g C m}^{-2}$ was calculated for the bag incubations.

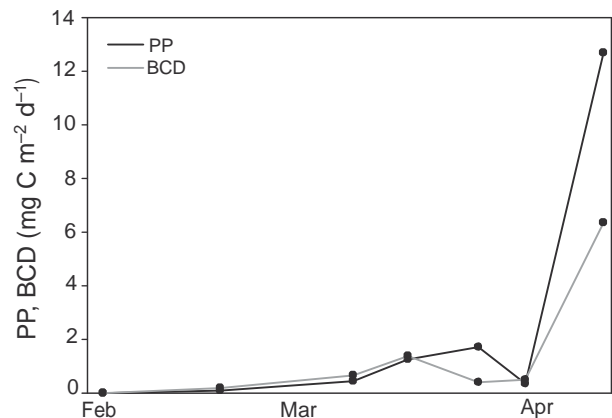


Fig. 5. Primary production (PP, $\text{mg C m}^{-2} \text{ d}^{-1}$) and bacterial carbon demand (BCD, $\text{mg C m}^{-2} \text{ d}^{-1}$) in bulk sea ice

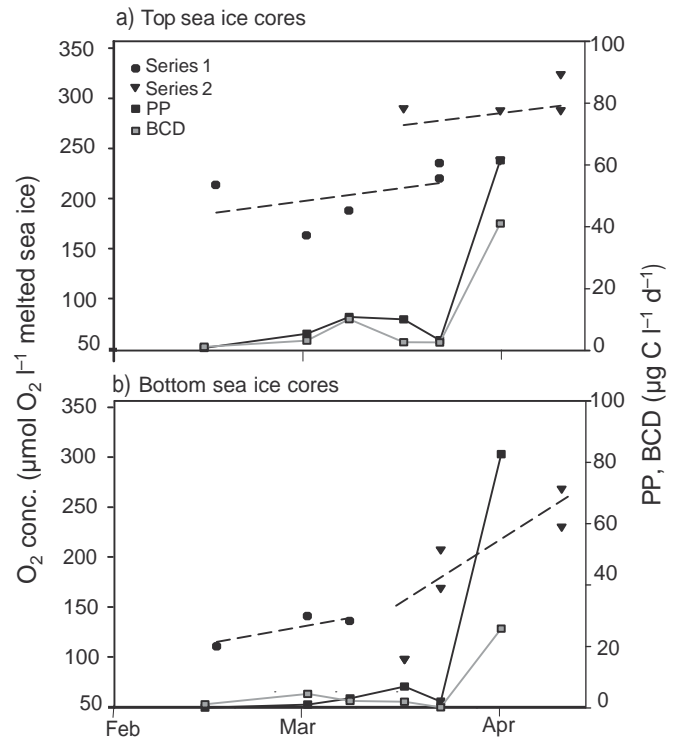


Fig. 6. Measurements of O_2 concentration (d,z: $\mu\text{mol O}_2 \text{ l}^{-1}$ melted sea ice), primary production (PP) (j: $\mu\text{g C l}^{-1}$ melted sea ice d^{-1}) and bacterial carbon demand (BCD) (h: $\mu\text{g C l}^{-1}$ melted sea ice d^{-1}) in (a) top half and (b) bottom half of sea ice cores. Dashed lines represent regression lines

Heterogeneity

On 23 February the abiotic and biotic conditions, i.e. bulk salinity, brine volume, temperature, chl *a*, primary production and bacterial carbon demand, were measured in top and bottom sections of the sea ice cores ($n = 10$) along a 10 m transect (Table 1). There

Table 1. Abiotic and biotic parameters in sea ice of Malene Bight: bulk salinity, relative brine volume (%), temperature (°C), chl *a* ($\mu\text{g l}^{-1}$), primary production ($\mu\text{g C l}^{-1}$ melted sea ice d^{-1}) and bacterial carbon demand ($\mu\text{g C l}^{-1}$ melted sea ice d^{-1})

	Bulk salinity	Relative brine volume (%)	Temperature (°C)	Chl <i>a</i> ($\mu\text{g l}^{-1}$)	Primary production ($\mu\text{g C l}^{-1}$ melted sea ice d^{-1})	Bacterial carbon demand ($\mu\text{g C l}^{-1}$ melted sea ice d^{-1})
Top sea ice	2.06 ± 0.13	2.38 ± 0.20	-4.65 ± 0.35	0.15 ± 0.09	0.24 ± 0.012	0.37 ± 0.06
Bottom sea ice	1.83 ± 0.18	3.09 ± 0.39	-3.15 ± 0.39	0.34 ± 0.25	0.36 ± 0.012	0.18 ± 0.06

was a significant effect of depth on chl *a* levels (2-way ANOVA: $F_{1,19} = 7.452$, $p = 0.023$) with the bottom section having a higher phototrophic biomass than the top section of the ice cores. The primary production rates were also highest in the bottom sections and lowest in the top sections (2-way ANOVA: $F_{9,19} = 119.180$, $p < 0.0005$), while the bacterial carbon demand was higher in the top sections than in the bottom sections (2-way ANOVA: $F_{1,19} = 6.521$, $p < 0.031$) (Table 1).

Along a 10 m transect there was no significant horizontal variation across all biotic and abiotic conditions (2-way ANOVA: $F_{9,19} = 0.142$, $p = 0.142$). However, for all the parameters there was a significant vertical variability (2-way ANOVA: $F_{5,49-50} = 15.215$, $p < 0.0005$).

Performing a similar statistical analysis on the temporal variations showed that, for all conditions, there was a significant temporal variability (2-way ANOVA: $F_{6,49-50} = 37.157$, $p < 0.0005$). Thus, for all conditions the horizontal variability in February was remarkably smaller than the seasonal variability.

Algal biomass (i.e. as chl *a*), bulk salinity and temperature in the lower section (5 cm) of the sea ice, and snow and sea ice thickness were measured along a 367 m transect to assess the horizontal distribution of these parameters. Moran's *I* was used to estimate the spatial autocorrelation within the data set (Moran 1950, Legendre & Legendre 1998, Rysgaard et al.

2001). Positive or negative values indicated positive or negative autocorrelation, respectively. The change from positive to negative values of Moran's *I* for chl *a* occurred from the 20.5 m distance class to the 50.5 m distance class (Fig. 7). This indicates that the average sea ice algae biomass patch radius was between 20.5 and 50.5 m. The change from positive to negative values of Moran's *I* for sea ice temperatures and bulk salinity also occurred from the 20.5 m class of distance to the 50.5 m class of distance. In contrast, the average sea ice thickness, snow thickness and relative brine volume patch radius was >100.5 m, i.e. where the first change from positive to negative values of Moran's *I* occurred.

DISCUSSION

Sea ice algae are known to be adapted to low ambient light levels and able to grow at light intensities as low as 7 to 20 $\mu\text{mol photons m}^{-2} \text{s}^{-1}$ (Gosselin et al. 1990, Gradinger & Ikävalko 1998). Before April, snow cover inhibited any significant sea ice primary production ($<1.5 \text{ mg C m}^{-2} \text{d}^{-1}$) due to high attenuation coefficients and low light availability ($<7 \mu\text{mol photons m}^{-2} \text{s}^{-1}$). As snow cover diminished, light availability increased to above 7 $\mu\text{mol photons m}^{-2} \text{s}^{-1}$ and sea ice algae began to flourish; thus, the community became net autotrophic as light availability increased late in the season.

The annual succession of the sea ice organisms in Malene Bight followed a distinctive pattern, with a winter stage in February and March characterised by low and almost balanced heterotrophic and autotrophic activities. During February and March, the oxygen level in the bag incubations remained constant, validating the low, balanced heterotrophic and autotrophic activity (Fig. 6). As light availability increased in late March and April the now net autotrophic community led to a significant net oxygen accumulation of $6.30 \pm 2.30 \mu\text{mol O}_2 \text{d}^{-1}$ in the bottom sea ice cores whereas no significant oxygen accumulation ($0.80 \pm 3.50 \mu\text{mol O}_2 \text{l}^{-1} \text{d}^{-1}$) was observed in the top sea ice cores.

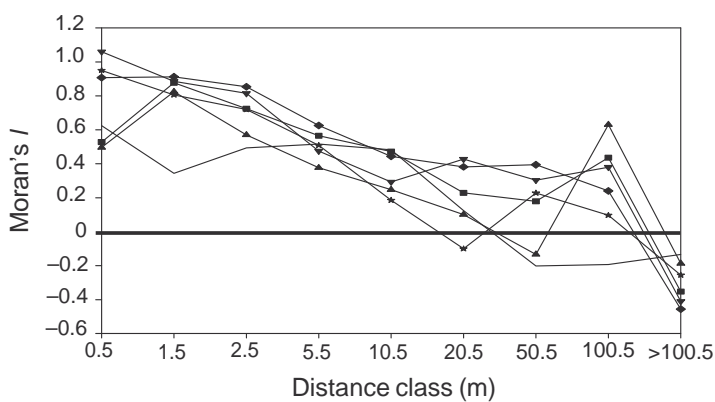


Fig. 7. Moran's *I* as a function of distance class (m) between sites. \star : temperature; M: bulk salinity; z: sea ice thickness; f: snow thickness; J: relative brine volume; —: chl *a*

To correctly assess primary production and heterotrophic activity it is essential to have insight into *in situ* light availability. In the present study, high snow reflectance caused strong light attenuation for most of the sea ice season. The snow attenuation coefficient varied (from 4 to 32 m^{-1}) throughout the sea ice season with the highest attenuation coefficient of 32 m^{-1} found in March (Fig. 1b). The snow attenuation coefficients in Malene Bight were within the range of <4 to 40 m^{-1} reported by Weller & Schwerdtfeger (1967) and Thomas (1963) for natural snow cover in the Arctic and Antarctic. Dry and fresh snow as observed in Malene Bight has a significantly higher light attenuation than did compressed or wet snow at subzero temperatures (Perovich 1996, Perovich et al. 1998, Glud et al. 2007), resulting in low *in situ* primary productivity as was observed in February and March.

The average attenuation coefficient of 8 m^{-1} in the sea ice of Malene Bight was also relatively high compared with the attenuation coefficient during the summer thaw as reported by Glud et al. (2007) and L uthje et al. (2006). The air humidity above the ice in Malene Bight was, on average, only 70% and in areas with low air humidity, air pockets could form due to brine drainage from surface layer, resulting in a high degree of scatter and increasing attenuation coefficients (Perovich 1996, Andreas & Ackley 1982, Trodahl & Buckley 1990). Overall our data on snow and sea ice attenuations are generally higher than values reported elsewhere, and as snow cover regulates light availability and therefore spatial patchiness of ice algae (Gosselin et al. 1986, Rysgaard et al. 2001), the phototrophic rates obtained during the present study were low. Sea ice algal biomass (chl *a*) patch size followed the snow and sea ice temperature patch size with an average radius of 20.5 to 50.5 m (Fig. 7). This suggests that snow cover and temperature (via brine volume) in sea ice were the main factors controlling sea ice algal patchiness. However, snow cover, temperature and light availability are crosscorrelated, and all exert a regulating effect on sea ice algal biomass in Malene Bight.

The maximum depth-integrated sea ice algal biomass of 0.07 to 0.5 $\text{mg chl } a \text{ m}^{-2}$ (Fig. 4b) was >2 orders of magnitude lower compared with the values of 50 to 150 $\text{mg chl } a \text{ m}^{-2}$ that were reported by Arrigo (2003) to be common in Arctic sea ice. Likewise, primary production measurements were low during February and March but gradually increased during the season, reaching a peak activity of only 12.6 $\text{mg C m}^{-2} \text{ d}^{-1}$ in early April, which is low compared with other studies (Arrigo 2003 and references therein). Integrated over the entire measuring period the annual sea ice algal carbon production was 350 mg C m^{-2} , which was 47% lower than measurements made in the neighbouring

Kobbefjord during 2006 (Mikkelsen et al. 2008). Furthermore, the sympagic primary production of 350 mg C m^{-2} corresponded to <1% of the annual pelagic primary production of the region (Juul-Pedersen et al. 2009).

The low biomass and primary production values of the sea ice in Malene Bight can be attributed to relatively low light availability and a relatively thick dense snow cover, which was also observed in NE Greenland by Glud et al. (2007). However, nutrient supply and different physical conditions, e.g. ice temperature, brine salinity and flushing of sea ice brine, and biological interactions also regulate the distribution and activity of sea ice organisms. The sea ice contained relatively high concentrations of NH_4^+ , while PO_4^{3-} , Si(OH)_4 and $\text{NO}_3^- + \text{NO}_2^-$ concentrations in the sea ice were low (0.70 to 0.05 $\mu\text{mol l}^{-1}$, 2.30 to 0.02 $\mu\text{mol l}^{-1}$ and 3.2 to 0.5 $\mu\text{mol l}^{-1}$, respectively (Figs. 2 & 3). The algal biomass was low at the bottom of the sea ice after mid-March, suggesting that the sea ice biomass was nutrient-limited late in the sea ice season. Nutrient concentration in sea ice is affected by biological activity as well as by exchange of nutrients between the sea ice, water and atmosphere. Previous studies have shown that during sea ice formation, dissolved constituents (including inorganic nutrients) are rejected from the ice matrix (Clarke & Ackley 1984, Giannelli et al. 2001). The nutrient–salt plots in Fig. 3 indicate that some import or accumulation of nutrients occurred during February and March. However, late in the sea ice season nutrients were generally depleted (Fig. 3), presumably due to microbial uptake (Fig. 4), which correlated with high primary productivity and a net autotrophic sea ice.

Plots of salinity– NH_4^+ suggested NH_4^+ enrichment, which occurred during the entire season, indicating an input from the atmosphere and/or heterotrophic activity by bacteria mineralising organic material encapsulated during sea ice formation. The standard laboratory-based incubations indicate a low net heterotrophic activity in February and March (Figs. 4 & 5). Calculated average bacterial carbon demand in this period was 1.60 $\mu\text{g C l}^{-1} \text{ d}^{-1}$. At a C:N ratio of 7:1, this is equivalent to a remineralisation rate of 0.02 $\mu\text{mol N l}^{-1} \text{ d}^{-1}$, which is lower than the values of Riedel et al. (2007) who reported NH_4^+ regeneration rates of 0.1 to 1.2 $\mu\text{mol N l}^{-1} \text{ d}^{-1}$ corresponding to only 20% of the winter–spring increase in NH_4^+ concentrations in the sea ice of Malene Bight. This suggests that NH_4^+ regeneration rates were not the main source of NH_4^+ accumulation in the sea ice. Thus, additional atmospheric input could potentially cause the high NH_4^+ concentrations in the sea ice of Malene Bight. In previous studies, high NH_4^+ values in sea ice have been measured in Arctic and Antarctic sea ice caused by

regeneration of nitrogen compounds within the sea ice (Thomas et al. 1995, Kaartokallio 2001, Riedel et al. 2007).

Bacteria production rates of 0.05 to $1.3 \text{ mg C m}^{-3} \text{ d}^{-1}$ in Malene Bight compare with rates of 0.004 to $6.0 \text{ mg C m}^{-3} \text{ d}^{-1}$ reported by Kottmeier et al. (1987), 0.2 to $10 \text{ mg C m}^{-3} \text{ d}^{-1}$ by Grossmann & Dieckmann (1994) and 2.9 to $5.6 \text{ mg C m}^{-3} \text{ d}^{-1}$ by Mock et al. (1997).

The annual net bacterial carbon demand of 130 mg C m^{-2} was 37% of the co-occurring primary production of 350 mg C m^{-2} . This observation is similar to findings reported in the world's oceans (Ducklow 1983) and in benthic systems (Fenchel & Glud 2000). However, the ratio reported in the present study is significantly higher than the few percent reported from Antarctic (Kottmeier et al. 1987) and Arctic sea ice (Smith et al. 1989, Smith & Clement 1990). Our bag incubations from winter, however, support results from our traditional standard incubations that a close connection exists between phototrophic and heterotrophic communities and, considering that both algae and bacteria are situated close together in the sea ice brine matrix, a tight metabolic coupling would be expected. Positive correlation has also been demonstrated in some sea ice habitats (e.g. Gradinger & Zhang 1997, Meiners et al. 2003). However, limited data on the coupling between phototrophic and heterotrophic communities in sea ice exists and further investigations are required to elucidate the metabolic coupling in sea ice.

In the standard incubations, primary production of sea ice algae was determined by the ^{14}C method (Stee-man-Nielsen 1952). One problem with this technique is that melting or crushing of sea ice is required to homogeneously distribute ^{14}C in the media, which separates organisms from the surrounding sea ice and alters the complex sea ice microenvironment. The photosynthetic performance may be considerably affected when the sea ice environment (i.e. irradiance, substrate, salinity, temperatures and spectral composition) is altered. Secondly, melting of the sea ice may influence algal abundance and species diversity (Gradinger et al. 1999). In the present study the samples were melted slowly (48 h) in darkness at $3 \pm 1^\circ\text{C}$. In general decreasing or increasing salinity from that typical of seawater results in decreasing photosynthetic rates. Kirst & Wiencke (1995) showed that most sea ice algae are more tolerant to reduced rather than elevated salinities. Salinity-induced stress to sea ice algae is light dependent, such that incubated samples only suffered photosynthetic damage when irradiance was applied (Ralph et al. 2007). Furthermore, a potential problem when melting sea ice samples in darkness is inactivation of phototrophs, which might remain inactive during a subsequent ^{14}C incubation period in light. However, sea ice algae can adapt to increasing light

intensity within hours (Smith & Sakshaug 1990). In addition, Peters & Thomas (1996b) showed that some algae cells are able to sustain an active photosynthetic apparatus for months in darkness, which allows carbon assimilation immediately after reintroduction to light. Also, photosynthetic rates in sea ice algae can be influenced by temperature (Palmisano et al. 1987, Ralph et al. 2005). Optimum temperature for ice algal photosynthesis is between 2 and 15°C , with a rapid decline in photosynthetic rate at temperatures above 15°C and below -10°C (Bunt 1964, Palmisano et al. 1987, Kottmeier & Sullivan 1988, Ralph et al. 2005). In the present study the sea ice was slowly melted at $3 \pm 1^\circ\text{C}$; thus, the primary production was measured at higher temperatures than *in situ*. This suggests that the primary production might be overestimated in the winter period, where the difference between *in situ* temperature and laboratory temperature was greatest. However, it is a nontrivial task to incubate samples at low bulk salinity at 0°C or subzero temperature without introducing freezing and thawing artefacts. Overall, it is difficult to assess the extent to which our (and other) procedures for ^{14}C incubations result in under- or over-estimation of the *in situ* primary production.

While calculation of phototrophic activity is relatively straightforward, the assessment of the bacteria production and bacterial carbon demand is based on a number of debatable assumptions. The method assumes that all bacteria assimilate exogenous thymidine and that eukaryotes do not. Uptake of [^3H]thymidine by eukaryotic microalgae has been clearly demonstrated (Rivkin 1986). However, Fuhrman & Azam (1980) have shown that at low concentrations and relatively short incubation periods the uptake of [^3H]thymidine by eukaryotes should be negligible. The [^3H]thymidine method is a widely used index of bacteria production but requires a conversion factor to relate DNA production to production of bacterial cells. In the present study, we extrapolated incorporation data to bacteria production by applying the early season data of Smith & Clement (1990). They calculated the conversion factor for high Arctic sea ice bacteria as $2.09 \cdot 10^{18} \text{ cells mol}^{-1}$ in the early sea ice season and as $0.47 \cdot 10^{18} \text{ cells mol}^{-1}$ in the late sea ice season. The conversion factor from the early sea ice season fell within the commonly reported range of 1 to $4 \cdot 10^{18} \text{ cells mol}^{-1}$ (e.g. Fuhrman & Azam 1982, Riemann et al. 1987), and Smith & Clement (1990) suggested that this factor was more appropriate than the lower conversion factor from the late season. Other factors used for the conversion of thymidine incorporation into bacteria production include the average bacterial cell size ($\text{Cell}_{\text{size}}$) and the volume-specific carbon content (C_{factor}), which combined provide the cell-specific carbon content (N_c) and which are affected by environmental changes

(Coveney & Wetzel 1988). Integrated over the entire measuring season, the sea ice of Malene Bight was net autotrophic. However, when using different N_c factors discussed in the literature (Riemann et al. 1987, Smith & Clement 1990, Gradinger and Zhang 1997, Kaartokallio et al. 2005), the annual bacterial carbon demand ranged by a factor of 6 from 70 to 400 mg C m⁻² depending on which N_c value is used. In the present study, we used an N_c value measured in the high Arctic (Smith & Clement 1990) and, thus, we observed an annual carbon demand of 130 mg C m⁻².

Rivkin & Legendre (2001) reported that the bacterial growth efficiency was an inverse function of temperature. We used a growth efficiency measured in polar oceans of 0.50 (Rivkin & Legendre 2001). However, small changes in temperature would influence growth efficiency and, hence, bacterial carbon demand (~2.5% decrease in growth efficiency per 1°C increase). Using the 3 different growth efficiencies of 0.10, 0.25 and 0.90 (Bjørnsen 1986, Bjørnsen & Kuparinen 1991, Gradinger & Zhang 1997, Middelboe & Søndergaard 1993, Rivkin & Legendre 2001 and references therein, M. Middelboe & R. Glud unpubl. data), the annual bacterial carbon demand ranged by a factor of 5 from 71 to 635 mg C m⁻² depending on the growth efficiency we used. The conclusion would change from an annual net autotrophic sea ice to a net heterotrophic sea ice if we used the growth efficiency of 0.10. However, when using the growth efficiencies of 0.25 and 0.90 the sea ice is still net autotrophic. According to Rivkin & Legendre (2001), growth efficiency increases with decreasing temperatures. Thus, the conversion of bacteria production to bacterial carbon demand by assuming a growth efficiency of 0.5 appears to be a realistic compromise among the conflicting literature values of 0.10 to 0.90 (Bjørnsen 1986, Bjørnsen & Kuparinen 1991, Gradinger & Zhang 1997, Middelboe & Søndergaard 1993, Rivkin & Legendre 2001 and references therein). It would be ideal to determine the respective factors at different seasonal conditions to improve the assessment of bacterial production and carbon demand, but in practice this would be an unrealistically large effort for most studies.

The O₂ concentration of sea ice is regulated by photosynthesis and respiration (Gleitz et al. 1995, Günther et al. 1999) and is also affected by freezing and thawing of sea ice (Glud et al. 2002). The temporal and spatial variations in snow cover thickness can introduce variability in sea ice temperatures and consequently in O₂ concentrations. During the present study, the snow cover varied from 0 to 26 cm and the sea ice temperature varied from 0 to -6°C (Fig. 1a), and only slight changes in temperature can lead to leakage of super-saturated and subsaturated water from the sea ice matrix (Glud et al. 2002). It is generally accepted that

to obtain realistic estimates of *in situ* microbial activity in sea ice, the microenvironment (i.e. temperature, salinity, nutrient concentration) should be maintained (e.g. McMinn & Ashworth 1998). The bag incubations were incubated *in situ* and, thus, the sea ice microenvironment was better maintained compared with standard incubations. This supports the use of bag incubations for determination of net O₂ production or consumption under natural conditions. In the present study, oxygen levels remained almost constant during February and March, indicating no or low net oxygen accumulation in the top sea ice cores of $0.50 \pm 3.00 \mu\text{mol O}_2 \text{ l}^{-1} \text{ d}^{-1}$ and in the bottom sea ice cores of $1.30 \pm 5.00 \mu\text{mol O}_2 \text{ l}^{-1} \text{ d}^{-1}$ (Fig. 6). The permeability of the bags was tested and could be responsible for a maximum O₂ exchange of $0.48 \pm 0.20 \mu\text{mol O}_2 \text{ l}^{-1} \text{ d}^{-1}$, which may compromise the results in February and March when no or low net oxygen accumulation was observed.

The autotrophic activity exceeded the heterotrophic activity in late March and April, resulting in a high net oxygen accumulation in the bottom sea ice cores of $6.30 \pm 2.30 \mu\text{mol O}_2 \text{ l}^{-1} \text{ d}^{-1}$, whereas no significant oxygen accumulation occurred in the top sea ice cores ($0.80 \pm 3.50 \mu\text{mol O}_2 \text{ l}^{-1} \text{ d}^{-1}$). The O₂ measurements showed high variability, indicating small-scale heterogeneity in oxygen. Thus, we suggest that more replicates be applied from all time intervals to quantify net oxygen consumption or production in future studies.

The temperature of sea ice enclosed in the bags did not differ from the ambient temperature profiles (data not shown). However, enclosure might have a number of consequences for the measured microbial activity. In case of high sea ice algal primary production and low nutrient concentrations, enclosing sea ice cores in bags creates a risk of underestimating primary production, as nutrient consumption sets an upper limit to production. In the present study, primary production measured in the bags from the bottom of the sea ice during peak activity late in the season was $60 \mu\text{g C l}^{-1} \text{ d}^{-1}$. Assuming a C:N Redfield ratio of 6.6 this represents a sufficient nitrogen pool for only 7 d of incubation. This indicates that the enclosed primary producers could have been nutrient-limited during the late part of the season (Fig. 6b), which suggests that oxygen production in the bottom sea ice section in the final incubation was underestimated. However, the annual net carbon fixation in the bag incubations was 8-fold higher than the annual net carbon fixation of 220 mg C m⁻² quantified from the standard incubations. We cannot, on this basis, pinpoint the reason for the apparent mismatch or evaluate which estimate is most correct. However, bags incubated for <7 d create a minimum disturbance of the microenvironment within the sea ice and might be a strong complementary tool to standard techniques

when assessing the net activity of microbial communities in sea ice. Hence, further work with the bag incubation technique *in situ* is clearly needed to better elucidate whether sea ice, on an annual scale, is net autotrophic or net heterotrophic.

Acknowledgements. We thank A. Haxen and M. R. Schröder for assistance in field and laboratory, and T. Juul-Pedersen, K. Arendt, D. M. Mikkelsen and P. Batty for valuable comments. We are thankful for the irradiance data provided by Asiaq (Greenland Survey). This study received financial support from the Danish Agency for Science, Technology and Innovation, KVUK Commission for Scientific Research in Greenland, is a part of the Greenland Climate Research Centre (GCRC 6507) and is a contribution to the Nuuk Basic and Zackenberg Basic programmes.

LITERATURE CITED

- Andreas EL, Ackley SF (1982) On the differences in ablation seasons of the Arctic and Antarctic sea ice. *J Atmos Sci* 39: 440–447
- Arrigo KR (2003) Primary production in sea ice. In: Thomas DN, Dieckmann GS (eds) *Sea ice: an introduction to its physics, chemistry, biology and geology*. Blackwell Science, Oxford, p 143–183
- Bjørnsen PK (1986) Bacterioplankton growth yield in continuous seawater cultures. *Mar Ecol Prog Ser* 30:191–196
- Bjørnsen PK, Kuparinen J (1991) Determination of bacterioplankton biomass, net production and growth efficiency in the Southern Ocean. *Mar Ecol Prog Ser* 71:185–194
- Braman RS, Hendrix SA (1989) Nanogram nitrite and nitrate determination in environmental and biological materials by vanadium (III) reduction with chemiluminescence detection. *Anal Chem* 61:2715–2718
- Brinkmeyer R, Knittel K, Jürgens J, Weyland H, Amann R, Helmke E (2003) Diversity and structure of bacterial communities in Arctic versus Antarctic pack ice. *Appl Environ Microbiol* 69:6610–6619
- Bunch JH, Harland RC (1990) Bacterial production in the bottom surface of sea ice in the Canadian Subarctic. *Can J Fish Aquat Sci* 47:1986–1995
- Bunt JS (1964) Primary productivity under sea ice in Antarctic waters. Influence of light and other factors on photosynthetic activities of Antarctic marine microalgae. *Antarct Res Ser* 1:27–31
- Clarke DB, Ackley SF (1984) Sea ice structure and biological activity in the Antarctic marginal ice zone. *J Geophys Res* C4 89:2087–2096
- Cota GF, Horne EPW (1989) Physical control of arctic ice algal production. *Mar Ecol Prog Ser* 52:111–121
- Coveney MF, Wetzel RG (1988) Experimental evaluation of conversion factors for the [³H]thymidine incorporation assay of bacterial secondary productivity. *Appl Environ Microbiol* 54:2018–2026
- Cox GFN, Weeks WF (1983) Equations for determining the gas and brine volumes in sea-ice samples. *J Glaciol* 29: 306–316
- Ducklow HW (1983) Production and fate of bacteria in the ocean. *Bioscience* 33:494–501
- Fenichel T, Glud RN (2000) Benthic primary production and O₂-CO₂ dynamics in a shallow-water sediment: spatial and temporal heterogeneity. *Ophelia* 53:159–171
- Fuhrman JA, Azam F (1980) Bacterioplankton secondary production estimates for coastal waters of British Columbia, Antarctica, and California. *Appl Environ Microbiol* 39: 1085–1095
- Fuhrman JA, Azam F (1982) Thymidine incorporation as a measure of heterotrophic bacterioplankton production in marine surface waters: evaluation and field results. *Mar Biol* 66:109–120
- Giannelli V, Thomas DN, Haas C, Kattner G, Kennedy H, Dieckmann GS (2001) Behavior of dissolved organic matter and inorganic nutrients during experimental sea ice formation. *Ann Glaciol* 33:317–321
- Gleitz M, vd Loeff MR, Thomas DN, Dieckmann GS, Millero FJ (1995) Comparison of summer and winter inorganic carbon, oxygen and nutrient concentrations in Antarctic sea ice brine. *Mar Chem* 51:81–91
- Glud RN, Rysgaard S, Kühl M (2002) A laboratory study on O₂ dynamics and photosynthesis in ice algal communities: quantification by microsensors, O₂ exchange rates, ¹⁴C incubations and a PAM fluorometer. *Aquat Microb Ecol* 27: 301–311
- Glud RN, Rysgaard S, Kühl M, Hansen JW (2007) The sea ice in Young Sound: implications for C cycling. In: Rysgaard S, Glud RN (eds) *Carbon cycling in Arctic marine ecosystems: case study Young Sound*. Bioscience Vol 58. Commission for Scientific Research in Greenland (Meddelselser om Grønland), Copenhagen, p 62–85
- Gosselin M, Legendre L, Therriault JC, Demers S, Rochet M (1986) Physical control of the horizontal patchiness of sea-ice microalgae. *Mar Ecol Prog Ser* 29:289–298
- Gosselin M, Legendre L, Therriault JC, Demers S (1990) Light and nutrient limitation of sea ice microalgae (Hudson Bay, Canadian Arctic). *J Phycol* 26:220–232
- Gosselin M, Levasseur M, Wheeler PA, Horner RA, Booth BC (1997) New measurements of phytoplankton and ice algal production in the Arctic Ocean. *Deep-Sea Res II* 44: 1623–1644
- Gradinger R, Ikävalko J (1998) Organism incorporation into newly forming Arctic sea ice in the Greenland Sea. *J Plankton Res* 20:871–886
- Gradinger R, Zhang Q (1997) Vertical distribution of bacteria in Arctic sea ice from the Barents and Laptev Seas. *Polar Biol* 17:448–454
- Gradinger R, Friedrich C, Spindler M (1999) Abundance, biomass and composition of the sea ice biota of the Greenland pack ice. *Deep-Sea Res II* 46:1457–1472
- Grasshoff K, Erhardt M, Kremling K (eds) (1983) *Methods of seawater analysis*, 2nd edn. Verlag Chemie, Weinheim
- Grossmann S, Dieckmann GS (1994) Bacterial standing stock, activity, and carbon production during formation and growth of sea ice in the Weddell Sea, Antarctica. *Appl Environ Microbiol* 60:2746–2753
- Grossmann S, Gleitz M (1993) Microbial responses to experimental sea-ice formation: implications for the establishment of Antarctic sea-ice communities. *J Exp Mar Biol Ecol* 173:273–289
- Günther S, Gleitz M, Dieckmann GS (1999) Biogeochemistry of Antarctic sea ice: a case study on platelet ice layers at Drescher Inlet, Weddell Sea. *Mar Ecol Prog Ser* 177:1–13
- Hansen JW, Thamdrup B, Jørgensen BB (2000) Anoxic incubation of sediment in gas-tight plastic bags: a method for biogeochemical process studies. *Mar Ecol Prog Ser* 208: 273–282
- Holmes RM, Aminot A, Kérouel R, Hooker BA, Peterson BJ (1999) A simple and precise method for measuring ammonium in marine and freshwater ecosystems. *Can J Fish Aquat Sci* 56:1801–1808
- Horner R, Schrader GC (1982) Relative contribution of ice

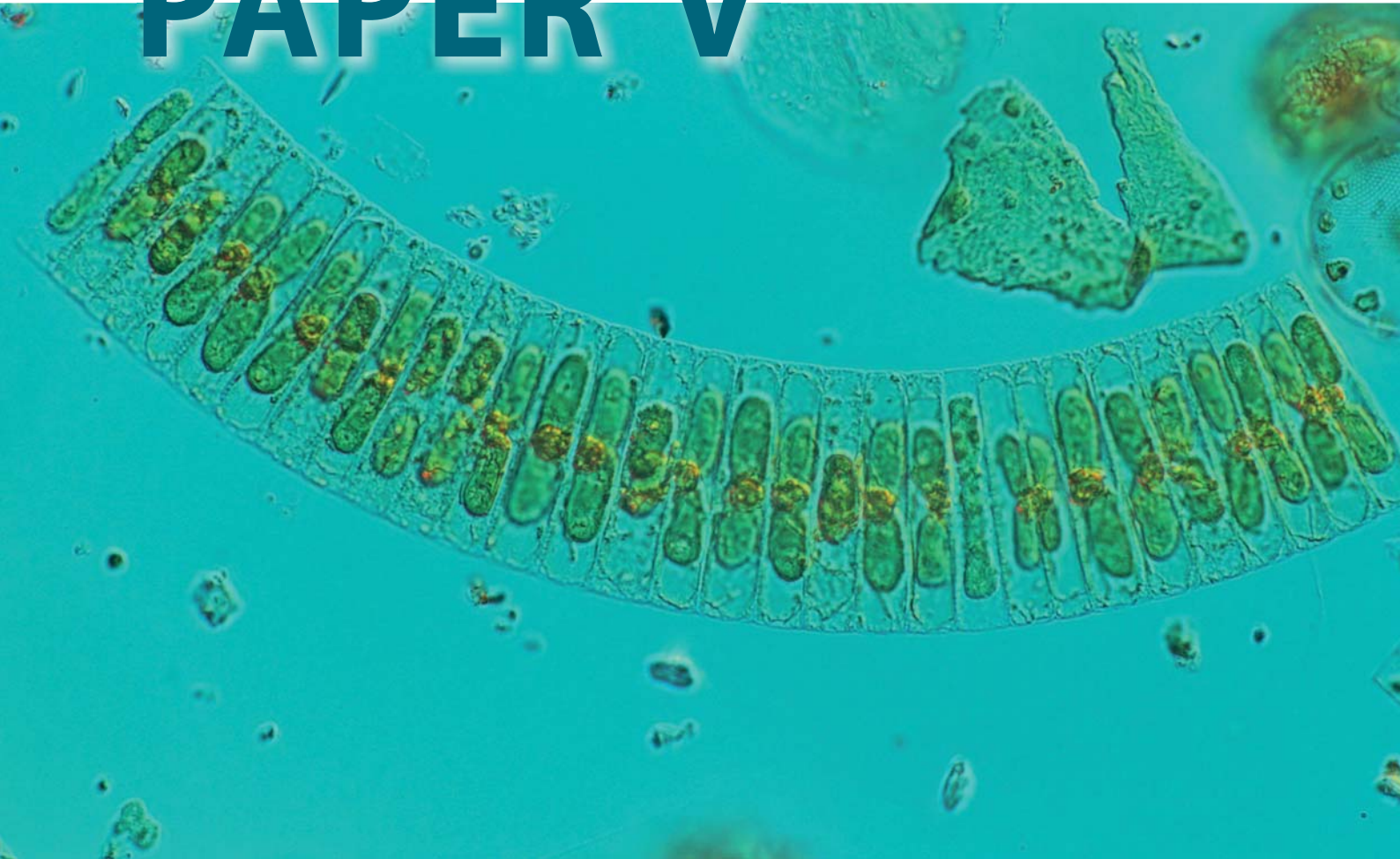
- algae, phytoplankton, and benthic microalgae to primary production in nearshore regions of the Beaufort Sea. *Arctic* 35:485–503
- Jespersen AM, Christoffersen K (1987) Measurements of chlorophyll-a from phytoplankton using ethanol as extraction solvent. *Arch Hydrobiol* 109:445–454
- Juul-Pedersen T, Rysgaard S, Batty P, Mortensen J and others (2009) Nuuk Basic: the marine basis programme 2008. In: Jensen LM, Rasch M (eds) Nuuk ecological research operations, 2nd Annu Rep 2008. National Environmental Research Institute, Aarhus University (Chapter 5)
- Kaartokallio H (2001) Evidence for active microbial nitrogen transformations in sea ice (Gulf of Bothnia, Baltic Sea) in midwinter. *Polar Biol* 24:21–28
- Kaartokallio H (2004) Food web components, and physical and chemical properties of Baltic Sea ice. *Mar Ecol Prog Ser* 273:49–63
- Kaartokallio H, Laamanen M, Sivonen K (2005) Responses of Baltic sea ice and open-water natural bacterial communities to salinity change. *Appl Environ Microbiol* 71:4364–4371
- Kaartokallio H, Kuosa H, Thomas DN, Granskog MA, Kivi K (2006) Biomass, composition and activity of organism assemblages along a salinity gradient in sea ice subjected to river discharge in the Baltic Sea. *Polar Biol* 30:183–197
- Kirst GO, Wiencke C (1995) Ecophysiology of polar algae. *J Phycol* 31:181–199
- Kottmeier ST, Sullivan CW (1988) Sea ice microbial communities (SIMCO) 9. Effects of temperature and salinity on rates of metabolism and growth of autotrophs and heterotrophs. *Polar Biol* 8:293–304
- Kottmeier ST, Grossi SM, Sullivan CW (1987) Sea ice microbial communities. VIII. Bacterial production in annual sea ice of McMurdo Sound, Antarctica. *Mar Ecol Prog Ser* 35:175–186
- Krembs C, Eicken H, Junge K, Deming JW (2002) High concentrations of exopolymeric substances in Arctic winter sea ice: implications for polar ocean carbon cycle and cryoprotection of diatoms. *Deep-Sea Res I* 49:2163–2181
- Legendre P, Legendre L (1998) Numerical ecology, 2nd edn. Developments in environmental modelling, Vol 20. Elsevier Science, Amsterdam
- Leppäranta M, Manninen T (1988) The brine and gas content of sea ice with attention to low salinities and high temperatures. *Finnish Inst Mar Res Internal Rep* 88-2
- Lizotte MP (2003) The microbiology of sea ice. In: Thomas DN, Dieckmann GS (eds) Sea ice: an introduction to its physics, chemistry, biology and geology. Blackwell Science, Oxford, p 184–210
- Lüthje M, Feltham DL, Taylor PD, Worster MG (2006) Modeling the summertime evolution of sea ice melt ponds. *J Geophys Res* 111:C02001, doi:10.1029/2004JC002818
- McMinn A, Ashworth C (1998) The use of oxygen microelectrodes to determine the net production by an Antarctic sea ice algal community. *Antarct Sci* 10:39–44
- Meiners K, Gradinger R, Fehling J, Civitarese G, Spindler M (2003) Vertical distribution of exopolymer particles in sea ice of the Fram Strait (Arctic) during autumn. *Mar Ecol Prog Ser* 248:1–13
- Middelboe M, Søndergaard M (1993) Bacterioplankton growth yield: seasonal variations and coupling lability and -glucosidase activity. *Appl Environ Microbiol* 59:3916–3921
- Mikkelsen DM, Rysgaard S, Glud RN (2008) Microalgal composition and primary production in Arctic sea ice: a seasonal study from Kobbefjord (Kangerluarsunnguag), West Greenland. *Mar Ecol Prog Ser* 368:65–74
- Mock T, Meiners KM, Giesenhagen HC (1997) Bacteria in sea ice and underlying brackish water at 54° 26' 50" N (Baltic Sea, Kiel Bight). *Mar Ecol Prog Ser* 158:23–40
- Moran PAP (1950) Notes on continuous stochastic phenomena. *Biometrika* 37:17–23
- Palmisano AC, SooHoo JB, Sullivan CW (1987) Effects of four environmental variables on photosynthesis-irradiance relationships in Antarctic sea-ice microalgae. *Mar Biol* 94:299–306
- Perovich DK (1996) The optical properties of sea ice. US Army Cold Regions Research and Engineering Laboratory (CRREL) Monogr 96-1, Hanover, NH
- Perovich DK, Roesler CS, Pegau WS (1998) Variability in Arctic sea ice optical properties. *J Geophys Res* 103:1193–1208
- Peters E, Thomas DN (1996b) Prolonged nitrate exhaustion and diatom mortality: a comparison of polar and temperate *Thalassiosira* species. *J Plankton Res* 18:953–968
- Platt T, Gallegos CL, Harrison WG (1980) Photoinhibition of photosynthesis in natural assemblages of marine phytoplankton. *J Mar Res* 38:687–701
- Ralph PJ, McMinn A, Ryan KG, Ashworth C (2005) Short-term effect of temperature on the photokinetics of microalgae from the surface layers of Antarctic pack ice. *J Phycol* 41:763–769
- Ralph PJ, Ryan KG, Martin A, Fenton G (2007) Melting out of sea ice causes greater photosynthetic stress in algae than freezing in. *J Phycol* 43:948–956
- Reimnitz E, Marincovich L Jr, McCormick M, Briggs WM (1992) Suspension freezing of bottom sediment and biota in the Northwest Passage and implications for Arctic Ocean sedimentation. *Can J Earth Sci* 29:693–703
- Riedel A, Michel C, Gosselin M, Leblanc B (2007) Enrichment of nutrients, exopolymeric substances and microorganisms in newly formed sea ice on the Mackenzie shelf. *Mar Ecol Prog Ser* 342:55–67
- Riemann B, Bjornsen PK, Newell S, Fallon R (1987) Calculation of cell production of coastal marine bacteria based on measured incorporation of [³H]thymidine. *Limnol Oceanogr* 32:471–476
- Rivkin RB (1986) Incorporation of tritiated thymidine by eukarotic microalgae. *J Phycol* 22:193–198
- Rivkin RB, Legendre L (2001) Biogenic carbon cycling in the upper ocean: effects of microbial respiration. *Science* 291:2398–2400
- Rysgaard S, Glud RN (2004) Anaerobic N₂ production in Arctic sea ice. *Limnol Oceanogr* 49:86–94
- Rysgaard S, Kühl M, Glud RN, Hansen JW (2001) Biomass, production and horizontal patchiness of sea ice algae in a high-Arctic fjord (Young Sound, NE Greenland). *Mar Ecol Prog Ser* 223:15–26
- Smith REH, Clement P (1990) Heterotrophic activity and bacterial productivity in assemblages of microbes from sea ice in the high Arctic. *Polar Biol* 10:351–357
- Smith WO Jr, Sakshaug E (1990) Polar phytoplankton. In: Smith WO Jr (ed) Polar oceanography. Part B. Chemistry, biology and geology. Academic Press, San Diego, CA, p 477–525
- Smith REH, Clement P, Cota GF (1989) Population dynamics of bacteria in Arctic sea ice. *Microb Ecol* 17:63–76
- Steeman-Nielsen E (1952) The use of radio-active carbon (¹⁴C) for measuring organic production in the sea. *J Cons Int Explor Mer* 18:117–140
- Strickland JDH, Parsons TR (1972) A practical handbook of seawater analysis. Fish Res Board Can Bull 167, Ottawa
- Thomas CW (1963) On the transfer of visible radiation through sea ice and snow. *J Glaciol* 4:481–484

-
- Thomas DN, Lara RJ, Eicken H, Kattner G, Skoog A (1995) Dissolved organic matter in Arctic multi-year sea ice during winter: major components and relationships to ice characteristics. *Polar Biol* 15:477–483
 - Trodahl HJ, Buckley RG (1990) Enhanced ultraviolet transmission of Antarctic sea ice during the austral spring. *J Geophys Res* 17:2177–2179
 - Vézina AF, Demers S, Laurion I, Sime-Ngando T, Juniper SK, Devine L (1997) Carbon flows through the microbial food web of first-year ice in Resolute Passage (Canadian High Arctic). *J Mar Syst* 11:173–189
 - Weeks WF, Ackley SF (1986) The growth, structure and properties of sea ice. In: Untersteiner N (ed) *The geophysics of sea ice*. NATO ASI Series Ser B Physics. Plenum Press, New York, NY, p 9–164
 - Weller G, Schwerdtfeger P (1967) Radiation penetration in Antarctic plateau and sea ice. In: *Polar meteorology*. World Meteorol Org Tech Note 87:120–141

*Editorial responsibility: Graham Savidge,
Portaferry, UK*

*Submitted: January 8, 2010; Accepted: September 27, 2010
Proofs received from author(s): November 26, 2010*

PAPER V



Sea ice diatom (*Fragilariopsis sp.*) Photo: Diana W. Krawczyk.

Growth limitation of three Arctic sea ice algal species: effects of salinity, pH, and inorganic carbon availability

D.H Sjøgaard • P.J. Hansen • S. Rysgaard • R.N. Glud

Polar Biology 34:1157 – 1165, doi: 10.1007/s00300-011-0976-3

Growth limitation of three Arctic sea ice algal species: effects of salinity, pH, and inorganic carbon availability

Dorte Haubjerg Søggaard · Per Juel Hansen ·
Søren Rysgaard · Ronnie Nøhr Glud

Received: 14 October 2010/Revised: 18 January 2011/Accepted: 19 January 2011/Published online: 3 March 2011
© Springer-Verlag 2011

Abstract The effect of salinity, pH, and dissolved inorganic carbon (TCO₂) on growth and survival of three Arctic sea ice algal species, two diatoms (*Fragilariopsis nana* and *Fragilariopsis* sp.), and one species of chlorophyte (*Chlamydomonas* sp.) was assessed in controlled laboratory experiments. Our results suggest that the chlorophyte and the two diatoms have different tolerance to fluctuations in salinity and pH. The two species of diatoms exhibited maximum growth rates at a salinity of 33, and growth rates at a salinity of 100 were reduced by 50% compared to at a salinity of 33. Growth ceased at a salinity of 150. The chlorophyte species was more sensitive to high salinities than the two diatom species. Growth rate of the chlorophyte was greatly reduced already at a salinity of 50 and it could not grow at salinities above 100. At salinity 33 and constant TCO₂ concentration, all species exhibited maximal growth rate at pH 8.0 and/or 8.5. The two diatom species stopped growing at pH > 9.5, while the chlorophyte species still was able to grow at a rate which was 1/3

of its maximum growth rate at pH 10. Thus, *Chlamydomonas* sp. was able to grow at high pH levels in the succession experiment and therefore outcompeted the two diatom species. Complementary experiments indicated that growth was mainly limited by pH, while inorganic carbon limitation only played an important role at very high pH levels and low TCO₂ concentrations.

Keywords Arctic · Sea ice algae · Salinity · pH · TCO₂ · In situ succession patterns

Introduction

Sea ice is permeated with pores and brine channels, which host a unique microbial community. The total brine channel volume of sea ice typically ranges between 1 and 30% depending on salinity, temperature, and ionic composition of the brine fluid (Weeks and Ackley 1986). When the temperature decreases, the thermodynamic phase equilibrium drives the sea ice toward a lower brine volume with higher salinities (Cox and Weeks 1983). Thus, the temperature and brine of sea ice are interrelated. At brine temperature between -1.9 and -6.7°C, the brine salinity may range from 34 to 108 (Gleitz et al. 1995). However, when sea ice is exposed to temperatures below -20°C, the brine salinity can be well above 200 (Cox and Weeks 1983). In the summer when sea ice melts, the salinity of the brine can be as low as one-third of normal sea water, e.g., salinity <10 (Ryan et al. 2004). Brine salinity also fluctuates vertically within the sea ice, with the lowest salinities usually encountered in the bottom sea ice layers (Gradinger 1999; Lizotte 2003; Ryan et al. 2004). Thus, sea ice algae must cope with severe physicochemical stress factors caused by natural variations in salinity. Only a few studies

D. H. Søggaard (✉) · S. Rysgaard · R. N. Glud
Greenland Climate Research Centre
(C/O Greenland Institute of Natural Resources),
Kivioq 2, Box 570, 3900 Nuuk, Greenland
e-mail: doso@natur.gl

P. J. Hansen
Marine Biological Laboratory, University of Copenhagen,
Strandpromenaden 5, 3000 Helsingør, Denmark

D. H. Søggaard · R. N. Glud
University of Southern Denmark, Campusvej 55,
5230 Odense M, Denmark

R. N. Glud
Dumstaffnage Marine Laboratory,
Scottish Association for Marine Science,
PA37 1QA Dunbeg, Scotland, UK

include investigations into the effect of salinity stress on growth rates of sea ice algae (Grant and Horner 1976; Arrigo and Sullivan 1992; Thiel et al. 1996; Ryan et al. 2004). A study on the sea ice diatoms (*Amphiprora kuffnerathii*, *Nitzschia*, and *Thalassiosira Antarctica*) isolated from ice cores from Weddell Sea revealed growth at salinities up to 90 at -5.5°C , and the diatoms were found to survive for 20 days at salinities up to 145 (Thiel et al. 1996). Other studies have shown that the growth of different sea ice diatoms from the Weddell Sea ceased at salinities above 50 (Grant and Horner 1976). Furthermore, studies have shown that most flagellate species of algae e.g., chlorophytes, dinoflagellates, and chrysophytes have been reported in the sea ice (Arrigo et al. 2010). These flagellate species is especially found in the top sea ice layer, where the highest salinity and lowest temperatures is encountered.

The differences in tolerance between sea ice algal species have been ascribed to various abilities for osmotic acclimations, e.g., production of osmolytes (such as proline), which balances the ionic pressure during changes in salinity (Gleitz and Thomas 1992). Moreover, changes in sea ice salinity and associate factors may be the key drivers for microbial succession in sea ice communities (Mikkelsen et al. 2008). The sea ice algal species that are capable to cope with a broad range of salinity may have an advantage and become dominant in the sea ice community. An understanding of the effect of fluctuating salinities in sea ice brine indicates which factors drive the distribution and succession of sea ice algae and might give important information that can be used to modeling sea ice species succession and carbon dynamics within the brine.

Variation in seawater pH levels can also have a marked effect on the growth and survival of sea ice algae. In sea ice, a number of biological and physical processes influence pH. Studies of sea ice have shown that in regions characterized by high primary production, the sea ice brine has considerably reduced concentrations of dissolved inorganic carbon (TCO_2) and elevated pH levels as high as 10.0 (Gleitz et al. 1995; Thomas et al. 2001). Furthermore, changes in carbon chemistry alone can result in significant changes in pH of the sea ice brine. One mechanism behind this is CaCO_3 precipitation that can occur at low temperatures (Rysgaard et al. 2007; Dieckmann et al. 2008). Carbonate precipitation will initially lead to a buildup of CO_2 in the brine system leading to a decrease in pH. With time, CO_2 can be transported to the water column through brine drainage. This net export of CO_2 out of the sea ice brine will lead to increased pH in the brine, especially when sea ice starts to melt. In sea water, changes in pH influence the equilibrium of the carbonate system and therefore the

inter-speciation of TCO_2 , i.e., CO_2 (aq), HCO_3^- , CO_3^{2-} , which may influence microalgae species succession and distribution (Hansen 2002; Rost et al. 2003; Trimborn et al. 2008). Limitation in the supply of CO_2 due to elevated pH levels may restrict photosynthesis and growth of some algal species (Hansen 2002; Rost et al. 2003; Hansen et al. 2007) and favor species that utilize HCO_3^- as an inorganic carbon source (Korb et al. 1997; Huertas et al. 2000; Hansen 2002). Diatoms have been found to actively take up HCO_3^- and convert it into intracellular CO_2 by extracellular enzymes (e.g., Korb et al. 1997; Tortell et al. 1997). Additionally, diatoms can utilize HCO_3^- directly for carbon fixation through C_4 photosynthesis (Tortell et al. 1997; Reinfelder et al. 2000). However, a previous study has shown that the ability to tolerate high pH is not related to particulate algal groups, but rather is species specific (Hansen 2002). In this study, we investigated the upper limit for growth with respect to salinity, pH, and TCO_2 for three common Arctic sea ice algal species; the diatoms *Fragilariopsis nana*, *Fragilariopsis* sp. and the chlorophyte *Chlamydomonas* sp. The physiological response toward these stress factors are evaluated and discussed in relation to in situ succession patterns. This study is important to understand the factors controlling the growth, survival, composition, and distribution of the sea ice algal communities within the brine and can be used to accurately model the species succession and the productivity of this complex system.

Materials and methods

Algae species and maintenance of sea ice algae cultures

Three sea ice algae were selected for the study (Arrigo et al. 2010). The diatom *Fragilariopsis* sp. (CCMP2297) and the chlorophyte *Chlamydomonas* sp. (CCMP2294) originated from sea ice from Baffin Bay and were provided by Guillard National Center for Culture of Marine Phytoplankton (CCMP), and the diatom *Fragilariopsis nana* (SCCAP K-0637) was isolated from the Labrador Sea and provided by the Scandinavian Culture Collection of Algae and Protozoa, Department of Phycology, University of Copenhagen. The two species of diatoms were selected as representatives for pennate diatoms, which are very common in sea ice (Arrigo et al. 2010). We deliberately chose *Fragilariopsis nana* because it is a relatively small species (length 8.0–9.4 μm ; width 1.9–2.0 μm) and *Fragilariopsis* sp. because it is somewhat larger diatom species (length 12–16 μm ; width 6–10 μm). The chlorophyte *Chlamydomonas* sp. (length 8–10 μm ; width 4.0–6.0 μm) was selected because chlorophytes are common in sea ice as well (Arrigo et al. 2010).

Algal cultures were grown in L1 growth medium (Guillard and Hargraves 1993) based on autoclaved seawater with a salinity of 33. The stock cultures were maintained at $3 \pm 1^\circ\text{C}$ and $50 \mu\text{E m}^{-2} \text{s}^{-1}$ following a light:dark cycle of 16:8 h. Illumination was provided by cool fluorescent lamps, and irradiance was measured using a LiCor 1400 (Li-Cor, NE, USA).

Experimental conditions

All experiments were carried out at $3 \pm 1^\circ\text{C}$ and at an irradiance of $50 \mu\text{E m}^{-2} \text{s}^{-1}$ following a light:dark cycle of 16:8 h. Only cells from exponentially growing cultures were used for inoculation of the experiments. However, the first 6–10 days were considered as an acclimation period; therefore, cell counts from these samplings were not included in the calculations of growth rates. All experiments were carried out in 62-ml polystyrene bottles, except for the pH-drift experiments that were carried out in gas-tight laminated NEN/PE plastic bag (Hansen et al. 2000) fitted with a gas-tight Tygon tube and valve for sampling. All experiments were carried out in triplicates, i.e., each experiment was carried out in three separate bottles.

Cultures were kept suspended through the use of a plankton wheel, and an external cooling system was used to prevent heating associated with radiation absorption. The L1 growth medium was selected to make sure that algal cultures were not nutrient limited at anytime during the experiment.

Enumeration of cells was carried out using subsamples fixed in acidic Lugol's iodine (2.5% final concentration), and cells were counted in a Sedgewick-Rafter chamber. Each count was based on at least 400 cells.

Growth rates (μ) were measured as increase in cell number and were calculated assuming exponential growth:

$$\mu(d^{-1}) = \frac{(\ln N_1 - \ln N_0)}{(t_1 - t_0)} \quad (1)$$

where N_0 and N_1 are number of cells at time t_0 and t_1 , and t is the difference in time (d) between t_0 and t_1 samples (Hansen 2002). We determined the exponential phase of growth (straight line). Two points, N_0 and N_1 , at the extremes of this linear phase was taken and substituted into the equation (same approach was used for determining the two points, t_0 and t_1). All experiments were carried out in triplicates; thus, this was done for each replicate and the mean of the three maximum growth rates was determined. The calculations of the growth rates were corrected for any dilutions. pH values were measured using a Sentron[®] 2001 pH-meter equipped with a Red Line electrode, which is an ISFET[®] sensor (Semiconductor Ion Field Effect Transistor) with detection limit

of 0.01. The pH sensor was calibrated (2 point) using Sentron buffers of pH 7.0 and 10.0. The concentration of dissolved inorganic carbon (TCO_2) was measured in the growth medium by transferring samples (12 ml) to Exetainer tubes (12 ml Exetainer[®], Labco High Wycombe, UK) spiked with $20 \mu\text{l}$ HgCl_2 (saturated solution, 5% w/v) and was measured using a CO_2 analyzer (CM5012 CO_2 Coulometer).

Experimental setup

Growth rate of sea ice algae at different salinities

In the first set of experiments, growth rates of the three sea ice algae *Fragilariopsis nana*, *Fragilariopsis sp.*, and *Chlamydomonas sp.* were measured at different salinities ranging from 5 to 150 (i.e., salinity of 5, 20, 33, 50, 75, 100, and 150). The salinity was adjusted from a salinity of 33 by addition of artificial seawater based on Red Sea salt with known TCO_2 concentrations to the L1 medium. The pH value was kept constant at 8.0 throughout the experiment. If the pH differed by more than 0.03 from the set point, it was adjusted by the aliquot addition of 0.1 M NaOH or HCl. The experiment was initiated with an inoculation of $1,000 \text{ cells ml}^{-1}$ and was allowed to run for minimum 18 d and maximum 20 d. Every second day, pH was measured, and subsamples (1 ml) were taken for enumeration of algae cells. After subsampling, the bottles were refilled to capacity with L1 growth medium (1 ml). The L1 growth medium was at each event adjusted to the correct salinity to prevent salinity in the experimental bottles to drift. Salinity and TCO_2 concentrations were measured initially and at the termination of the experiment.

To test the effect of lowered salinity on the growth of the three species of sea ice algae, a second set of experiments was conducted. The algal cultures were grown in L1 growth medium (Guillard and Hargraves 1993) based on autoclaved seawater with a salinity of 75 and a known TCO_2 concentration for a month. The salinity was adjusted from a salinity of 75 to different salinities of 5, 20, and 33 to mimic the transition from cold to melting sea ice. The pH value was kept constant at 8.0 throughout the experiment. If the pH differed by more than 0.03 from the set point, it was adjusted by the aliquot addition of 0.1 M NaOH or HCl. The experiment was initiated with an inoculation of $1,000 \text{ cells ml}^{-1}$ and was allowed to run for a minimum of 18 d and a maximum of 20 d.

Growth rate of the sea ice algae at different pH and TCO_2

In the first set of pH experiments, growth rates of the three species of sea ice algae: *Fragilariopsis nana*,

Fragilariopsis sp., and *Chlamydomonas* sp. were measured at different pH values ranging from 8.0 to 10.0 (i.e., pH 8.0, 8.5, 9.0, 9.5, and 10.0). The salinity was 33 throughout the experiment. The pH was adjusted by addition of 0.1 M HCl or NaOH to the medium. The experiment was initiated by inoculating 1,000 cells ml⁻¹ and was allowed to run for 20 d. The TCO₂ concentration was, in all instances, 2.4 mM. Every second day, pH of the culture media was measured, and subsamples (1 ml) were taken for enumeration of algae cells. After subsampling, the bottles were refilled to capacity with pH adjusted-L1 growth medium (i.e., pH 8.0, 8.5, 9.0, 9.5, 10.0), and the bottles were remounted on the plankton wheel. If the pH differed by more than 0.03 from the set point, it was adjusted by addition of aliquots of 0.1 M HCl or NaOH.

In the pH-drift experiment, *Fragilariopsis* sp. and *Chlamydomonas* sp. were inoculated (1,000 cells ml⁻¹) in media with a pH of 8.0 and initial TCO₂ concentrations of c. 1.2 or 2.4 mM and were allowed to grow into stationary growth phase (up to 26 d). The 1.2 mM TCO₂ concentration medium was obtained by mixing the 2.4 mM L1 growth medium with a very low TCO₂ concentration medium (<0.5 mM). The very low TCO₂ medium was prepared by acidifying the growth medium (to pH < 3), followed by heating to 110°C for 30 min and aerating the medium. The pH was then adjusted to 8.0 by the addition of 0.1 or 1.0 M NaOH or HCl (Hansen et al. 2007). The experiment was carried out in gas-tight laminated NEN/PE plastic bags (Hansen et al. 2000). Every second day, the pH of the culture medium was measured, and subsamples were withdrawn for enumeration of algae cell concentration (3 ml) and for measurements of the TCO₂ concentration (36 ml). The NEN/PE plastic bags were not refilled after each sampling. The [CO₂ + HCO₃⁻] concentrations were calculated from measurements of TCO₂, temperature, salinity, and pH (Lewis and Wallace 1998).

Succession experiment

The three sea ice algal species were inoculated in a mixed culture (i.e., 1,000 cells ml⁻¹) at a pH of 8.0 and a salinity of 33 and an initial TCO₂ concentration of 2.4 mM. The three sea ice algal species were allowed to grow well into stationary growth phase (up to 22 d). Every second day, pH of the culture media was measured, and subsamples (1 ml) were taken for enumeration of the mixed algae cells. After subsampling, the bottles were refilled to capacity with pH adjusted-L1 growth medium and the bottles were remounted on the plankton wheel. TCO₂ concentration was measured at the initiation and the termination of the experiment to ensure that the concentration was sufficient for algae growth during the experiments.

Results

Effect of salinity on the growth rates of three Arctic sea ice algae

The two sea ice diatoms exhibited similar growth rates as a function of salinity, and no significant differences were observed between acclimation salinities (33 or 75) used in the salinity experiments (Student's *t*-test, *P* > 0.05). Maximum growth rates were obtained at a salinity of 33 (Fig. 1a). At salinities above 33, growth rates gradually decreased with salinity. However, growth rates at a salinity of 100 were reduced by 50%, and none of the diatoms could grow at a salinity of 150. At salinities below 33, growth rates of the two diatoms decreased only slightly and they were still quite high at a salinity of 5 (Fig. 1a, b). The two diatom species showed significantly more reduced growth rates at high salinities than at low salinities (*Fragilariopsis nana* OLS, *P* = 0.005, one-sided and

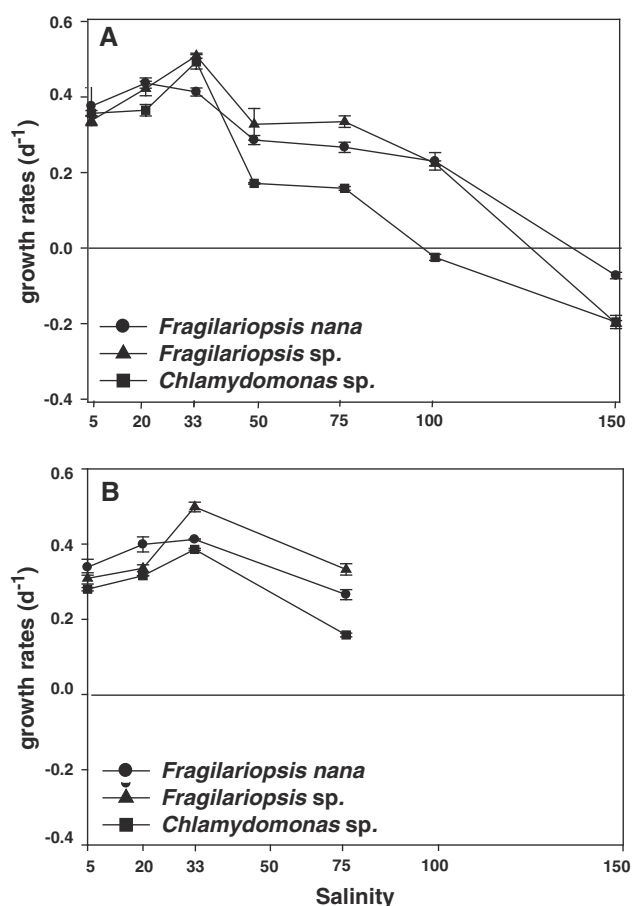


Fig. 1 *Fragilariopsis nana*, *Fragilariopsis* sp., and *Chlamydomonas* sp. Growth rates of the three sea ice algae as a function of salinity. **a** Salinity adjusted from 33 to the experimental salinity. **b** Salinity adjusted from 75 to the experimental salinity. Data points represent treatment means SE ± (*n* = 3)

Fragilariopsis sp., $P = 0.005$). The growth response of the chlorophyte as a function of salinity was similar to that of the two diatoms showing more reduced growth rates at high salinities (*Chlamydomonas* sp. OLS, $P = 0.009$, one-sided) (Fig. 1a). Growth rates of the chlorophyte was greatly reduced already at a salinity of 50 and it could not grow at salinities above 100 (Fig. 1a, b). *Effect of pH and TCO₂ limitation on the growth rate of the three sea ice algae.*

A very profound effect of the pH was observed on the growth rates of all three species (Fig. 2). All species exhibited maximum growth rates at a pH of 8.0–8.5 (Fig. 2). Above a pH of 8.5, a negative effect of increasing pH was observed on the growth rate of all species. However, all species were still able to grow at half the maximum growth rate at pH 9.5. The diatom species could not grow at pH 10, while the chlorophyte species demonstrated a growth rate of one-third its maximum. The growth rates of the two diatoms were significantly reduced at pH > 9.0 (Student's *t*-test *Fragilariopsis nana*, $P = 0.0066$; *Fragilariopsis* sp., $P = 0.0061$).

In the pH-drift experiments of *Fragilariopsis* sp., the pH reached a maximum of 9.5 and 9.7 in the experiments initiated at a TCO₂ concentration of 1.4 and 2.4 mM, respectively (Fig. 3). Final TCO₂ concentrations in these experiments were 1.0 and 1.5 mM, respectively.

For the pH-tolerant species, *Chlamydomonas* sp., the pH reached 9.8, when grown at initially high and low TCO₂ concentrations (Fig. 3). The final TCO₂ concentration was 1.0 mM in the experiments initiated at a high TCO₂ concentration, whereas the concentrations decreased from 1.4 to 1.0 mM for this species in experiments initiated at a low TCO₂ concentration (Fig. 3).

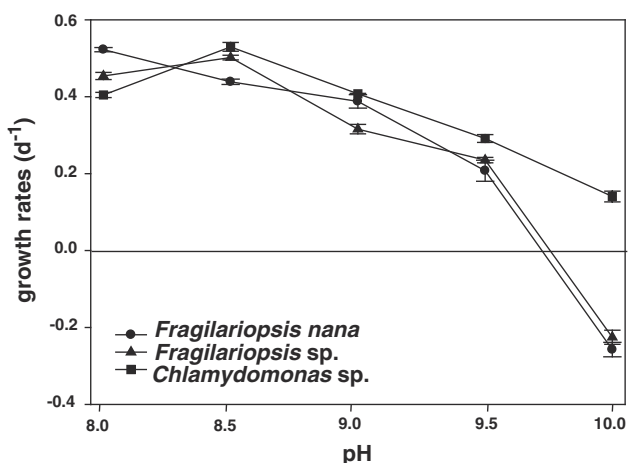


Fig. 2 *Fragilariopsis nana*, *Fragilariopsis* sp., and *Chlamydomonas* sp. Growth rates of the three sea ice algae as a function of different fixed pH levels. Dissolved inorganic carbon (TCO₂) concentration was initially between 2.2 and 2.4 mM in the experiment flasks. Data points represent treatment means SE ± ($n = 3$)

Succession experiment

The importance of pH in succession of sea ice algae species was studied using mixed cultures of three sea ice algal species (*Fragilariopsis nana*, *Fragilariopsis* sp., and *Chlamydomonas* sp.) with an initial pH of 8.0 (Fig. 4). All three species grew until pH reached 9.4 to 9.5 on Day 18. At Day 20, the pH had increased to above 9.6, and the two diatoms stopped growing, while the chlorophyte species maintained a positive growth rate.

Discussion

Growth of sea ice algae at different salinities

The ability of sea ice algae to grow within the physiochemical gradient found in the sea ice suggests that the algae are well adapted to cope with fluctuations in light, temperature, salinity, pH, and TCO₂ concentrations. However, salinity has a pronounced effect on growth, photosynthetic efficiency, and metabolism (Misra et al. 2001). Some microalgae are considered euryhaline, since they can adapt to varying external salinities (Hellebust 1985). However, the salinity range over which active growth takes place differs greatly among species, and the physiochemical conditions in the sea ice will provide a selection pressure that influences the final community composition (Ryan et al. 2004). A previous study has indicated that most sea ice algae are more tolerant to reduced, rather than elevated salinities (Bates and Cota 1986). The present study supports the results of Bates and Cota (1986), as the three sea ice algae showed more reduced growth rates at high salinity levels than at low salinity levels. The experiments suggest that the two diatoms have a competitive advantage in sea ice, where brine salinity is greater than 50. These salinity conditions are typically encountered where the sea ice temperature is between -1.9 and -6.7°C (Gleitz et al. 1995).

When sea ice melts, the algae are exposed to altered salinities and subsequently the algal growth may be influenced. A previous study showed that diatom species are only slightly affected by decreasing salinities, whereas decreasing salinities may result in substantial losses of ciliates and flagellate species (Garrison and Buck 1986; Ryan et al. 2004; Mikkelsen and Witkowski 2010). In the present study, the three sea ice algal species were exposed to changes in salinity conditions with different initial salinities of 33 or 75 to test the effect of rapid shifts in salinity from high to low on the growth rates. The salinity stress had the smallest effect on the growth rate of the two diatoms compared to the effect on the chlorophyte. This suggests that sea ice diatoms are less affected by

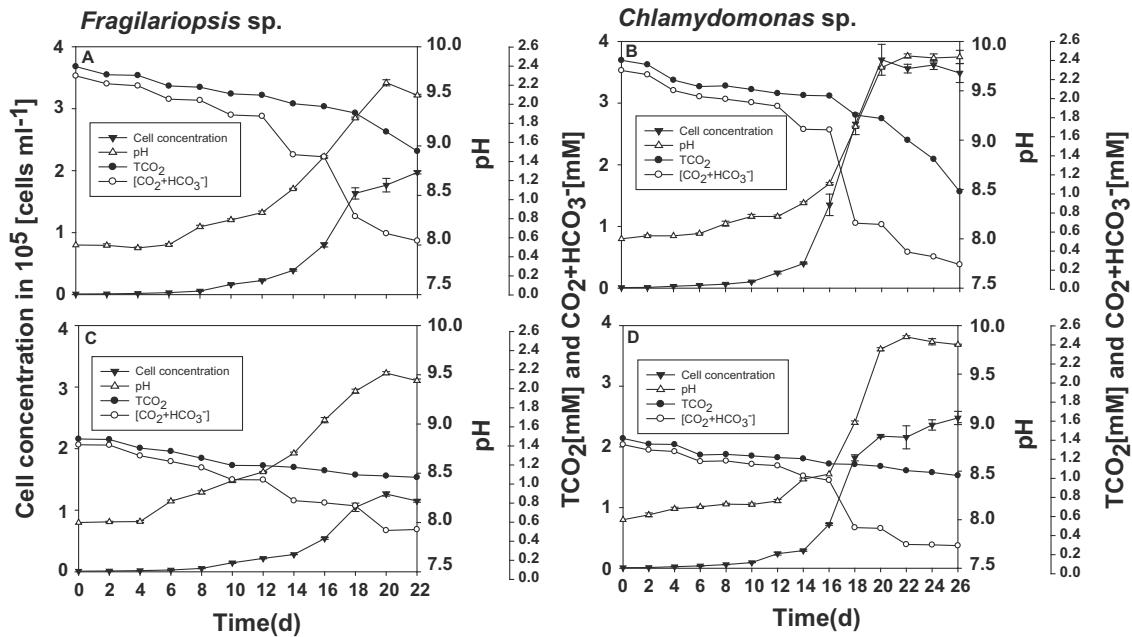


Fig. 3 *Fragilariopsis* sp. and *Chlamydomonas* sp. Cell concentration in 10⁵, pH, dissolved inorganic carbon (TCO₂) and available inorganic carbon [CO₂ + HCO₃⁻] as a function of time for pH-drift

experiments at initial TCO₂ concentration for the two sea ice algae. Initial TCO₂: (a, b) 2.4 mM and (c–d) 1.4 mM. Data points represent treatment means ± (*n* = 3)

decreasing salinities and thus may have a competitive advantage during summer and spring thaw when sea ice salinity becomes low. This result compares with previous studies showing that sea ice diatoms dominates during sea ice summer and spring thaw (Palmisano and Garrison 1993; Ikävalko and Thomsen 1997; Mikkelsen et al. 2008). Furthermore, the present study shows that some sea ice algal species are better adapted to changes in salinity than other algal species, and thus, the changes in sea ice salinity may drive species succession of sea ice algae.

All the experiments were conducted at higher temperatures ($3 \pm 1^\circ\text{C}$) than the in situ temperatures observed in sea ice (Søgaard et al. 2010). Previous studies have shown that photosynthetic rates in sea ice algae are influenced by temperature (Palmisano et al. 1987; Ralph et al. 2005). This suggests that the growth rates of the three sea ice algae might be overestimated compared to growth rates at in situ temperatures. However, it is a nontrivial task to incubate samples at low bulk salinity at 0 or sub-zero temperature without introducing freezing and thaw artifacts.

Tolerance of sea ice algae to elevated pH

The effect of high pH on the growth rates of marine planktonic algae is well established. Some species are very sensitive to elevated pH and cannot grow when pH exceeds 8.8, while others still grow at pH above 10 (e.g., Hansen 2002; Lundholm et al. 2004). Several studies have also shown that the tolerance to high pH is species specific, and

large differences exist within important marine algal groups, such as diatoms and dinoflagellates (Hansen 2002; Lundholm et al. 2004; Sørensen and Hansen 2007).

The knowledge of the effect of high pH on growth rates of sea ice algae is however, very limited. High pH is observed in sea ice with high primary production (Gleitz et al. 1995; Thomas et al. 2001) and thus prevails during spring when irradiance increase (Cota and Horne 1989; Köhl et al. 2001). In the present study, influence of high pH levels on the growth rate of the three species of sea ice algae was studied at pH levels ranging from pH 8.0 to 10.0 in nutrient-rich growth media. We did not measure the nutrient concentrations in the nutrient rich media during all the experiments, but the amount of nutrients left at the termination of the experiments assuming Redfield stoichiometry documents that nutrients were not limiting at any point during the experiments (see Table 1).

In the present study, our results clearly demonstrate that all species were restricted by high pH even at a high initial TCO₂ concentration. Growth rates were significantly reduced for both diatom species at pH > 9.0 (Fig. 2). Above pH 9.5, the two sea ice diatoms stopped growing irrespective of TCO₂, showing that pH had a direct effect on algal growth. Only a limited number of diatoms have been studied with respect to effect of pH on growth; however, among those studied the effect of pH on growth varied (Lundholm et al. 2004). Lundholm et al. (2004) found that smaller diatoms have a higher upper pH limit for growth than larger diatom. In present study, we

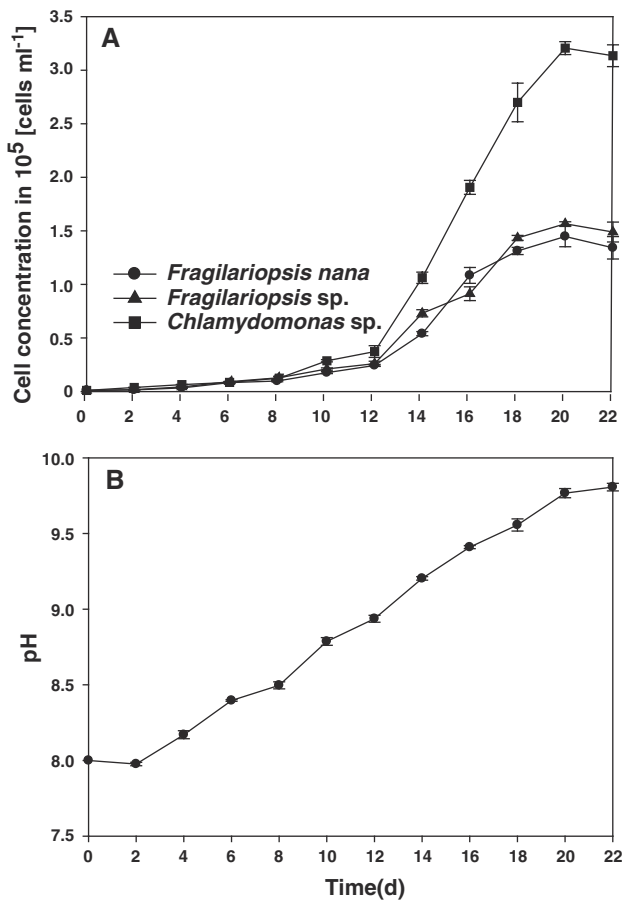


Fig. 4 Succession experiment. **a** Change in cell concentration in 10⁵ of the three sea ice algae species. *Fragilariopsis nana*, *Fragilariopsis sp.*, and *Chlamydomonas sp.* as a function of time (d) from inoculation at pH 8.0. **b** pH as a function of time from inoculation. Data points represent treatment means SE ± (n = 3)

deliberately chose *Fragilariopsis nana* because it is a relatively small diatom species and *Fragilariopsis sp.* because it is somewhat larger diatom species. Despite the difference in cell volume, the two diatom species showed the same upper pH limit. The sea ice chlorophyte showed an extreme pH tolerance as only a small reduction in growth rate was observed above this pH level. The results suggest that these sea ice algal species are not limited by inorganic carbon at pH

8.0–9.0 (Fig. 3), a pH level close to that found in sea ice brine (Papadimitriou et al. 2007). However, pH increases in colonized sea ice because of a decline in TCO₂ as a result of photosynthetic carbon assimilation (Thomas et al. 2010). This may affect species such as *Fragilariopsis nana* and *Fragilariopsis sp.* (Figs. 2, 3 and 4). Other species such as *Chlamydomonas sp.* can tolerate much higher pH levels and thus will have a competitive advantage in sea ice with high pH levels (Figs. 2, 3 and 4). However, this species was limited by low TCO₂ concentrations and thus may be out-competed by algal species in the sea ice, which are able to grow at high pH levels and very low TCO₂ concentrations. Algae can only utilize CO₂ and HCO₃⁻ for photosynthesis (e.g., Stumm and Morgan 1996; Korb et al. 1997), and it is well known that the speciation of inorganic carbon species depends upon pH. For instance, at pH 9.3, only half of the TCO₂ is available in the form of [CO₂ and HCO₃⁻]. In the pH-drift experiments initiated at a low TCO₂, the algae were able to deplete the available inorganic carbon [CO₂ and HCO₃⁻] to a lower limit of 0.45 mM for *Fragilariopsis sp.* and 0.25 mM for *Chlamydomonas sp.*, assuming equilibrium in the carbonate system (Fig. 3). At those low concentrations of [CO₂ and HCO₃⁻], growth rates of the algal species may have become restricted by carbon, as has been shown previously for dinoflagellates (Hansen et al. 2007).

For plankton communities, pH changes have been shown to drive species succession, because many planktonic algae appear to be quite sensitive to high pH (Hansen 2002; Pedersen and Hansen 2003). However, possible role of elevated pH in the succession of Arctic sea ice algae has received little attention. The succession experiment carried out in the present study suggested that elevated pH may well drive species succession, as the pH-tolerant species (*Chlamydomonas sp.*) out-grew the two sea ice diatoms (Fig. 4). However, how can we be sure that the observed succession pattern in the study is due to pH changes and not due to for instance production of toxic substances (allelochemicals) that affect the growth of the two diatoms? Well, we cannot completely out rule that the chlorophyte exudes allelochemicals, as we did not test this specifically. However, no marine chlorophytes have yet been

Table 1 Estimated uptake of C, N, and P in pH-drift experiments at dissolved inorganic carbon concentration (TCO₂) of 2.4 and 1.4 mM in *Fragilariopsis nana*, *Fragilariopsis sp.*, and *Chlamydomonas sp.* cultures that have reached maximum cell concentration in L1 medium

Algae species	Maximum cell concentration (cell ml ⁻¹)	TCO ₂ initial 2.4 mM					
		C uptake (μm)	N uptake (μm)	P uptake (μm)	C uptake (μm)	N uptake (μm)	P uptake (μm)
<i>Fragilariopsis nana</i>	4.1 × 10 ⁵	919	139	8.7	329	50	3.1
<i>Fragilariopsis sp.</i>	2.4 × 10 ⁵	887	139	8.4	405	61	3.8
<i>Chlamydomonas sp.</i>	4.0 × 10 ⁵	1,384	209	13.0	398	60	3.8

Addition of N and P to the seawater in L1 medium was 1,111 and 47 μm, respectively. Estimation was based on a Redfield ratio of 106C:16N:1P

convincingly shown to produce allelochemicals (see review by Granéli and Hansen 2006). Secondly, the growth of the two diatom species in the mixed culture experiment can be explained by pH changes alone, and there are no indications in our data set which suggest that allelochemicals were produced. Our study has only dealt with a few species of ice algae. Thus, much more attention is required in this topic. It would be particularly interesting to study how elevated pH and therefore decreasing TCO₂ affects in situ succession pattern and the growth rates of the algal species in the sea ice.

Conclusions

Our results suggest that the three sea ice algal species have different tolerance to fluctuations in salinity and pH. The results suggest that the three sea ice algal species were mainly limited by pH, whereas TCO₂ concentrations only played a role at high pH levels and low TCO₂ concentrations. The salinity stress had the smallest effect on the growth rate of the two diatoms compared to the effect on the chlorophyte. This suggests that sea ice diatoms are less affected by salinities changes and thus may have a competitive advantage compared to the chlorophyte in sea ice with rapid fluctuations in salinity. Finally, the fluctuations in pH levels may drive species succession of sea ice algae. The chlorophyte was able to tolerate much higher pH levels than the two diatom species. Thus, *Chlamydomonas* sp. was able to grow even at high pH levels in the succession experiment and therefore outcompeted the two diatom species.

Consequently, sea ice algal species, which are able to grow at fluctuating pH and salinity conditions, may have an advantage in surviving in the harsh environment of forming and melting sea ice.

Acknowledgments We thank Anna Haxen and Michael R. Schrøder for assistance in field and laboratory and Thomas Juul-Pedersen, Kristine Arendt and Paul Batty for valuable comments. Furthermore, we want to thank Nina Lundholm from the Scandinavian Culture Collection of Algae and Protozoa, Department of phycology, University of Copenhagen for providing the diatom *Fragilariopsis nana*. The study received financial support from the Danish Agency for Science, Technology and Innovation, KVUK Commission for Scientific Research in Greenland and is a part of the Greenland Climate Research Centre (GCRC 6507) and a contribution to the Nuuk Basic and Zackenberg Basic programmes.

References

- Arrigo KR, Sullivan CW (1992) The influence of salinity and temperature covariation on the photophysiological characteristics of Antarctic sea ice microalgae. *J Phycol* 28:746–756
- Arrigo KR, Mock T, Lizotte MP (2010) Primary producers and sea ice. In: Thomas DN, Dieckmann GS (eds) *Sea ice*, 2nd edn. Blackwell Science, Oxford, pp 283–325
- Bates SS, Cota GF (1986) Fluorescence induction and photosynthetic responses of arctic ice algae to sample treatment and salinity. *J Phycol* 22:421–429
- Cota GF, Horne EPW (1989) Physical control of arctic ice algal production. *Mar Ecol Prog Ser* 52:111–121
- Cox GFN, Weeks WF (1983) Equations for determining the gas and brine volume in sea ice samples. *J Glaciol* 29:306–316
- Dieckmann GS, Nehrke G, Papadimitriou S, Göttlicher J, Steininger R, Kennedy H, Wolf-Gladrow D, Thomas DN (2008) Calcium carbonate as ikaite crystals in Antarctic sea ice. *Geophys Res Lett* 35:L08501. doi:10.1029/2008GL033540
- Garrison DL, Buck KR (1986) Organisms losses during melting: a serious bias in sea ice community studies. *Polar Biol* 6:237–239
- Gleitz M, Thomas DN (1992) Physiological responses of a small Antarctic diatom (*Chaetoceros* sp.) to simulated environmental constraints associated with sea ice formation. *Mar Ecol Prog Ser* 88:271–278
- Gleitz G, Rutgers VD, Thomas DN, Dieckmann GS, Millero FJ (1995) Comparison of summer and winter inorganic carbon, oxygen and nutrient concentrations in Antarctic sea ice brine. *Mar Chem* 51:81–91
- Gradinger R (1999) Vertical fine structure of the biomass and composition of algal communities in Arctic pack ice. *Mar Biol* 133:745–754
- Granéli E, Hansen PJ (2006) Allelopathy in harmful algae: a mechanism to compete for resources? In: Granéli E, Turner JT (eds) *Ecology of Harmful Algae*, Ecological Studies series of Springer-Verlag, vol 189. Springer, Chap 15 pp 189–201
- Grant WS, Horner RA (1976) Growth responses to salinity variation in four Arctic ice diatoms. *J Phycol* 12:180–185
- Guillard RRL, Hargraves PE (1993) *Stichochrysis immobilis* is a diatom, not a chrysophyte. *Phycologia* 32:234–236
- Hansen PJ (2002) The effect of high pH on the growth and survival of marine phytoplankton: implications for species succession. *Aquat Microb Ecol* 28:279–288
- Hansen JW, Thamdrup B, Jørgensen BB (2000) Anoxic incubation of sediment in gas-tight plastic bags: a method for biogeochemical process studies. *Mar Ecol Prog Ser* 208:273–282
- Hansen PJ, Lundholm N, Rost B (2007) Growth limitation in marine red-tide dinoflagellates: effects of pH versus inorganic carbon availability. *Mar Ecol Prog Ser* 334:63–71
- Hellebust JA (1985) Mechanisms of response to salinity in halotolerant microalgae. *Plant Soil* 89:69–81
- Huertas IE, Colman B, Espie GS, Lubian LM (2000) Active transport of CO₂ by the three species of marine microalgae. *J Phycol* 36:314–320
- Ikävalko J, Thomsen HA (1997) The Baltic Sea ice biota (March 1994): a study of the protistan community. *Eur J Protistol* 33:229–243
- Korb RE, Saville PJ, Johnston AM, Raven J (1997) Sources of inorganic carbon for photosynthesis by three species of marine diatoms. *J Phycol* 33:433–440
- Kühl M, Glud RN, Borum J, Rygaard S (2001) Photosynthetic performance of surface-associated algae below sea ice as measured with a pulse-amplitude-modulated (PAM) fluorometer and O₂ microsensors. *Mar Ecol Prog Ser* 223:1–14
- Lewis E, Wallace D (1998) Program developed for CO₂ system calculations. Environmental Science Division. No. 4735
- Lizotte MP (2003) The microbiology of sea ice. In: Thomas DN, Dieckmann GS (eds) *Sea ice an introduction to its physics, chemistry, biology and geology*. Blackwell Science, Oxford, pp 184–210

- Lundholm N, Hansen PJ, Kotaki Y (2004) Effect of pH on growth and domoic acid production by potentially toxic diatoms of the genera *Pseudo-nitzschia* and *Nitzschia*. *Mar Ecol Prog Ser* 273:1–15
- Mikkelsen DM, Witkowski A (2010) Melting sea ice for taxonomic analysis: a comparison of four melting procedures. *Polar Res*. doi:10.1111/j.1751-8369.2010.00162.x
- Mikkelsen DM, Rysgaard S, Glud RN (2008) Microalgal composition and primary production in Arctic sea ice: a seasonal study from Kobbefjord (Kangerluarsunnguag), West Greenland. *Mar Ecol Prog Ser* 368:65–74
- Misra AN, Srivastava A, Strasser RJ (2001) Utilization of fast chlorophyll a fluorescence techniques in assessing salt/ion sensitivity of mung bean and Brassica seedlings. *J Plant Physiol* 158:1173–1181
- Palmisano AC, Garrison DL (1993) Microorganisms in Antarctic sea ice. In: Friedmann EI (ed) *Antarctic microbiology*. Wiley-Liss, New York, pp 167–218
- Palmisano AC, SooHoo JB, Sullivan CW (1987) Effects of four environmental variables on photosynthesis-irradiance relationships in Antarctic sea ice microalgae. *Mar Biol* 94:299–306
- Papadimitriou S, Thomas DN, Kennedy H, Hass C, Kuosa H, Krell A, Dieckmann GS (2007) Biochemical composition of natural sea ice brines from the Weddell Sea during early austral summer. *Limnol Oceanogr* 52:1809–1823
- Pedersen MF, Hansen PJ (2003) Effects of high pH on a natural marine planktonic community. *Mar Ecol Prog Ser* 260:19–31
- Ralph PJ, McMinn A, Ryan KG, Ashworth C (2005) Short-term effect of temperature on the photokinetics of microalgae from the surface layers of Antarctic pack ice. *J Phycol* 41:763–769
- Reinfelder JR, Kraepiel AM, Morel FM (2000) Unicellular C4 photosynthesis in a marine diatom. *Nature* 407:996–999
- Rost B, Riebesell U, Burkhardt S, Sültermeyer D (2003) Carbon acquisition of bloom-forming marine phytoplankton. *Limnol Oceanogr* 48:55–67
- Ryan KG, Ralph PJ, McMinn A (2004) Acclimation of Antarctic bottom-ice algal communities to lowered salinities during melting. *Polar Biol* 27:679–686
- Rysgaard S, Glud RN, Sejr MK, Bendtsen J, Christensen PB (2007) Inorganic carbon transport during sea ice growth and decay: A carbon pump in polar seas. *J Geophys Res* 112:C03016. doi:10.1029/2006JC003572
- Søderberg LM, Hansen PJ (2007) Growth limitation due to high pH and low inorganic carbon concentrations in temperate species of the dinoflagellate genus *Ceratium*. *Mar Ecol Prog Ser* 351:105–112
- Søgaard DH, Kristensen M, Rysgaard S, Glud RN, Hansen PJ, Hilligsøe KM (2010) Autotrophic and heterotrophic activity in Arctic first-year sea ice: seasonal study from Malene Bight, SW Greenland. *Mar Ecol Prog Ser* 419:31–45
- Stumm W, Morgan J (1996) *Chemical equilibria and rates in natural waters*. Aquatic chemistry. Wiley, New York
- Thiel H, Pörtner HO, Arntz WE (1996) Marine life at low temperatures—a comparison of polar and deep-sea characteristics. *Biosys Ecol Ser* 11:183–219
- Thomas DN, Kennedy H, Kattner G, Gerdes D, Gough C, Dieckmann GS (2001) Biogeochemistry of platelet ice: its influence on particle flux under fast ice in the Weddell Sea, Antarctica. *Polar Biol* 24:486–496
- Thomas DN, Papadimitriou S, Michel C (2010) Biogeochemistry of sea ice. In: Thomas DN, Dieckmann GS (eds) *Sea ice*, 2nd edn. Blackwell Science, Oxford, p 432
- Tortell PD, Reinfelder JR, Mortel FMM (1997) Active uptake of bicarbonate by diatoms. *Nature* 390:243–244
- Trimborn S, Lundholm N, Thoms S, Richter K-U, Krock B, Hansen PJ, Rost B (2008) Inorganic carbon acquisition in potentially toxic and non-toxic diatoms: the effect of pH-induced changes in the seawater carbonate chemistry. *Physiol Plant* 133:92–105
- Weeks WF, Ackley SF (1986) The growth, structure and properties of sea ice. In: Understeiner N (ed) *The geophysics of sea ice*. Martinus Nijhoff Publisher, Dordrecht

PAPER VI



Photo: Michael Fischer.

Short-term variability in bacterial abundance, cell properties, and incorporation of leucine and thymidine in subarctic sea ice

H. Kaartokallio • D. H. Søgaard • L. Norman • S. Rysgaard • J.-L. Tison • B. Delille • D. N. Thomas

Aquatic Microbial Ecology 71:57 – 73, doi: 10.3354/ame01667

Short-term variability in bacterial abundance, cell properties, and incorporation of leucine and thymidine in subarctic sea ice

H. Kaartokallio^{1,*}, D. H. Søgaard^{2,3}, L. Norman⁴, S. Rysgaard^{2,5,6},
J.-L. Tison⁷, B. Delille⁸, D. N. Thomas^{1,4,5}

¹Marine Research Center, Finnish Environment Institute, Erik Palmenin aukio 1 00560, Helsinki, Finland

²Greenland Climate Research Centre, c/o Greenland Institute of Natural Resources, Kivioq 2, Nuuk 3900, Greenland

³University of Southern Denmark, Campusvej 55, 5230 Odense M, Denmark

⁴School of Ocean Sciences, Bangor University, Menai Bridge, Anglesey LL59 5AB, UK

⁵Arctic Research Centre, Aarhus University, C.F. Møllers Allé 8, Bldg. 1110, 8000 Aarhus C, Denmark

⁶Centre for Earth Observation Science, 535 Wallace Building, University of Manitoba, Winnipeg R3T 2N2, Canada

⁷Glaciology Unit, Department of Earth and Environmental Science, Université Libre de Bruxelles, ULB CP 160/03 50 Avenue F. D. Roosevelt, 1050 Bruxelles, Belgium

⁸Unité d'Océanographie Chimique, MARE, Université de Liège, Allée du 6 Août, 17-4000 Liège, Belgium

ABSTRACT: Sea ice is a biome of immense size and provides a range of habitats for diverse microbial communities, many of which are adapted to living at low temperatures and high salinities in brines. We measured simultaneous incorporation of thymidine (TdR) and leucine (Leu), bacterial cell abundance and cell population properties (by flow cytometry) in subarctic sea ice in SW Greenland. Short-term temporal variability was moderate, and steep environmental gradients, typical for sea ice, were the main drivers of the variability in bacterial cell properties and activity. Low nucleic acid (LNA) bacteria, previously linked to oligotrophic ecotypes in marine habitats, were more abundant in the upper ice layers, whereas high nucleic acid (HNA) bacteria dominated in lower ice, where organic carbon was in high concentrations. Leu incorporation was saturated at micromolar concentrations, as known from freshwater and marine biofilm systems. Leu:TdR ratios were high (up to >300) in lowermost ice layers, and when compared to published respiration measurements, these results suggest non-specific Leu incorporation. There was evidence of polyhydroxyalkanoate (PHA)-containing bacteria in the sea ice, shown by brightly fluorescing intracellular inclusions after Nile Blue A staining. High Leu saturating concentrations coupled with the occurrence of PHA-producing organisms further highlight the similarity of sea ice internal habitats to biofilm-like systems rather than to open-water systems.

KEY WORDS: Sea ice · Bacteria · Temporal variability · Leucine · Thymidine · Flow cytometry · Polyhydroxyalkanoates

Resale or republication not permitted without written consent of the publisher

INTRODUCTION

Sea ice is a defining feature of the marine ecosystems of polar and some subarctic seas, and is an ephemeral biome of immense size comparable to the world's deserts or grasslands (Thomas & Dieckmann

2002, 2010). Sea ice has characteristically strong and highly variable gradients in temperature, salinity, space and light that are ultimately governed by air temperature and depth of snow cover (Thomas & Dieckmann 2002). The internal sea ice habitat, i.e. small pores and channels filled with hyper-saline

*Email: hermanni.kaartokallio@ymparisto.fi

© Inter-Research 2013 · www.int-res.com

brines, can be thought of as resembling biofilm-like systems due to the high densities of organisms and large amounts of exopolymeric substances (EPS) produced by both sea ice algae and bacteria (Krembs & Deming 2008, Underwood et al. 2010, 2013, Krembs et al. 2011). It is also an extreme habitat since salinity varies as a function of ice temperature and can exceed 200, and the temperature is constantly below seawater freezing temperature, reaching down to -30°C in the uppermost parts of the ice on occasions (Petrich & Eicken 2010).

Heterotrophic bacteria are the most abundant organism group in ice and important in terms of carbon cycling and biodiversity. The typical bacteria found in sea ice in all ice-covered marine waters belong to the *Bacteroidetes* (e.g. *Flavobacteria*) as well as *Alpha*- and *Gammaproteobacteria*, although other bacterial groups are also found (Deming 2010). Dissolved organic carbon and nitrogen resources are generally thought to be non-limiting for bacteria in sea ice (Pomeroy & Wiebe 2001, Thomas et al. 2010). Many of the sea ice bacteria are copiotrophs, and up to 60% of them can be cultured (Junge et al. 2002).

Generally marine bacteria can be divided into high nucleic acid (HNA) bacteria and low nucleic acid (LNA) bacteria based on their DNA content detected by flow cytometry, and also related to cell size (Gasol & del Giorgio 2000, Lebaron et al. 2001). Bacteria in sea ice have been enumerated by flow cytometry (Fransson et al. 2011, Martin et al. 2011, Mundy et al. 2011), although the proportions of HNA and LNA populations in the total bacterial abundance have not been reported. HNA bacteria are often attributed to the dynamic part of the bacterial community that is able to respond to changes in nutrient and carbon availability (Morán et al. 2007), whereas abundance of LNA bacteria is generally linked to oligotrophic ecotypes in both freshwater and marine environments (Mary et al. 2006, Wang et al. 2009). In sea ice, algal and bacterial biomass is often concentrated in lower ice layers, and HNA and LNA bacteria can be expected to exist in different proportions in different horizons of the ice; for example, Collins et al. (2010) found dominance of SAR11 cluster bacteria in upper horizons of winter Arctic sea ice, a group whose single cultivated member is an obligate oligotroph (Rappé et al. 2002).

Since the late 1980s, bacterial production in sea ice has been measured, to our knowledge, in less than 15 studies in both polar oceans and the Baltic Sea. These have primarily used thymidine (TdR, Fuhrman & Azam 1980, 1982) or leucine (Leu, Kirchman et al. 1985) incorporation methods, both widely utilized in

aquatic studies. TdR and Leu methods are based on biochemical theory allowing incorporation of radiochemical tracer by DNA (TdR) or protein (Leu) synthesis to be extrapolated into bacterial cell or biomass growth. Bacterial production measurements in sea ice have mostly been made on melted ice samples (e.g. Smith & Clement 1990, Mock et al. 1997, Søgaard et al. 2010), brines extracted from ice cores or ice cube/crush slurries (e.g. Kottmeier et al. 1987, Helmke & Weyland 1995, Kaartokallio 2004). Normally only one of the incorporation methods has been applied, and measurements combining both tracers are limited to the Antarctic (Grossmann & Dieckmann 1994) and Baltic Sea ice (Mock et al. 1997, Kaartokallio et al. 2006, 2008, Kuosa & Kaartokallio 2006). To our knowledge, dual-labeling has never been done in Arctic or subarctic sea ice investigations. Previous studies in polar and sub-polar sea ice have mostly used only one tracer or revealed conflicting or unclear patterns of Leu and TdR incorporation (Grossmann & Dieckmann 1994, Helmke & Weyland 1995, Guglielmo et al. 2000, Pusceddu et al. 2008).

The aim of this paper was to study short-term temporal variability in ice bacterial abundance, cell properties and production with particular emphasis on use of both Leu and TdR methods and the saturation kinetics of the tracers employed. We also applied flow cytometry to study nucleic acid content and apparent size of bacterial cells.

MATERIALS AND METHODS

Sampling

Sampling was conducted from 11 to 15 March 2010 in first-year land fast ice in a small fjord belonging to Kangerluat fjord system in SW Greenland, close to the Kapisillit settlement ($64^{\circ} 26' \text{N}$, $50^{\circ} 13' \text{W}$). Further details are given by Long et al. (2012) and Søgaard et al. (2013). Sampling was done over 5 consecutive days at the same sampling site (within 10 m^2), situated approximately 100 m from the fast ice edge. The water depth at the sampling site was 42 m. The sea ice thickness was 64 cm and snow thickness was 2 cm over the entire study period.

On each sampling occasion, 2 to 4 ice cores were retrieved within an area of 0.5 m^2 with a Kovacs MARK II CRREL-type core auger. The first core was used for determination of bacterial activity, cell counts and population characteristics. The second was used for salinity, dissolved organic matter (DOM) and inorganic nutrient determinations. The

remaining cores were used for more detailed salinity, temperature and brine volume profile determination. For investigation of small-scale variability, 5 separate 10 cm ice top sections were retrieved on each sampling day and analyzed in the same way as the second core above. The first 2 cores were sectioned using a stainless steel hand saw within minutes from retrieval. As biomass is typically concentrated in the lowermost centimeters of ice, a 4 cm section was cut from the bottom, and the remaining core was divided into 12 cm sections. Ice sections were put into 1 l plastic pots and transported to the laboratory.

Bacterial production was measured immediately after sampling using crushed ice, for the other variables, samples were processed after complete melting in a cool laboratory deck. Direct melting was used for all ice samples. Water samples were obtained immediately below the ice and, on Days 3 and 5, also from 9 m under the ice using a peristaltic pump (Cole-Palmer, Master Flex, E/P) with trace metal-free tygon tubing.

To construct detailed ice temperature, salinity and brine volume profiles, temperature and salinity were measured on Days 1, 3 and 5 with a 4 cm depth resolution. Temperature was measured, *in situ*, directly after extraction of the cores, using a calibrated probe (Testo 720) inserted in pre-drilled holes (perpendicular to core side) at the exact diameter of the probe and with a depth resolution of 4 cm. The precision of the measurements was $\pm 0.1^\circ\text{C}$. Bulk ice salinity measurements were centered on the temperature probe measurements. The temperature core was immediately sliced in the field and stored in polyethylene containers, and left to melt in the laboratory. Salinities were measured after melting at room temperature, with a portable salinometer (Orion Star Series Meter) with a precision of ± 0.1 .

To get additional information on bacteria moving with the brine in the ice, brines were collected by coring sackholes at about 40 (sackhole 1) and 50 (sackhole 2) cm depth, to allow gravity-driven brine collection (Thomas & Dieckmann 2010). Brines were collected after 15 to 45 min (depending on the rate of percolation into the hole) using the portable peristaltic pump described above for temperature, salinity and further measurements.

The theoretical brine volume fraction (V_b/V , Eq. 1) and brine salinity (S_b , Eq. 2) are calculated from ice temperature (T) and bulk ice salinity (S) using the formulae of Petrich & Eicken (2010), neglecting the air volume fraction (V_a/V) and using the coefficients $F1(T)$ and $F2(T)$ from Cox & Weeks (1983) to define 2 empirical functions related to the temperature. ρ_i and S_i are pure ice density and bulk ice salinity respectively.

$$V_b/V = (1 - V_a/V) (\rho_i/1000) S_i / [F1(T) - (\rho_i/1000) S_i F2(T)] \quad (1)$$

$$S_b (\text{‰}) = (1 - 54.11/T)^{-1} \times 1000 \quad (2)$$

Salinity, dissolved organic carbon/nitrogen and inorganic nutrients

To obtain the salinity value corresponding to inorganic nutrients, the salinity of melted ice, brine and water samples was measured at laboratory temperature using a SEMAT Cond 315i/SET salinometer with a WTW Tetracon 325 probe. Samples were filtered through Whatman GF/F syringe filters (pore size 0.45 μm), stored on ice and frozen (-18°C) on return to the laboratory until further analysis. The concentrations of the major dissolved inorganic nutrients, nitrate (NO_3^-), nitrite (NO_2^-), SRP (soluble reactive phosphorus), and silicic acid ($\text{Si}(\text{OH})_4$) were determined by standard colorimetric methods (Grasshoff et al. 1983) as adapted for flow injection analysis (FIA) on a LACHAT Instruments Quick-Chem 8000 autoanalyzer (Hales et al. 2004). The concentration of dissolved ammonium (NH_4^+) was determined with the fluorimetric method of Holmes et al. (1999) using a HITACHI F2000 fluorescence spectrophotometer. Dissolved organic nitrogen (DON) concentrations were determined by subtraction of the concentration of dissolved inorganic nitrogen ($\text{DIN} = [\text{NO}_2^-] + [\text{NO}_3^-] + [\text{NH}_4^+]$) from that of the total dissolved nitrogen (TDN) determined by FIA on the LACHAT autoanalyzer using on-line peroxodisulfate oxidation coupled with UV radiation at pH 9.0 and 100°C (Kroon 1993). The concentrations of dissolved organic carbon (DOC) were determined by high temperature combustion of acidified samples on an MQ 1001 TOC Analyzer (Qian & Mopper 1996).

Bacterial abundance and cell population characteristics

Bacterial abundance and cell population characteristics were determined by flow cytometry following the methods outlined by Gasol et al. (1999) and Gasol & del Giorgio (2000). Samples for determination of bacteria abundances were fixed with 0.2 μm filtered electron microscopy-grade glutaraldehyde (final concentration of 0.5%) and stored at 4°C . Cells were stained with SYBR Green I (Molecular Probes) and samples were analyzed with an LSR II flow cytometer (BD Biosciences) using a 488 nm laser. A known

amount of CountBright absolute counting beads (Molecular Probes) were added to each sample to calculate the accurate measured volume of each sample. Bacterial data were typically acquired until 50 000 events were recorded and HNA and LNA cell populations identified from bivariate plots of green fluorescence (FITC) vs. right-angle light scatter (SSC). Gating analysis was performed using FACS Diva software (BD Biosciences). Cell abundance was calculated from processed sample volumes and number of events recorded. In addition, the median SSC parameter was defined for each cell population.

Microscopic detection of polyhydroxyalkanoate-containing bacteria

Potential polyhydroxyalkanoate (PHA) production in bacteria was identified using a modification of the widely used Nile Blue A staining method of Ostle & Holt (1982) as follows: 5 ml of each sample (same samples as for flow cytometry) were filtered onto a black 0.2 μm polycarbonate filter (Osmonics) and stained for 15 min with 0.2 μm -filtered 1% (w/v) aqueous solution of Nile Blue A sulfate (Sigma Aldrich). After staining, filters were rinsed 3 times with deionized water to remove excess stain. Filters were examined using a Leitz Aristoplan epifluorescence microscope with blue excitation (I3 filter) and a PL Fluotar 100 \times 12.5/20 oil-immersion objective. Cells with orange-fluorescing bodies within them were imaged using a Photometrics CH250/A charged-couple device camera connected to a Leitz Aristoplan epifluorescence microscope and PMIS image-acquisition software. In addition to PHA, Nile Blue A can also selectively stain neutral lipid or wax ester inclusions inside bacterial cells. However, the production of these compounds has only been reported in a limited number of bacterial phyla that do not generally occur in sea ice (Ishige et al. 2003, Wältermann & Steinbüchel 2005, Deming 2010). In contrast, the ability to produce PHA is widespread among prokaryotes.

TdR and Leu incorporation, bacterial production

For the measurement of bacterial production, samples containing a known amount of ice crush and seawater (Kaartokallio 2004) were prepared as follows: Each intact 5 to 10 cm ice core section was crushed using a spike and electrical ice cube crusher. Approximately 10 ml of crushed ice was placed in a

scintillation vial and weighed (with an accuracy of ± 0.1 g). To maintain salinity and ensure even distribution of labeled substrate, 2 to 4 ml sterile-filtered (through 0.2 μm Sartorius minisart syringe filters) seawater was added to the scintillation vials. All ice processing work was done in a cool laboratory deck at near-zero temperatures.

Bacterial production was measured using ^{14}C -Leu (Kirchman et al. 1985) and ^3H -TdR (Fuhrman & Azam 1980, 1982) incorporation methods and dual labeling. Two replicate samples and a formaldehyde-killed absorption blank were amended with L-[U- ^{14}C] Leu (PerkinElmer, specific activity 324 mCi mmol^{-1}) diluted with carrier Leu at a proportion of 1:5 and [methyl- ^3H] TdR (PerkinElmer, specific activity 20 Ci mmol^{-1}). Working concentrations of 20 nmol l^{-1} for TdR (all sample types) and 1000 nmol l^{-1} (ice and brine samples) and 500 nmol l^{-1} (water samples) for Leu were used. We used high concentrations of Leu exceeding typical concentrations used for seawater by 2 orders of magnitude, whereas the TdR concentrations used were of same order of magnitude as typically used for marine waters. The choice of the concentrations had to be made in advance due to the logistical constraints of working at a remote field station and the lack of opportunity to re-evaluate the working concentrations during the investigation. The concentrations were based on previous experience with Baltic Sea ice (Kaartokallio 2004, Kaartokallio et al. 2006).

Samples were incubated in the dark in a seawater-ice crush water bath (at $-0.5 \pm 0.3^\circ\text{C}$) for 17 to 18 h, and incubations were stopped by adding formaldehyde. Samples were processed using a standard cold trichloroacetic acid (TCA) extraction (with 5% TCA) and filtration procedure (using Advantec MFS 0.2 μm MCE filters). A Wallac Win-Spectral 1414 counter and InstaGel (Perkin-Elmer) cocktail were used for scintillation counting. Bacterial production was calculated using a cell conversion factor of 2.09×10^{18} cells mol^{-1} , cell volume of $0.473 \mu\text{m}^3$ and carbon conversion factor of $0.12 \text{ pg C } \mu\text{m}^3$ for TdR (Smith & Clement 1990). Leu-based bacterial production was calculated using a factor of $3.0 \text{ kg C } \text{mol}^{-1}$ (Bjørnsen & Kuparinen 1991).

A saturation kinetics experiment was conducted on Day 2 for both TdR and Leu and the 3 major sample types. Ice samples were combined from 4 separate bottom ice sections taken alongside the normal sampling on Day 2, brine was sampled from the upper brine horizon on Day 1 (sackhole depth approximately 40 cm) and water was taken from 9 m depth on Day 2. The concentrations used were 5, 10, 14, 30

and 50 nmol l⁻¹ TdR for all sample types, 200, 700, 1500, 2000 and 2500 nmol l⁻¹ Leu for ice and brine samples, and 100, 350, 750, 1000 and 1250 nmol l⁻¹ Leu for water samples.

Experimental data were fitted with the single kinetic Michaelis-Menten equation $V = V_{\max} \times S / (K_t + S_n + S)$, (where V = incorporation rate, V_{\max} = maximum incorporation rate, $K_t + S_n$ = apparent half-saturation constant, i.e. half-saturation constant + natural leucine/thymidine concentration), S = added leucine/thymidine concentration), using SigmaPlot 10 software (SPSS). Saturating concentrations were defined as substrate concentrations where 90% of V_{\max} was reached and calculated as $V_{\max 90} = 9 \times K_t + S_n$ (Ayo et al. 2001). Isotope dilution was assessed as a ratio of V_{\max} and V_{measured} at the saturating concentration (van Looij & Riemann 1993, Buesing & Gessner 2003). Incorporation kinetics experiments were conducted with a 16 h incubation at 4 h intervals for all 3 sample types on Day 3 using water from immediately under the ice, and brine and bottom ice samples from Day 3 sampling.

Statistical analyses

Statistical analyses were done using base, Psych, Vegan and MASS packages of R software (R Development Core Team 2011). Differences between more than 2 sample types were verified using the Kruskal-Wallis rank (KW) sum test with the pairwise Wilcoxon rank sum post hoc test (Wp-h) and Bonferroni adjustment or, when comparing 2 sample types using Wilcoxon rank sum tests (W). For non-metric multidimensional scaling (NMDS), Spearman's rank-order correlations between bacterial and environmental parameters were calculated. NMDS was performed on a Bray-Curtis dissimilarity matrix of bacterial parameters with metaMDS wrapper routine included in the Vegan package (Oksanen et al. 2012). Environmental parameters were fitted on the NMDS plot using the function, *ef*, included in the Vegan package.

RESULTS

For analyses, ice core sections were divided into 3 classes: 'upper ice', the 2 uppermost ice sections (upper-

most 24 cm of ice), 'bottom ice', the lowermost 4 cm ice section at ice-water interface, and 'middle ice', the ice sections between the other 2 classes. Brine samples from both brine sampling horizons as well as water samples from 2 sampling depths were pooled to form sample classes 'brine' and 'water', respectively.

Physical and chemical parameters

Ice temperature, salinity and brine volumes are presented in Fig. 1 and Table 1. Differences in the 3 parameters between sampling days were not statistically significant as verified by the KW tests. The ice temperature varied from -3.8 to -0.8°C, displaying typical near-linear profiles increasing with ice depth (Fig. 1). Ice bulk salinity was significantly higher in bottom ice compared to upper and middle ice (KW² = 17.64, $p < 0.001$, Wp-h both $p < 0.008$). Calculated brine volumes were generally below 10% except in the bottom ice. The underlying water had median salinity of 33.1 with small temporal variability.

Inorganic and organic nutrient concentrations are presented in Table 1. Both DOC and DON concentrations were higher in bottom ice compared to middle and upper ice (KW, DOC: ² = 8.39, $p = 0.015$, DON: ² = 11.89, $p < 0.003$). NO₃⁻ concentrations were significantly higher in bottom ice compared to middle ice (NO₃⁻: ² = 10.61, $p < 0.005$) but not upper ice (Wp-h for DOC, DON and NO₃ all $p < 0.05$). Surprisingly, apart from silicate, brine and ice concentrations of dissolved inorganic nutrients were similar, despite the salinity contrast between bulk ice and

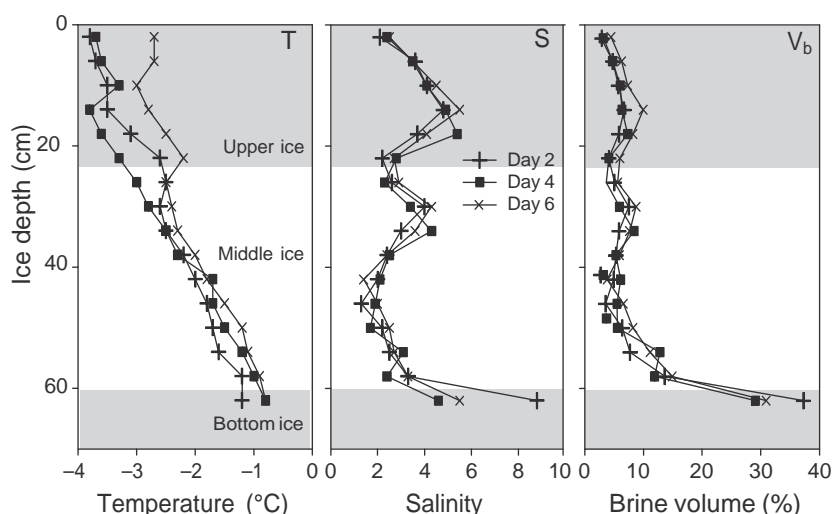


Fig. 1. Temperature (T), salinity (S) and brine volume (V_b) profiles in ice on Days 2, 4 and 6. The 3 ice layers used are indicated by different shading

Table 1. Salinity, inorganic nutrients, dissolved organic carbon (DOC) and nitrogen (DON) in melted sea ice, brine and water. SRP = soluble reactive phosphorus, Si = silicic acid (Si(OH)₄). Mean, range (in parentheses) and standard deviation for each sample class are given

	Upper ice	Middle ice	Bottom ice	Brine	Water
Salinity	3.42 (2.90–4.00) 0.46, n=10	2.55 (1.8–3.5) 0.62, n=15	5.18 (4.6–6.1) 0.66, n=5	48.3 (42.9–55.6) 4.61, n=8	33.1 (32.7–33.4) 0.36, n=3
SRP (μmol l ⁻¹)	0.13 (0.06–0.26) 0.07, n=10	0.19 (0.04–0.72) 0.2, n=15	0.63 (0.1–2.56) 1.08, n=5	0.2 (0.16–0.32) 0.05, n=8	1.42 (0.78–2.56) 0.99, n=3
Si (μmol l ⁻¹)	5.38 (2.80–7.74) 2.16, n=10	4.72 (2.29–7.96) 2.0, n=15	5.97 (5.2–6.7) 0.65, n=5	83.1 (75.6–97.1) 7.43, n=8	6.87 (6.68–7.01) 0.15, n=3
NO ₃ ⁻ (μmol l ⁻¹)	0.77 (0.31–1.66) 0.40, n=10	0.40 (0.06–0.95) 0.2, n=15	0.93 (0.68–1.47) 0.31, n=5	0.82 (0.41–2.2) 0.57, n=8	8.67 (8.60–8.80) 0.12, n=3
NO ₂ ⁻ (μmol l ⁻¹)	0.05 (0.0–0.10) 0.03, n=10	0.04 (0.0–0.11) 0.03, n=15	0.04 (0.0–0.12) 0.05, n=5	0.03 (0.0–0.09) 0.04, n=8	0.07 (0.03–0.11) 0.04, n=3
NH ₄ ⁺ (μmol l ⁻¹)	0.47 (0.01–0.86) 0.27, n=10	0.64 (0.24–2.75) 0.62, n=15	0.71 (0.35–1.34) 0.38, n=5	0.76 (0.56–0.94) 0.11, n=8	0.31 (0.28–0.35) 0.04, n=3
DON (μmol l ⁻¹)	2.51 (1.49–3.06) 0.53, n=8	3.35 (1.64–7.4) 1.48, n=13	6.09 (5.14–7.03) 0.7, n=5	24.3 (21.1–28.0) 2.34, n=8	1.6 (1.50–1.70) 0.1, n=3
DOC (μmol l ⁻¹)	56.0 (34.6–80.9) 12.6, n=10	52.1 (34.2–78.5) 14.9, n=15	80.2 (64.0–106) 17.0, n=5	620 (581–651) 25.6, n=8	62.9 (55.3–68.5) 56.8, n=3
DOC:DON	22.0 (15.9–28.9) 4.8, n=8	16.9 (5.89–26.7) 6.53, n=13	13.1 (11.0–15.2) 1.56, n=5	25.7 (23.2–30.9) 2.64, n=8	39.3 (37.0–42.0) 2.51, n=3

brine. Small scale spatial variability, measured from 5 separate upper ice sections, was lowest for salinity and Si(OH)₄ with a coefficient of variation (CV) of 9%. The CV was 16% for DOC and DOC:DON, 25 to 32% for DON, NO₃⁻, SRP and NH₄⁺, and 54% for NO₂⁻. Temporal variability in the top 12 cm section over the study period was lowest for salinity (CV 2%), 63% for NH₄⁺, and 21 to 41% for all other parameters mentioned above. Temporal variability significantly exceeded small-scale spatial variability in the ice top section as seen in higher average CVs (W = 85, p < 0.0005).

Bacterial abundance, cell population characteristics

Bacterial abundance was rather low in all sample types (Fig. 2), but comparable to the abundances described by Middelboe et al. (2012) in the water column of an adjacent fjord system. Bacterial abundance in ice was highest in the bottom ice layer (KW² = 21.18, p < 0.001, Wp-h p < 0.004). Abundances in water and brines were similar and not significantly different from bottom ice. Bacterial abundance in brine was signifi-

cantly higher than in the corresponding ice sections (W = 120, p < 0.001), but approximately 2 times lower than expected based on the calculated brine volume fraction.

HNA and LNA cells contributed almost equally to the total bacterial abundance in ice. HNA:LNA ratios (Table 2) ranged from 0.66 in upper ice to 1.09 in bottom ice and were significantly different between sample types (KW² = 9.85, p < 0.008). The HNA:LNA ratio in water was only 0.33, and significantly lower than in bottom ice (W = 34, p < 0.05). The HNA

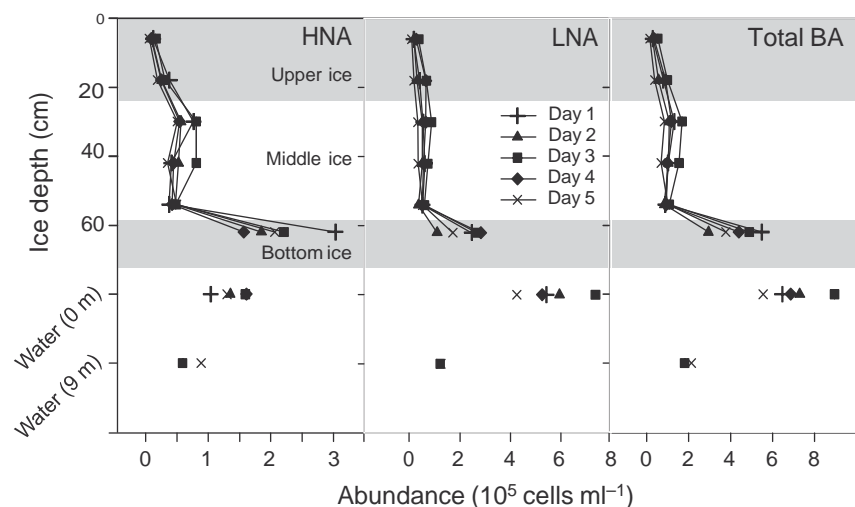


Fig. 2. Abundance of high-nucleic-acid (HNA), low-nucleic-acid (LNA) and total (HNA + LNA) bacteria (BA) in ice layers and underlying water

Table 2. Leucine (Leu) and thymidine (TdR) incorporation, bacterial production (BP) and bacterial abundance in melted sea ice, brine and underlying water. HNA = high nucleic acid, LNA = low nucleic acid. **Mean**, range (in parentheses) and standard deviation for each sample class are given

	Upper ice	Middle ice	Bottom ice	Brine	Water
Leu (pmol l ⁻¹ h ⁻¹)	23.4 (0.9–48.8) 15.1, n=8	24.4 (9.22–52.8) 13.2, n=12	737 (546–1030) 219, n=4	179 (141–229) 27.64, n=8	181.6 (148–210) 25.1, n=5
TdR (pmol l ⁻¹ h ⁻¹)	0.17 (0.02–0.32) 0.10, n=10	0.41 (0.17–0.65) 0.16, n=15	2.55 (1.45–3.8) 1.08, n=5	3.45 (1.84–5.56) 1.21, n=8	2.65 (1.83–3.88) 0.83, n=7
Leu:TdR	145 (41.7–202) 46.7, n=8	60.1 (42.3–85.8) 14.4, n=12	269 (205–313) 46.0, n=4	57.6 (35.7–98.8) 21.4, n=8	69.1 (52.3–80.9) 12.2, n=5
BP Leu (μgC l ⁻¹ h ⁻¹)	0.07 (0–0.15) 0.05, n=8	0.07 (0.03–0.16) 0.04, n=12	2.21 (1.64–3.09) 0.66, n=4	0.54 (0.42–0.69) 0.08, n=8	0.45 (0.03–0.63) 0.23, n=5
BP TdR (μgC l ⁻¹ h ⁻¹)	0.02 (0–0.04) 0.01, n=10	0.05 (0.02–0.08) 0.02, n=15	0.30 (0.17–0.45) 0.13, n=5	0.41 (0.22–0.66) 0.14, n=8	0.32 (0.22–0.46) 0.10, n=7
HNA bacteria (×10 ⁴ cells ml ⁻¹)	1.91 (0.59–3.79) 1.05, n=10	5.32 (3.43–8.08) 1.48, n=15	21.4 (15.7–30.3) 5.54, n=5	25.4 (17.5–34.4) 6.52, n=8	13.0 (8.88–16.1) 2.89, n=7
LNA bacteria (×10 ⁴ cells ml ⁻¹)	3.36 (1.0–6.81) 2.00, n=10	5.49 (3.43–8.83) 1.43, n=15	21.6 (11.0–28.3) 7.31, n=5	21.0 (11.0–36.1) 8.62, n=8	49.2 (12.5–73.7) 20.1, n=7
HNA:LNA	0.61 (0.32–0.97) 0.23, n=10	0.99 (0.67–1.48) 0.24, n=15	1.09 (0.55–1.67) 0.43, n=5	1.30 (0.89–1.77) 0.32, n=8	0.33 (0.19–0.71) 0.19, n=7
Total bacteria (×10 ⁴ cells ml ⁻¹)	5.28 (1.58–9.92) 2.85, n=10	10.9 (6.98–16.9) 2.64, n=15	43.0 (29.4–55.0) 9.9, n=5	46.4 (28.6–68.4) 14.3, n=8	62.2 (21.3–89.6) 23.0, n=7

Table 3. Right-angle light scatter (SSC) parameter for the high (HNA) and low nucleic acid (LNA) populations and cell-specific thymidine (TdR cell⁻¹) and leucine (Leu cell⁻¹) incorporation in sea ice, brine and underlying water. **Mean**, range (in parentheses) and standard deviation for each sample class are given

	Upper ice	Middle ice	Bottom ice	Brine	Water 0 m	Water 9 m
HNA SSC	688 (421–913) 131, n=10	763 (610–914) 97.8, n=15	926 (747–1135) 140, n=5	989 (846–1111) 82, n=8	748 (678–838) 66.5, n=4	512 (499–524) 18, n=2
LNA SSC	444 (327–582) 84, n=10	446 (386–523) 53.4, n=15	375 (283–568) 112, n=5	528 (399–582) 62, n=8	328 (299–349) 18.0, n=5	364 (361–367) 4, n=2
Leu cell⁻¹ (×10 ⁻⁷ pmol cell ⁻¹ h ⁻¹)	7.13 (0.30–30.8) 9.97, n=8	2.38 (0.70–5.21) 1.43, n=12	16.5 (10.8–23.4) 6.48, n=4	4.14 (2.06–5.77) 1.10, n=8	2.69 (2.27–3.13) 0.46, n=5	8.01 n=1
TdR cell⁻¹ (×10 ⁻⁹ pmol cell ⁻¹ h ⁻¹)	5.19 (0.50–18.9) 5.80, n=10	4.02 (1.29–7.02) 1.95, n=15	6.15 (3.45–10.1) 2.89, n=5	7.84 (4.06–12.8) 3.11, n=8	3.85 (2.83–5.07) 0.95, n=5	10.7 n=1

bacteria cell size proxy in brines (mean SSC parameter, Table 3) was significantly higher than in under-ice water, and the upper and middle ice layers ($KW^2 = 23.74$, $p < 0.001$, Wp-h all $p < 0.015$) but there was no significant difference for bottom ice. In ice, HNA SSC was significantly higher in bottom ice than upper ice ($KW^2 = 8.81$, $p < 0.013$, Wp-h $p < 0.04$). Under-ice water had lower mean HNA SSC than bottom ice or brine, although only the differences between brine and water were statistically significant ($W = 36$, $p < 0.008$). The variability of LNA SSC was generally low with significantly higher LNA SSC in brine and middle ice layers as compared to under-ice water ($KW^2 = 21.43$, $p < 0.001$, Wp-h all $p < 0.015$).

TdR and Leu incorporation, bacterial production and respiration

Bacterial production data are presented in Table 2 and Fig. 3. For both Leu and TdR, temporal variability was moderate and pronounced incorporation in the bottom ice occurred throughout the study period. Leu incorporation in the bottom ice significantly exceeded the under-ice water values ($W = 32$, $p < 0.005$), whereas bottom ice and under-ice TdR values were not significantly different. Temporal variability of TdR in under-ice water was higher than for Leu, and both under-ice water and water from 9 m depth had comparable values. In the brines, both Leu and TdR exceeded upper and middle ice values by a fac-

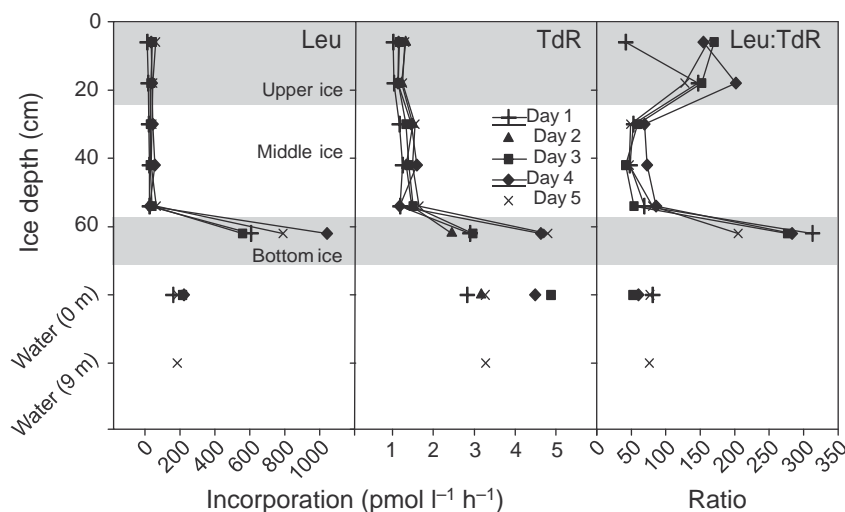


Fig. 3. Leucine (Leu) and thymidine (TdR) incorporation and their ratios in ice and water

tor of 7 to 8, which is in line with the estimated brine volume fraction in the middle layer (Fig. 1). Bacterial production estimates produced with the 2 tracers were not significantly different in middle ice, brine and water, whereas the mean Leu-based production estimates for the upper and bottom ice were significantly higher than the TdR-based estimates, being 3.5 times ($W = 65$, $p < 0.03$) and 7.3 times ($W = 20$, $p < 0.016$) higher, respectively.

To assess whether bacterial productivity measurements gave realistic results they were related to independent oxygen flux measurements from the same site and study period, published by Long et al. (2012). Bacterial respiration was calculated for the bottom ice layer, using 3 different bacterial growth efficiencies and 2 Leu conversion factors to generate a range of values. The bacterial growth efficiency values used were (1) a calculated value of 0.384 according to Rivkin & Legendre (2001), (2) a mean value of 0.386 for a control unit at 0°C presented by Kuparinen et al. (2011), and (3) the high Arctic sea ice-bottom average value of 0.24 from Nguyen & Maranger (2011).

For respiration estimates, theoretical conversion factor extremes of 1.5 and 3.0 kg C mol⁻¹ Leu were used (Simon & Azam 1989), which have also been empirically validated for cold seawater environments (Bjørnsen & Kuparinen 1991, Ducklow et al. 2000, Ducklow 2003). Bacterial carbon respiration was converted to oxygen consumption assuming a respiratory quotient of 1. Ranges and median (in parentheses) values for bottom-ice bacterial respiration for the entire study period were 1.7 to 6.72 (3.37) O₂ m⁻² d⁻¹ for Leu-, and 0.50 to 1.02 (0.52) O₂ m⁻² d⁻¹ for TdR-based production estimates.

Leu:TdR ratios

Leu:TdR ratios in the ice were consistently lowest in the middle ice layers and highest in the upper and bottom ice layers during the sampling period (Fig. 3). The ratio was higher ($W = 32$, $p < 0.005$) in the bottom ice and variability was lower in bottom than in upper ice horizons (Fig. 3). In middle ice layers and brine and under-ice waters, the Leu:TdR ratios were not significantly different. The Leu:TdR ratios in under-ice water were at the higher end of the range reported for other marine systems (Chin-Leo & Kirchman 1990, Kirchman 1992, Shiah & Ducklow 1997).

Saturation and incorporation kinetics

Apparent half-saturation constants ($K_t + S_n$) were variable across sample types for both Leu and TdR tracers (Fig. 4). We did not take natural background concentrations into account in the calculations, and apparent ($K_t + S_n$) values include the ambient Leu and TdR concentrations. The results indicated that, despite the high Leu working concentrations used, the ice samples were still under-saturated in respect to both tracers ($V_{\max 90}$:working concentration ratio was 1.6 for TdR and 2.07 for Leu). In brines, the $V_{\max 90}$:working concentration ratio was 1.8 for TdR, whereas added tracer concentration exceeded the estimated saturation level in brines for Leu and in water for both tracers. Isotope dilution was estimated to be small and varied little across sample types and tracers (range 1.02 to 1.08 for TdR and 1.08 to 1.10 for Leu). V_{\max} values reflecting the maximum incorporation potential in samples were equal in brine and water for both tracers, but 2 times higher for TdR, and an order of magnitude higher for Leu in bottom ice. In a separate incorporation linearity test, the incorporation rates were stable over the 16 h incubation used for both tracers and for all sample types (data not shown).

Cell-specific incorporation

Cell-specific incorporation for Leu and TdR was calculated using total bacterial abundance and incorporation (Table 3). Cell-specific TdR was less variable as a function of ice layer than cell-specific Leu. Cell-

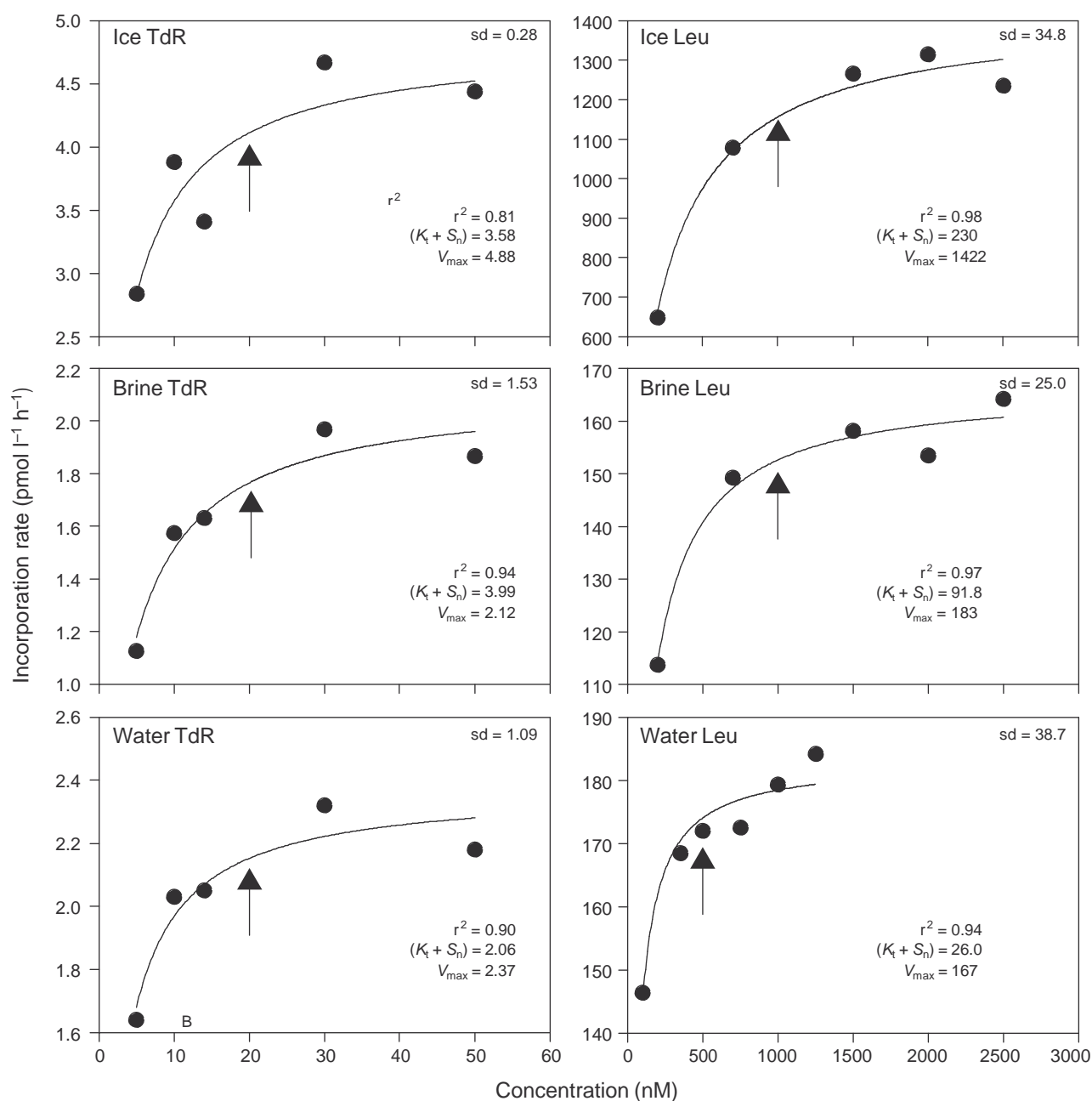


Fig. 4. Saturation experiment results with fitted non-linear Michaelis-Menten kinetics. V_{\max} , $K_t + S_n$ and adjusted r^2 values are shown. The arrows indicate working concentrations used in the measurements. 'sd' denotes the overall standard deviation of all thymidine (TdR) or leucine (Leu) measurements for Days 1 to 3

specific TdR was not significantly different in ice layers ($KW^2 = 2.250$, $p < 0.325$), whereas mean cell-specific Leu was almost 7-fold and significantly higher in the bottom ice ($\chi^2 = 9.037$, $p < 0.011$) compared to middle ice (Wp-h $p < 0.013$), but not upper ice samples ($p < 0.152$). In brines, the cell-specific TdR and Leu were significantly higher than in the middle ice layers (Leu: $W = 79$, $p < 0.016$; TdR: $W = 102$, $p < 0.006$). In the under-ice water, the cell-specific incorporation

was not significantly different from upper and middle ice layers for both tracers, but significantly lower than in bottom ice for Leu ($W = 0$, $p < 0.007$).

NMDS

Following NMDS analysis, different ice layers were separated into distinct clusters (Fig. 5), whereas

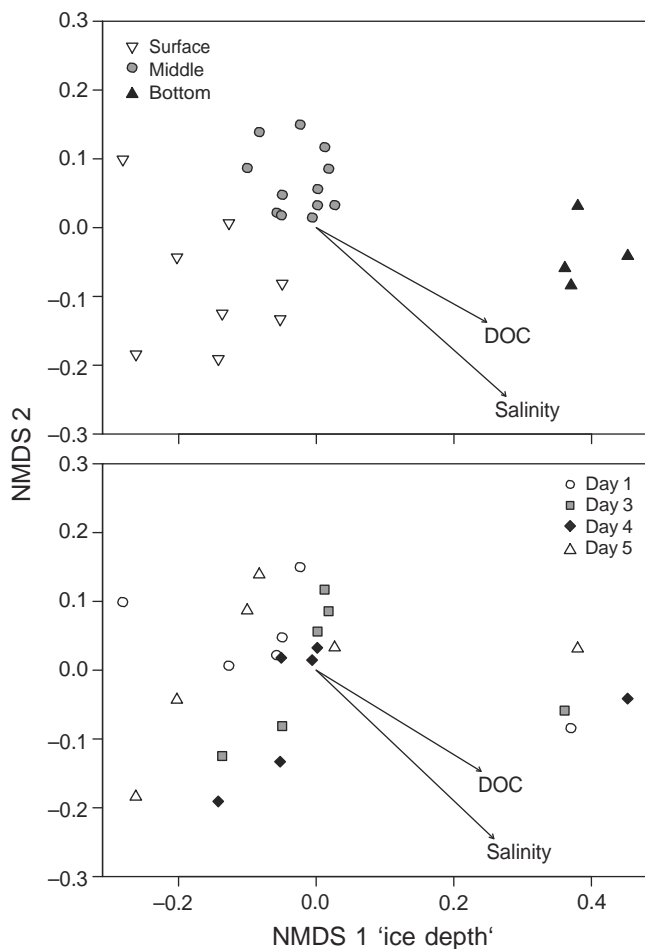


Fig. 5. Non-metric multi-dimensional scaling (NMDS) of bacterial parameters in ice (presented in Table 2) with physicochemical parameters (presented in Table 1) correlated with the distance matrix (correlations with $p < 0.05$ are displayed). Ice sections are plotted in the upper panel and sampling days in the lower panel

sampling days were not different from each other. Based on the NMDS results, the main NMDS axis 1 was identified as 'ice depth'. Parameters presented in Table 1 were correlated with the NMDS distance matrix and only the DOC:DON ratio and salinity were correlated on a 95% significance level. Highest non-significant correlations were with DOC:DON (80% confidence level) and DON, SRP and NO_3^- (70% confidence level).

Cells containing putative PHA granules

Cells containing putative PHA granules (i.e. brightly fluorescing intracellular inclusions observed following the Nile Blue A stain) were found in all ice layers and in the underlying water samples (Fig. 6).

They were most abundant in the bottom ice, although they were only a minor portion of all bacterial cells present. Unfortunately, the method employed did not allow their quantitative determination. Three main morphotypes of 'PHA-containing' cells were found: (1) long filaments with numerous PHA granules inside the cells; (2) shorter filaments or elongated rods with 3 to 4 granules inside the cell; and (3) cells with single and double granules. In doubles, one of the granules was typically brighter, the less-intense granule possibly being inside a daughter cell. All 3 general morphotypes were present in bottom, middle and upper ice, and brine. In the under-ice waters, only single or double granules were observed. Granule-containing bacteria were often associated with diatoms in bottom ice and detrital particles in other parts of the ice. In acridine orange-stained samples, bacterial cells and filaments with visible inclusions corresponding to the shape and size of PHA granules were recorded (not shown).

DISCUSSION

The sea ice sampling design covered both temporal and small-scale spatial variability. Limited assessment of small-scale spatial variability of salinity, dissolved nutrients, DOC and DON indicated that it was significantly lower than the temporal variability over the study period (c.f. Sogaard et al. 2013). The small-scale spatial variability investigation did not include bacterial parameters, but low spatial variability in salinity and nutrients is expected to be reflected in bacterial parameters as, based on NMDS, environmental variables seemed to drive changes in them (see below). Furthermore, snow cover, a major controlling factor for organism biomass variability in lower ice (Gosselin et al. 1986), was low and consistent throughout the study and sampling site. Temporal variability for ice bacterial and background parameters was not pronounced over the 5 d, suggesting that during stable weather conditions and excluding periods of fast biomass increase (ice algal blooms), a single ice sampling event can be temporally representative on weekly scales, a commonly used sampling interval in time series studies including biological parameters (Kaartokallio 2004, Mikkelsen et al. 2008, Sogaard et al. 2010). Pronounced vertical gradients, typical for sea ice and with highest values in the bottom ice, were seen in the salinity and calculated brine volume (Fig. 1) profiles as well as all bacterial parameters (Figs. 2 & 3). Based on the NMDS analysis (Fig. 5), distance from interfaces (water-ice and air-

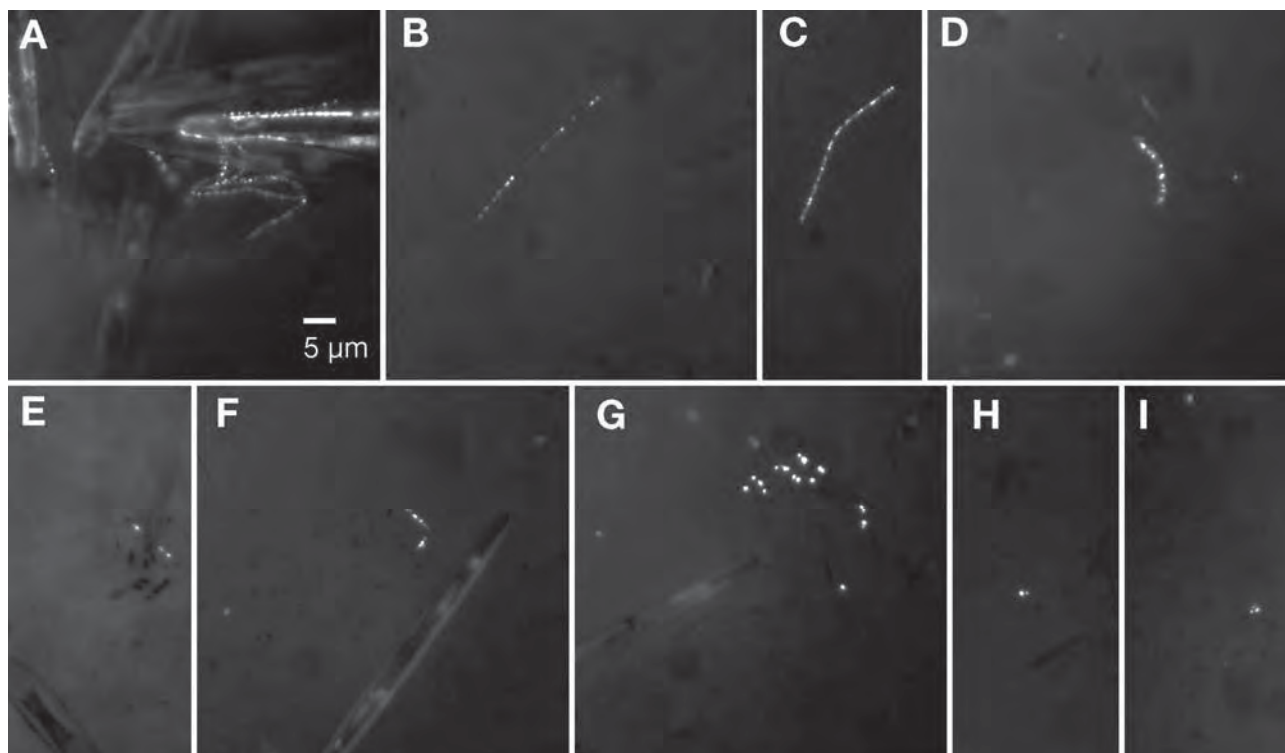


Fig. 6. Photomicrographs of Nile Blue A-stained bacterial cells containing polyhydroxyalkanoate granules. (A to C) Long filaments, (D) cells embedded in exopolymeric substance (EPS) matrix, (E) short filament, (F) long rods with multiple granules and (G to I) single and double granules. (A) to (G) are from bottom ice sections, (H) is from a brine sample and (I) is from an upper ice section

ice interface), which drive the steep environmental gradients, is a key parameter influencing the constitution and activity of the bacterial communities. The observed significant correlations (Fig. 5) between bacterial and environmental variables in NMDS illustrate the effect of environmental drivers on bacterial communities (salinity) or substrate availability produced by ice algae in bottom ice (i.e. DOM).

The proportion of HNA bacteria was higher in bottom ice than in upper ice, where LNA bacteria were dominant (Fig. 2). This observation is supportive of the findings of Collins et al. (2010), who found a dominance of oligotrophic bacterial lineages in upper sea ice layers. In under-ice water, the HNA:LNA ratio was more than 3 times lower than in bottom ice. This pattern is coherent with the assumption of greater carbon availability (as seen in the highest DOC and DON concentrations, Table 1) leading to higher abundance of HNA cells in bottom sections of ice. Also, the HNA bacterial cell size was larger in bottom ice. In the LNA populations, cell size was stable, indicating that the LNA bacteria indeed formed a natural distinct population of small cells (oligotrophs) and were not senescent large HNA bacteria with low nucleic acid content.

Simultaneous sampling of ice and brine provides insights into the partitioning between the brine fraction (that moves inside the brine channel system into the collection sackholes) and the total bacterial community within the ice matrix (that contains the entire bacterial population in ice including brines). We sampled brines at 40 and 50 cm depth, corresponding to the depth of the middle ice layers. The bacteria in brine (Tables 2 & 3) had a higher HNA:LNA ratio, and the cells were larger and more active than those in the whole ice fraction in middle ice layers, indicating that LNA bacteria were present in the upper ice horizons and did not move as readily with brines as HNA bacteria. The sackhole sampling technique used to extract brines is based on gravity drainage of brines and it may lead to under-representation of particulate material or bacteria associated with particles or trapped in EPS. Collins et al. (2010) discuss entrapment in EPS as a potential refuge for oligotrophic bacterial lineages in upper sea ice, which is in keeping with our results of higher proportions of LNA bacteria being retained within the ice matrix and not moving into brine sackholes by gravity.

The low concentrations of SRP and dissolved nitrogenous nutrients in the brines are evidence of

their non-conservative partitioning relative to salinity within the brine channel system. Similar low concentrations of dissolved nutrients in brine have been reported from Antarctic sea ice (Becquevort et al. 2009). As NO_3^- and SRP concentrations in brine and bulk ice were low, and upper and middle ice layers were not biomass-rich, it can be assumed that the reason for similar concentrations was more likely entrapment of nutrients inside the brine channel system than release of nutrients from organisms or particulate matter during direct melting of bulk ice samples (c.f. Thomas et al. 1998). Becquevort et al. (2009) discuss entrapment within EPS as a potential cause for low nutrient concentrations in brines obtained by sackhole sampling, as in this study. For NH_4^+ , direct incorporation into the ice matrix in addition to entrapment in EPS has been discussed by Zhou et al. (2013).

Although the bottom ice and under-ice water represent strongly diverging habitats by nature, the bacterial abundance, activities and cell properties in them were not significantly different (apart from the Leu incorporation and abundance of LNA cells), pointing to the influence of ice cover on waters immediately below the ice (0 m depth). This influence was likely mediated by ice melt and brine transporting sea ice bacteria across the ice-water interface (Long et al. 2012). Nguyen & Maranger (2011) attribute the presence of large bacteria in under-ice water to the immediate proximity of ice in the western Arctic. Belzile et al. (2008) found a higher proportion of HNA bacteria under ice cover in spring compared to the open water season on the Beaufort Shelf, which also indicates the effect of ice on surface water bacterial communities.

In marine pelagic environments, saturation of both TdR and Leu incorporation is typically observed at 5 to 20 nmol l^{-1} extracellular concentrations of labeled substrate (e.g. Fuhrman & Azam 1982, Simon & Azam 1989, Ducklow et al. 2000), whereas saturation levels for Leu in eutrophic or freshwater systems can be an order of magnitude higher (100 to 200 nmol l^{-1} , Jørgensen 1992, van Looij & Riemann 1993, Fischer & Pusch 1999). In biofilms, saturating concentrations of Leu are in the range of 1000 to 2000 nmol l^{-1} (Fischer & Pusch 1999, Törnblom & Søndergaard 1999, Buesing & Gessner 2003, Miranda et al. 2007) and 15 to 100 $\mu\text{mol l}^{-1}$ in freshwater sediments (Tuominen 1995, Fischer & Pusch 1999, Buesing & Gessner 2003). We estimated high saturating concentrations (Fig. 4) for Leu in bottom ice crush samples (2100 nmol l^{-1}) and brine originating from middle ice layers (830 nmol l^{-1}), which were close to the biofilm satu-

rating concentration range and clearly higher than in underlying water (230 nmol l^{-1}).

The use of Leu in bacterial production measurements in sea ice has been limited to a few studies in Antarctica and in the Baltic Sea, but these provide clear indications that Leu working concentrations used in oceanic waters are not adequate in sea ice. Grossmann & Dieckmann (1994) used a 10 nmol l^{-1} Leu concentration for Weddell Sea brine samples and discuss possible Leu under-saturation as a reason for anomalous low Leu:TdR ratios. Guglielmo et al. (2000) and Pusceddu et al. (2008) also used a 10 nmol l^{-1} Leu concentration for Antarctic fast ice crush samples and report extremely low or negligible bacterial carbon production compared to measured enzyme activities. However, they did not discuss the effect of under-saturation on their results. Studies done on Baltic Sea ice that have used 1 (Mock et al. 1997) to 2 orders of magnitude higher Leu saturating concentrations (Kaartokallio 2004, Kuosa & Kaartokallio 2006, Kaartokallio et al. 2006, Piiparinen & Kuosa 2011) do not report problems attributable to under-saturation.

The calculated isotope dilution in ice corresponds to the 80 to 100 nmol l^{-1} natural Leu concentration. This is in the same range as the measured 54 nmol l^{-1} Leu concentration in melted multiyear Arctic ice floe (Amon et al. 2001), but is perhaps unrealistically high for under-ice water. Based on the TdR saturation kinetics experiment, the TdR working concentrations used were still not saturating in ice and brine. However, the estimated degree of under-saturation was comparable in both Leu and TdR and we assume their ratios to be valid without correction to the saturating level.

Sea ice brine channels have been thought to resemble biofilm-like habitats, due to the high organism densities and large amounts of EPS creating gel-like matrices (Krembs & Deming 2008). Also, based on our results, Leu-saturating concentrations are close to those measured in aquatic biofilm systems, mostly freshwater and marine epi- and periphyton, where TdR and Leu methods have been routinely used. Nearly identical Leu saturating concentrations of 1 to 2 $\mu\text{mol l}^{-1}$ over a wide range of biofilm systems and sea ice in this study point to a common underlying cause, possibly related to the bacterial adaptation to the biofilm environment.

We hypothesize that the variation in Leu incorporation saturating concentrations over 5 orders of magnitude in adjacent natural aquatic habitats (open water, biofilm, sediment) and the striking cross-system (fresh and marine waters, sea ice) stability in sat-

urating concentrations might be explained by the bacterial communities' differential use of the primary and secondary Leu transport systems in these environments. Heterotrophic bacteria are known to possess bi- or multiphasic uptake systems for low molecular weight compounds, operating from nanomolar to millimolar concentration ranges (Azam & Hodson 1981, Nissen et al. 1984, Fuhrman & Ferguson 1986). Biphaseic amino acid or Leu uptake/incorporation kinetics have been reported in marine waters (Unanue et al. 1999), bacterial culture experiments (Logan & Fleury 1993) and freshwater submerged plant litter (Gillies et al. 2006). A bi- or multiphasic Leu incorporation kinetic pattern is consistent with the 3 known separate transport systems for branched-chain amino acids, or specifically Leu in gram-negative bacteria: 2 associated high-affinity primary ATP-binding cassette (ABC) transporter systems (LIV-1 and LS) and a secondary low-affinity Na⁺-dependent symporter system (LIV-2, Calvo & Matthews 1994, Saier 2000). Both general types of amino acid transporter are also expressed by natural marine coastal bacterioplankton (Poretsky et al. 2010) as a response to DOC addition.

If the first 2 of the 3 distinct Leu saturation regimes mentioned above can be attributed to the ABC transporters LIV-1 and LS, the very much higher saturating concentrations of between 15 and 100 $\mu\text{mol l}^{-1}$ possibly reflect the use of the secondary low-affinity Leu transport system LIV-2. This would be in keeping with the findings of Logan & Fleury (1993), who reported a Leu saturation plateau between 1 and 1000 $\mu\text{mol l}^{-1}$. ABC transporters are typically highly conserved, and a novel binding-protein-related homotropic autoregulation model for the maltose ABC transporter described by Bao & Duong (2012) may also be valid for Leu ABC transporters. Under the homotropic autoregulation model, saturating behavior is an inherent property of the transporter system and the actual saturating concentration dependent on the amount of transporters on the cell membrane, i.e. their expression level. Variation within the lower 2 regimes could thus possibly be due to community composition or expression levels of particular ABC transport systems.

As in aquatic biofilms, TdR-saturating concentrations in the ice were close to open-water values (Törnblom & Søndergaard 1999, Pollard 2010) and in good agreement with earlier results from Arctic ice-associated waters (Garneau et al. 2008). TdR uptake activity in gram-negative bacteria is regulated by immediate phosphorylation inside the cell (Mizushima et al. 1997), resulting in non-saturated kinetics at higher

concentrations (Logan & Fleury 1993). Use of TdR concentrations of 10 nmol l^{-1} in Antarctic sea ice have produced realistic production estimates (Grossmann & Dieckmann 1994, Helmke & Weyland 1995). For TdR, under-saturation at 20 nmol l^{-1} (ratios added to $V_{\text{max}90}$ 1.6 to 1.8) in ice and brines point to a need for higher TdR working concentrations in ice and brines than used in cold polar surface waters.

Unfortunately, our saturation kinetics experiment did not extend to a higher range of TdR concentrations, or lower range of Leu concentrations, but were initially designed to validate the working concentrations used. Thus, we cannot verify the existence of bi- or multiphasic TdR or Leu incorporation kinetics in sea ice but point to the existence of differing saturating concentrations across the sample types and tracers used. Our results suggest that in sea ice bacterial production measurements, Leu concentrations typical for biofilms, rather than oceanic seawater, should be used, and saturating concentrations for both TdR and Leu should be tested over a broad range.

The Leu:TdR ratio is a widely employed indicator for physiological or metabolic status of bacterial communities, since it reflects the ratio of the 2 major basic metabolic functions in bacteria: protein and DNA synthesis. In a range of aquatic systems, the Leu:TdR ratios typically vary between 5 and 70, and departure from balanced growth is indicated by increased ratios (Chin-Leo & Kirchman 1990, Kirchman 1992, Shiah & Ducklow 1997). Leu:TdR ratios presented in this study were generally high and showed a consistent pattern in ice over the entire study period: ratios were highest in bottom ice, elevated in upper ice sections and lowest in the middle ice section. The obvious explanations for high Leu:TdR ratios in the upper and bottom ice are unbalanced growth (i.e. bacteria increasing their biomass without DNA synthesis) or non-specific incorporation of Leu into non-protein macromolecules. Uncoupling between Leu and TdR has also been reported in coastal marine epiphytic biofilms, where increasing Leu incorporation was positively correlated with the age of the biofilm (Törnblom & Søndergaard 1999).

To estimate the validity of divergent Leu- and TdR-based bacterial production estimates, we calculated the production estimate based on previously published data for oxygen exchange at the ice-water interface obtained during the same campaign at the same site (Long et al. 2012), which gave a net mean oxygen flux into bottom ice of $-2.13 \text{ mmol O}_2 \text{ m}^{-2} \text{ d}^{-1}$ and an average gross primary productivity equal to production of $0.69 \text{ mmol O}_2 \text{ m}^{-2} \text{ d}^{-1}$ (assuming a 1:1 C:O₂ ratio). Primary productivity was mostly confined

to the lowermost ice layers (Søgaard et al. 2013). Our mean bacterial respiration estimates for bottom ice, 0.52 and 3.37 mmol O₂ m⁻² d⁻¹ for TdR and Leu, respectively, are in the same range as the oxygen exchange values presented by Long et al. (2012), suggesting that bacterial respiration alone was close to the observed oxygen fluxes. However, bacterial respiration accounts for only a part of the community respiration. If bacterial respiration is assumed to be 44% of community respiration (Robinson 2008, Kirchman et al. 2009, Nguyen & Maranger 2011), TdR and Leu incorporation results provide an estimated community respiration of 1.18 and 8.45 mmol O₂ m⁻² d⁻¹, respectively, the latter being unrealistically high. If estimated tracer under-saturation in ice is taken into account, the TdR community respiration estimate is 1.89 mmol O₂ m⁻² d⁻¹, being close to the oxygen flux estimate of Long et al. (2012).

The saturation-level-corrected estimate for Leu is almost an order of magnitude too high, a difference unexplained by the conversion factors used. The high Leu incorporation implies that the incorporated Leu is not only ending up in the protein fraction. Mock et al. (1997), working on Baltic Sea brines, found 2-fold lower Leu incorporation after hot TCA extraction as compared to cold TCA extraction, which also points to non-protein incorporation. One possible route for non-protein Leu incorporation is the inclusion into PHA granules via the branched-chain amino acid degradation pathway to the important PHA precursor acetyl-coenzyme A (CoA). The full Leu degradation pathway is known to be present in some ice-inhabiting proteobacterial genera (Kazakov et al. 2009). A key enzyme of this degradation pathway, methylcrotonyl-CoA carboxylase, has been recently associated with high dark bicarbonate uptake and possible Leu degradation by natural Arctic surface water *Gamma-proteobacteria* (Alonso-Sáez et al. 2010). Leu usage for intracellular polymer production has also been proposed by Ducklow & Yager (2007) to explain rapid Leu turnover in cold polynya surface waters.

PHAs are highly reduced, structurally simple macromolecules that are deposited into water-insoluble inclusion bodies within bacterial cells (Anderson & Dawes 1990, Madison & Huisman 1999) and can be used as carbon and energy storage and to alleviate oxidative stress (Ayub et al. 2009). The regulation of PHA production may be directly linked to biofilm formation (Campisano et al. 2008, Tribelli et al. 2012). PHA-producing bacteria in marine habitats have so far been mostly found in sediments or biofilms (Koller et al. 2011), although 2 species of the genus *Oceani-cola* (*Alphaproteobacteria*), isolated from seawater at

the Bermuda-Atlantic Time-series Study Site, have been shown to produce intracellular PHA granules in culture (Cho & Giovannoni 2004). We found various bacterial morphotypes containing putative PHA granules in the bottom ice samples (Fig. 6), suggesting actual PHA production by multiple sea ice bacterial species beyond the only currently known (by genomic traits) sea ice-inhabiting PHA producer *Colwellia psychrerythrea* (Méthé et al. 2005). A hypothetical ecological function for PHA production by sea ice bacteria could be storage of excess carbon (Pomeroy & Wiebe 2001), thereby enhancing their survival in the more dilute planktic environment following ice melt.

CONCLUSIONS

Our results demonstrate small diel variability in bacterial parameters and suggest that a weekly sampling strategy can be temporally representative in sea ice bacteria monitoring studies in subarctic sea ice. Under climatically unstable conditions (e.g. ice warming introducing melting and brine instability) or during periods of rapid biomass growth in spring, more frequent sampling may be needed to adequately cover the variability (Maranger et al. 1994, Riedel et al. 2007).

Our results support earlier views of sea ice habitats acting as biofilm-like systems rather than being analogous to open-water systems. We found biofilm-like saturating concentrations for Leu incorporation in bottom sea ice horizons and we suggest that it would be pertinent for future investigations into sea ice and adjacent permanently cold waters to test a wide concentration range and establish saturating concentrations.

Bacterial cell properties as revealed by flow cytometry imply a distribution of copiotrophic and oligotrophic ecotypes in ice and underlying water, reflecting DOM distribution, and show that flow cytometry is a useful tool for studying sea ice bacteria. We have provided evidence that subarctic sea ice bacteria in the natural environment can produce PHA. Taking into account the vast areal coverage of sea ice, our results suggest that there may be a significantly wider spatial and geographical occurrence of natural bacterial PHA production in marine environments than previously acknowledged. Furthermore, our results point to the influence of ice cover on the underlying water bacterial community and the need to consider ice-covered surface waters as a habitat for bacteria that is quite distinct from open marine waters not influenced by sea ice.

Acknowledgements. The study received financial support from the Greenland Climate Research Centre, and D.H.S. was financially supported by the commission for scientific Research in Greenland (KVUG). D.N.T. and L.N. are grateful to the Royal Society and NERC for support for their participation in the work. H.K. and D.N.T. are also grateful to the Academy of Finland (FiDiPro programme) for their support. S.R. acknowledges the support of the Canada Excellence Research Chair (CERC) program.

LITERATURE CITED

- Alonso-Sáez L, Galand PE, Casamayor EO, Pedrós-Alió C, Bertilsson S (2010) High bicarbonate assimilation in the dark by Arctic bacteria. *ISME J* 4:1581–1590
- Amon RMW, Fitznar HP, Benner R (2001) Linkages among the bioreactivity, chemical composition, and diagenetic state of marine dissolved organic matter. *Limnol Oceanogr* 46: 287–297
- Anderson AJ, Dawes EA (1990) Occurrence, metabolism, metabolic role, and industrial uses of bacterial polyhydroxyalkanoate. *Microbiol Rev* 54:450–472
- Ayo B, Unanue M, Azua I, Gorsky G, Turley C, Iriberry J (2001) Kinetics of glucose and amino acid uptake by attached and free-living marine bacteria in oligotrophic waters. *Mar Biol* 138:1071–1076
- Ayub ND, Tribelli PM, López NI (2009) Polyhydroxyalkanoates are essential for maintenance of redox state in the Antarctic bacterium *Pseudomonas* sp. 14-3 during low temperature adaptation. *Extremophiles* 13:59–66
- Azam F, Hodson RE (1981) Multiphasic kinetics for D-glucose uptake by assemblages of natural marine bacteria. *Mar Ecol Prog Ser* 6:213–222
- Bao H, Duong F (2012) Discovery of an auto-regulation mechanism for the maltose ABC transporter MalFGK2. *PLoS ONE* 7:e34836
- Becquevort S, Dumont I, Tison J-L, Lannuzel D, Sauvee M-L, Chou L, Schoemann V (2009) Biogeochemistry and microbial community composition in sea ice and underlying seawater off East Antarctica during early spring. *Polar Biol* 32: 879–895
- Belzile C, Brugel S, Nozais C, Gratton Y, Demers S (2008) Variations of the abundance and nucleic acid content of heterotrophic bacteria in Beaufort Shelf waters during winter and spring. *J Mar Syst* 74:946–956
- Bjørnsen PK, Kuparinen J (1991) Determination of bacterioplankton biomass, net production and growth efficiency in the Southern Ocean. *Mar Ecol Prog Ser* 71:185–194
- Buesing N, Gessner MO (2003) Incorporation of radiolabeled leucine into protein to estimate bacterial production in plant litter, sediment, epiphytic biofilms, and water samples. *Microb Ecol* 45:291–301
- Calvo JM, Matthews RG (1994) The leucine-responsive regulatory protein, a global regulator of metabolism in *Escherichia coli*. *Microbiol Rev* 58:466–490
- Campisano A, Overhage J, Rehm BHA (2008) The polyhydroxyalkanoate biosynthesis genes are differentially regulated in planktonic- and biofilm-grown *Pseudomonas aeruginosa*. *J Biotechnol* 133:442–452
- Chin-Leo G, Kirchman DL (1990) Unbalanced growth in natural assemblages of marine bacterioplankton. *Mar Ecol Prog Ser* 63:1–8
- Cho JC, Giovannoni SJ (2004) *Oceanicola granulosa* gen. nov., sp. nov. and *Oceanicola batsensis* sp. nov., polyhydroxybutyrate-producing marine bacteria in the order ‘*Rhodobacterales*’. *Int J Syst Evol Microbiol* 54:1129–1136
- Collins RE, Rocap G, Deming JW (2010) Persistence of bacterial and archaeal communities in sea ice through an Arctic winter. *Environ Microbiol* 12:1828–1841
- Cox GFN, Weeks WF (1983) Equations for determining the gas and brine volumes in sea ice samples. *J Glaciol* 29: 306–316
- Deming JW (2010) Sea ice bacteria and viruses. In: Thomas DN, Dieckmann GS (eds) *Sea ice*, 2nd edn. Wiley-Blackwell, Oxford, p 247–282
- Ducklow HW (2003) Seasonal production and bacterial utilization of DOC in the Ross Sea, Antarctica. *Antarctic Res Ser* 78:143–158
- Ducklow HW, Yager PL (2007) Pelagic bacterial processes in Polynyas. In: Smith WO Jr., Barber DG (eds) *Polynyas: Windows into polar oceans*. Elsevier Oceanography Series 74, Elsevier BV, p 323–361
- Ducklow H, Dickson M, Kirchman D, Steward G, Orchardo J, Marra J, Azam F (2000) Constraining bacterial production, conversion efficiency and respiration in the Ross Sea, Antarctica, January–February, 1997. *Deep-Sea Res II* 47: 3227–3247
- Fischer H, Pusch M (1999) Use of the [¹⁴C] leucine incorporation technique to measure bacterial production in river sediments and the epiphyton. *Appl Environ Microbiol* 65: 4411–4418
- Fransson A, Chierici M, Yager PL, Smith WO Jr. (2011) Antarctic sea ice carbon dioxide system and controls. *J Geophys Res* 116(C12), C12035, doi:10.1029/2010JC006844
- Fuhrman JA, Azam F (1980) Bacterioplankton secondary production estimates for coastal waters of British Columbia, Antarctica, and California. *Appl Environ Microbiol* 39: 1085–1095
- Fuhrman JA, Azam F (1982) Thymidine incorporation as a measure of heterotrophic bacterioplankton production in marine surface waters: evaluation and field results. *Mar Biol* 66:109–120
- Fuhrman JA, Ferguson RL (1986) Nanomolar concentrations and rapid turnover of dissolved free amino acids in seawater: agreement between chemical and microbiological measurements. *Mar Ecol Prog Ser* 33:237–242
- Garneau ME, Roy S, Lovejoy C, Gratton Y, Vincent WF (2008) Seasonal dynamics of bacterial biomass and production in a coastal arctic ecosystem: Franklin Bay, western Canadian Arctic. *J Geophys Res* 113(C7), C07S91, doi:10.1029/2007JC004281
- Gasol JM, del Giorgio PA (2000) Using flow cytometry for counting natural planktonic bacteria and understanding the structure of planktonic bacterial communities. *Sci Mar* 64:197–224
- Gasol JM, Zweifel UL, Peters F, Fuhrman JA, Hagström Å (1999) Significance of size and nucleic acid content heterogeneity as measured by flow cytometry in natural planktonic bacteria. *Appl Environ Microbiol* 65:4475–4483
- Gillies JE, Kuehn KA, Francoeur SN, Neely RK (2006) Application of the [³H]leucine incorporation technique for quantification of bacterial secondary production associated with decaying wetland plant litter. *Appl Environ Microbiol* 72:5948–5956
- Gosselin M, Legendre L, Therriault J-C, Demers S, Rochet M (1986) Physical control of the horizontal patchiness of sea-ice microalgae. *Mar Ecol Prog Ser* 29:289–298
- Grasshoff K, Ehrhardt M, Kremling K (1983) *Methods of seawater analysis*, 2nd edn. Verlag Chemie, Weinheim
- Grossmann S, Dieckmann GS (1994) Bacterial standing stock, activity, and carbon production during formation and growth of sea ice in the Weddell Sea, Antarctica. *Appl Environ Microbiol* 60:2746–2753

- Guglielmo L, Carrada G, Catalano G, Dell'Anno A and others (2000) Structural and functional properties of sympagic communities in the annual sea ice at Terra Nova Bay (Ross Sea, Antarctica). *Polar Biol* 23:137–146
- Hales B, van Greer A, Takahashi T (2004) High-frequency measurements of seawater chemistry: Flow-injection analysis of macronutrients. *Limnol Oceanogr Methods* 2: 91–101
- Helmke E, Weyland H (1995) Bacteria in sea ice and underlying water of the eastern Weddell Sea in midwinter. *Mar Ecol Prog Ser* 117:269–287
- Holmes RM, Aminot A, Kerouel R, Hocker BA, Peterson BJ (1999) A simple and precise method for measuring ammonium in marine and fresh water. *Can J Fish Aquat Sci* 56: 1801–1808
- Ishige T, Tani A, Sakai Y, Kato N (2003) Wax ester production by bacteria. *Curr Opin Microbiol* 6:244–250
- Jørgensen NOG (1992) Incorporation of [³H] leucine and [³H] valine into protein of freshwater bacteria: Uptake kinetics and intracellular isotope dilution. *Appl Environ Microbiol* 58:3638–3646
- Junge K, Imhoff F, Staley T, Deming JW (2002) Phylogenetic diversity of numerically important Arctic sea-ice bacteria cultured at subzero temperature. *Microb Ecol* 43:315–328
- Kaartokallio H (2004) Food web components, and physical and chemical properties of Baltic Sea ice. *Mar Ecol Prog Ser* 273:49–63
- Kaartokallio H, Kuosa H, Thomas DN, Granskog MA, Kivi K (2006) Biomass, composition and activity of organism assemblages along a salinity gradient in sea ice subjected to river discharge in the Baltic Sea. *Polar Biol* 30:183–197
- Kaartokallio H, Tuomainen J, Kuosa H, Kuparinen J, Martikainen PJ, Servomaa K (2008) Succession of sea-ice bacterial communities in the Baltic Sea fast ice. *Polar Biol* 31: 783–793
- Kazakov AE, Rodionov DA, Alm E, Arkin AP, Dubchak I, Gelfand MS (2009) Comparative genomics of regulation of fatty acid and branched-chain amino acid utilization in Proteobacteria. *J Bacteriol* 191:52–64
- Kirchman DL (1992) Incorporation of thymidine and leucine in the subarctic Pacific: application to estimating bacterial production. *Mar Ecol Prog Ser* 82:301–309
- Kirchman D, K'nees E, Hodson R (1985) Leucine incorporation and its potential as a measure of protein synthesis by bacteria in natural aquatic systems. *Appl Environ Microbiol* 49:599–607
- Kirchman DL, Hill V, Cottrell MT, Gradinger R, Malmstrom RR, Parker A (2009) Standing stocks, production, and respiration of phytoplankton and heterotrophic bacteria in the western Arctic Ocean. *Deep-Sea Res II* 56:1237–1248
- Koller M, Gasser I, Schmid F, Berg G (2011) Linking ecology with economy: Insights into polyhydroxyalkanoate-producing microorganisms. *Eng Life Sci* 11:222–237
- Kottmeier S, Grossi SM, Sullivan CW (1987) Sea ice microbial communities. VIII. Bacterial production in annual sea ice of McMurdo Sound, Antarctica. *Mar Ecol Prog Ser* 35: 175–186
- Krembs C, Deming JW (2008) The role of exopolymers in microbial adaptation to sea ice. In: Margesin R, Schinner F, Marx J-C, Gerday C (eds) *Psychrophiles: from biodiversity to biotechnology*. Springer-Verlag, Heidelberg, p 247–264
- Krembs C, Eicken H, Deming JW (2011) Exopolymer alteration of physical properties of sea ice and implications for ice habitability and biogeochemistry in a warmer Arctic. *Proc Natl Acad Sci USA* 108:3653–3658
- Kroon H (1993) Determination of nitrogen in water: comparison of continuous flow method with on-line UV digestion with the original Kjeldahl method. *Anal Chim Acta* 276: 287–293
- Kuosa H, Kaartokallio H (2006) Experimental evidence on nutrient and substrate limitation of Baltic Sea sea-ice algae and bacteria. *Hydrobiologia* 554:1–10
- Kuparinen J, Autio R, Kaartokallio H (2011) Sea ice bacterial growth rate, growth efficiency and preference for inorganic nitrogen sources in the Baltic Sea. *Polar Biol* 34: 1361–1373
- Lebaron P, Servais P, Agogue H, Courties C, Joux F (2001) Does the high nucleic-acid content of individual bacterial cells allow to discriminate active cells in aquatic systems? *Appl Environ Microbiol* 67:1775–1782
- Logan BE, Fleury RC (1993) Multiphasic kinetics can be an artifact of the assumption of saturable kinetics for microorganisms. *Mar Ecol Prog Ser* 102:115–124
- Long MH, Koopmans D, Berg P, Rysgaard S, Glud RN, Søgaard DH (2012) Oxygen exchange and ice melt measured at the ice-water interface by eddy correlation. *Biogeosciences* 9:1957–1967
- Madison LL, Huisman GW (1999) Metabolic engineering of poly(3-hydroxyalkanoates): from DNA to plastic. *Microbiol Mol Biol Rev* 63:21–53
- Maranger R, Bird DF, Juniper SK (1994) Viral and bacterial dynamics in Arctic sea ice during the spring algal bloom near Resolute, N.W.T., Canada. *Mar Ecol Prog Ser* 111:121–127
- Martin A, Anderson MJ, Thorn C, Davy SK, Ryan KG (2011) Response of sea-ice microbial communities to environmental disturbance: an *in situ* transplant experiment in the Antarctic. *Mar Ecol Prog Ser* 424:25–37
- Mary I, Heywood JL, Fuchs BM, Amann R, Tarran GA, Burkill PH, Zubkov MV (2006) SAR11 dominance among metabolically active low nucleic acid bacterioplankton in surface waters along an Atlantic meridional transect. *Aquat Microb Ecol* 45:107–113
- Méthé BA, Nelson KE, Deming JW, Momen B and others (2005). The psychrophilic lifestyle as revealed by the genome sequence of *Colwellia psychrerythraea* 34H through genomic and proteomic analyses. *Proc Natl Acad Sci USA* 102:10913–10918
- Middelboe M, Glud RN, Sejr MK (2012) Bacterial carbon cycling in a subarctic fjord: A seasonal study on microbial activity, growth efficiency, and virus-induced mortality in Kobbefjord, Greenland. *Limnol Oceanogr* 57:1732–1742
- Mikkelsen DM, Rysgaard S, Glud RN (2008) Microalgal composition and primary production in Arctic sea ice: a seasonal study from Kobbefjord (Kangerluarsunnguag), West Greenland. *Mar Ecol Prog Ser* 368:65–74
- Miranda MR, Guimarães JRD, Coelho-Souza AS (2007) [³H]Leucine incorporation method as a tool to measure secondary production by periphytic bacteria associated to the roots of floating aquatic macrophyte. *J Microbiol Methods* 71:23–31
- Mizushima T, Yokoyama K, Mima S, Tsuchiya T, Sekimizu K (1997) Inhibition of thymidine transport in *dnaA* mutants of *Escherichia coli*. *J Biol Chem* 272:21195–21200
- Mock T, Meiners KM, Giesenhagen HC (1997) Bacteria in sea ice and underlying brackish water at 54° 26' 50" N (Baltic Sea, Kiel Bight). *Mar Ecol Prog Ser* 158:23–40
- Morán XAG, Bode A, Ángel Suárez L, Nogueira E (2007) Assessing the relevance of nucleic acid content as an indicator of marine bacterial activity. *Aquat Microb Ecol* 46: 141–152
- Mundy CJ, Gosselin M, Ehn JK, Belzile C and others (2011) Characteristics of two distinct high-light acclimated algal communities during advanced stages of sea ice melt. *Polar Biol* 34:1869–1896

- Nguyen D, Maranger R (2011) Respiration and bacterial carbon dynamics in Arctic sea ice. *Polar Biol* 34:1843–1855
- Nissen H, Nissen P, Azam F (1984) Multiphasic uptake of D-glucose by an oligotrophic marine bacterium. *Mar Ecol Prog Ser* 16:155–160
- Oksanen JF, Blanchet G, Kindt R, Legendre P and others (2012) *Vegan: Community Ecology Package*. R package version 2.0-5. CRAN.R-project.org/package=vegan
- Ostle AG, Holt JG (1982) Nile blue A as a fluorescent stain for poly-beta-hydroxybutyrate. *Appl Environ Microbiol* 44:238–241
- Petrich C, Eicken H (2010) Growth, structure and properties of sea ice. In: Thomas DN, Dieckmann GS (eds) *Sea ice*, 2nd edn. Wiley-Blackwell, Oxford, p 23–78
- Piiparinen J, Kuosa H (2011) Impact of UVA radiation on algae and bacteria in Baltic Sea ice. *Aquat Microb Ecol* 63:75–87
- Pollard PC (2010) Bacterial activity in plant (*Schoenoplectus validus*) biofilms of constructed wetlands. *Water Res* 44:5939–5948
- Pomeroy LR, Wiebe WJ (2001) Temperature and substrates as interactive limiting factors for marine heterotrophic bacteria. *Aquat Microb Ecol* 23:187–204
- Poretsky RS, Sun S, Mou X, Moran MA (2010) Transporter genes expressed by coastal bacterioplankton in response to dissolved organic carbon. *Environ Microbiol* 12:616–627
- Pusceddu A, Dell'Anno A, Vezzulli L, Fabiano M and others (2008) Microbial loop malfunctioning in the annual sea ice at Terra Nova Bay (Antarctica). *Polar Biol* 32:337–346
- Qian J, Mopper K (1996) High performance high temperature combustion total organic carbon analyzer. *Anal Chem* 68:3090–3097
- R Development Core Team (2011) *R: A language and environment for statistical computing*. R Foundation for Statistical Computing, Vienna
- Rappé MS, Cannon SA, Vergin KL, Giovannoni SJ (2002) Cultivation of the ubiquitous SAR11 marine bacterioplankton clade. *Nature* 418:630–633
- Riedel A, Michel C, Gosselin M (2007) Grazing of large-sized bacteria by sea-ice heterotrophic protists on the Mackenzie Shelf during the winter–spring transition. *Aquat Microb Ecol* 50:25–38
- Rivkin RB, Legendre L (2001) Biogenic carbon cycling in the upper ocean: effects of microbial respiration. *Science* 291:2398–2400
- Robinson C (2008) Heterotrophic bacterial respiration. In: Kirchman DL (ed) *Microbial ecology of the oceans*. Wiley-Blackwell, Oxford, p 299–334
- Saier MH (2000) Families of transmembrane transporters selective for amino acids and their derivatives. *Microbiology* 146:1775–1795
- Shiah FK, Ducklow HW (1997) Bacterioplankton growth responses to temperature and chlorophyll variations in estuaries measured by thymidine:leucine incorporation ratio. *Aquat Microb Ecol* 13:151–159
- Simon M, Azam F (1989) Protein content and protein synthesis rates of planktonic marine bacteria. *Mar Ecol Prog Ser* 51:201–213
- Smith REH, Clement P (1990) Heterotrophic activity and bacterial productivity in assemblages of microbes from sea ice in the high Arctic. *Polar Biol* 10:351–357
- Søgaard DH, Kristensen M, Rysgaard S, Glud RN, Hansen PJ, Hilligsøe KM (2010) Autotrophic and heterotrophic activity in Arctic first-year sea ice: seasonal study from Malene Bight, SW Greenland. *Mar Ecol Prog Ser* 419:31–45
- Søgaard DH, Thomas DN, Rysgaard S, Glud RN and others (2013) The relative contributions of biological and abiotic processes to the carbon dynamics in subarctic sea ice. *Polar Biol*. doi:10.1007/s00300-013-1396-3
- Thomas DN, Dieckmann GS (2002) Antarctic sea ice—a habitat for extremophiles. *Science* 295:641–644
- Thomas DN, Dieckmann GS (eds) (2010) *Sea ice*, 2nd edn. Wiley-Blackwell, Oxford
- Thomas DN, Lara RJ, Haas C, Schnack-Schiel SB and others (1998) Biological soup within decaying summer sea ice in the Amundsen Sea, Antarctica. In: Lizotte M, Arrigo K (eds) *Antarctic sea ice biological processes, interactions and variability*. *Antarctic Res Ser* 73:161–171
- Thomas DN, Papadimitriou S, Michel C (2010) The biogeochemistry of sea ice. In: Thomas DN, Dieckmann GS (eds) *Sea ice*, 2nd edn. Wiley-Blackwell, Oxford, p 425–467
- Törnblom E, Søndergaard M (1999) Seasonal dynamics of bacterial biomass and production on eelgrass *Zostera marina* leaves. *Mar Ecol Prog Ser* 179:231–240
- Tribelli PM, Di Martino C, López NI, Raiger Iustman LJ (2012) Biofilm lifestyle enhances diesel bioremediation and bio-surfactant production in the Antarctic polyhydroxyalkanoate producer *Pseudomonas extremaustralis*. *Biodegradation* 23:645–651
- Tuominen L (1995) Comparison of leucine uptake methods and a thymidine incorporation method for measuring bacterial activity in sediment. *J Microbiol Methods* 24:125–134
- Unanue M, Ayo B, Agis M, Slezak D, Herndl G, Iriberry J (1999) Ecto-enzymatic activity and uptake of monomers in marine bacterioplankton described by a biphasic kinetic model. *Microb Ecol* 37:36–48
- Underwood GJC, Fietz S, Papadimitriou S, Thomas DN, Dieckmann GS (2010) Distribution and composition of dissolved extracellular polymeric substances (EPS) in Antarctic sea ice. *Mar Ecol Prog Ser* 404:1–19
- Underwood GJC, Aslam SN, Michel C, Niemi A and others (2013) Broad-scale predictability of carbohydrates and exopolymers in Antarctic and Arctic sea ice. *Proc Natl Acad Sci USA* 110:15734–15739
- van Looij A, Riemann B (1993) Measurements of bacterial production in coastal marine environments using leucine: application of a kinetic approach to correct for isotope dilution. *Mar Ecol Prog Ser* 102:97–104
- Wältermann M, Steinbüchel A (2005) Neutral lipid bodies in prokaryotes: recent insights into structure, formation, and relationship to eukaryotic lipid deposits. *J Bacteriol* 187:3607–3619
- Wang Y, Hammes F, Boon N, Chami M, Egli T (2009) Isolation and characterization of low nucleic acid (LNA)-content bacteria. *ISME J* 3:889–902
- Zhou J, Delille B, Eicken H, Vancoppenolle M and others (2013) Physical and biogeochemical properties in landfast sea ice (Barrow, Alaska): Insights on brine and gas dynamics across seasons. *J Geophys Res Oceans* 118:3172–3189

Editorial responsibility: Hugh Ducklow,
Woods Hole, Massachusetts, USA

Submitted: April 22, 2013; Accepted: September 23, 2013
Proofs received from author(s): November 15, 2013

PAPER VII

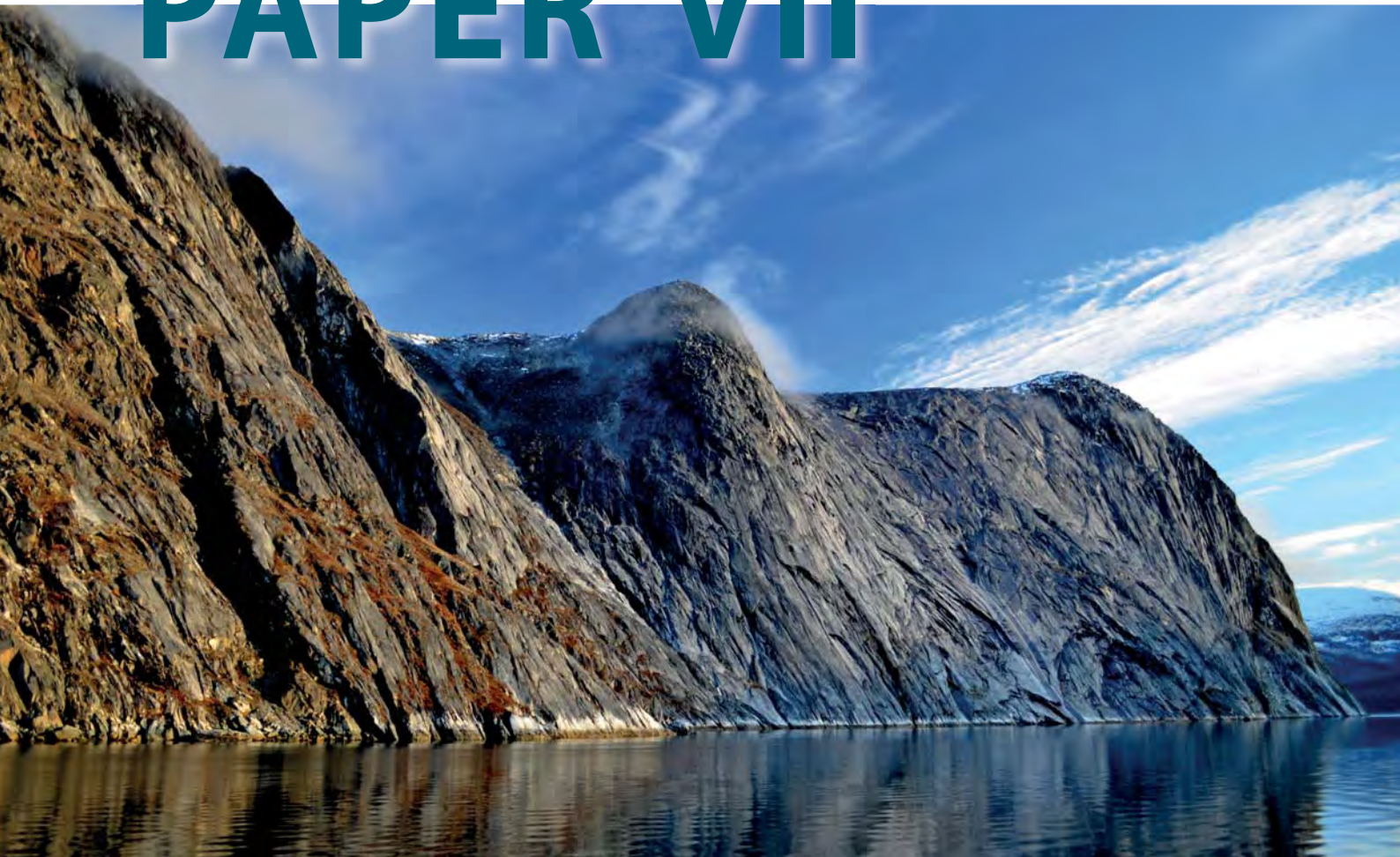
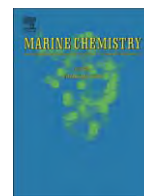


Photo: Thomas Juul-Pedersen.

High air-sea CO₂ uptake rates in nearshore and shelf areas of Southern Greenland: Temporal and spatial variability

S. Rysgaard • J. Mortensen • T. Juul-Pedersen • L.L. Sørensen •
K. Lennert • D.H. Søgaard • K.E. Arendt • M.E. Blicher • M.K. Sejr
• J. Bendtsen

Marine Chemistry 128-129:26 – 33, doi:10.1016/j.marchem.2011.11.002



High air–sea CO₂ uptake rates in nearshore and shelf areas of Southern Greenland: Temporal and spatial variability

S. Rysgaard^{a,*}, J. Mortensen^a, T. Juul-Pedersen^a, L.L. Sørensen^{a,b}, K. Lennert^a, D.H. Søgaard^{a,c}, K.E. Arendt^a, M.E. Blicher^a, M.K. Sejr^{a,b}, J. Bendtsen^a

^a Greenland Climate Research Centre, Greenland Institute of Natural Resources, Nuuk, Greenland

^b National Environmental Research Institute, Aarhus University, Aarhus, Denmark

^c University of Southern Denmark, Campusvej 55, 5230 Odense M, Denmark

ARTICLE INFO

Article history:

Received 12 May 2011

Received in revised form 10 November 2011

Accepted 11 November 2011

Available online 27 November 2011

Keywords:

Air–sea CO₂ exchange

Arctic shelf

Greenland

Primary production

Vertical sinking flux

Fjord

Glacial meltwater

ABSTRACT

The present study is based on hourly samplings of wind speed, monthly sampling sessions of temperature, salinity, dissolved inorganic carbon, alkalinity, nutrients, primary productivity and vertical export in the outer sill region (station GF3) of a sub-arctic SW Greenland fjord (Godthåbsfjord) through 2005–2010. Air–sea CO₂ fluxes varied at GF3 from c. $-20 \text{ g C m}^{-2} \text{ month}^{-1}$ (uptake from the atmosphere) to $25 \text{ g C m}^{-2} \text{ month}^{-1}$ (release to the atmosphere) during 2005–10. The average annual air–sea CO₂ flux of -83 to $-108 \text{ g C m}^{-2} \text{ yr}^{-1}$ was within the range of the local gross annual primary productivity of 76 – $106 \text{ g C m}^{-2} \text{ yr}^{-1}$. Furthermore, the estimated vertical export of phytoplankton carbon to depths below 60 m of 38 – 89 g C m^{-2} suggests that a large fraction of the mineralization (release of CO₂) occurs in deeper waters in the outer sill region of the fjord. However, there was no statistically significant correlation between average annual gross primary production and annual air–sea flux during 2005–2010, which suggests that regulation of pCO₂ in the fjord is more complex. Despite three confined periods with supersaturated pCO₂ conditions in surface waters during 2005–2010, Godthåbsfjord can be considered as a strong sink ($7.2 \text{ tons C month}^{-1} \text{ km}^{-2}$) for atmospheric CO₂. In addition, measurements from Godthåbsfjord during the summer season showed that mixing between glacial meltwater and coastal water could explain a large part of the low pCO₂-values observed in the innermost part of the fjord. Finally, a larger survey confirmed the existence of very low pCO₂ conditions in innershore and shelf waters around Southern Greenland.

© 2011 Elsevier B.V. All rights reserved.

1. Introduction

Over the global oceans, the seasonal and geographical variation of the partial pressure of CO₂ (pCO₂) is much greater than that of atmospheric pCO₂, and, hence, the direction and magnitude of the air–sea CO₂ flux are mainly regulated by oceanic pCO₂. A recent synthesis of worldwide measurements of pCO₂ indicates that most open shelves in the temperate and high-latitude regions are undersaturated with respect to atmospheric CO₂ during all seasons, although the low-latitude shelves seem to be supersaturated (Chen and Borges, 2009; Takahashi et al., 2002). Basic knowledge is still needed, however, to elucidate whether coastal waters are net sources or sinks of atmospheric CO₂, and whether organic carbon from primary production in coastal seas is exported or recycled (Mackenzie et al., 2000; Smith and Hollibaugh, 1993; Smith and Mackenzie, 1987; Thomas et al., 2004; Ver et al., 1999a,b). One of the arguments presented for

areas with CO₂ degassing to the atmosphere is based on the imbalance between the total river transport of c. 0.4 Pg C yr^{-1} and the oceanic organic carbon burial rate of c. $0.14 \text{ Pg C yr}^{-1}$. The difference of $0.26 \text{ Pg C yr}^{-1}$ would most likely be returned to the atmosphere (Smith and Hollibaugh, 1993; Smith and Mackenzie, 1987). Furthermore, there is an increasing evidence that a very large fraction of terrestrial/riverine organic matter is degraded in nearshore areas and emitted as CO₂ to the atmosphere there without ever reaching the continental shelves (Middelburg and Herman, 2007 and references therein). Based on carbon mass-balance calculations as well as scaled estimates of pCO₂ measurements, Chen and Borges (2009) established that open shelf areas are sinks for atmospheric CO₂, although many inner estuaries, nearshore coastal waters and intensive upwelling areas are supersaturated with respect to CO₂. Although the Arctic covers c. 25% of the global coastal region (areas with water depths <200 m, Menard and Smith, 1966) very few studies of pCO₂ uptake exist from these high-latitude nearshore areas and virtually none from Greenland waters (Anderson et al., 2000; Miller et al., 2002; Murata and Takizawa, 2003; Sejr et al., 2011; Yager et al., 1995). In addition, investigations have been restricted to short surveys and most measurements have been performed during summer.

* Corresponding author at: Centre for Earth Observation Science, University of Manitoba, Winnipeg, Canada.

E-mail address: Rysgaard@cc.umanitoba.ca (S. Rysgaard).

In the present study, we report monthly measurements of salinity, temperature, nutrients, total alkalinity (TA), total dissolved inorganic carbon (TCO₂) and primary production through 2005–2010 in a sub-Arctic Greenland fjord (Godthåbsfjord). Conductivity, temperature and depth (CTD) measurements, nutrients, TCO₂ and TA samples from the innermost part of the fjord, coastal areas and shelf locations further offshore, were also collected during summer around the southern part of Greenland during 2007–08 through a larger survey using the German research vessel Merian (2007), the Danish research vessel Dana (2008), and the coast guard vessel Agdlek from the Danish Navy (2007).

2. Method

Sampling in Godthåbsfjord was performed in the outer part of the fjord system connecting the Greenland Ice Sheet to shelf waters off West Greenland, and results reported in this study form part of the long-term Greenland Ecosystem Monitoring program (www.g-e-m.dk). Sampling took place from a small research boat every 3–4 weeks (2005–2010) at the station GF3 in the outer part of Godthåbsfjord (64°07'N, 51°53'W – water depth c. 350 m) located in Southwest Greenland (Fig. 1). Godthåbsfjord is a deep sill (170 m) fjord, which is in contact with the Greenland Ice Sheet through six glaciers. It covers an area of 2013 km², has a volume of 525 km³ and the mean depth is 260 m.

Shelf waters enter the fjord through a narrow 3–5-km entrance. Several deep sills are present in the fjord, the shallowest sill depth at the entrance to the fjord being 170 m. The warmer waters at depth located outside the Fyllas Banke represent the warm, saline and dense Atlantic water, (sub-polar mode water), flowing northwards along the West Greenland Shelf (Buch et al., 2004; Myers et al., 2007). Water masses and physical settings within the fjord have recently been described by Mortensen et al. (2011).

At GF3, vertical profiles of temperature, salinity, fluorescence and light intensity (PAR, Li-Cor 190SA quantum Q, Li-Cor) were obtained with a CTD profiler (SBE19+) from our smaller vessel. A Niskin bottle was used to collect water samples from depths of 1, 5, 10, 15, 20, 30, and 40 m. Water for analysis of TCO₂ and total alkalinity (TA) determination was transferred to 100-ml glass bottles with a gas-tight Tygon tube, allowing overflow of at least 3 times the volume of the bottle. Samples were preserved with HgCl₂ (saturated solution) to a final concentration of 0.02%. Samples were stored at 4 °C until analysis. Samples for nutrient analysis were filtered (GF/F) and frozen in polyethylene vials until later analysis. The vials were rinsed several times in GF/F filtered water from the specific depth before filling and freezing.

TCO₂ concentrations were measured coulometrically (Johnson et al., 1987) and TA by potentiometric titration (Haraldsson et al., 1997).

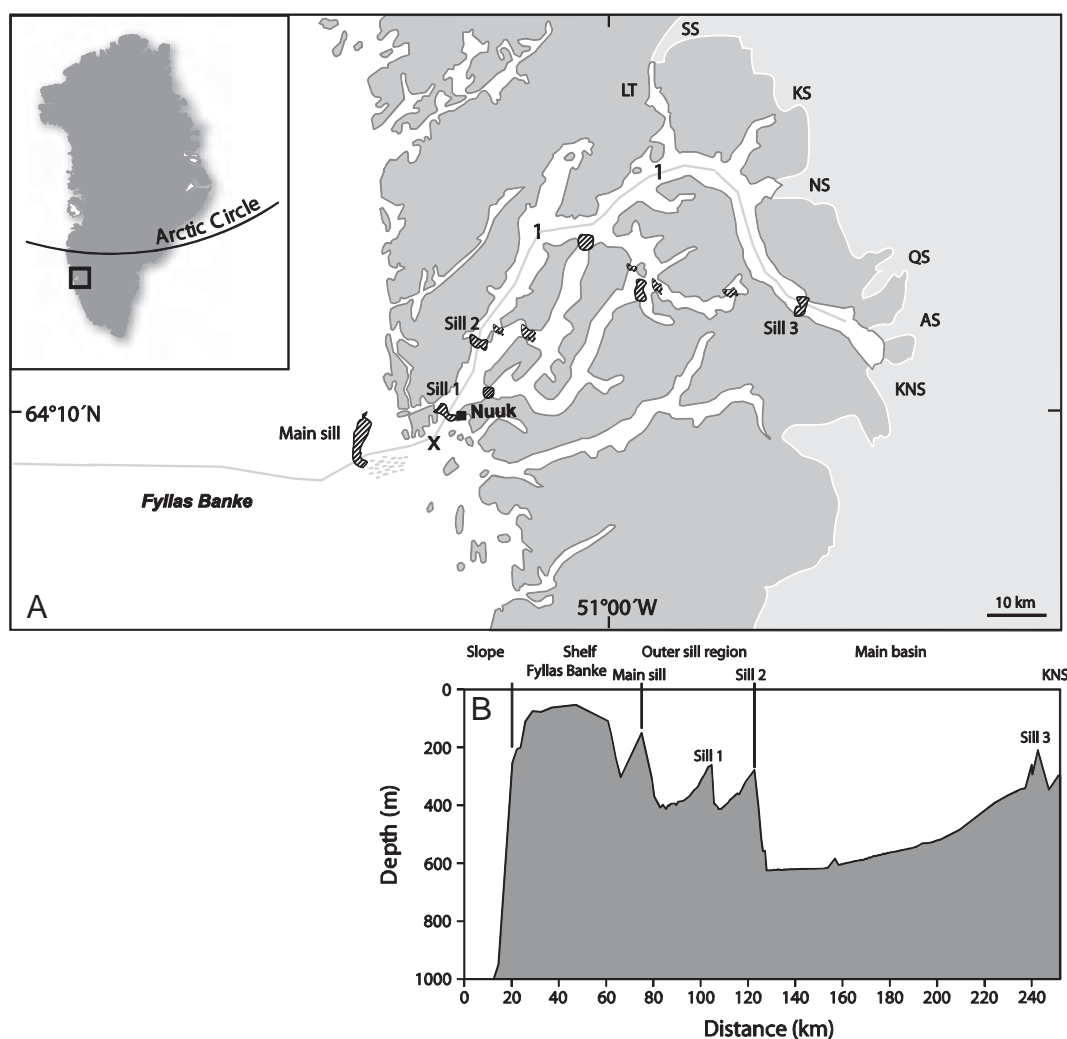


Fig. 1. (A) Sampling location (GF3, X) in Godthåbsfjord, southwest Greenland. The location of the meteorological station “522” used in the present study is indicated as “solid square in Nuuk”. Also shown are the positions of sills (hatched areas); 1, Godthåbsfjord or Nuup Kangerlua; KNS, Kangiata Nunaata Sermia; AS, Akullersuup Sermia; NS, Narsap Sermia; QS, Qamanaarsuup Sermia; KS, Kangilinnuata Sermia; SS, Saqqap Sermersua; LT, Lake Tasersuaq. (B) Bathymetry of a length section from the continental slope following the main branch of the fjord to the inner part near KNS is shown as a light gray line in Fig. 1A. Four sills and four domains are indicated: slope, shelf, outer sill region and main fjord basin.

Routine analysis of Certified Reference Materials (provided by A. G. Dickson, Scripps Institution of Oceanography; <http://andrew.ucsd.edu/co2qc/>) verified that the accuracy of TCO₂ and TA measurements was 0.5 μmol kg⁻¹ and 2 μmol kg⁻¹, respectively. Nutrients (phosphate and silicate) were analyzed by standard colorimetric methods (Grasshoff et al., 1983) against certified reference materials (provided by Eurofins, Denmark). Triplicate measurements were performed on each sample with standard deviations <0.05 μM (phosphate) and 0.2 μM (silicate).

At each sampling date, water from 5, 10, 20, 30, and 40 m was transferred to Winkler glass bottles to which 200 μl H¹⁴CO₃⁻ was added for determination of primary production (Steeaman-Nielsen, 1952). Two bottles were incubated in situ at the different water depths representing in situ light conditions and 1 bottle in the dark at each water depth. The incubation time was 2 h around local noon. The content of each bottle was GF/C filtered (max 0.3 bar). The filters were transferred to scintillation vials and 100 μl 1 M HCl was added onto the filters, which were then fumed for minimum 8 h. Following addition of scintillation cocktail (UltimaGold+), the samples were measured on a PerkinElmer Scintillation Counter.

Vertical sinking flux of particulate material was also measured monthly as part of the Marin Basis Nuuk program. Free-drifting sediment traps were deployed for 2 h at 60 m, i.e. below the euphotic zone. Chlorophyll *a* (along with other parameters) was determined by filtration of trap content onto GF/C filters (max 0.3 bar), after which filters were extracted in 96% ethanol for 24 h (at 4 °C in the dark) and analyzed fluorometrically (Turner Designs TD-700). Vertical sinking flux values were then converted to chlorophyll *a*-based carbon (Chl-C) using a carbon:Chl *a* ratio of 40 g:g (Lorenzen, 1968). It should be noted, however, that the carbon:Chl-*a* ratio in phytoplankton can vary from ≤10 to 300 g/g (e.g. Falkowski and Kiefer, 1985) and depends on temperature, nutrient availability, PAR (Photosynthetically Active Radiation), plankton diversity, etc. (e.g. Cloern, 1996).

Partial pressure of CO₂ (*p*CO₂) was calculated from measurements of temperature, salinity, TCO₂ and TA according to Millero (1995) also taking into account the measured concentrations of phosphate and silicate. However on two cruises with larger research vessels; one in August 2006 (Galathea cruise) and one in July 2008 (Dana cruise), *p*CO₂ was measured directly using an equilibrator system. The partial pressure of CO₂ in the water (water intake at 5 m) was determined by bringing a volume of air into equilibrium with a continuous stream of sea water. Air was sampled alternately from the equilibrator system, a calibration gas and the atmospheric air. In this manner, we could use the same instrument for determining *p*CO₂ in the ocean and the atmosphere. CO₂ in the samples was measured using an IR CO₂ monitor (LICOR-6262). The equilibrator was constructed according to Dickson and Goyet (1994) and consists of a glass cylinder into which water is pumped from the top where a series of small glass tubes increase the water–air contact surface in order to achieve equilibrium quickly. Air was sampled continuously from the equilibrator into the CO₂ monitor and the air flow from the CO₂ monitor was returned into the equilibrator in a circulating flow. The ocean–atmosphere difference in *p*CO₂ was determined as half-hour means during the cruise.

The net flux of CO₂ (*F*) was calculated from the bulk gas exchange equation: $F = ks(\Delta p\text{CO}_2)$, where *k* is the transfer velocity, and *s* the solubility of CO₂ (Weiss, 1974). $\Delta p\text{CO}_2$ was calculated by subtracting the atmospheric *p*CO₂ values from measured individual surface–water *p*CO₂ values. A variety of formulas have been proposed for estimating the transfer coefficient. In the present study we used the coefficient of Nightingale et al. (2000):

$$k = 0.333U + 0.222U^2 \quad (1)$$

where *U* is wind speed (m s⁻¹) 10 m above sea level obtained from the meteorological station “522” (Asiaq, Greenland Survey) close to

GF3 (Fig. 1). The equation of Nightingale et al. (2000) was chosen because it was derived for coastal environments.

Primary production was calculated from the in situ radio-carbon incubations around noon, subtracting dark fixation values obtained from the dark-incubated bottles. The measured concentration of TCO₂ from each individual depth was used to calculate primary production. Primary production was corrected for available PAR and integrated for the entire water column over 24 h, taking into account daily irradiance. The values were then integrated over the season using seasonally measured PAR values and assuming that measured activity on the sampling date accounted for half of the time from the previous and to the next measuring date, respectively.

3. Results

During 2005–2010, temperature and salinity conditions in surface water at GF3 in the outer part of Godthåbsfjord fluctuated over the season with a peak temperature of 7 °C and lowest salinity of 24.2 during summer. The lowest surface–water temperature during winter was –0.7 °C and the highest salinity 33.5 (Fig. 2). Average annual temperature in surface waters (0–1 m) during 2005–2010 was 2.0 °C. During winter, sea ice forms in the inner parts of the fjord and the smaller fjord branches, reaching up to 0.8 m in thickness. Surface–water TA concentrations were c. 1800 μmol kg⁻¹ during summer and c. 2300 μmol kg⁻¹ during winter. TCO₂ concentrations in surface waters varied from c. 1600 μmol kg⁻¹ during summer to c. 2100 μmol kg⁻¹ during winter. Surface–water concentrations of PO₄³⁻ and SiO₂ ranged from c. 0.1 μmol kg⁻¹ and 0.2 μmol kg⁻¹ during summer to 0.9 μmol kg⁻¹ and 6.7 μmol kg⁻¹, respectively, during winter.

Mean monthly wind speed varied from 3 to 9 m s⁻¹ during 2005–10, although wind speed in shorter periods (hours) was up to 34 m s⁻¹ (Fig. 3). $\Delta p\text{CO}_2$ determines whether the fjord acts as a source or a sink for atmospheric CO₂. During 2005–2010, $\Delta p\text{CO}_2$ was below 0 except for January–February 2008, October 2009 to February 2010 and during May 2010, indicating general undersaturation of the surface water compared with the atmosphere. Air–sea CO₂ fluxes ranged from c. –20 g C m⁻² month⁻¹ (uptake from the atmosphere) to 25 g C m⁻² month⁻¹ (release to the atmosphere) during 2005–10. Two different calculations were made; one based on the average monthly wind speed and one based on hourly wind speed. These correlated strongly (*r*² = 0.93; *P* < 0.001) but the air–sea CO₂ flux based on hourly wind speed exceeded the monthly estimates based on average monthly wind speed by 23%. The reason for this is the non-linear relationship between air–sea flux and wind speed (Eq. (1)) resulting in large exchanges during high wind speed events. Integrated annual air–sea fluxes are summarized in Table 1.

Daily primary production rates varied from 1 to 1500 mg C m⁻² d⁻¹ during 2005–10 (Juul-Pedersen et al., 2010). The highest daily rates of primary production varied between years from 700 mg C m⁻² d⁻¹ to 1500 mg C m⁻² d⁻¹, and annually integrated values varied between 76 g C m⁻² yr⁻¹ and 105 g C m⁻² yr⁻¹, respectively (Table 1). In some years, both the spring bloom and the post-bloom period could be detected, whereas in other years they could not. No statistically significant correlation between daily primary production rates and air–sea CO₂ flux rates was detected (*P* = 0.48, *r*² = 0.08).

Monthly vertical sinking fluxes of estimated chlorophyll *a*-based carbon (Chl-C) ranged between 2 and 1112 mg C m⁻² d⁻¹ from 2006 to 2010. The annually integrated Chl-C values decreased from 2007 to 2010 (from 89 to 38 g C m⁻² yr⁻¹, respectively; Table 1).

During summer (July–August) 2007–08 the $\Delta p\text{CO}_2$ values ranged from –20 to –330 μatm in surface waters of nearshore and offshore areas of southern Greenland showing a marked undersaturation of surface waters compared with the atmosphere (Fig. 4). Furthermore, very low *p*CO₂ values were recorded in the innermost part of Godthåbsfjord. There was a tendency towards more positive $\Delta p\text{CO}_2$ values off SE Greenland as compared with SW Greenland.

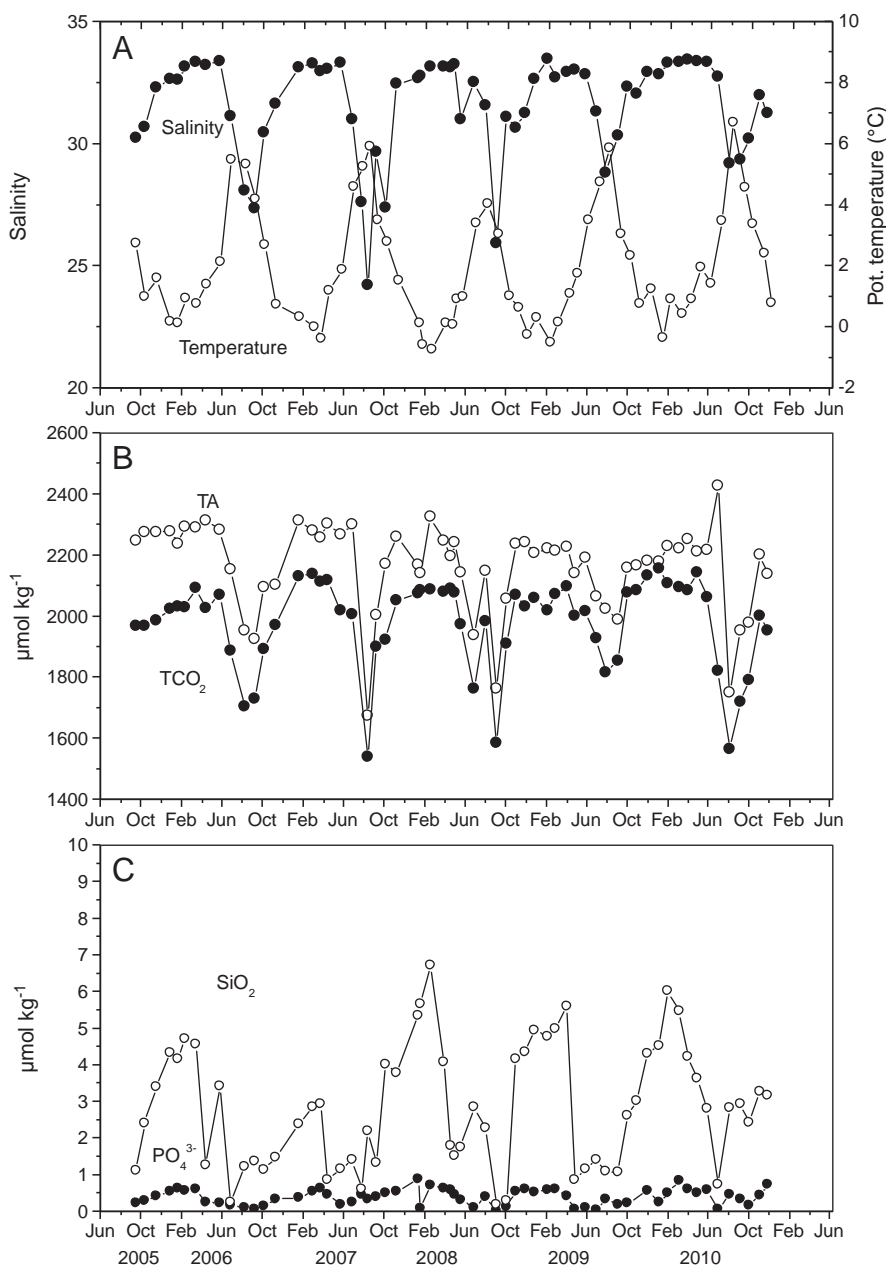


Fig. 2. Surface-water conditions during 2005–10 at GF3 in Godthåbsfjord of (A) salinity (closed circles) and temperature (open circles). (B) Total alkalinity, TA (open circles), and total inorganic carbon, TCO₂ (closed circles). (C) Silicate (open circles) and phosphate (closed circles).

4. Discussion

Despite some uncertainties (Borges, 2005; Borges et al., 2005; Cai et al., 2006), mounting evidence based on $p\text{CO}_2$ measurements (Chen and Borges, 2009) and mass-balance calculations (Chen, 2004; Chen et al., 2003) seem to indicate that the continental shelves are sinks for atmospheric CO_2 . The largest contributions to this CO_2 sink appear to be from sub-polar and polar biogeochemical provinces, whereas tropical and sub-tropical shelves tend to act as sources of CO_2 to the atmosphere (Chen and Borges, 2009). Despite variability in the annual air–sea CO_2 uptake rate at GF3 during 2005–2010 in Godthåbsfjord ($14\text{--}172\text{ g C m}^{-2}\text{ yr}^{-1}$ based on the equations by Nightingale et al., 2000; mean value $96\text{ g C m}^{-2}\text{ yr}^{-1}$; Table 1) it support the high uptake rates of $26\text{ g C m}^{-2}\text{ yr}^{-1}$ reported for Arctic shelves in general (Chen and Borges, 2009), and our data add further to the evidence that high-latitude shelves are indeed sinks for CO_2 . Computations based on several other parameterizations for evaluating the air–sea CO_2 flux

(Wanninkhof, 1992; Wanninkhof and McGills, 1999; Liss and Werlivat, 1986 and Wu, 1996) yield a mean air–sea CO_2 uptake rate of $87\text{ g C m}^{-2}\text{ yr}^{-1}$ (air–sea CO_2 flux; Min. = -4 ; Max. = $-173\text{ g C m}^{-2}\text{ yr}^{-1}$) further underlining the strong uptake of CO_2 at GF3.

We observed very low $p\text{CO}_2$ conditions in the inner parts of the fjords (Fig. 4). Surface $p\text{CO}_2$ correlated strongly with surface salinity along the length section ($y = 8.1e^{0.1x}$, $r^2 = 0.98$, where x and y indicate distance (km) and salinity, respectively) in Godthåbsfjord as discharge of cold meltwater from the ice sheet will maintain low $p\text{CO}_2$ conditions in the inner parts of the fjord during summer. In addition, high primary production rates exist in these inner parts, as evident from high Chlorophyll a concentrations and depleted nutrients in the upper 50 m of the water column during May–September, and will help maintain $p\text{CO}_2$ levels below atmospheric levels during the productive season (Fig. 4; Arendt et al., 2010; Arendt et al., 2011; Cruise Report, R/V 'Dana' 2008). Moreover, high TA levels relative to

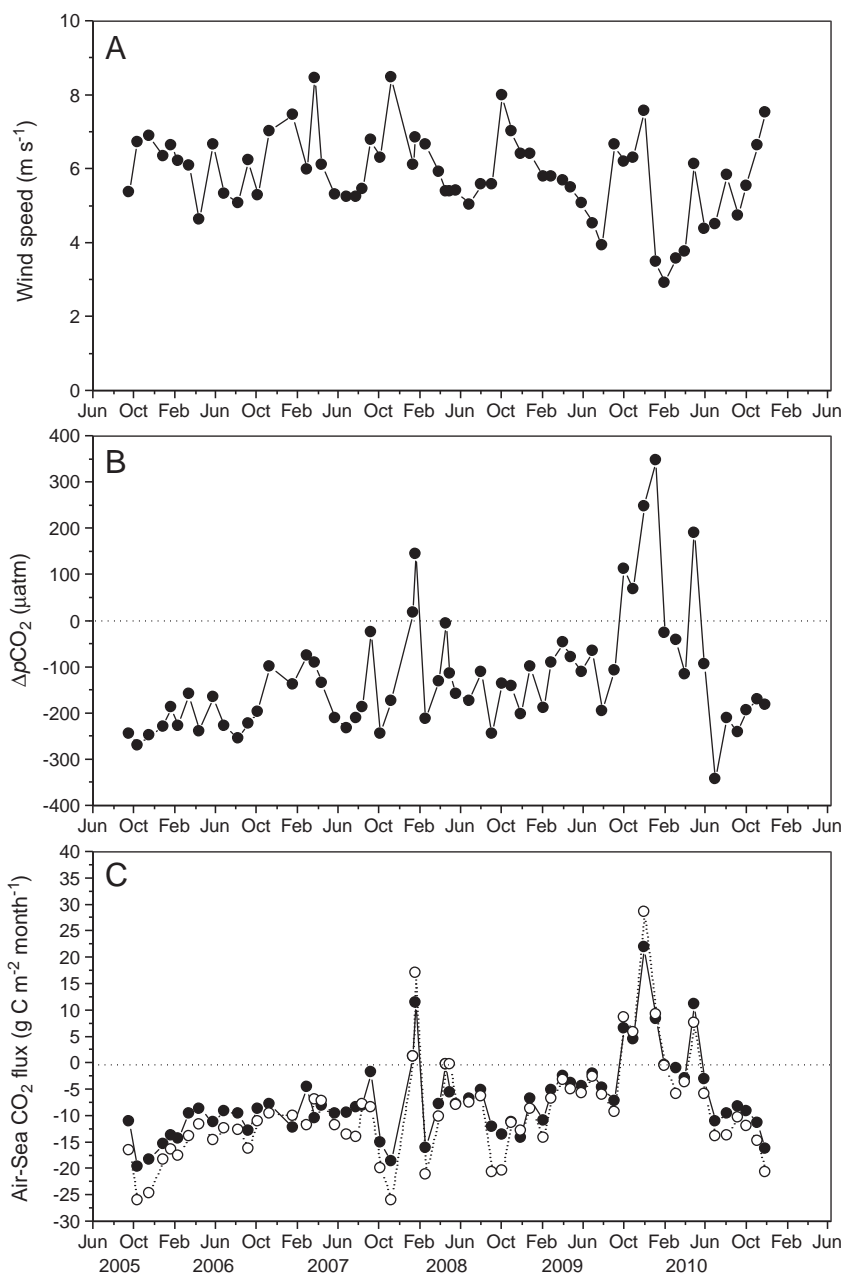


Fig. 3. (A) Mean monthly wind speed at the meteorological station "522". (B) Difference in $p\text{CO}_2$ between atmosphere and sea surface ($\Delta p\text{CO}_2$) at GF3. (C) Air–sea CO_2 flux rates during 2005–10 calculated from mean monthly wind speeds (close circles) and from hourly wind speeds (open circles).

TCO_2 levels in surface waters observed here during August–September when subglacial meltwater discharge peaks could suggest that glacial meltwater contains geochemically reactive carbonate minerals leading to low surface–water $p\text{CO}_2$ as also recently observed in other

glacier fjords in Svalbard (Krawczyk and Bartoszewski, 2008) and in East Greenland (Sejr et al., 2011). We analyzed a single transect to the innermost part of Godthåbsfjord occupied during August 2010 where TA and TCO_2 were measured at 1 m depth (Fig. 5). The increase

Table 1
Conditions at GF3 in the outer sill region of Godthåbsfjord. Computed annual air–sea CO_2 fluxes based on hourly and monthly average wind measurements. Integrated annual primary production rates and vertical export rates below 60 m water depth.

Year	Air–sea flux ($\text{g C m}^{-2} \text{ yr}^{-1}$) monthly values	Air–sea flux ($\text{g C m}^{-2} \text{ yr}^{-1}$) hourly values	Primary production (C-fixation) ($\text{g C m}^{-2} \text{ yr}^{-1}$)	Vertical export of chl. carbon (60 m) ($\text{g C m}^{-2} \text{ yr}^{-1}$)
2006	–128.4	–163.8	76.0	88.5
2007	–132.6	–172.8	104.3	89.1
2008	–87.7	–100.4	91.1	44.7
2009	–14.2	–18.5	99.7	40.3
2010	–53.7	–84.5	105.5	38.2

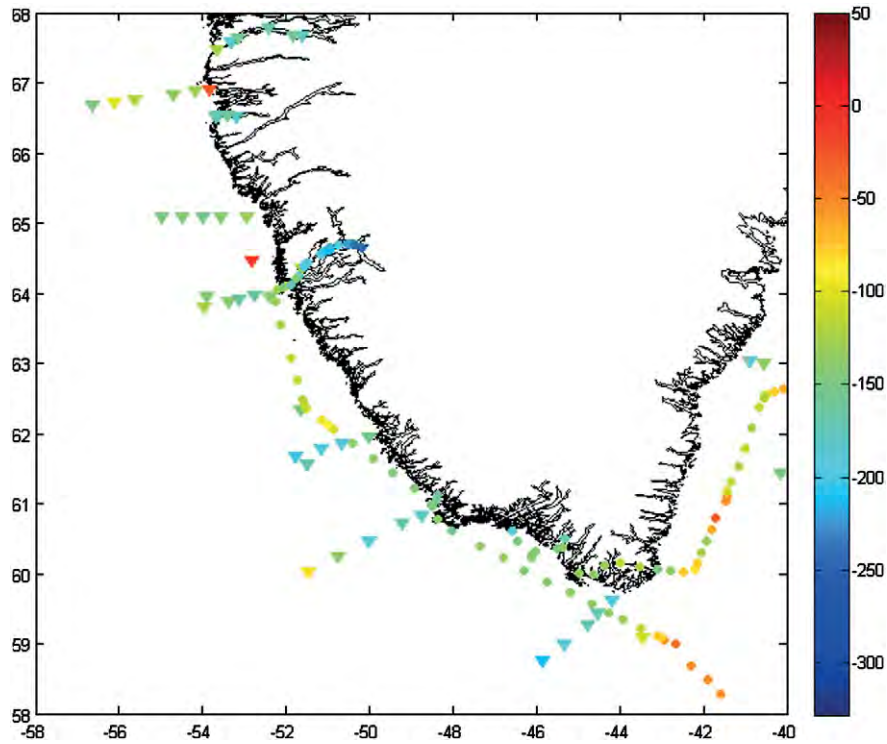


Fig. 4. Difference in $p\text{CO}_2$ between atmosphere and sea surface ($\Delta p\text{CO}_2$) in nearshore and offshore waters around southern Greenland. The data are both equilibrator online data from the Dana cruise in summer 2008, the Galathea cruise fall 2006 and data from various discrete sampling. $\Delta p\text{CO}_2$ values along the coast are mainly from the two cruises (circles), and $\Delta p\text{CO}_2$ measurements perpendicular to the coast are discrete sampling (triangles).

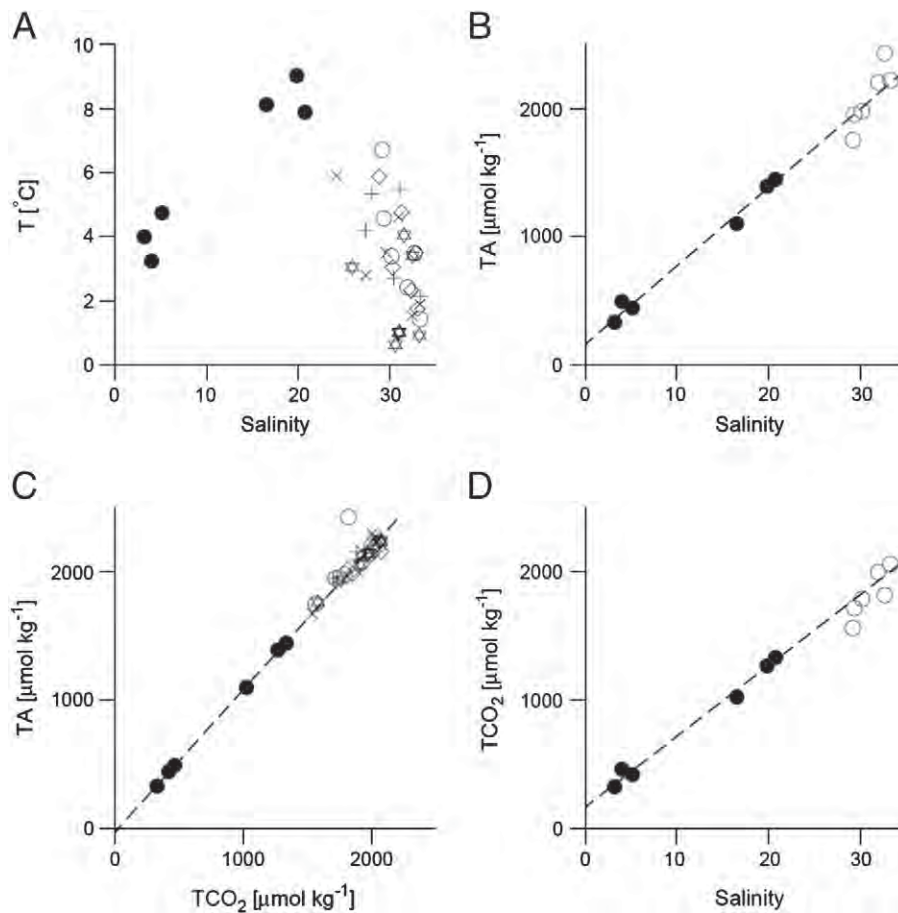


Fig. 5. Plot of (A) T-S, (B) TA-S, (C) TA- TCO_2 and (D) TCO_2 -S from 1 m depth along a length section in Godthåbsfjord (4th August 2010, bullets) and corresponding linear regression lines (dashed). Data from GF3 from June–November 2006–2010 (2006, plus; 2007, times; 2008, star; 2009, diamond; 2010, circle) are shown in (A, C) and from 2010 only (B, D).

of surface salinity from 5 at the inner part towards values of about 30 at GF3 reflected the gradual mixing between meltwater and coastal water. Linear regressions of TA and TCO_2 versus salinity, where uncertainties of TA and TCO_2 ($10 \mu\text{mol kg}^{-1}$) and salinity (1 salinity unit) were estimated from the spatial variations in the fjord, resulted in significant fits between TA and salinity (goodness of fit $Q=0.40$; $\text{TA}=161(\pm 47)+61(\pm 3) S$) and TCO_2 and salinity ($Q=0.48$; $\text{TCO}_2=169(\pm 42)+55(\pm 3) S$, where Q is the goodness of fit probability; Press et al., 1986). The corresponding linear relation between TCO_2 and TA resulted in a similar significant fit ($Q=0.79$, $\text{TCO}_2=-25(\pm 13)+1.11(\pm 0.01) \text{TA}$). The linear relationship implies a large decrease in $p\text{CO}_2$ from the mouth towards the inner part of the fjord of about 180 ppm (corresponding to the difference between $S=30$ and $S=5$ with $T=5^\circ\text{C}$) and therefore mixing between meltwater and coastal water can explain a significant part of the large decrease in surface $p\text{CO}_2$ in Godthåbsfjord. This may also apply to other fjord systems around Greenland with similar low $p\text{CO}_2$ values. An extrapolation of a corresponding significant linear regression ($Q=0.80$) between TA and TCO_2 was in accordance with the range of TA and TCO_2 values observed during the summer and fall seasons at GF3 (Fig. 5C) and this indicates that meltwater from the fjords also influences the coastal $p\text{CO}_2$ variability. A calculation based on the meltwater $p\text{CO}_2$ content of $86 \mu\text{atm}$ and a volume flux of c. 8 km^3 from glacier discharge (Mortensen et al., 2011) shows that this freshwater discharge can account for $1\text{--}2 \text{ g C m}^{-2} \text{ yr}^{-1}$ of the total air–sea CO_2 uptake in Godthåbsfjord. The potential uptake may be higher as the meltwater estimate of 8 km^3 does not include liquid meltwater discharge.

The average gross annual primary productivity over the period 2006–2010 of 95 g C m^{-2} is within the range of the air–sea flux of $83\text{--}108 \text{ g C m}^{-2}$ (Table 1, mean annual numbers are based on hourly and monthly air–sea CO_2 computations, respectively). Furthermore, the relatively high vertical sinking flux of Chlorophyll *a* to depths below 60 m suggests that a large fraction of carbon assimilated by phytoplankton at our investigated station is not degraded above the mixed layer in contact with the atmosphere, but rather mineralized in deeper waters. This would cause primary production to maintain a low $p\text{CO}_2$ concentration in surface waters, thus driving a high air–sea $p\text{CO}_2$ flux similar to what has been observed in shelf sea systems (Thomas et al., 2004). However, there was no statistically significant correlation between the average annual gross primary production and the annual air–sea flux during 2005–2010 ($r^2=0.18$, $P=0.47$), which suggests that regulation of $p\text{CO}_2$ in the fjord is more complex. Furthermore, removing the solubility effect of temperature by

normalizing to the average temperature of 2°C (2005–2010) did not improve the correlation.

A description of water masses and circulation patterns in Godthåbsfjord was provided recently by Mortensen et al. (2011). Here they describe 4 circulation modes in the fjord; estuarine circulation, subglacial circulation, intermediate baroclinic circulation and dense coastal inflows. Whereas the first three circulation modes largely affect local water masses within the fjord, dense coastal inflows of modified Subpolar Mode Water determined from larger circulation patterns outside the fjord can send old $p\text{CO}_2$ -rich water ($p\text{CO}_2>500 \mu\text{atm}$) into the fjord at depth and cause bottom water to be forced upwards in the fjord. These dense inflows may sometimes reach the surface, leading to a net CO_2 flux from the fjord to the atmosphere, and at other times they do not. The surface $\Delta p\text{CO}_2$ at GF3 during 2005–10 together with the density at 240 m depth (this depth captures dense inflows, see Mortensen et al., 2011) and primary production is shown in Fig. 6. Positive values of $\Delta p\text{CO}_2$ at GF3 seem to occur in connection with warm inflow events of modified Subpolar Mode Water, e.g. in winter 2007–08 and again in winter 2009–10. The warm and following cold inflow during 2005 were most likely too short to allow this water to reach the surface and/or water in the fjord prior to the inflow was so undersaturated in $p\text{CO}_2$ that it could maintain $p\text{CO}_2$ in surface waters below atmospheric levels (Fig. 3). Overall, except for the three confined CO_2 emissions to the atmosphere, GF3 in Godthåbsfjord was a strong sink for atmospheric CO_2 over the investigation period of 2005–2010.

The observations of low $p\text{CO}_2$ conditions in nearshore and offshore areas of southern Greenland add further to other existing observations of sub-Arctic seas showing a marked undersaturation of the sea surface compared with the atmosphere (Fig. 4, Takahashi et al., 2009). The strong $p\text{CO}_2$ undersaturation in the surface water from the different fjord systems along the Greenland coast line may be responsible for the low $p\text{CO}_2$ values observed on the shelf and most likely representative for the region. As the fjords also exports a lot of freshwater due to the large meltwater flux from Greenland Ice Sheet, the strong halocline will ensure that released CO_2 from mineralization of sedimenting material below this halocline will not reach surface waters in the study area during summer.

Unfortunately, not many measurements exist from the region during winter. However, through compilations of existing data and normalizing procedures, Takahashi et al. (2009) computed the $\Delta p\text{CO}_2$ level in surface waters for each month of a reference year (2000). According to their computations, $\Delta p\text{CO}_2$ levels in surface–water areas north of 50°N would on average vary by c. $40 \mu\text{atm}$ during a

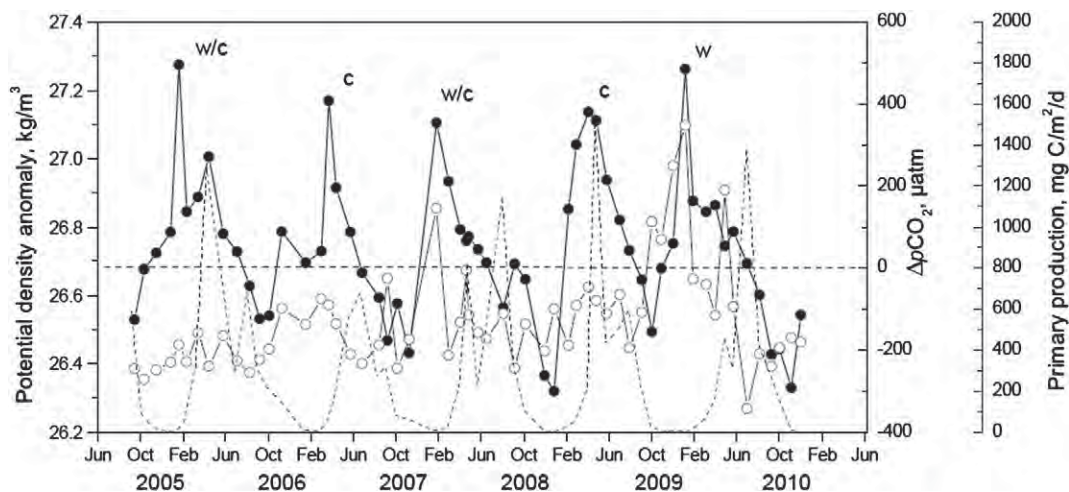


Fig. 6. Potential density anomaly at 240 m (filled circles) indicating cold (c) and warm (w) inflow events, $\Delta p\text{CO}_2$ conditions at 1 m (open circles) and primary production (dotted line) at GF3 in Godthåbsfjord during 2005–10.

season. If this also applies to our study area off the coast, surface-water $p\text{CO}_2$ conditions would still be undersaturated during winter at most of the stations and the area could, hence, be considered a strong sink for atmospheric CO_2 on an annual basis as well. Using an average wind speed of 6 m s^{-1} , a mean marine $p\text{CO}_2$ of $170 \mu\text{atm}$ and the atmospheric CO_2 content of $387 \mu\text{atm}$ from the investigated fjord area of c. 2000 km^2 , this accounts for an air–sea CO_2 flux of $5 \times 10^{-7} \text{ Pg C d}^{-1}$. This is a relatively large uptake compared to the area uptake of the total European shelf water ($5 \times 10^6 \text{ km}^2$) which is about $3.4 \times 10^{-4} \text{ Pg C d}^{-1}$ (Frankignoulle and Borges, 2001) or compared to the oceanic area ($16.2 \times 10^6 \text{ km}^2$) uptake north of 50°N which is about $8 \times 10^{-4} \text{ Pg C d}^{-1}$ (Takahashi et al., 2009). According to Takahashi et al. (2009), the high-latitude North Atlantic, including the Nordic Seas and portions of the Arctic Sea, is the most intense CO_2 sink region (based per unit area), with a mean of $2.5 \text{ tons C month}^{-1} \text{ km}^{-2}$. Hence, Godthåbsfjord must be considered a very strong sink indeed, with an uptake of about $7.5 \text{ tons C month}^{-1} \text{ km}^{-2}$. If the uptake here is typical for similar fjord systems in Greenland, then the coastal areas of Greenland constitute a much larger sink than anticipated.

Acknowledgments

The study received financial support from the Danish Agency for Science, Technology and Innovation, The Danish Energy Agency, The Danish Environmental Protection Agency, The Canada Excellence Research Chair (CERC) program, Nordic Council of Ministers and the Aage V Jensen Charity Foundation. Anna Haxen is thanked for linguistic corrections. The study is a part of the Greenland Climate Research Centre activities (www.natur.gl) and the Greenland Ecosystem Monitoring Program (www.g-e-m.dk). Finally, we would like to thank the Editor and two anonymous reviewers for their comments and suggestions to our manuscript.

References

- Anderson, L.G., Drange, V., Chierici, M., Fransson, A., Johannessen, T., Skjelvan, I., Rey, F., 2000. Annual variability of carbon flux in the upper Greenland Sea, as evaluated from measured data and a box model. *Tellus B* 52, 1013–1024.
- Arendt, K.E., Nielsen, T.G., Rysgaard, S., Tønnesson, K., 2010. Difference in plankton community structure along the Godthåbsfjord, from the Greenland Ice Sheet to offshore waters. *Mar. Ecol. Prog. Ser.* 401, 49–62.
- Arendt, K.E., Dutz, J., Jonasdóttir, S.H., Jung-Madsen, S., Mortensen, J., Moeller, E.F., Nielsen, T.G., 2011. Effects of suspended sediments on copepods feeding in a glacial influenced sub-Arctic fjord. *J. Plankton Res.* 33 (10), 1526–1537. doi:10.1093/plankt/fbr054.
- Borges, A.V., 2005. Do we have enough pieces of the jigsaw to integrate CO_2 fluxes in the coastal ocean? *Estuaries* 28, 3–27.
- Borges, A.V., Delille, B., Frankignoulle, M., 2005. Budgeting sinks and sources of CO_2 in the coastal ocean: diversity of ecosystems counts. *Geophys. Res. Lett.* 32, L14601.
- Buch, E., Pedersen, S.A., Ribergaard, M.H., 2004. Ecosystem variability in West Greenland waters. *J. Northwest Atl. Fish. Sci.* 34, 13–28.
- Cai, W.-J., Dai, M.H., Wang, Y.C., 2006. Air–sea exchange of carbon dioxide in ocean margins: a province-based synthesis. *Geophys. Res. Lett.* 33, L12603.
- Chen, C.T.A., 2004. Exchange of carbon in the coastal seas. In: Field, C.B., Raupach, M.R. (Eds.), *The Global Carbon Cycle: Integrating Human, Climate and the Natural World*. SCOPE, Washington DC, pp. 341–351.
- Chen, C.T.A., Borges, A.V., 2009. Reconciling opposing views on carbon cycling in the coastal ocean: continental shelves as sinks and near-shore ecosystems as sources of atmospheric CO_2 . *Deep Sea Res.* II 56, 578–590.
- Chen, C.T.A., Liu, K.K., MacDonald, R., 2003. Continental margin exchange. In: Fasham, M.J.R. (Ed.), *Ocean Biogeochemistry: A JGOFs Synthesis*. Berlin, Springer, pp. 53–97.
- Cloern, J.E., 1996. Phytoplankton bloom dynamics in coastal ecosystems: a review with some general lessons from sustained investigation of San Francisco Bay, California. *Rev. Geophys.* 34, 127–168.
- Dickson, A.G., Goyet, C., 1994. Handbook of Methods for the Analysis of the Various Parameters of the Carbon Dioxide System in Sea Water, Version 2 ORNL/CDIAC-74.
- Falkowski, P., Kiefer, D.A., 1985. Chlorophyll *a* fluorescence in phytoplankton: relationships to photosynthesis and biomass. *J. Plankton Res.* 7, 715–731.
- Frankignoulle, M., Borges, A.V., 2001. European continental shelf as a significant sink for atmospheric carbon dioxide. *Global Biogeochem. Cycles* 15, 569–576.
- Grasshoff, K., Erhardt, M., Kremling, K., 1983. *Methods of Sea Water Analysis*, 2nd Revised and Extended Version. Verlag Chemie, Weinheim, Deefield Beach, Fla.
- Haraldsson, C., Anderson, L.G., Hasselöv, M., Hult, S., Olsson, K., 1997. Rapid, high-precision potentiometric titration of alkalinity in ocean and sediment pore water. *Deep Sea Res.* I 44, 2031–2044.
- Johnson, K.M., Sieburth, J.M., Williams, P.J., Brändström, L., 1987. Coulometric total carbon dioxide analysis for marine studies: automation and calibration. *Mar. Chem.* 21, 117–133.
- Juul-Pedersen, T., Rysgaard, S., Batty, P., Mortensen, J., Retzel, A., et al., 2010. The MarineBasic programme 2010 The MarinBasis programme. In: Jensen, L.M., Rasch, M. (Eds.), *Nuuk Ecological Research Operations, 4th Annual Report*. National Environmental Research Institute, Aarhus University, Denmark.
- Krawczyk, W.E., Bartoszewski, S.A., 2008. Crustal solute fluxes and transient carbon dioxide drawdown in the Scottbreen Basis, Svalbard in 2002. *J. Hydrol.* 362, 206–219.
- Liss, P.S., Werliav, L., 1986. Air–sea gas exchange rates: introduction and synthesis. In: Buat-Menard, P.D. (Ed.), *The Role of Air–sea Exchange in Geochemical Cycling*. Reidel, Norwell, Mass, pp. 113–129.
- Lorenzen, C.J., 1968. Carbon/chlorophyll relationships in an upwelling area. *Limnol. Oceanogr.* 13, 202–204.
- Mackenzie, F.T., Ver, L.M., Lerman, A., 2000. Coastal-zone biogeochemical dynamics under global warming. *Int. Geol. Rev.* 42, 193–206.
- Menard, H.W., Smith, S.M., 1966. Hypsometry of ocean basin provinces. *J. Geophys. Res.* 71, 4305–4325.
- Middelburg, J.J., Herman, P.M.J., 2007. Organic matter processing in tidal estuaries. *Mar. Chim.* 106, 127–147.
- Miller, L.A., Yager, P.L., Erikson, K.A., Amiel, D., Bâcle, J., Cochran, J.K., et al., 2002. Carbon distributions and fluxes in the North Water, 1998 and 1999. *Deep Sea Res.* II 49, 5151–5170.
- Millero, F.J., 1995. Thermodynamics of the carbon dioxide system in the oceans. *Geochim. Cosmochim. Acta* 59, 661–677.
- Mortensen, J., Lennert, K., Bendtsen, J., Rysgaard, S., 2011. Heat sources for glacial melt in a sub-Arctic fjord (Godthåbsfjord) in contact with the Greenland Ice Sheet. *J. Geophys. Res.* 116, C01013.
- Murata, A., Takizawa, T., 2003. Summertime CO_2 sinks in shelf and slope waters of the western Arctic Ocean. *Cont. Shelf Res.* 23, 753–776.
- Myers, P.G., Kulan, N., Ribergaard, M., 2007. Irminger water variability in the West Greenland Current. *Geophys. Res. Lett.* 34, L17601.
- Nightingale, P.D., Malin, G., Law, C.S., Watson, A.J., Liddicoat, M.I., et al., 2000. In situ evaluation of the air–sea gas exchange parameterizations using novel conservative and volatile tracers. *Global Biogeochem. Cycles* 14.
- Press, W.H., Teukolsky, S.A., Vetterling, W.T., Flannery, B.P., 1986. *Numerical Recipes in FORTRAN: the Art of Scientific Computing*. Press Syndicate of the University of Cambridge, USA.
- Sejr, M.K., Krause-Jensen, D., Rysgaard, S., Sørensen, L.L., Christensen, P.B., Glud, R.N., 2011. Air–sea flux of CO_2 in arctic coastal waters influenced by glacial melt water and sea ice. *Tellus B* 63B, 815–822.
- Smith, S.V., Hollibaugh, J.T., 1993. Coastal metabolism and the oceanic organic carbon balance. *Rev. Geophys.* 31, 75–89.
- Smith, S.V., Mackenzie, F.T., 1987. The ocean as a net heterotrophic system; implications for the carbon biogeochemical cycle. *Glob. Biogeochem. Cycles* 1, 187–198.
- Steeman-Nielsen, E., 1952. The use of radio-active carbon (^{14}C) for measuring organic production in the sea. *J. Cons. Int. Explor. Mer* 18, 117–140.
- Takahashi, T., Sutherland, S.C., Sweeney, C., Poisson, A., Metzl, N., Tilbrook, B., et al., 2002. Biological and temperature effects on seasonal changes of $p\text{CO}_2$ in global surface waters. *Deep Sea Res.* II 49, 1601–1622.
- Takahashi, T., et al., 2009. Climatological mean and decadal change in surface ocean $p\text{CO}_2$ and net sea–air CO_2 flux over the global oceans. *Deep Sea Res.* II 56, 554–577.
- Thomas, H., Bozec, Y., Elkalay, K., de Baar, H.J.W., 2004. Enhanced open ocean storage of CO_2 from shelf sea pumping. *Science* 304, 1005–1008.
- Ver, L.M.B., Mackenzie, F.T., Lerman, A., 1999a. Carbon cycle in the coastal zone: effects of global perturbations and change in the past three centuries. *Chem. Geol.* 159, 283–304.
- Ver, L.M.B., Mackenzie, F.T., Lerman, A., 1999b. Biogeochemical responses of the carbon cycle to natural and human perturbations: past, present, and future. *Am. J. Sci.* 299, 762–801.
- Wanninkhof, R., 1992. Relationship between wind speed and gas exchange over the ocean. *J. Geophys. Res.* 97, 7373–7382.
- Wanninkhof, R., McGillis, W.R., 1999. A cubic relationship between air–sea CO_2 exchange and wind speed. *Geophys. Res. Lett.* 26, 1889–1892.
- Weiss, R.F., 1974. Carbon dioxide in water and seawater: the solubility of a non-ideal gas. *Mar. Chim.* 203–215.
- Wu, J., 1996. Air–sea gas transfer: mechanisms and parameterization. *J. Phys. Oceanogr.* 26, 1440–1447.
- Yager, P.L., Minnett, P.J., Deming, J.W., 1995. The Northeast Water Polynya as an atmospheric CO_2 sink: a seasonal rectification hypothesis. *J. Geophys. Res.* 100, 4389–4398.



ISBN: 87-91214-68-8

